UNIVERSITÀ
di VERONA

UNIVERSITY OF VERONA

DEPARTMENT OF
Neurosciences, Biomedicine and Movement

SECTION OF
Anatomy and Histology

PHD PROGRAM IN
Natural Sciences and Engineering
PhD in Nanoscience and Advanced Technologies

PRESENTED BY **FLAVIA CARTON**
31° CYCLE

BIOCOMPATIBLE NANOCARRIERS FOR DELIVERING DRUGS TO SKELETAL MUSCLE CELLS: A THERAPEUTIC OPTION FOR MYOTONIC DYSTROPHY?

S.S.D.: BIO/16 HUMAN ANATOMY

COORDINATOR: Prof. Franco TAGLIARO

TUTOR: Prof. Manuela MALATESTA

CO-TUTOR: Dr. Giovanna LOLLO

PHD STUDENT: Flavia CARTON

Biocompatible nanocarriers for delivering drugs to skeletal muscle cells: a therapeutic option for myotonic dystrophy? -Flavia Carton
Tesi di Dottorato
Verona, 17 Dicembre 2018
ISBN

A Bianca

ACKNOWLEDGMENTS

During my PhD studies, I had the chance to know, meet and cooperate with many people. I wish to express to all of them my deep gratitude. They gave me the opportunity to improve my knowledge, supported my activities, taught me how to overcome difficulties, and broadened my horizons, improving myself in life and work.

I am especially grateful to my supervisor, Professor Manuela Malatesta (University of Verona), not only for accepting me in her research group, but also for giving me her knowledge, experience and enthusiasm, and for encouraging me with her valuable lessons. I especially appreciated her willingness to generously devote her time to me: working with her was formative and pleasant.

I really would like to express my special thanks also to my co-supervisor, Doctor Giovanna Lollo (LAGEP UMR 5007, Université Claude Bernard Lyon 1), a memorable reference and guide. Giovanna guided me to discover the world of formulation, to improve my knowledge in this new field, and to take my first steps into an international research. I will never forget her patient guidance and valuable advice in my research work, her continuous help and especially her kindness. She has been, and still is, for me a very important person.

I also wish to thank Professor Silvia Arpicco and Professor Barbara Stella (University of Turin): they welcomed me in their laboratory and introduced me into the chemical word. With their enthusiasm, they gave me an unforgettable experience of fruitful collaboration, leaving me the confidence to willingly continue my work. They also pointed me towards my great “adventure” in Lyon, and I am so grateful for that. I thankfully remember all the students in Turin who kindly shared with me their expertise during my research in Professor Arpicco’s laboratory.

I wish to thank Professor Giovanni Meola and Doctor Rosanna Cardani (I.R.C.C.S. Policlinico San Donato, San Donato Milanese, Milan) who kindly provided me with the primary myoblast cultures from patients with myotonic

dystrophy: Professor Meola is a scientist and physician internationally renowned for his contributions to the research and therapy of myotonic dystrophies and introduced me to the study of this neuromuscular disorder.

I want to express my gratitude to Professor Franco Tagliaro, Coordinator of the PhD program in Nanoscience and Advanced Technologies at the University of Verona, who supported me in all the activities I undertook. My grateful thanks are also extended to Professor Federico Boschi (University of Verona) for his help in doing the analysis of morphometical data; to Professor Carlo Pellicciari (University of Pavia) who made available to me his experience in light microscopy and histochemistry; and to Professor Laura Calderan (University of Verona) who always devoted so much attention to me with her proficient suggestions during my research activity.

Many thanks are as well due to all my research fellows in Verona (Barbara Cisterna, Manuela Costanzo, Valeria Guglielmi, Enrica Cappellozza, and Mathieu Repellin) for their advices and assistance in keeping my progress on schedule, and for sharing with me precious moments in the lab as much as outside work.

Regarding my stay in France at the LAGEP UMR 5007-University Claude Bernard Lyon 1, it was an important training, both as a scientific and a personal experience. I am deeply indebted to Professor Stéphanie Briançon for accepting me at the LAGEP where I did have a great and memorable life experience. For this reason, I would like to thank Professor Yves Chevalier for the support and valuable advice that were crucial to improve my research program. I would like also to extend my thanks to the staff of the INSERM 1052 CNRS 5286 laboratory (Centre Léon Bérard, Centre de Recherche en Cancérologie de Lyon), and particularly to Doctor Lars Petter Jordheim and his collaborators (Émeline Cros and Zineb Bousfiha) who helped me to collect important original data. Thanks, to the technicians of the LAGEP UMR 5007 and C2P2 UMR 5265 laboratory, University of Lyon 1, Géraldine Agusti, Sebastien Urbaniak and Pierre-Yves Dugas, for their great patience to support me while learning new theoretical and practical skills. Memorable will be all the friends I met in Lyon, who made this experience *unique*:

they helped me in my work doings, and everyone contributed to my professional and personal growth.

In particular, a very singular gratitude goes to special friends (Valeria Gugliemi, Greta Magnano, Mathieu Repellin and Roberta Calmo) who made enormous contribution to my personal and work career for providing me constructive comments, warm encouragements, valuable suggestions, motivation and ideas during all these years.

Finally, I am wholeheartedly thankful to my family (Elles, Alberto, Guelfo, Bianca, Cristiana and Giacomo) who has always believed in me, supporting all my decisions and encouraging me during all my life.

SOMMARIO

Le distrofie miotoniche (DM) sono malattie neuromuscolari degenerative a base genetica caratterizzate dalla progressiva alterazione di diversi organi e tessuti (ad esempio, tessuto muscolare scheletrico, cardiaco e liscio, sistema nervoso centrale), dei quali uno dei più compromessi è il muscolo scheletrico. Esistono due tipi di DM: la forma più grave è denominata DM di tipo 1 (o malattia di Steinert) e la forma più lieve è detta DM di tipo 2 (conosciuta anche come "proximal Myotonic Myopathy" o "PROMM"). I meccanismi patogenetici molecolari sono, per la DM1, l'espansione della tripletta $(CTG)_n$ nella regione 3' UTR del gene Dystrophia Myotonica Protein Kinase (DMPK), mentre l'espansione della quadripletta $(CCTG)_n$ nel primo introne del gene Nucleic Acid Binding Protein/Zinc Finger 9 (CNBP/ZNF9) è responsabile della DM2. La trascrizione di queste sequenze ripetute produce RNA tossico che si accumula in aggregati ribonucleoproteici nucleari (chiamati foci) e provoca una generale alterazione dello splicing. Il principale problema di queste patologie è che, ad oggi, non esiste una terapia risolutiva e gli approcci terapeutici attualmente in uso sono puramente sintomatici. Attualmente, la ricerca farmacologica sta valutando l'efficacia di piccole molecole, come la pentamidina (PTM), in grado di limitare le alterazioni dello splicing associate alla DM: la PTM è un farmaco antiprotozoario e chemioterapico in grado di ridurre la formazione di foci nucleari nella DM; tuttavia rappresenta una terapia scarsamente applicabile a causa della elevata tossicità a livello sistemico. Per superare queste limitazioni, un approccio adeguato può essere la veicolazione di farmaci mediante nanovettori biocompatibili, in grado di migliorare la somministrazione mirata e diminuire la tossicità sistemica.

Pertanto, l'obbiettivo principale di questo lavoro di tesi è stato quello di individuare una strategia terapeutica innovativa per la DM basata su nanovettori biocompatibili per la veicolazione di PTM.

A questo scopo, su linee cellulari tumorali e su colture primarie di cellule muscolari umane è stata testata *in vitro,* la biocompatibilità di differenti tipologie di nanovettori [liposomi, nanoparticelle a base di poly(lactic-co-glycolic acid)

(PLGA), nanoparticelle di silice mesoporosa]. Mediante microscopia a fluorescenza convenzionale e confocale e la microscopia elettronica a trasmissione, si è studiato il meccanismo di internalizzazione, la distribuzione intracellulare e la degradazione delle differenti tipologie di nanosistemi testati. Tutte le nanoparticelle sperimentate sono risultate biocompatibili per tutti tipi cellulari considerati, sebbene le cellule di origine muscolare (in particolare i miotubi) abbiano mostrato una capacità di internalizzazione inferiore rispetto ai modelli tumorali.

Inoltre, in collaborazione con l'Università di Lione, sono state sviluppate nanoparticelle a base di acido ialuronico in grado di incapsulare farmaci idrofilici. Tali nanoparticelle sono risultate biocompatibili sia per le cellule tumorali che per quelle muscolari, dimostrandosi efficaci nella veicolazione di PTM a cellule tumorali; è attualmente in corso lo studio degli effetti di questo trattamento sulle cellule muscolari.

Infine, nel tentativo di colmare il divario esistente tra le tecniche convenzionali di coltura cellulare *in vitro* e la sperimentazione *in vivo*, abbiamo messo a punto un'innovativa applicazione della tecnologia fluidodinamica per migliorare la preservazione di muscoli espiantati e studiare così la biodistribuzione di nanovettori in questi organi. I primi dati hanno rivelato come le nanoparticelle di PLGA, che pure sono facilmente internalizzate dalle cellule muscolari in coltura, riescano difficilmente a penetrare nelle miofibre nel muscolo intero, poiché la maggior parte di esse si accumula nel tessuto connettivo. A seguito di questo risultato, abbiamo intrapreso studi di funzionalizzazione delle nanoparticelle di PLGA, allo scopo di favorirne la penetrazione all'interno delle fibre muscolari.

ABSTRACT

Myotonic dystrophy (DM) represents a genetic disorder characterized by progressive dysfunction of multiple organs and tissues (*e.g.* skeletal, cardiac, and smooth muscle; the central nervous systems) among which the most severely affected is the skeletal muscle; this condition leads patients to a progressive muscle weakness, wasting and myotonia. The molecular pathogenetic mechanism of DM type 1 (or Steinert's) disease is the expansion of a $(CTG)_n$ triplet in 3' UTR region of the Dystrophia Myotonica Protein Kinase (DMPK) gene, while the $(CCTG)_n$ quadruplet expansion in the first intron of the cellular Nucleic Acid Binding Protein/Zinc Finger 9 (CNBP/ZNF9) is responsible for DM type 2 (previously named "proximal Myotonic Myopathy" or "PROMM"). These expanded repeats are transcribed into toxic RNA that accumulates in nuclear RNA-protein aggregates (called foci), and lead to a general splicing alteration. The main problem of DM pathologies is that no therapies are currently available, and the commonly used treatments are administered to only manage symptoms. At present, the pharmaceutical research is screening small molecules such as pentamidine (PTM) able to repair the DM-associated splicing defects: PTM is an antimicrobial and antitumor compound that can mitigate the DM missplicing, but has limited applicability in humans due to its high systemic toxicity. To overcome these limitations, the administration *via* biocompatible nanoparticles (NPs) may represent a suitable approach, improving targeted delivery of the therapeutic drug and decreasing its systemic toxicity.

Therefore, the main goal of the present experimental thesis was to set up an innovative experimental therapeutic strategy for DM based on biocompatible NPs loaded with PTM.

To this aim, different types of NPs potentially suitable for drug delivery [liposomes, poly(lactic-co-glycolic acid) (PLGA) NPs, mesoporous silica NPs] were tested for biocompatibility *in vitro* on stabilized tumor cell lines and cultured primary human muscle cells. Conventional and confocal fluorescence microscopy and transmission electron microscopy allowed elucidating the mechanisms of NP internalization, intracellular distribution, fate and degradation. The tested NPs

proved to be biocompatible for all the cell types investigated, although muscle-derived cells (especially the differentiated myotubes) showed lower internalization capability than cancer cells.

In addition, novel hyaluronic acid-based nanocomplexes for hydrophilic drug encapsulation were synthesized in collaboration with the University of Lyon; these NPs proved to be biocompatible for both cancer and cultured muscle cells, and to efficiently deliver PTM to cancer cells; the effects of PTM-loaded NPs on muscle cells are currently under investigation.

Finally, in the attempt to fill the gap between the conventional cell cultures and the organ complexity *in vivo*, an *in vitro* fluid dynamic system was set up to improve the preservation of explanted muscles and was then used for monitoring the biodistribution of NPs in this organ. Preliminary results revealed that PLGA NPs, which are easily internalized by cultured muscle cells, hardly enter the myofibers in the whole muscle since most of them accumulate in the connective tissue; consequently, modifications of the NP surface are in progress to improve targeting to and uptake by the muscle fibers.

INDEX

ACRONYMS **17**

LIST OF FIGURES **19**

LIST OF TABLES **21**

I. INTRODUCTION **23**

1. Myotonic dystrophy **25**

1.1. Morphological and functional features of human skeletal muscle 25

1.2. Pathogenic mechanisms of myotonic dystrophy 29

1.3. Current therapeutic development in myotonic dystrophy 31

2. Nanotechnology in biomedical research **35**

2.1. Nanoparticles for drug delivery 35

2.2. Nanoparticle testing for biomedical application 37

2.2.1. *In vitro* studies 38

2.2.2. *In vivo* studies 40

2.2.3. Fluid dynamic *in vitro* technologies 41

2.3. Nanoparticles for skeletal muscle 43

2.3.1. Liposomes 44

2.3.2. Mesoporous silica nanoparticles 47

2.3.3. Polymeric nanoparticles 49

3. Aim of the work **54**

II. RESULTS **57**

M. Costanzo, F. Carton, A. Marengo, G. Berlier, B. Stella, S. Arpicco, M. Malatesta (2016): Fluorescence and electron microscopy to visualize the intracellular fate of nanoparticles for drug delivery *63*

M. Costanzo, F. Carton, M. Malatesta (2017a). Monitoring the uptake and intracellular fate of nanovectors by microscopical technique. In: Small is beautiful: nanovectors for biomedical research and therapy *75*

M. Costanzo, F. Carton, M. Malatesta (2017b): Microscopy techniques in nanomedical research *97*

V. Guglielmi, F. Carton, G. Vattemi, S. Arpicco, B. Stella, G. Berlier, A. Marengo, F. Boschi, M. Malatesta (2018): Uptake and intracellular distribution of different types of nanoparticles in primary human myoblasts and myotubes *105*

A. Preliminary results I 131

F. Carton, Y. Chevalier, L. Nicoletti, M Tarnowska, B. Stella, S. Arpicco, M. Malatesta, LP. Jordheim, S. Briançon, and G. Lollo: Hyaluronic acid-based nano-complexes for hydrophilic drug encapsulation (in preparation) *135*

B. Preliminary results II 176

F. Carton, L. Calderan, M. Malatesta (2017): Incubation under fluid dynamic conditions markedly improves the structural preservation in vitro of explanted skeletal muscles *181*

C. Priminary results III 188

III. DISCUSSION 191

IV. APPENDIX 203

BIBLIOGRAPHY 229

ACRONYMS

3Rs: Three Rs (replacement, refinement and reduction)

ActD: Actinomycin D

ASO: Antisense oligomer

ATP: adenosine triphosphate

CELF1/CUGBP1: CUGBP/Etav-like family member 1

cET: 2'-4'-constrained ethyl

Clcn1: Chloride channel 1

CNS: Central nervous system

CNBP; ZNF9: CCHC-type zinc finger nucleic acid binding protein

DM: Myotonic dystrophy

DM1: Myotonic dystrophy type 1 (Steinert's disease, OMIM160900)

DM2: Myotonic dystrophy type 2 (proximal myotonic myopathy PROMM, OMIM602668)

DMPK: Dystrophia myotonica protein kinase

ECM: Extracellular matrix

EDTA: Ethylenediaminetetraacetic Acid

EMA: European Medicine Agency

FBS: Fetal Bovine Serum

FDA: Food and Drug Administration

FITC: Fluorescein isothiocyanate

GAG: glycosaminoglycan polysaccharide

GSK3β: Glycogen synthase kinase 3 beta

HA: Hyaluronic acid

HA-PArg NPs: Hyaluronic acid and polyarginine nanoparticles

IUPAC: International union of pure and applied chemistry

LPs: Liposomes

MBNL1: Muscleblind like 1 protein

MOE: 2'-O-methoxyethyl

MTT: 3-(4,5-dimethylthiazol-2-yl)-2,5-diphenyltetrazolium bromide

MSNs: Mesoporous silica nanoparticles

NPs: Nanoparticles

PBS: Phosphate-Buffered Saline

PLGA: Poly(lactic-*co*-glycolic acid)

PNPs: Polymeric nanoparticles

PTM: Pentamidine

PTM-S: Pentamidine isethionate salts

PTM-B: Pentamidine base

RES: Reticuloendothelial system

T tubules: Transverse tubules

LIST OF FIGURES

Figure 1. Development of skeletal muscle cell. The fusion of myoblasts forms myotubes, precursors of the mature muscle fibers. 26

Figure 2. Sarcomeric organization in myofibrils. 27

Figure 3. Microanatomical organisation of skeletal muscles. 28

Figure 4. NPs commonly used in biomedical fields. Modified from https://www.ema.europa.eu/documents/presentation/presentation-quality-aspects-nano-based-medicines-dolores-hernan-pacrez-de-la-ossa_en.pdf 36

Figure 5. Viability and cytotoxicity biomarkers commonly used to assess the occurrence of apoptotic or necrotic events due to the cytotoxic effect of nanomaterials (modified from Niles et al., 2008). 39

Figure 6. Different types of signals from which the activity of cells and organs depend. Using a bioreactor with an appropriate design and engineering, it is possible to reproduce these factors occurring *in vivo* (modified from Sbrana et al., 2012). 42

Figure 7. Self-assembly representation of a LPs (modified from Su et al., 2018). 46

Figure 8. Encapsulation of hydrophobic and hydrophilic drugs inside different types of LPs (modified from Sercombe et al., 2015). 47

Figure 9. Different types of functionalization on MSNs (modified from Chen et al., 2018). 49

Figure 10. Different type of PNPs: A nanospheres and B nanocapsules. 51

Figure 11. Various techniques for preparation of PNPs (modified from Say et al., 2017). 51

Figure 12. Structure of HA monomer. 52

Figure 13. Hydrolysis of PLGA (modified from Danhier et al., 2012). 52

Figure 14. Schema of the fluidic dynamic experimental system. 61

Figure 15. Mean±SD of cell viability of primary human myoblasts obtained from a patient affected by DM1. The effect of free PTM-B, and PLGA 50:50 and 75:25 NPs loaded with PTM-B was measured by the MTT assay 24 h after treatment at different PTM-B concentrations. Asterisks indicate values significantly different from 0µM PTM-B samples (control) (*$p<0.05$, one-way Anova test). 132

Figure 16. (a) Conventional fluorescence micrograph of a myoblast nucleus immunolabelled with anti-MBNL1 antibody (green fluorescence) and counterstained for DNA with Hoechst 33342 (blue fluorescence); note the green

spots (foci). Bar: 10 µm. (b) Quantitative evaluation of foci in myoblast nuclei of a DM1 patient: their number is significantly decreased (asterisk) after incubation with 30 µM PTM-loaded PLGA 75:25 NPs in comparison to untreated (untr) samples (n=25, one-way Anova test). 133

Figure 17. Mean±SD percentage of dead C2C12 cells. The effect of HA-Parg NPs, NPs loaded with PTM-S and free PTM-S was assessed by the Trypan blue test 2h, 24h and 72h after treatment at different PTM-S concentrations. Asterisks indicate values significantly different from 0µM PTM samples (control) (*p<0.05, Kruskal Wallis test). 178

Figure 18. Cross-section of soleus muscle, conventional fluorescence microscopy. After 3h incubation post-i.m. injection, Nile red-labeled PLGA NPs (red fluorescence) mostly accumulate in the endomysium and perimysium. Arrows indicate the few NPs inside the muscle fibers. Green fluorescence, sarcoplasm; blue fluorescence, cell nuclei. Bar: 30 µm. 189

Figure 19. Cross-section of soleus muscle, conventional fluorescence microscopy. After 6h incubation post-administration in the medium, most of the PLGA NPs (red fluorescence) accumulate in the epimysium. Green fluorescence, sarcoplasm; blue fluorescence, cell nuclei. Bar: 30 µm. 189

LIST OF TABLES

Table 1. Main characteristics of the three types of muscle tissue present in Vertebrates. 25

Table 2. Pharmacokinetic steps of NPs inside the body. 37

Table 3. FDA approved liposome-based drug delivery systems for biomedical applications (modified from Zylberberg et al., 2016). 45

Table 4. Most commonly natural and synthetic polymers. 50

Table 5. Mechanisms of internalization and cell viability of different types of NPs into primary human myoblasts 195

I. INTRODUCTION

1. Myotonic dystrophy

1.1. Morphological and functional features of human skeletal muscle

In humans as well as in the other vertebrates, there are three types of muscle tissue: the skeletal, cardiac and smooth muscle (Table 1) (Andrew G. Engel, 2004). Skeletal muscle is a striated voluntary muscle: it is connected to the bones and, by the contraction of its cells, it is responsible for the body movements. Cardiac muscle is a striated involuntary muscle that constitutes the main tissue constituents of the heart: its contractions induce the movement of blood in the circulatory system. Smooth muscle is a non-striated involuntary muscle; sheaths or bundles of smooth muscle cells are present in the walls of hollow organs (*e.g.*, the gut, the uterus and the urinary bladder) or of the arteries and veins of the blood circulatory system.

Table 1. Main characteristics of the three types of muscle tissue present in Vertebrates.

Three main types of muscle in the human body			
	Skeletal	**Cardiac**	**Smooth**
Cellular lengh	1 nm – 20 cm	50 – 100 µm	20 – 200 µm (0.5 mm in uterus in pregnancy)
Cellular diameter	10 – 100 µm	10 – 20 µm	5 – 10 µm
Cellular morfology	cylindrical with more than one nucleus, non striated	roughly rectangular, single central nucleus striated	fusiform shape, single central nucleus striated
Connexion	bundles of fibers and tendons	intercalated discs, encased by collagen fibres and other substances forming the extracellular matrix	connective tissue, gap junctions and desmosomes
Control	Voluntary control by the central nervous system	involuntary contraction	involuntary contraction
Power	quick and vigorous	rhythm variable and continuous for all life	slow and rhythmic

All muscle cells share various properties: the excitability (*i.e.*, the capability to respond to a stimulus producing electrical signals called action potential or impulse); contractility (the ability to contract after stimulation induced by an action potential); extensibility (the capability of muscle to be stretched without damage); and elasticity (the ability to recoil back to the initial length after being stretched).

Through prolonged contractions and/or cycles of contractions and relaxation, the muscle tissue carries out four fundamental functions: production of body movements, maintenance of posture, thermoregulation and movement of fluids (*e.g.*, the blood and the lymphatic fluid) and materials (*e.g.*, the food and waste).

Skeletal muscles are organs specialized for the movement and stability of the body. It is a voluntary organ, which means that the central nervous systems (CNS) controls actively its contraction. Most of the skeletal muscles are anchored to bones by bundles of collagen fibres know as tendons. Skeletal muscles are made of elongated multinucleated syncytia known as muscle fibres formed by fusion of precursor cells (the myoblasts) during the embryonic development (Figure 1).

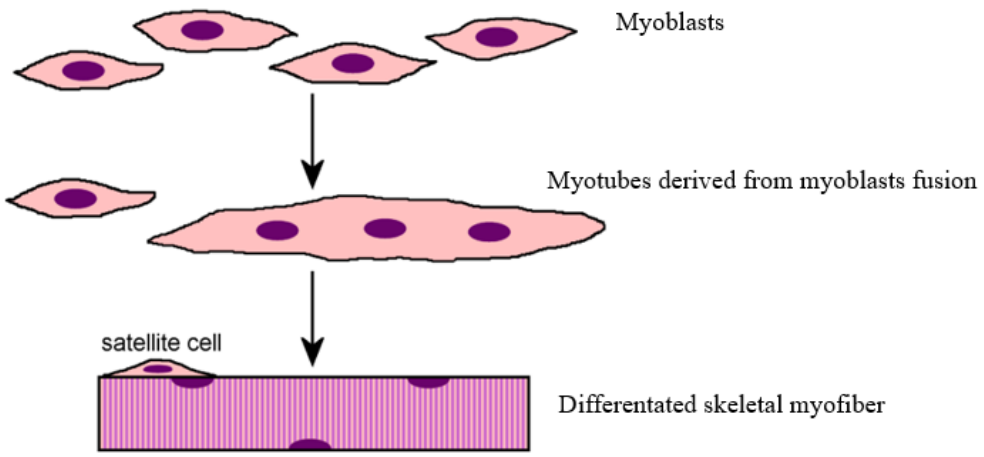

Figure 1. Development of skeletal muscle cell. The fusion of myoblasts forms myotubes, precursors of the mature muscle fibers.

The muscle fibres (also called muscle cells or myofibres) are cylindrical, multinucleated cells, generally long from 10 to 100 µm in diameter and sometimes several centimetres in length. The cell membrane of muscle fibers is called sarcolemma and presents characteristic invaginations termed transverse tubules (T tubules) that penetrate into the myofibre cytoplasm, called sarcoplasm. T tubules permit the rapid propagation of the electrical potential and also play an important role in regulating cellular calcium concentration. Sarcoplasm is mostly occupied by myofibrils that run parallel to the length of the fibre. In each myofibril, sets of thick and thin filaments partially overlap give rises to alternate bands of dark and light

regions. The thick filaments (with a diameter around 11-12 nm) are mainly made of myosin, while the thin filaments (around 5-6 nm in diameter) are predominantly made of actin. The thin and thick filaments partially overlap to give rise to the typical striated pattern unit that occurs with a periodicity of about 2 to 3 µm; this typical repetitive unit is called the sarcomere (Figure 2). The sarcomere is bordered at each extremity by a dark, narrow line (about 0.1 µm thick) known as the Z line; each Z line bisects an I band (isotropic, in polarized light) which is common to the adjacent sarcomeres. The centre of the sarcomeres is dark due to the presence of the A band (anisotropic, in polarized light) which is itself bisected by a less dense H zone; in the middle of the H zone there is a lighter region often called the pseudo H zone or bare zone which contains a region of higher density called the M line. The presence of these dark and clear zones is responsible of the typical transverse banding that characterized the striated muscle cells. Actin and myosin filaments are responsible for the sarcomere shortening and muscle contraction, after the release of calcium from the sarcoplasmic reticulum, *i.e.*, the endoplasmic reticulum which wraps around the myofibrils and is an important regulator of muscle contraction being an intracellular calcium storage depot. In the sarcoplasm, mitochondria are aligned along the myofibrils, and glycogen granules are abundantly present.

.

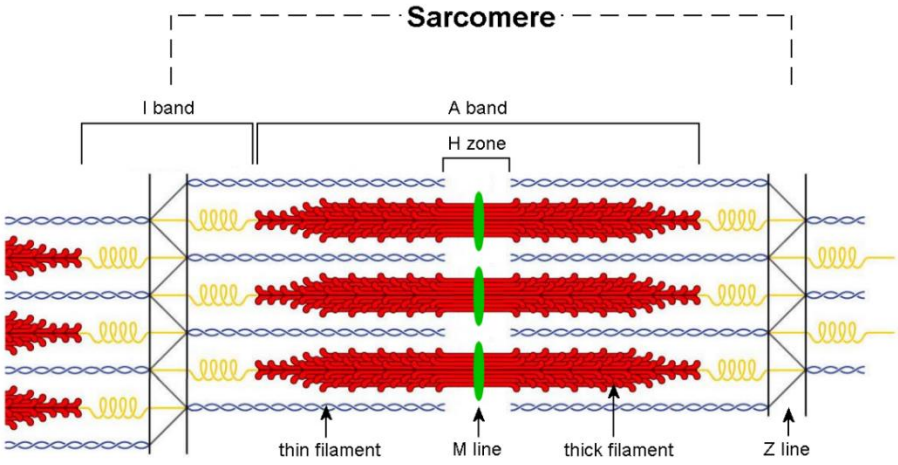

Figure 2. Sarcomeric organization in myofibrils.

In the skeletal muscle, each myofibre is surrounded by a loose connective tissue called endomysium. Muscle cells bundles form fascicles surrounded by a dense irregular connective tissue called perimysium, while the hole fascicles that form the entire muscle are surrounded by a dense connective tissue called epimysium. (Figure 3).

Skeletal muscle fibres are terminally differentiated cells that have lost the ability to proliferate. However, a damaged skeletal muscle is able to regenerate thanks to the presence of undifferentiated stem cells termed satellite cells (Yin et al., 2013). They are located between the sarcolemma and the basal lamina, and are normally quiescent; however, following appropriate stimulation (*e.g.*, a muscle damage), they undergo activation, and proliferate; some of the resulting daughter cells fuse with pre-existing myofibres and differentiate thus restoring the muscle mass, while others return to quiescence and maintain the satellite cell pool.

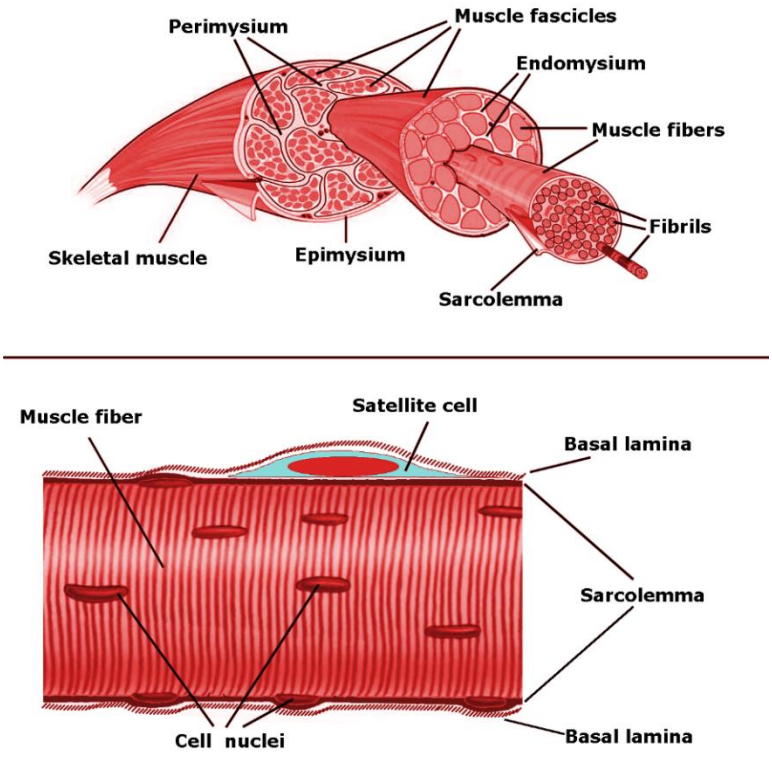

Figure 3. Microanatomical organisation of skeletal muscles.

1.2. Pathogenic mechanisms of myotonic dystrophy

Among the numerous pathologies affecting skeletal muscle there is myotonic dystrophy (DM). It is a genetically heterogeneous neuromuscular disorder with autosomal dominant inheritance and it has been estimated that it affects 1:8000 individuals worldwide (Harper, 2001). However, that estimation is based solely on diagnosed cases of DM and, given that the diagnosis sometimes takes more than ten years, it is likely that diagnosed cases represent only a fraction of the population bearing DM mutations. Studies aimed at understanding DM prevalence are currently ongoing in USA and in Europe.

A CTG repeat expansion in the 3' UTR region of the Dystrophia Myotonica Protein Kinase (*DMPK*) gene is responsible for DM type 1 (DM1; Steinert's disease; OMIM 160900), whereas the instability of a CCTG repeat in the first intron of the CCHC-type zinc finger nucleic acid binding protein (*CNBP*, also known as *ZNF9*) gene is linked to DM type 2 (DM2; proximal myotonic myopathy PROMM; OMIM 602668) (Brook et al., 1992; Fu et al., 1992; Mahadevan et al., 1992; Liquori et al., 2001). Mutations in these two unrelated genes cause similar phenotypes, with multisystem pathological features mostly affecting skeletal muscle (muscular dystrophy, myotonia) but involving also other organs and systems (dilated cardiomyopathy, cardiac conduction defects, insulin-resistance, cataracts, disease-specific serological abnormalities) (Harper, 2001). Clinical manifestations are highly variable, depending on the number of repeats, and range from minimal features, to moderately severe facial and distal limb muscle wasting and weakness, to severe congenital disorder that often lead to premature death (Harper, 2001; Meola and Cardani, 2015). The most severe form is congenital DM1, found in infants with markedly expanded CTG repeats. DM2 displays a milder clinical phenotype and a more benign prognosis, with no congenital form nor severe involvement of the CNS (Meola et al., 2002; Meola and Cardani, 2015).

The most accepted pathogenic hypothesis is an "RNA gain-of-function" due to expanded RNAs that accumulate in nuclear foci and alter the expression of specific RNA-binding splicing regulators such as muscleblind like 1 (MBNL1) and CUGBP/Elav-like family member 1 (CELF1/CUGBP1) (Meola and Cardani, 2009); alteration in MBNL1 and CUGBP1 activity results in splicing deregulation

of a subset of genes in multiple tissues (Miller et al., 2000). It has been demonstrated (Perdoni et al., 2009) that in DM2 nuclear foci sequester also the splicing factors snRNPs and hnRNPs, suggesting that a general alteration of the post-transcriptional pathway could contribute to the multifactorial DM2 phenotype. It has been suggested that the spliceopathy cannot fully explain the multisystem DM phenotype, which might also depend on changes in gene expression and translation efficiency, antisense transcripts, nonconventional translation and micro-RNA deregulation (Sicot et al., 2011).

1.3. Current therapeutic development in myotonic dystrophy

Currently, no disease-modifying therapies are available for DM1 or DM2 patients, and treatments are made to only manage the various symptoms; in particular, to reduce myotonia drugs blocking Na^+ channels have been proposed: Mexiletine, an anti-arrhythmic agents belonging to the class 1b, which will be probably commercialized soon as the medicinal product NaMuscla^{TM} intended for the symptomatic treatment of myotonia in adults with certains hereditary muscle disorders (recommendation of the Committee for Medicinal Products for Human Use, EMA, www.lupin.com); Flecainide, another anti-arrhythmic agent belonging to the class 1c (Cavalli et al., 2018); or Lamotrigine, an anticonvulsant agent used for epilepsy and bipolar disorder (Andersen et al., 2017). Although at present no specific agents activating Cl^- channels have been identified, Acetazolamide, a carbonic anhydrase inhibitor involved in Cl^- activation, is used in cases of myotonia non-responsive to Na^+ channels blocker agents (Markhorst et al., 2014).

At present the pharmaceutical research aimed at developing innovative drugs for the treatment of DM is quite limited. In recent years, Ionis Pharmaceuticals tested a new drug to treat DM1. This antisense drug, called IONIS-DMPKRx, was designed to target the toxic DMPK RNA in the skeletal muscle that is responsible for myotonia or muscle dysfunction. Unfortunately, in January 2017 the company announced that the 1/2 phase clinical trial failed. At present, Ionis Pharmaceuticals,Inc and Biogen are developing a technology aimed at increasing the efficiency of drug uptake and delivery by adding specific conjugates (https://us8.campaign-archive.com/?u=8f5969cac3271759ce78c8354&id=1109538bcf&e=cd1f4d18fe).

Another clinical trial is currently ongoing by AMO Pharma to test the efficacy of AMO-02 (tideglusib) for the treatment of the CNS and neuromuscular dysfunctions in the severe form of congenital myotonic dystrophy (Goudron and Meola, 2017). AMO-02 is an inhibitor of glycogen synthase kinase 3 beta (GSK3ß), a protein especially active in patients affected by this particular DM form, and has been shown to correct the activity of regulatory proteins, such as CUGBP1, in animal models of DM1

(https://www.myotonic.org/sites/default/files/Horrigan%20-%20AMO%20Pharma%20Tideglusib%20001%20Study%20-%20MDF%20conference%20-%20September%202016%20-%20v3.pdf).

Apart from the two above clinical trials, to date two main experimental therapeutic approaches have been described for DM1 to target expanded RNA repeats: i) antisense oligomer (ASO)-induced degradation of toxic CUG-containing RNA, and ii) inhibition of pathogenic interaction of CUG-containing RNA with nuclear proteins (without causing degradation of the expanded RNA) by means of small compounds or antisense oligonucleotides binding the CUG repeat hairpin. Both treatments are intended to prevent MBNLs sequestration and/or significantly reduce nuclear foci formation thus correcting alternative splicing abnormalities (Jog et al., 2012).

Therapeutic antisense technology has great potential to target disease-associated RNA molecules (Bennett and Swayze, 2010), and the systemic administration of unformulated ASOs gave positive clinical trial data for several diseases (Raal et al., 2010; Saad et al. 2011; van Deutekom et. al., 2007; Goemans et al., 2011; Büller et al. 2014; Gaudet et al. 2014). Importantly, the systemically administered ASO mipomersen sodium has been approved by FDA as a treatment for homozygous familial hypercholesterolemia (Lee et al., 2013). Second generation ASOs have chemically modified 2′-O-methoxyethyl (MOE) residues and a phosphorothioate backbone; a MOE modified ASO targeting noncoding RNAs showed a potent activity in skeletal muscles of the HSALR mouse model of DM1 (Wheeler et al., 2012). Lee et al. (2012) generated gapmer ASOs with CAG repeat sequences able to reduce expanded CUG transcripts and RNA foci in both cell cultures from DM1 patients and in DM1 mouse models. These antisense agents were tested in clinical trials in DM1 patients to evaluate the safety and tolerability of multiple doses but, as stated above, the results were unsatisfying. A novel ASO class containing 2′-4′ constrained ethyl (cEt) modifications (Seth et al., 2009) showed enhanced potency *in vivo* and favorable safety profile (Seth et al., 2009; Burel et al., 2013). Pandey et al. (2015) characterized *in vitro* and *in vivo* a cEt ASO that targets mouse, monkey and human DMPK mRNA. When administered subcutaneously, this ASO has

potent activity against DMPK in skeletal and cardiac muscle in normal mice, human DMPK transgenic mice, and *Cynomolgus* monkeys.

A second approach to reduce RNA dominance involves prevention of abnormal interactions between toxic transcripts and RNA binding proteins, either through the use ASOs or other small molecules. $(CAG)_{25}$ morpholino ASO was designed to bind CUG RNA repeat expansions; its local injection into the skeletal muscle of HSALR mice inhibited the binding of MBNL1 to the expanded RNA, induced MBNL1 redistribution and a partial correction of spliceopathy, and eliminated myotonia (Leger et al., 2013).

Attempts have been made to identify small molecules that may bind RNAs of interest by examining the secondary structural motifs: small molecules (*e.g.* pentamidine (PTM)) would present an advantage over the ASO protocols, due to their less problematic administration, biodistribution and bioavailability. PTM is a small compound with high affinity for CUG repeats, able to inhibit MBNL1 binding and sequestration. Although reverting the spliceopathy in the skeletal muscle of HSA^{LR} mice (Warf et al., 2009), PTM has limited therapeutic application due to its high toxicity. An improved PTM ligand partially reverted DM1 associated missplicing when injected intraperitoneally into HSA^{LR} mice (Parkesh et al., 2012). Recent reports indicate that DM does not simply depend on spiceopathy, suggesting that binding CUGexp may not be enough to reverse all disease pathways. Thus, efforts to destroy toxic RNA transcript or inhibit its formation have particular appeal. Childs-Disney et al. (2012) developed a small molecule that photodegrades the toxic transcript, and analogs of PTM were reported to inhibit the synthesis of CUGexp by binding to the $(CTG{\cdot}CAG)_n$ duplex (Coonrod et al., 2013). Nguyen et al. (2015) have identified three small molecules that intervene in three separate steps of DM1 pathobiology: each of these molecules shows RNase A-like activity in selectively cleaving $(CUG)_{16}$ *in vitro* and inhibits both the *in vitro* transcription of CTGexp and the sequestration of MBNL1 into the nuclear foci in a DM1 model cell culture. One of the agents showed enhanced phenotypic reversal in two separate DM1 Drosophila assays. Recently, Siboni et al. (2015) demonstrated that Actinomycin D (ActD), a known transcription inhibitor with affinity and specificity for GC-rich DNA (Kamitori and Takusagawa, 1992), reduces CUG RNA transcript

levels in both DM1 cells and mouse models, and rescues MBNL1 dependent missplicing events in a mouse model. Currently, ActD is most commonly used as a key component in the multimodal treatment of several cancers (Hill et al., 2014; Osborne et al., 2011).

As for DM2 pathology, Lee et al. (2009) described a series of multivalent ligands displaying kanamycin A units which inhibited the r(CCUG)$_{47}$–MBNL1 interaction *in vitro* (Lee et al., 2009). A triaminopyrimidine-acridine ligand was reported to be an *in vitro* inhibitor of the MBNL1-r(CCUG)$_6$ complex but proved to be toxic in cellular assays (Wong et al., 2011). To improve the therapeutic potential of this compound a new set of ligands was developed; they maintained the key triaminopyrimidine recognition unit but replaced the acridine intercalator with a bisamidinium groove binder. The optimized ligands have low cytotoxicity and were able to disrupt the MBNL1-r(CCUG)n foci in DM2 cell cultures (Nguyen et al., 2014).

Despite the promising results obtained in experimental models *in vivo* and *in vitro*, at present all the tested molecules have scarce therapeutic applicability in humans because of their low bioavailability (due to enzymatic degradation) or high systemic toxicity.

Nanocarriers, protecting the encapsulated agents from enzymatic degradation and to allow drug delivery and sustained release inside the cells, may represent a suitable approach for improving the administration of therapeutic agents and decreasing adverse systemic side effects. These nanocarriers must obviously be biocompatible and biodegradable to play their therapeutic action without damaging patient's organism.

To our knowledge, scarce information is available about experiments aimed at delivering therapeutic molecules for DM by using biocompatible nanoparticles (NPs). Therefore, nanotechnology represents a truly innovative approach to face the still unsolved problems of DM treatment.

2. Nanotechnology in biomedical research

2.1. Nanoparticles for drug delivery

Over the last years, nanotechnology has been receiving a great interest in daily life. The Food and Drug Administration (FDA) has never given a definition for "nanotechnology", "nanomaterials" or "nanoscale", but mentions nanotechnology as the science able to manipulate materials with extremely small size, usually with a dimension between 1 and 100 nm (Soares et al., 2018). Nowadays, nanotechnologies are very important in different fields including medicine, chemistry and environment, energy, information-communication and heavy industry (Kavoosi et al., 2018).

Nanomedicine is defined as a part of the medical science that utilizes nanoscale materials for various applications including diagnosis, therapeutics and regenerative medicine (Patra et al., 2018; Kavoosi et al., 2018). The European medicine agency (EMA) has defined nanomedicine as a science that design systems having at least one component at nanoscale size for clinical application (https://www.ema.europa.eu/documents/presentation/presentation-quality-aspects-nano-based-medicines-dolores-hernan-pacrez-de-la-ossa_en.pdf). The term of nanomedicine can cover a wide variety of materials and structures, and NPs represent the main material employed. The most commonly used NPs are showed in Figure 4.

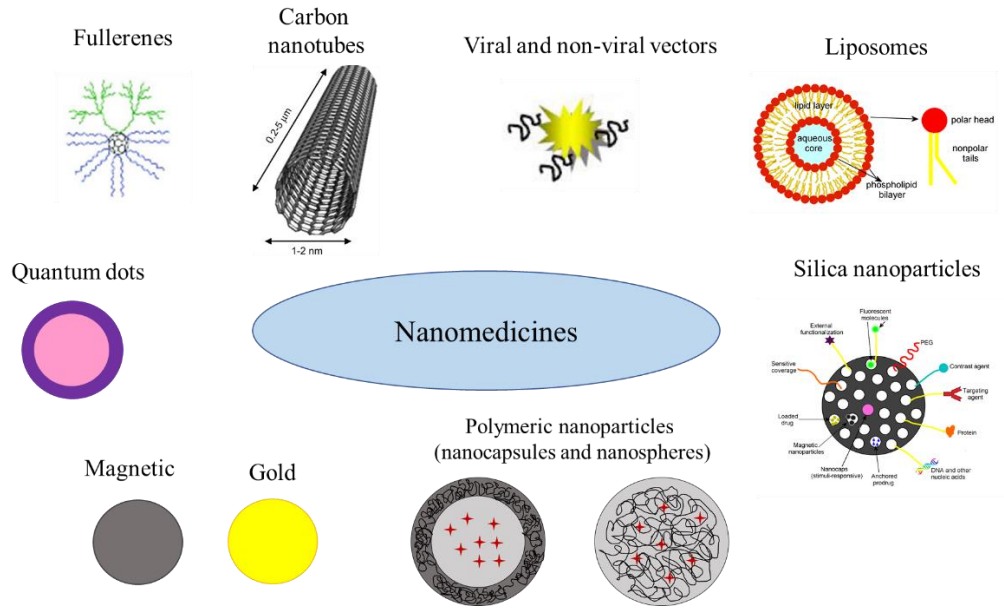

Figure 4. NPs commonly used in biomedical fields. Modified from https://www.ema.europa.eu/documents/presentation/presentation-quality-aspects-nano-based-medicines-dolores-hernan-pacrez-de-la-ossa_en.pdf

The rational use of NPs has revolutionized the application of pharmaceutical drugs for therapeutic and diagnostic purposes. Due to their small size, NPs have unique structural, chemical, mechanical, magnetic, electrical and biological properties that are different from those of the equivalent bulk materials (Patra et al., 2018). The use of such delivery systems may improve drug stability *in vivo* and prolong its blood circulation times; this can increase drug bioavailability thus making it possible to lower the doses to be administered, with a reduction of systemic toxicity and side effects.

The clearance of NPs by the hepatic, renal and immune systems represents, in fact, one of the most important drawbacks in drug delivery technology because NPs may undergo opsonization and removal before reaching the target organs and tissues (Sahay et al., 2010; Adabi et al, 2017). To overcome these problems a local administration, the block of the activity of phagocytic cells or the modification of NPs surface with hydrophilic polymers represent possible solutions (Adabi et al. 2017). When NPs reach the target organs, they NPs undergo metabolic processing, to be finally excreted from the organism. The following table summarises the main

pharmacokinetics steps of NPs in the body: absorption, distribution, metabolism and excretion (Table 2).

Table 2. Pharmacokinetic steps of NPs inside the body.

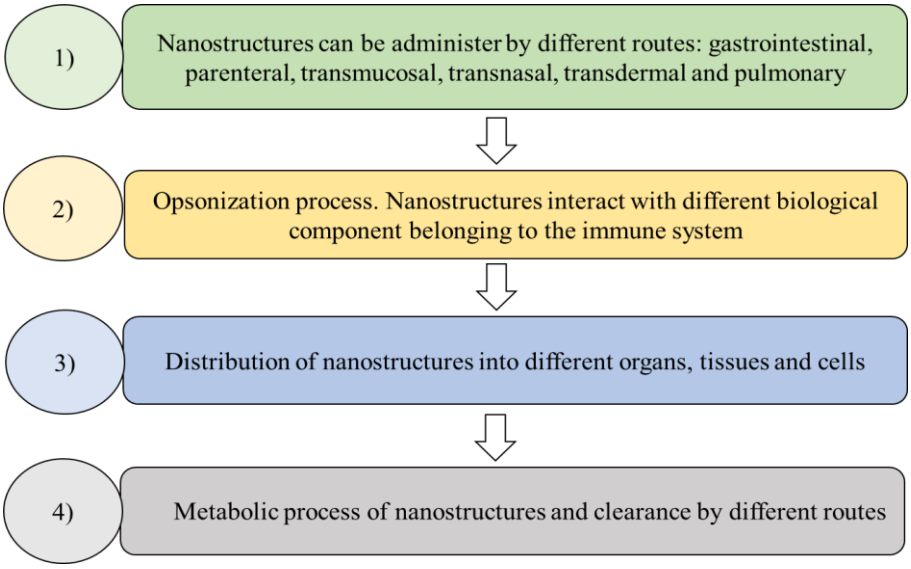

2.2. Nanoparticle testing for biomedical application

An important aspect in drug delivery technology is represented by the study of the relationships between NPs and the possible responses that can occur in living systems. For this reason, pre-clinical evaluations of the biocompatibility of NPs in *in vitro* and in *in vivo* systems represent an essential step for developing safe and efficient drug delivery systems.

Biocompatibility was refined in 1987 as follow: "Biocompatibility refers to the ability of a material to perform with an appropriate host response in a specific situation" (Williams, 1987). The notion of biocompatibility is strictly related to that of biodegradability, *i.e.* the ability of the NPs system to be eliminated from the cell/organism without undesired negative effects. The definition of biocompatibility encompasses a wide and varied panel of analyses, from the chemical characterization of the material to the tests *in vitro* (cytotoxicity) and *in vivo* (*e.g.* hemocompatibility, irritation/intracutaneous reactivity, sensitization, systemic toxicity, pyrogenicity, implantation). These tests must be applied at both short and long term.

The most used methods *in vitro*, *in vivo* and *ex vivo* for testing NPs intended for biomedical application are briefly described in the following chapters, with special

reference to the recent technological advancement of *in vitro/ex vivo* systems aimed at mimicking to the biological environment.

2.2.1. *In vitro* studies

Regarding the interaction of nanoconstructs with the biological systems, *in vitro* studies are the first to be performed for evaluating NPs cytotoxicity.

In general, NPs are able to easily enter the cells and to interact with their organelles, thanks to their small size. Once in contact or inside the cells, NPs can affect cellular viability through chemical or physical interactions which may induce structural and/or functional changes (Nel et al., 2009).

Chemical mechanisms hindering cell viability include the production of reactive oxygen species (because of the destruction of balance of redox systems caused by the nanomaterials: Soares et al., 2018), the release of toxic ion (Xia et al., 2008), the disturbance of the cell membrane electron/ion-transport activity (Auffan et al., 2008), the oxidative damage through catalysis (Foley et al., 2002) and lipid peroxidation (Kamat et al., 2000). On the other hand, physical mechanism includes disruption of the membranes (Hussain et al., 2005) or their activity (Navarro et al., 2008; Elsaesser and Howard, 2012), altered transport processes (Ovrevik et al., 2004), protein misfolding (Hauck et al., 2008), and protein aggregation/fibrillation (Chen and Von Mikecz, 2005).

To identify the cytotoxic effects of nanomaterials, different *in vitro* assays may be performed. These tests are usually applied to cultured cells, in order to evaluate cell proliferation and death, or stress responses following exposure to nanomaterials. For example, the mitochondrial activity, the release of lactate dehydrogenase, or the activation of death-related proteins (such as activated caspases) are popular and practical markers for assessing the cytotoxicity of NPs (Niles et al., 2008; Soares et al., 2018).

Necrotic cells undergo early plasmalemmal and mitochondrial damage, with ensuing release of cytosolic enzymes and sudden adenosine triphosphate (ATP) depletion; as a consequence, the live-cell assays based on the reduction of compounds (such as tetrazolium and resuzarin) by the mitochondria electron transport chain become negative. Contrary to necrotic cells, apoptotic cells preserve

functional plasma membranes until the late stages of this regulated form of cell death (*i.e.*, until karyorrhexis and cell fragmentation into apoptotic bodies): this allows cells to retain their cytosolic enzymes and the capability to reduce tetrazolium and resazurin. In addition, in apoptotic (but not in necrotic) cells, specific proteases called caspases are activated (Kabakov et al., 2011; Riss et al.,2016).

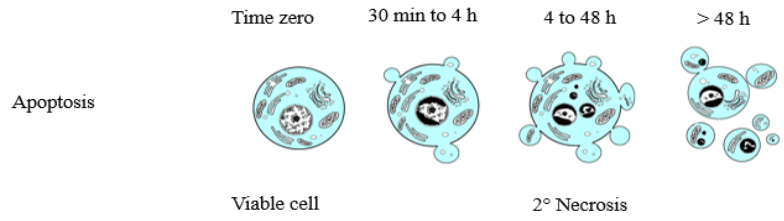

Enzyme release	0	+	++++	+
Caspase	0	++	++++	0
ATP	++++	+++	+	0
Tetrazolium	++++	+++	+	0
Resazurin	++++	+++	+	0
Enzyme retention	++++	+++	+	0

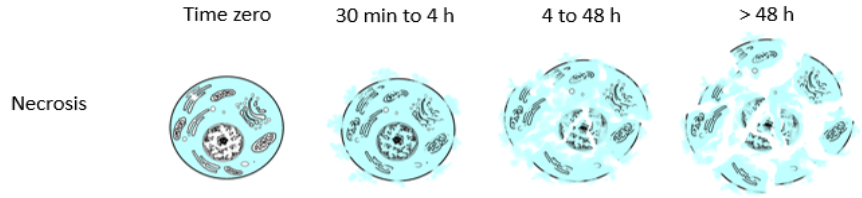

Enzyme release	0	++++	++	0
Caspase	0	0	0	0
ATP	++++	0	0	0
Tetrazolium	++++	0	0	0
Resazurin	++++	0	0	0
Enzyme retention	++++	0	0	0

Figure 5. Viability and cytotoxicity biomarkers commonly used to assess the occurrence of apoptotic or necrotic events due to the cytotoxic effect of nanomaterials (modified from Niles et al., 2008).

However, it is worth remarking that the results of the conventional toxicity assays following NPs administration may sometimes be questionable, due to the following reasons. The chemical composition of NPs can directly influence the results of some enzyme-based assays or can change the pH or nutrient balance in

the culture medium thus altering the cell growth conditions (Mahmoudi et al., 2018): all these events are potentially able to affect cell viability or proliferation, irrespective of the occurring interaction between NPs and the cultured cells.

2.2.2. *In vivo* studies

The main drawback of *in vitro* tests is the inability to fully reproduce the complexity of living organisms, and for this reason *in vitro* studies are insufficient alone to predict possible hazards to humans. In the literature there is a considerable number of newly synthetized nanocomposites successfully tested in *in vitro* models that then proved to be unsuitable when applied *in vivo*; the knowledge of the NPs behaviour in a living organism is therefore mandatory, to predict the fate, possible toxicity and therapeutic efficacy of NPs suitable for drug delivery in humans.

Actually, *in vivo* studies allowed to optimize several parameters to make NPs able to more easily enter the cells and to overcome the biological barriers. Numerous works focused their attention on the study of the *in vivo* biodistribution of NPs into different organ and tissues using mice and rats us animal models (review in Li et al., 2012). From these studies, inorganic (*e.g.* gold, silver, ferric oxide, quantum dots) and organic NPs (*e.g.* liposomes (LPs), solid lipid) are found mainly in liver, spleen, lung, brain, heart and kidney. As expected, the biodistribution of the different NPs into organs and tissues, depend on the different routes of administration and on the physicochemical properties (such us size, surface chemistry and composition) of nanovectors. For example, Nel and collaborators (2009) studied *in vivo* the cytotoxic effect of NPs taking into account their size, hydrophobicity and surface charge: these authors found that cationic NPs are more toxic than the anionic ones due to the electrostatic interactions between the negative cell membrane and the positive NPs which enhances cellular uptake; moreover, they demonstrated that hydrophobic NPs generally have a short half-life *in vivo* (hence a relatively low bioavailability) as they are rapidly removed by the reticuloendothelial system (RES).

The administration route may also strongly influence NPs bioavailability in the organs and tissues of a living body. When NPs directed to a given organ are systemically administered (*e.g.*, by intravenous injection) it is important to study

their presence and effects not only on the organs of interest, but also in others to clarify where NPs are efficiently taken up and to detect the possible occurrence of tissue damage or inflammation response.

There are however limits for the tests *in vivo* too. This is usually a long and costly experimentation, which is sometimes believed as insufficient to directly prove the efficacy of a treatment on humans. In addition, especially in recent years, the ethical concern on the use of animals in testing has grown in the public opinion, and the Three Rs (3Rs: replacement, refinement and reduction) (Russell and Burch, 1959) is nowadays the guiding principle for more ethical use of animals in experimentation: 3Rs are aimed at ameliorating the animal welfare and the scientific quality when the use of animals is unavoidable, and also encouraged to develop alternatives to animal testing.

2.2.3. Fluid dynamic *in vitro* technologies

The currently available *in vitro* systems from the conventional 2D cell cultures to the 3D co-cultures cannot efficiently mimic the functional and structural complexity of a living organism.

Several alternative cell culture methods have been proposed in recent years in order to avoid a simplistic *in vitro* representation (Wei et al., 2006; Mazzei et al., 2010; Giusti et al., 2014). The first generation involved low shear perfusion systems (Chen, 1992), sired tank bioreactors (Reuss, 1995) and airlift bioreactors (Saxena et al., 2007). The peculiar feature of these kind of systems, that makes them more suitable than conventional cell culture, is the introduction of fluid dynamics mimicking the flow of the physiological fluids. As shown in Figure 6, in a physiological environment, cells coordinate their behaviour and function in response to different signals: biochemical, physico-chemical and mechano-chemical cues. One of the most important physicochemical cues is the oxygen concertation. Using a dynamic system, it is possible to maximize the transport of this gas thanks to the recirculation of fresh medium (Sbrana and Ahluwalia, 2012). Under fluidic dynamic conditions, cells in culture are subjected to shear stress, flow-dependent mechanical stimuli, concentration gradients, movement and local

increase of nutrients, all features that are known to positively influence cell functions and stimulate growth (Vozzi et al, 2011).

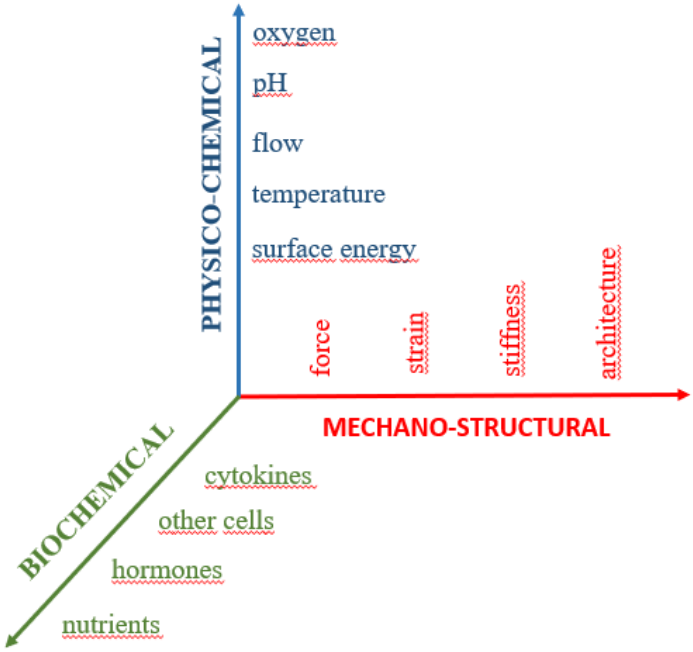

Figure 6. Different types of signals from which the activity of cells and organs depend. Using a bioreactor with an appropriate design and engineering, it is possible to reproduce these factors occurring *in vivo* (modified from Sbrana et al., 2012).

The second generation of bioreactors are composed by a membrane or fibres housing supported by a ring containing an outlet and inlet ports. All the system is connected to a glass medium reservoir, glass medium waste and a micro-peristaltic pump. These types of bioreactors offer a high degree of oxygenation thanks to the diffusion of humidified air across the membrane. (De Bartolo et al., 2006 ; Schwartlander et al., 2007; Ye et al., 2007).

Finally, the third generation is represented by micro-fluidic systems. These devices include microarray bioreactors (Powers et al., 2002), the micro cell culture chamber assay (Lee et al., 2006) and the micro cell culture analogue (Sung and Shuler, 2009). However, the microfluidic systems are limited by their microscale size. In order to overcome the disadvantages of all these systems, new fluid dynamic technologies for *in vitro* models have been developed in order to avoid this problem. These devices offer the same mechanical stimuli from flow and are normally

composed of different culture chambers made of polydimethylsiloxane that can be collected and joined together, in parallel or in series, offering the possibility also to simulate a multiple organ system. Three different bioreactors were developed: a laminar flow chamber, for the simulation of shear stress, a multicompartmental bioreactor and its evolution, presently under experimentation, for the metabolic study of organs and tissues. Previous works have successfully demonstrated the validity of these bioreactors demonstrating the increase of integrity and tight junction of epithelial cells (Caco-2) in comparison to the static condition (Giusti et al., 2014). Also, Vozzi and collaborators (2009) underlined the advantages of these multisystemic bioreactor showing the improved of metabolic function of Hepatocyte-HUVEC cells under dynamic conditions.

These new fluid dynamic *in vitro* systems allow to fill the gap between the conventional *in vitro* cell cultures and the *in vivo* complexity thanks to the possibility to use directly explanted organs. When applied to explanted tissues or organs (such as the skin, muscle or gut), this technology may provide reliable organotypic information thus helping to reduce the number of animals to be used for pre-clinical tests.

2.3. Nanoparticles for skeletal muscle

A wide variety of NPs have been proposed as drug nanocarriers for biomedical use; however, their application to the treatment of muscular dystrophies has so far been quite limited. The studies essentially focussed on Duchenne muscular dystrophy (Nance et al, 2018), and several different NPs were tested: polymeric NPs (PNPs) proved to efficiently deliver oligonucleotides (Rimessi et al., 2009; Sirsi et al., 2009; Falzarano et al., 2013, 2014; Wang et al., 2015); LPs were used to deliver gentamicin (Yukihara et al., 2011) and morpholino oligomer (Negishi et al., 2014); cationic LPs were used to deliver siRNA to skeletal muscles *in vivo* (Mori et al., 2014); a nanolipodendrosome carrier was loaded with MyoD and myogenin as novel therapeutic agents in mice with muscular dystrophy phenotype (Afzal et al., 2013); perfluorocarbon NPs were used to deliver rapamycin (Bibee et al., 2014). Recently, gold NPs have been tested *in vitro* and *in vivo* to deliver Cas9 and correct the DNA mutation causing Duchenne muscular dystrophy (Glass et al.,

2017; Lee et al., 2017). Gold NPs and fluorescent copper nanoclusters were also proposed for diagnostic purposes (Qin et al., 2010; Chen et al., 2015).

On the other hand, to our knowledge, only few studies focussed so far on nanocarriers intended for DM treatment: Bubble LPs were used to deliver antisense oligonucleotides to correct chloride channel 1 (Clcn1) alternative splicing and limit myotonia in a DM1 mouse model (Koebis et al., 2013; Negishi et al., 2018), and methods to obtain encapsulation and controlled release of PTM in mesoporous silica nanoparticles (MSNs) intended for DM treatment have been recently set up (Peretti et al., 2018).

For the experimental work of this thesis, we chose to test nanocarriers already demonstrated to be biocompatible in different biological systems. Their main characteristics are described below.

2.3.1. Liposomes

LPs were discovered in 1960 by Bangham and Horne and approved for the clinical use in 1995 (Bozzuto and Molinari, 2015; Zylberberg and Matosevic, 2016). Due to their unique properties and the high biocompatibility, LPs are widely used in biomedical application for drug delivery and gene therapy (Zylberberg and Matosevic, 2016). Nowadays, about a dozen of LP-based drug-carrier systems are available in the market (Zylberberg and Matosevic, 2016; Chang et al., 2012) (Table 3).

Table 3. FDA approved liposome-based drug delivery systems for biomedical applications (modified from Zylberberg et al., 2016).

Drug	Administration	Product	Particle type
Ampotericin B	Intrevenous	Ambisome	Liposome
Ampotericin B	Intrevenous	Abelcet	Lipid complex
Ampotericin B	Intrevenous	Amphotec	Lipid complex
Daunorubicin	Intrevenous	DaunoXome	Liposome
Cytarabine	SpinalEpidural	Depocyt	Liposome
Morphone sulfate	Intrevenous	Depodur	Liposome
Doxorubicin	Intrevenous	Doxil	PEGylated liposome
Inactivated hepatitis A virus	Intramuscolar	Epaxal	Liposome
Inactivated hemaglutinine of Influenza virus strains A and B	Intramuscolar	Inflexal	Liposome
Doxorubicin	Intrevenous	Myocet	Liposome
Doxorubicin	Intrevenous	Lipodox	PEGylated liposome
Vincristine	Intrevenous	Marqibo	Liposome
Verteporphin	Intravenous	Visudyne	Liposome

LPs are colloidal aggregates of phospholipids that assemble in water forming a spherical vesicle made of a single bilayer or of multiple concentric lipid bilayers encapsulating an aqueous compartment. The main components of LPs are phospholipids, *i.e.*, amphiphilic molecules containing a hydrophilic head and two hydrophobic chains (Figure 7, Su et al., 2018). In an aqueous environment, due to their amphiphilic nature, they are able to form membranes where the polar head locates at the surface and the fatty acid chains are in the inner part, far from the water.

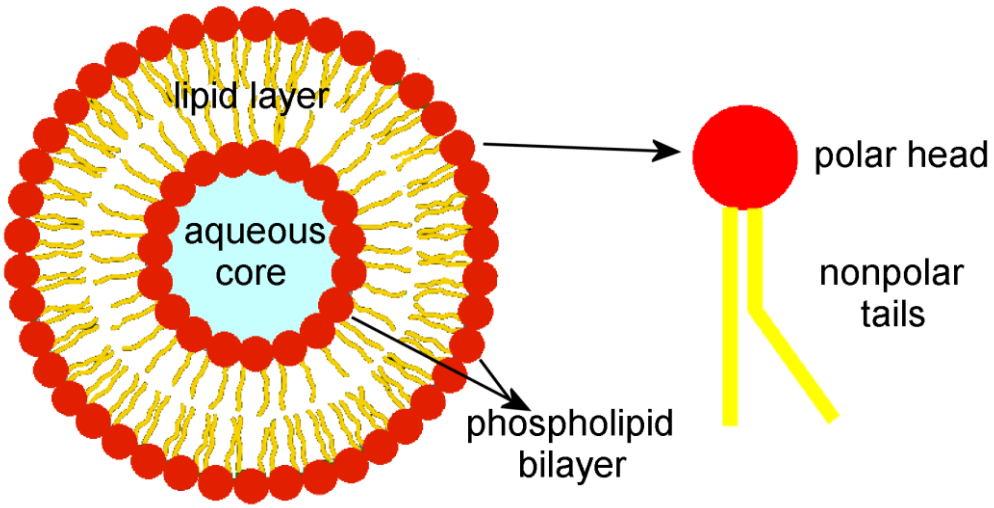

Figure 7. Self-assembly representation of a LPs (modified from Su et al., 2018).

Thanks to their amphiphilic nature, LPs may be loaded with both lipophilic and hydrophilic molecules: hydrophilic drugs are normally dissolved in the aqueous core, while lipophilic compounds are entrapped inside the lipid bilayer (Figure 8). Conventional LPs were the first generation of this NPs type; they consist of a cationic, anionic or neutral lipid bilayer containing also cholesterol that surrounds an aqueous core. To increase stability and extend the blood circulation times, LPs with surface-bound PEG were developed. Moreover, to improve targeting, LPs may be functionalized with different compounds (peptides, carbohydrates, antibodies) that can interact with ligands specifically expressed on the surface of the target cells.

LPs can be formulated and processed to different size, charge, and lamellarity according to the specific requirements such as drug loading, application, cost and reproducibility (Bozzuto and Molinari, 2015).

Changing the concentration and type of phospholipids, it is possible to modify the plasticity, stability and pharmacokinetic of LPs. For example, cholesterol improves the phospholipid packing thus stabilizing the LPs membrane and improving its stability *in vivo* and *in vitro*. Moreover, to prolong the half-life of LPs in blood circulation and reduce the uptake by the reticuloendothelial system, it is possible to use cholesterol for anchoring specific molecules (*e.g.*, polyethylene glycol, PEG) able to modify the pharmacokinetic features.

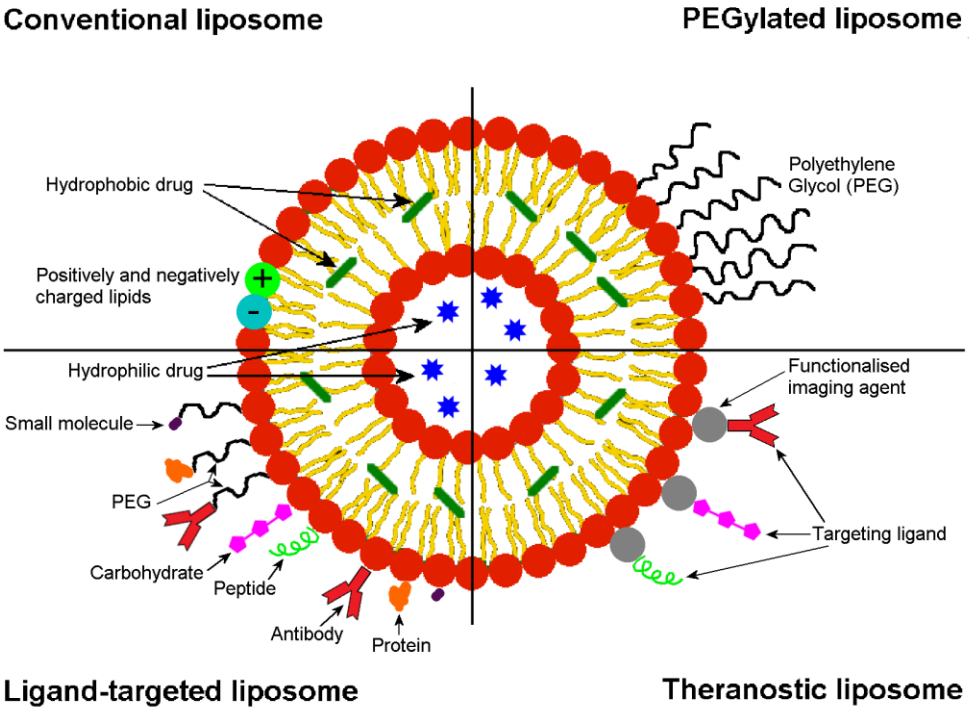

Figure 8. Encapsulation of hydrophobic and hydrophilic drugs inside different types of LPs (modified from Sercombe et al., 2015).

2.3.2. Mesoporous silica nanoparticles

Among the nanocarriers for delivering pharmaceutical agents, MSNs are very promising, due to their versatility and unique structural features. MSNs may have different sizes (from 50 to 300 nm) and shapes (from spheres to rods), uniform cylindrical mesopores, high surface areas (1000 m^2/g) and easily functionalizable surfaces (Manzano and Vallet-Regí, 2018). Moreover, MSNs are mechanically, thermally and chemically more stable in the biological environment than other biomaterials such as polymers. According to the description by the International Union of Pure and Applied Chemistry (IUPAC), a mesoporous material is defined as a porous material with pore diameter between 2 and 50 nm and a high volume (1 cm^3/g) in which it is possible to load a wide variety of chemical compounds. Thanks to this versatility, MSNs are therefore suitable for different biomedical applications as host materials for pharmaceuticals or bioactive molecules, or as bioimaging,

biocatalytic and biosensing tools (Trewyn et al., 2007; Slowing et al., 2008; Liong et al., 2008; Manzano et al., 2009; Viviero-Escoto et al., 2010).

Recent investigation demonstrated the possibility to design MSNs for single-drug or multi-drug release. The pores may be closed to avoid the leak of the drug by covering the whole NPs with a shell sensitive to specific internal or external stimuli (such as the pH, light, magnetic fields, ultrasound) that trigger the release of the cargo at the target site (Manzano and Vallet-Regí, 2018). In MSNs designed for multi-drug loading, one therapeutic agent is loaded into the pores while the other one in the shell (Baeza et al., 2012). In addition, other studies developed an alternative preparation system where a cytotoxic drug is loaded in an inactivate state (as a pro-drug) that is enzymatically activated at the target site: for example, Baeza et al. (2015) used MSNs where the non-toxic pro-drug, indol-3-acetic acid was loaded in the pore while its switchable activating enzyme (horseradish peroxidase) was in the shell.

Irrespective of the method used for manufacturing, it is relatively simple to prepare MSNs with various structural features of size, shape and pore volume; moreover, similarly to LPs, MSNs may be functionalized by adding on their internal or external surfaces either functional groups to avoid their interaction with blood components and the reticuloendothelial cells, or ligands to improve their interaction with cells expressing specific receptor. All these structural and compositional features can affect the pharmacokinetic and pharmacodynamic behaviour, and the modes of cell interaction and internalization of the MSNs. Figure 9 shows different functionalization strategies of MSNs.

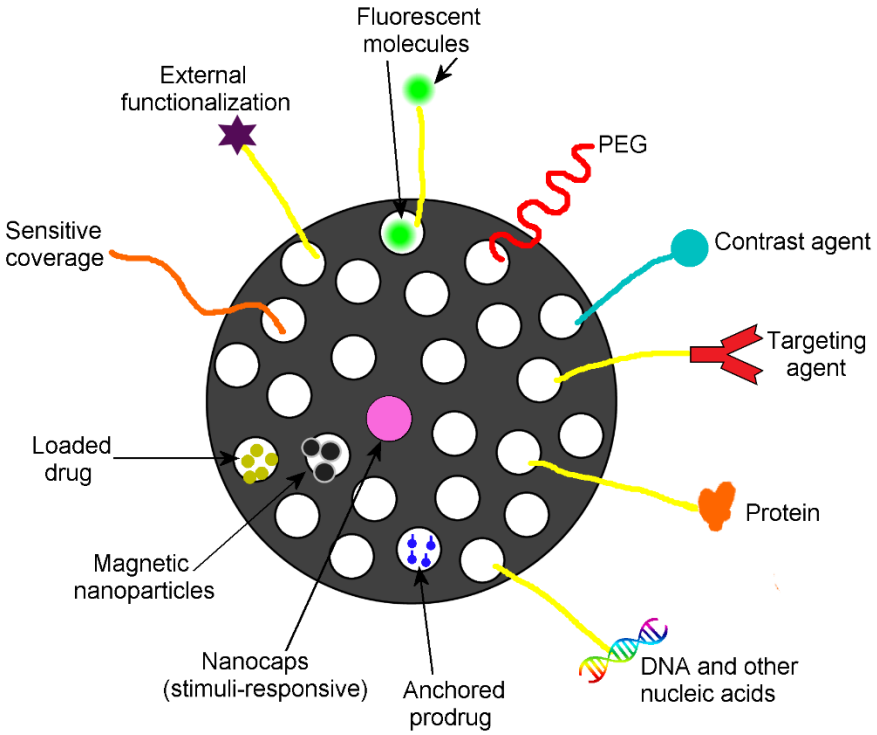

Figure 9. Different types of functionalization on MSNs (modified from Chen et al., 2018).

Previous studies have demonstrated an optimal biocompatibility *in vitro* using a MSNs dosage lower than 100 µg/kg (Hudson et al., 2014), while *in vivo* MSNs are well tolerated at dosages lower than 200 mg/kg (Lu et al., 2010). This great biocompatibility is probably due to the fact that NPs are degraded to non-toxic silicic acid (Shen et al., 2014), which is normally present in many tissue and physiologically excreted through the urine (Park et al., 2009). This makes MSNs very promising nanocarriers for theragnostic and diagnostic applications, and good candidates for future tests in clinical trials.

2.3.3. Polymeric nanoparticles

PNPs are considered as optimal vectors for drug delivery due to their simple formulation design, versatility, safety, efficacy, absence of immunogenicity, biological inactivity, good pharmacokinetics, and tunable release of both hydrophobic and hydrophilic drug. Polymers are macromolecules formed by a large number of similar units bonded together and are characterised by multiple structures

and properties related to the chemical composition, molecular weight, and number and type of reactive groups.

Natural or synthetic polymers can be used to manufacture PNPs (Table 4). Natural polysaccharides have various origin (microbial, vegetal, or animal) and can be classified in cationic (chitosan), anionic (alginate, heparin, pectin, hyaluronic acid), or neutral (pullulan, dextran), based on their intrinsic charge. Natural materials are less toxic, more biocompatible and biodegradable in comparison to the synthetic ones, but they are difficult to reproduce (due to the high degree of variability) and to purify. Conversely, synthetic polymers are more immunogenic, which prevents their long-term usage.

Table 4. Most commonly natural and synthetic polymers.

Natural polymers	Synthetic polymers
• Chitosan • Gelatin • Sodium alginate • Albumin	• Polylactides(PLA) • Polyglycolides(PGA) • Poly(lactide coglycolides) (PLGA) • Polyanhydrides • Polyorthoesters (POE) • Polycyanoacrylates • Polycaprolactone (PCL) • Polyglutamic acid (PGA) • Polymalic acid (PMLA) • Poly(N-vinyl pyrrolidone) • Poly(methyl methacrylate)Poly(vinyl alcohol) • Poly(acrylic acid) (PAA) • Poly acrylamide (PAM) • Poly(ethylene glycol) • Poly(methacrylic acid)

Generally, PNPs have a size between 10 and 1000 nm and are classified as nanocapsules and nanospheres, depending on the preparation method (Nagavarma et al., 2012). Nanocapsules are vesicular structures in which the drug can be confined inside an aqueous or non-aqueous liquid core surrounded by a polymeric shell; nanospheres are solid/matrix systems in which the drug may be trapped within the polymeric mass or adsorbed at the surface (Figure 10).

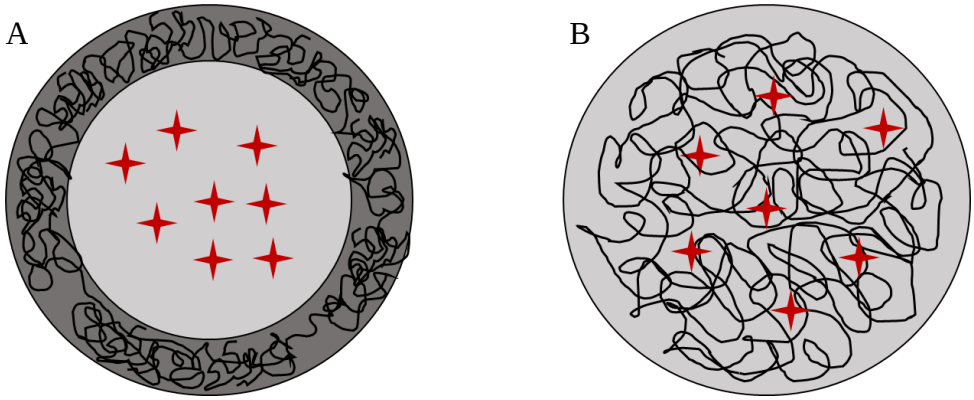

Figure 10. Different type of PNPs: A nanospheres and B nanocapsules.

PNPs can be either formulated from direct monomeric polymerization or from preformed polymers.

Figure 11 shows the most common polymerization techniques to synthesize PNPs (El-Say and El-Sawy, 2017).

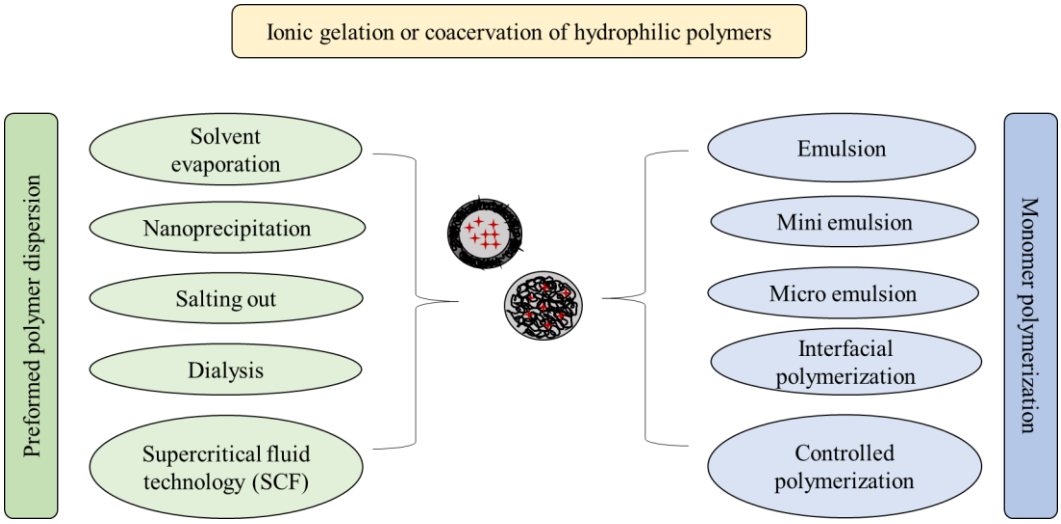

Figure 11. Various techniques for preparation of PNPs (modified from Say et al., 2017).

The therapeutic agent can be dissolved, entrapped, encapsulated or attached to the PNPs matrix. The release of the drug from PNPs may occur in three different ways: by enzymatic reaction that causes polymer rupture or degradation at the delivery site; by hydration and swelling of the polymer followed by diffusion of the drug through the matrix; by dissociation of the drug from the polymer.

Among the different natural polysaccharides, hyaluronic acid (HA) has been widely use in the pharmaceutical field thanks to its biocompatibility, biodegradability, non-toxicity, and non-immunogenicity properties (Morra, 2015). HA is a negatively-charged linear glycosaminoglycan (GAG) made of several identical subunits (D-glucuronic acid and N-acetyl-D-glucosamine disaccharide) linked together by glyosidic bonds (Figure 12).

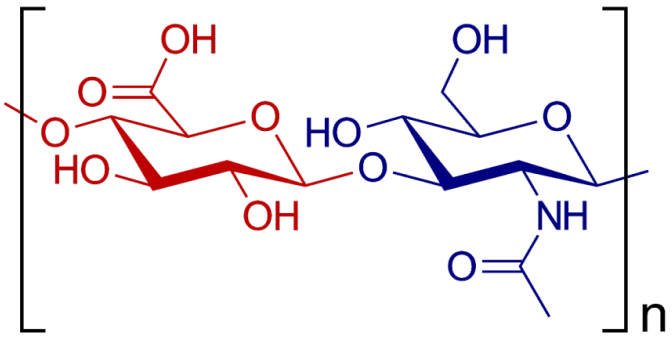

Figure 12. Structure of HA monomer.

HA is an important component of the extracellular matrix, being widely distributed throughout the connective, epithelial, muscular and nervous tissues.

Among the synthetic polymers, poly(lactic-*co*-glycolic acid) (PLGA) NPs are very promising nanoconstructs for drug delivery (Danhier et al., 2012). PLGA hydrolysis forms two endogenous and biocompatible monomers, lactic acid and glycolic acid, which are easily metabolised *via* the Krebs cycle (Figure 13).

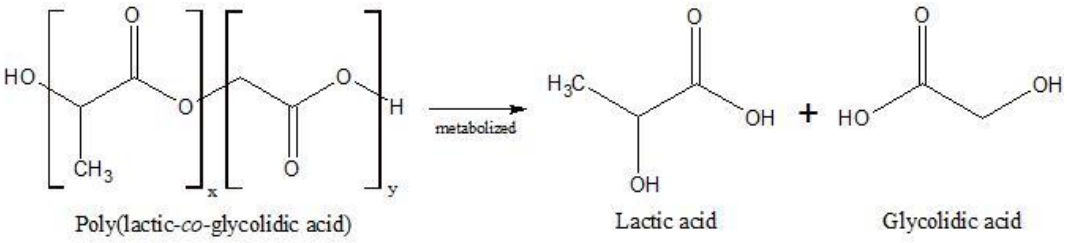

Figure 13. Hydrolysis of PLGA (modified from Danhier et al., 2012).

In addition, PLGA NPs are able to encapsulate both soluble and insoluble drugs ensuring a high loading efficiency. The presence of reactive groups on their surface allows an easy modification and functionalization, thus empowering the stability of NPs in physiological conditions and improving cell and tissue targeting. PLGA NPs are approved by the FDA and EMA as drug delivery systems for biomedical applications such as the administration of vaccines, or the treatment of cancer as well as of cardiovascular (Pascual-Gil et al., 2017), inflammatory (Gu et al., 2013; Ikoba et al., 2015), infectious (Darvishi et al., 2015; Kumar et al., 2015) or neurodegenerative diseases. Nowadays eleven types of products for medical application using PLGA NPs are available on the market (Sun et al., 2017).

3. Aim of the work

During my doctoral program, I focused my attention on the still unsolved problem of the lack of therapy for DM1 and DM2.

As already reported, the most accepted pathogenic hypothesis for these genetic neuromuscular disorders is an RNA gain-of-function due to expanded RNAs that accumulate in nuclear foci where RNA-binding splicing regulators are sequestered; this leads to a general splicing deregulation.

Several molecules among which PTM proved either to induce the degradation of the expanded RNA repeats or to inhibit the sequestration of splicing factors in *in vivo* and *in vitro* experimental models; however, serious delivery or toxicity drawbacks prevent their clinical application.

Nanotechnology may offer a solution to this problem. In fact, drug-loaded NPs may improve the therapeutic efficacy thanks to their ability to protect the encapsulated molecules from enzymatic degradation and to ensure their delivery and sustained release inside the cell.

Therefore, the main goal of my work was to set up an innovative experimental therapeutic strategy for DM based on biocompatible nanocarriers loaded with therapeutic agents that were selected among the ones accredited by the scientific literature.

To this aim:

1) the suitability for muscle cells of different biocompatible nanocarriers was tested *in vitro* on both established cell lines and primary cultures;

2) novel biocompatible nanocarriers that efficiently encapsulate pentamidine were synthesized and preliminarily tested *in vitro*;

3) an *in vitro* system able to maintain explanted mouse skeletal muscles under fluid dynamic conditions was set up and used to investigate the biodistribution of selected NPs in the whole muscle.

The synthesis of the new nanocarriers was achieved by a chemical and pharmaceutical approach, while the studies on the relationships between NPs and the biological environment were mainly performed by fluorescence (conventional and confocal) microscopy and transmission electron microscopy.

II. RESULTS

The first aim of my doctoral project was to verify the suitability for muscle cells of different biocompatible NPs. In pilot studies, the cell uptake, the interactions with cellular components, and the intracellular degradation of LPs, PNPs and MSNs were investigated *in vitro* on established cell lines (Costanzo et al., 2016, 2017a). Analyses at light and electron microscopy (Costanzo et al., 2017b) allowed us to demonstrate that each investigated NPs was characterized by specific interactions with the cells, and to understand the cellular basis of their biocompatibility; in addition, these results gave us an experimental background to proceed with the evaluation of the impact of these NPs on muscle cells.

Therefore, LPs, MSNs and PLGA NPs (pilot tests demonstrated the unsuitability for muscle cells of polymeric NPs, thus replaced by PLGA NPs) were applied to primary human myoblasts and myotubes from healthy human subjects (Guglielmi et al., submitted). During this study, I became aware of the complexity of the primary muscle cell cultures, where cycling myoblasts and resting differentiating myotubes may occur, with significant consequences on NPs experimentation. The results demonstrated the biocompatibility of all the tested nanocarriers for both myoblasts and myotubes but highlighted the reduced uptake efficiency of muscle cells in comparison to the established cancer cell lines usually employed for NPs evaluation. Since this study suggested PLGA NPs as the most promising nanocarriers for muscle cells among those tested, we performed a pilot study to preliminarily assess the therapeutic efficacy of PLGA NPs loaded with PTM base (PTM-B) using cultured myoblasts obtained from skeletal muscle biopsies of a DM1 patient (see preliminary results I). The results showed a reduced toxicity of NPs-loaded PTM coupled with a reduction of the intranuclear foci containing toxic RNA typical of DM1.

The second aim of my doctoral project arouse from the promising results obtained on DM1 myoblasts treated with PTM-B released by PLGA NPs. In order to synthesize novel biocompatible nanocarriers encapsulating PTM, I worked for nine months at the Laboratoire d'automatique et de génie des proceeds (LAGEP) of the Claude Bernard University, in Lyon (France). Under the guidance of Prof. Giovanna Lollo, I synthesized novel HA-based NPs suitable for efficiently encapsulating PTM isethionate salts (PTM-S) (Carton et al., submitted). Studies *in*

vitro are in progress to assess the impact of these NPs on an established murine muscle cell line. The first results demonstrated their full biocompatibility for myoblasts and suggested a high internalization efficiency, which however needs to be checked by further experiments (see preliminary results II).

In order to validate the tested NPs for biomedical application, a nanocarrier must be faced not only with cultured cells but also with the complex biological environment of the target organ and the living organism. However, the use of laboratory animals implies several ethical and economic problems.

In this view, as the third aim of my doctoral project, I undertook a new challenge to set up an *in vitro* system able to preserve explanted organs and tissues from control animals used for other experimental protocols, in order to respect the 3R principles. A fluidic dynamic system (IVTech Srl, Massarosa, Lucca, Italy) originally developed to improve cell cultures, was adapted to preserve explanted skeletal muscles *in vitro* for prolonged times, thus offering an experimental model mimicking the functional and structural complexity of the whole organ (Carton et al., 2017). In addition, the muscles necessary for our experiments were explanted from control animals used in other experimental protocols, thus reducing the number of laboratory animals. This novel experimental system allowed to monitor the biodistribution in the whole muscle of the PLGA NPs successfully tested in cultured cells, highlighting the NPs retention in the connective tissue (see preliminary results III) and opening the way to new studies aimed at improving NPs targeting by means of surface functionalization (Figure 14).

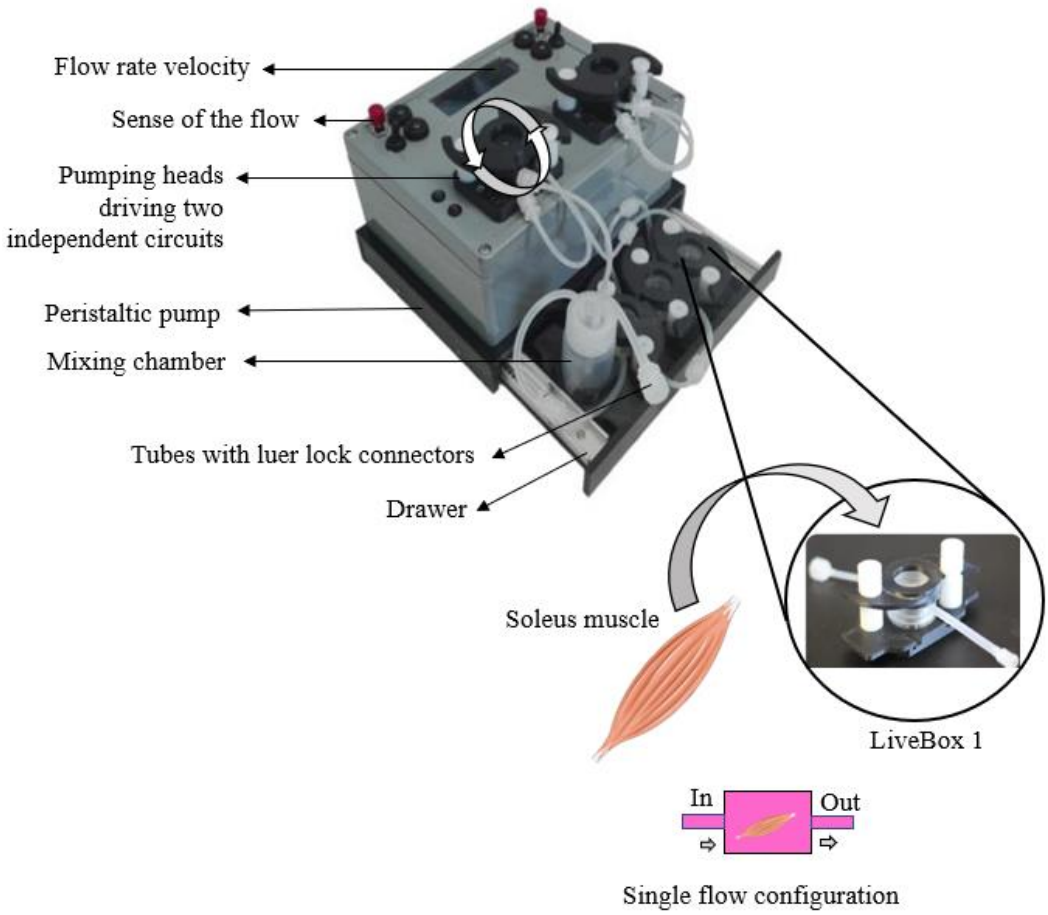

Figure 14. Schema of the fluidic dynamic experimental system.

The above-described studies have been carried out in collaboration with the research teams headed by Prof. Silvia Arpicco and Prof. Barbara Stella (Department of Drugs Science and Technology, University of Torino, Italy), Prof. Giovanna Lollo (LAGEP, Claude Bernard University, Lyon, France), and Prof. Giovanni Meola (Department of Neurology, IRCCS Policlinico San Donato, San Donato Milanese, and Department of Biomedical Sciences for Health, University of Milano, Italy).

The results summarized above are described in detail in the published or submitted scientific articles, as well as in the preliminary results reported below. The published articles have been reproduced with the permission of the journals' Publishers.

M. Costanzo, F. Carton, A. Marengo, G. Berlier, B. Stella, S. Arpicco, M. Malatesta (2016): Fluorescence and electron microscopy to visualize the intracellular fate of nanoparticles for drug delivery. Eur J Histochem 60:2640, DOI: 10.4081/ejh.2016.2640.

Fluorescence and electron microscopy to visualize the intracellular fate of nanoparticles for drug delivery

M. Costanzo,[1] F. Carton,[1] A. Marengo,[2] G. Berlier,[3] B. Stella,[2] S. Arpicco,[2] M. Malatesta[1]

[1]Department of Neurosciences, Biomedicine and Movement Sciences, Anatomy and Histology Section, University of Verona
[2]Department of Drug Science and Technology, University of Turin
[3]Department of Chemistry and NIS Research Centre, University of Turin, Italy

Abstract

In order to design valid protocols for drug release *via* nanocarriers, it is essential to know the mechanisms of cell internalization, the interactions with organelles, and the intracellular permanence and degradation of nanoparticles (NPs) as well as the possible cell alteration or damage induced. In the present study, the intracellular fate of liposomes, polymeric NPs and mesoporous silica NPs (MSN) has been investigated in an *in vitro* cell system by fluorescence and transmission electron microscopy. The tested nanocarriers proved to be characterized by specific interactions with the cell: liposomes enter the cells probably by fusion with the plasma membrane and undergo rapid cytoplasmic degradation; polymeric NPs are internalized by endocytosis, occur in the cytoplasm both enclosed in endosomes and free in the cytosol, and then undergo massive degradation by lysosome action; MSN are internalized by both endocytosis and phagocytosis, and persist in the cytoplasm enclosed in vacuoles. No one of the tested nanocarriers was found to enter the nucleus. The exposure to the different nanocarriers did not increase cell death; only liposomes induced a reduction of cell population after long incubation times, probably due to cell overloading. No subcellular damage was observed to be induced by polymeric NPs and MSN, whereas transmission electron microscopy revealed cytoplasm alterations in liposome-treated cells. This important information on the structural and functional relationships between nanocarriers designed for drug delivery and cultured cells further proves the crucial role of microscopy techniques in nanotechnology.

Introduction

Nanomedicine bears nanotechnology and medicine together, with the aim to obtain new therapeutic approaches and improve current treatments.[1] The unique features of nanomaterials, such as *e.g.*, increased surface area and quantum effects, are responsible for their remarkable efficacy in establishing molecular interactions at the cellular and subcellular level. Due to these peculiarities, nanocarriers received special attention in recent years, as suitable tools for efficiently delivering drugs or diagnostic agents to the target sites. Nanoparticles (NPs) may be loaded with relatively large variety of drug molecules (*e.g.*, small molecules, peptides, nucleic acids) which are protected from cleavage by external agents, and the encapsulated drugs do not participate in the control over pharmacokinetic and biodistribution. Thus, NP-based targeted therapy has emerged as a unique strategy to maintain a drug therapeutic dose at the target site, while reducing systemic drug toxicity and adverse side effects to healthy tissues.[2,3]

A plethora of nanosized drug-delivery systems has been developed, and particular attention has been paid to liposomes and biodegradable polymeric NPs, as biocompatible and versatile systems to encapsulate active agents.

Liposomes are nanoconstructs made of natural or synthetic phospholipids surrounding a water core. Liposomes spontaneously form when phospholipids are dispersed in water, and are non-toxic, biodegradable, and biocompatible, being phospholipids their major component. A wide variety of drugs may be encapsulated in liposomes into either the aqueous core or the surrounding bilayer.[4,5] Liposomes, especially the cationic ones, are also used for gene therapy, and are considered the most suitable transfecting vectors among the currently used synthetic (non-viral) carriers.[6-10]

Polymeric NPs include nanospheres and nanocapsules composed of natural or synthetic polymers, in which drugs can be adsorbed, dissolved, entrapped or encapsulated. Nanospheres are matrix systems where the loaded drug is uniformly dispersed, while in nanocapsules the drug is confined to the inner aqueous or oily cavity surrounded by a tiny polymeric membrane.[11] Polymeric NPs have good encapsulation efficiency and high stability in plasma, and increase the solubility and stability of hydrophobic drugs while lowering their toxicity, thus permitting a controlled release at the target site at relatively low doses.[12-15]

Mesoporous silica NPs (MSN) have recently attracted attention as promising components of multimodal NP systems, owing to their straightforward synthesis and functionalization, tunable pore size, large drug loading capacity, good chemical stability, and adequate biocompatibility.[16,17] MSN can encapsulate both small molecules and oligonucleotides.[18]

Despite the numerous studies on the physicochemical and pharmacological properties of liposomes, polymeric NPs and MSN, little attention has so far been paid to investigate the mechanisms of cell internalization, organelle interactions, and intracellular permanence and degradation as well as the possible NP-related cell alteration or damage. This information is essential for designing suitable protocols for NP-mediated drug delivery,[19-21] and in the present study the intracellular fate of liposomes, polymeric NPs and MSN has been investigated in an *in vitro* cell system by fluorescence and transmission electron microscopy.

Correspondence: Manuela Malatesta, Department of Neurosciences, Biomedicine and Movement Sciences, Anatomy and Histology Section, University of Verona, Strada Le Grazie 8, 37134 Verona, Italy.
Tel. +39.045.8027155 - Fax: 39.045.8027163.
E-mail: manuela.malatesta@univr.it

Key words: Liposomes; mesoporous silica nanoparticles; polymeric nanoparticles; fluorescence microscopy; electron microscopy.

Acknowledgments: we thank Dr. Federico Boschi for skillful assistance in confocal fluorescence analysis. M.C. and F.C. are PhD students in receipt of a fellowship from Doctoral Programs of the University of Verona. This work was supported by MIUR - University of Turin Fondi Ricerca Locale (ex-60%).

Received for publication: 1 March 2016.
Accepted for publication: 4 April 2016.

European Journal of Histochemistry 2016; 60:2640
doi:10.4081/ejh.2016.2640

Materials and Methods

Preparation and characterization of NPs

Fluorescent labelled liposomes were prepared by thin lipid film hydration and extrusion method. Briefly, a chloroform solution of the lipid components (Avanti Polar-Lipids distributed by Spectra 2000 Rome, Italy) 1,2-dipalmitoyl-sn-glycero-3-phosphocholine (DPPC), cholesterol (Chol), and L-α phosphatidyl-DL-glycerol sodium salt (PG) (70:30:3

molar ratios) was evaporated and the resulting lipid film was dried under vacuum overnight. Lipid films were hydrated with a 10 mM solution of fluorescein-5-(and-6)-sulfonic acid trisodium salt (Invitrogen, Life Technologies, Monza, Italy) in HEPES [4-(2-hydroxyethyl) piperazine-1-ethanesulforic acid] buffer (pH 7.4), and the suspension was vortex mixed for 10 min and bath sonicated. The formulations were extruded (Extruder, Lipex, Vancouver, Canada) at 60°C passing the suspension 10 times under nitrogen through 220 nm polycarbonate membrane (Costar, Corning Incorporated, NY). To prepare hyaluronated liposomes, HA_{17000}-DPPE conjugate was previously prepared as reported by Arpicco *et al.*[4] The lipid films were made up of DPPC/Chol (70:30 molar ratio) and then hydrated using a solution of HA_{17000}-DPPE conjugate (3 molar ratio) in HEPES.

Fluorescent labelled polymeric nanoparticles were prepared by nanoprecipitation of the copolymer poly(methoxypolyethyleneglycol cyanoacrylate-*co*-hexadecyl cyanoacrylate) (poly(MePEGCA-*co*-HDCA)) obtained as earlier reported[22]. Practically, 12 mg of the copolymer and 16.8 µg of Nile red ((9-diethylamino-5*H*-benzo[α]phenoxazine-5-one), Sigma-Aldrich, Milan, Italy) were dissolved in 2 mL of warm acetone; this solution was then added to 4 ml of MilliQ® water under magnetic stirring. Precipitation of nanoparticles occurred spontaneously. After solvent evaporation under reduced pressure, an aqueous suspension of fluorescent nanoparticles was obtained.[23] Fluorescent liposomes and polymeric NPs were purified from non-incorporated dye by gel filtration on a Sepharose CL-4B column.

The mean particle size and the polydispersity index (PI) of liposomes and polymeric nanoparticles were determined at 25°C by quasi-elastic light scattering (QELS) using a nanosizer (Nanosizer Nano Z, Malvern Inst., Malvern, UK). The selected angle was 173° and the measurement was made after dilution of the nanoparticle suspension in MilliQ® water. Each measure was performed in triplicate.

Amino-mesoporous silica NPs (NH_2-MSN) were prepared by using cetyltrimethylammonium bromide (CTAB) as structure directing agent (SDA) as previously described.[17] Fluorescein isothiocyanate (FITC) labelled MSN were prepared as reported by[24] with minor modifications. Briefly, at a suspension of 1 mg of NH_2-MSN in 150 µL of MilliQ® water 250 µL of FITC ethanol solution (0.3 mg/mL) were added. The mixture was maintained for 5 h under stirring in the dark and then the nanoparticles were centrifuged and washed with ethanol three times until the supernatants were colorless.

The particle surface charge of all formulations was investigated by zeta potential measurements at 25°C applying the Smoluchowski equation and using the Nanosizer Nano Z. Measurements were carried out in triplicate.

In vitro cell culture

HeLa cells, a human cell line commonly used for basic research as a standardised *in vitro* system, were grown in Dulbecco's modified Eagle medium supplemented with 10% (v/v) fetal calf serum, 1% (w/v) glutamine, 10,000 units/mL of penicillin and 10,000 µg/mL of streptomycin (Gibco by Life Technologies, Milan, Italy), at 37°C in a 5% CO_2 humidified atmosphere. Cells were trypsinized (0.25% trypsin in PBS containing 0.05% EDTA) when sub-confluent, and seeded either on 12 multi-well plastic microplates (2×10^4 per well) for cell viability evaluation or glass coverslips in 12-multi-well plastic microplates (1×10^4 per well) for fluorescence and transmission electron microscopy (TEM). One day after seeding, the initial medium was replaced with a fresh one containing fluorescent NP suspensions: both uncoated and hyaluronic acid-coated liposomes were administered at the concentration of 500 µg/mL, MSN at 50 µg/mL and polymeric NPs at 100 µg/ml. The chosen NP concentrations were previously demonstrated to be non-cytotoxic for various cultured cells.[4,14,25] Cells were incubated with NPs for 2 h, 24 h and 48 h and then processed as described below; in parallel, untreated cells were used as control. HeLa are highly proliferating cells with a cell cycle of about 20 h,[26] therefore a 48 h incubation time allows the completion of two cycles.

Cell viability assay

To estimate the effect of NPs on cell viability, HeLa cultures at all the incubation times were detached by mild trypsinization and stained in suspension for 2 min with 0.01% Trypan blue in the culture medium: cells that were permeable to Trypan blue were considered as non-viable and their percentage was estimated by microscope counting on a Burker hemocytometer; cell samples not exposed to NPs were considered as controls. Results were expressed as the mean ± standard error (SE) of three independent experiments.

To evaluate cell growth, 2×10^4 cells/well were seeded on 12 multi-well plastic microplates and the total cell number was estimated after the different incubation times. The cells were detached by mild trypsinization and counted in a Burker hemocytometer, and the data were expressed as the mean of three independent experiments ± SE.

In order to evaluate the effect of NPs administration on cell proliferation, the S-phase cells fraction was estimated 2 h, 24 h and 48 h after NPs exposure: cells grown on coverslips were pulse-labelled with 20 µM bromodeoxyuridine (BrdU, Sigma) for 30 min at 37°C, then fixed with 70% ethanol and treated for 20 min at room temperature in 2 N HCl, to denature DNA partially. After neutralization with 0.1 M sodium tetraborate (pH 8.2) for 3 min, samples were washed in PBS, permeabilized for 15 min in PBS containing 0.1% bovine serum albumin and 0.05% Tween-20, and incubated for 1 h with a mouse monoclonal antibody recognizing BrdU (BD, Franklin Lakes, NJ, USA) diluted 1:20 in PBS. After two washings with PBS, samples were incubated for 1 h with an Alexafluor 594-conjugated anti-mouse secondary antibody (Molecular Probes, Invitrogen, Milan), diluted 1:200 in PBS. The cell samples were washed with PBS, stained for 5 min with 1 µg/mL Hoechst 33342 (Sigma) in PBS, and finally mounted in PBS:glycerol (1:1) to be observed and scored in fluorescence microscopy (see below). Data were expressed as the mean of three independent experiments ± SE.

Analysis of NPs intracellular distribution

At each incubation time, HeLa cells were fixed for fluorescence microscopy with 4% (v/v) paraformaldehyde in PBS, pH 7.4, for 30 min at room temperature.

The samples were stained for DNA with Hoechst 33342 (1 µg/mL in PBS for 5 min; Sigma), counterstained with 0.1% Trypan blue in PBS for 30 sec, rinsed in PBS, and mounted in a 1:1 mixture of glycerol:PBS (Calbiochem, Inalco, Milan, Italy): this allowed to visualize the intracellular presence of fluorescent NPs and to verify their possible intranuclear location. An Olympus BX51 microscope equipped with a 100W mercury lamp (Olympus Italia Srl, Milan, Italy) was used under the following conditions: 450-480 nm excitation filter (excf), 500 nm dichroic mirror (dm), and 515 nm barrier filter (bf), for FITC; 540 nm excf, 580 nm dm, and 620 nm bf, for Nile red; 330–385 nm excf, 400 nm dm, and 420 nm bf, for Hoechst 33342. Images were recorded with an QICAM Fast 1394 digital camera (QImaging, Surrey, BC, Canada) and processed using Image-Pro Plus 7.0 software (Media Cybernetics Inc., Rockville, MD, USA). For confocal laser scanning microscopy, a Leica TCS-SP system mounted on a Leica DMIRBE inverted microscope (Leica Microsystems Italia, Milan, Italy) was used; for fluorescence excitation, an Ar/Vis laser at 488 nm for FITC, a He/Ne laser at 543 nm for Nile red, and an Ar/UV laser at 364 nm for Hoechst 33258 were used. Spaced (0.5 µm) optical sections were recorded using a 63x oil immersion objective. Images were collected in the 1024×1024 pixel format, stored on a magnetic mass memory and processed by the Leica confocal software. For TEM, HeLa cells were fixed with 2.5% (v/v) glutaraldehyde and 2% (v/v) paraformalde-

hyde in 0.1 M phosphate buffer, pH 7.4, at 4°C for 2 h, post-fixed with 1% OsO_4 and 1.5% potassium ferrocyanide at room temperature for 1h, dehydrated with acetone and embedded in Epon.

Ultrathin sections were weakly stained with uranyl acetate and observed in a Philips Morgagni transmission electron microscope (FEI Company Italia Srl, Milan, Italy) operating at 80 kV and equipped with a Megaview II camera for digital image acquisition.

Results

Characterization of NPs

Liposomes (both uncoated and hyaluronic acid-coated) showed diameters around 230 nm (uncoated liposomes, 220±6 nm; hyaluronic acid-coated liposomes, 245±3 nm, PI<0.1). As previously reported,[4] liposome size increases with the addition of HA-DPPE conjugate. Zeta potential was negative for both formulations and was -15.0±0.70 mV for uncoated liposomes and more negative (-43.0±1.11 mV) for hyaluronic acid-coated ones due to the presence of the carboxylic negative residues of HA on their surface. At TEM, they appeared as spherical vesicles of low electron density (Figure 1 a,b).

Polymeric NPs were 104±25 nm in diameter (PI 0.1) and had a zeta potential of -41±0.50 mV; at TEM, they appeared as spherical particles of moderate electron density (Figure 1c).

MSN were 100±23 nm in diameter with mesopores of about 3.5 nm, and a zeta potential of 12.4±0.91 mV. At TEM, MSN appeared as spherical particles of moderate electron density, with well-ordered mesopores (Figure 1d).

Cell viability

The Trypan blue exclusion test showed that the percentage of dead cells in all NP-treated HeLa samples was lower than 1.5% at all incubation times, at no variance with control samples (Figure 2a).

The total number of cells was similar in control samples and in samples exposed to polymeric NPs and MSN at all times considered. Conversely, cell populations exposed to liposomes underwent significant modification in comparison to control samples; in detail, uncoated liposomes induced a decrease after 48 h incubation, while hyaluronic acid-coated liposomes induced a decrease after both 24 h and 48 h (Figure 2b).

The S-phase fraction did not significantly change after 2 h incubation with all NPs except from MSN, which showed a significant increase in BrdU incorporation. After 24 h incubation, no change was found in all samples while, after 48 h NPs incubation, BrdU incorporation significantly decreased in cells incubated with hyaluronic acid-coated liposomes and polymeric NPs (Figure 2c).

Intracellular distribution of NPs

Liposomes

Microscopic observations were similar for uncoated and hyaluronic acid-coated liposomes. Fluorescence microscopy showed that, after 2 h incubation, several liposomes had entered HeLa cells; they appeared as isolated NPs and never accumulated nor formed intracellular aggregates even after 48 h incubation (Figure 3 a-c). Confocal microscopy confirmed the limited number of liposomes inside the cells, and demonstrated that they always localized in the peripheral region of the cell never entering the nucleus (Figure 4a). At TEM, liposomes were strongly electron dense due to the lipid staining by osmium tetroxide, and showed roundish shapes and *shaggy* profiles (Figure 5). Many liposomes - both singly and as small aggregates - were found adhering to the cell surface, while others occurred inside the cells, just below the plasma membrane or in the peripheral region of the cytoplasm (Figure 5 a,c). No internalization processes such as endocytosis or phagocytosis were observed, suggesting a direct translocation through the cell membrane. Liposomes never occurred in the inner part of the cytoplasm nor inside the cell nuclei. After cell internalization, many liposomes showed a loose filamentous content, and electron dense fine granular material occurred nearby in the cytosol (Figure 5b). Moreover, in the cells exposed to liposomes many lipid droplets were found: they frequently occurred close to the liposomes and contained the electron dense fine granular material, which appeared preferentially - although not exclusively- distributed at their periphery (Figure 5b). After 2 h, but especially after 24 h incubation, many lipid droplets accumulated in the outer cytoplasmic region, often budding from the cell surface until their extrusion in the extracellular milieu (Figure 5 c,d). These lipid droplets were absent in the controls and in the cells treated with the other NP types. All HeLa cells incubated with liposomes contained large amounts of vesicular and membranous structures, although nuclei and cytoplasmic organelles did not show morphological alterations. This phenomenon was particularly evident after 24 h incubation and in cells treated with hyaluronic acid-coated liposomes. Consistent with the results on cell viability, no necrotic nor apoptotic figures were ever observed.

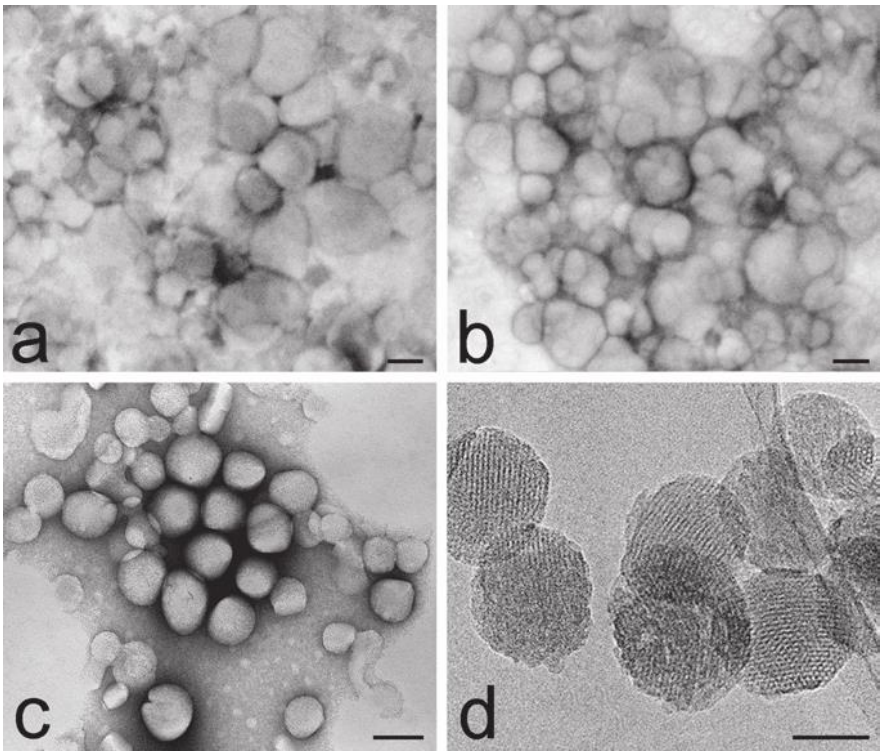

Figure 1. Transmission electron micrographs of uncoated liposomes (a), hyaluronic acid-coated liposomes (b), polymeric NPs (c) and MSN (d). Well-ordered mesopores are clearly visible in MSN. a-c). Negative staining. Scale bars: a-c) 100 nm; d) 50 nm.

Polymeric NPs

Fluorescence microscopy revealed that polymeric NPs entered HeLa cells after 2 h incubation: they appeared as isolated NPs that progressively increased in number and accumulated in perinuclear areas, after 24 h (Figure 3 a'-c'). Confocal microscopy confirmed their cytoplasmic distribution and their absence in the cell nuclei (Figure 4b). At TEM, polymeric NPs showed a regular round shape and a moderate electron density (Figure 6). Single NPs were rarely found to adhere to the cell surface (Figure 6), and in the cytoplasm they appeared both inside membrane-bounded endosomes (Figure 6b) and free in the cytosol (Figure 6a); they never occurred inside the nucleus. After 24 h incubation, a large number of roundish electron dense residual bodies accumulated in the perinuclear region of the cytoplasm (Figure 6e); this phenomenon did not occur in control cells or in samples treated with MSN or liposomes. Some polymeric NPs were surrounded by double membranes, as typical of autophagic figures (Figure 6 c,d).

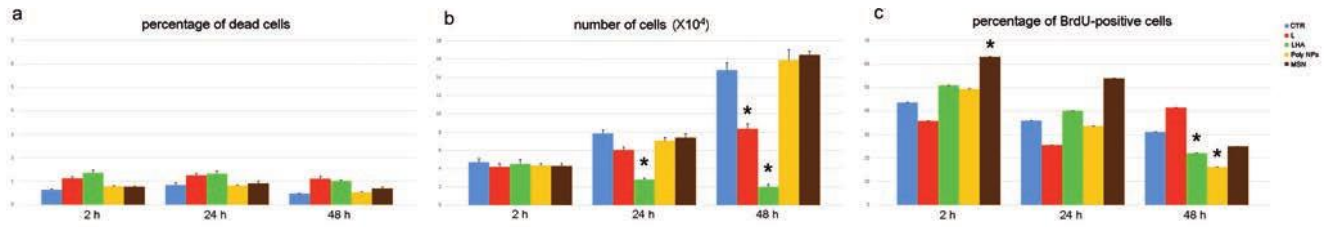

Figure 2. Effect of NP treatment on cell proliferation. a) Mean values±SE of dead cell percentage after 2, 24 and 48 h incubation with the different NPs. b) Mean values±SE of cell number after 2, 24 and 48 h incubation with the different NPs. c) Mean values±SE of BrdU-positive cell percentage after 2, 24 and 48 h incubation with the NPs. In the histograms, values identified with asterisks are significantly different from the control (untreated) cells at the same incubation time. CTR, control; L, liposomes; LHA, hyaluronic acid-coated liposomes; Poly NPs, polymeric NPs; MSN, mesoporous silica nanoparticles.

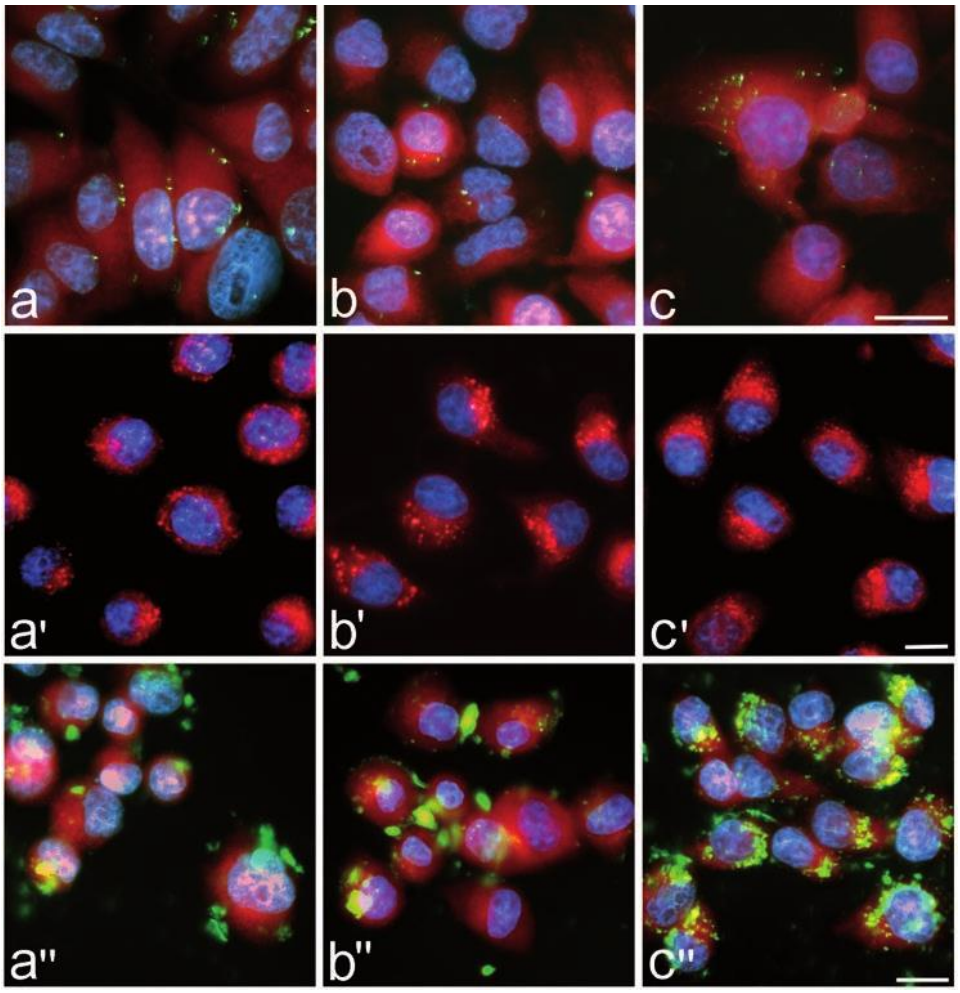

Figure 3. Conventional fluorescence microscopy analysis of liposome (green fluorescence, a-c), polymeric NP (red fluorescence, a'-c') and MSN (green fluorescence, a''-b'') intracellular distribution after 2 h (a-a''), 24 h (b-b'') and 48 h (c-c'') incubation. All NPs are distributed in the whole cytoplasm, especially in the perinuclear region, but are apparently absent from nuclei. Polymeric NPs and MSN progressively accumulate inside the cells, whereas liposomes do not show evident accumulation at increasing treatment times. DNA is stained with Hoechst 33342 (blue fluorescence); in a-c and a''-b'' the cytoplasm is counterstained with Trypan blue (red fluorescence). Scale bars: 20 µm.

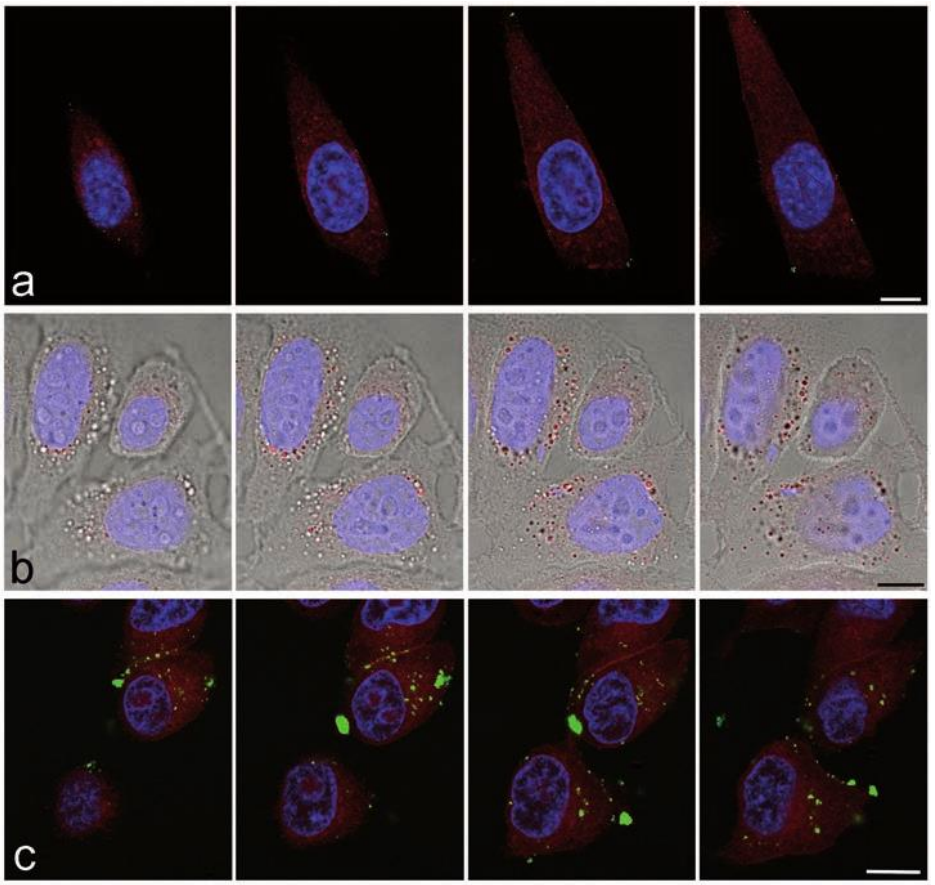

Figure 4. Confocal 500 nm-spaced optical sections of HeLa cells after 24 h incubation with liposomes (green fluorescence, a), polymeric NPs (red fluorescence, b) and MSN (green fluorescence, c). Al the NPs are distributed in the cytoplasm but are absent from the nucleus; note the peripheral location of liposomes. DNA is stained with Hoechst 33342 (blue fluorescence). In a and c the cytoplasm is counterstained with Trypan blue (red fluorescence); in b the red fluorescent signal of polymeric NPs has been merged with the brighfield image. Scale bars: 20 µm.

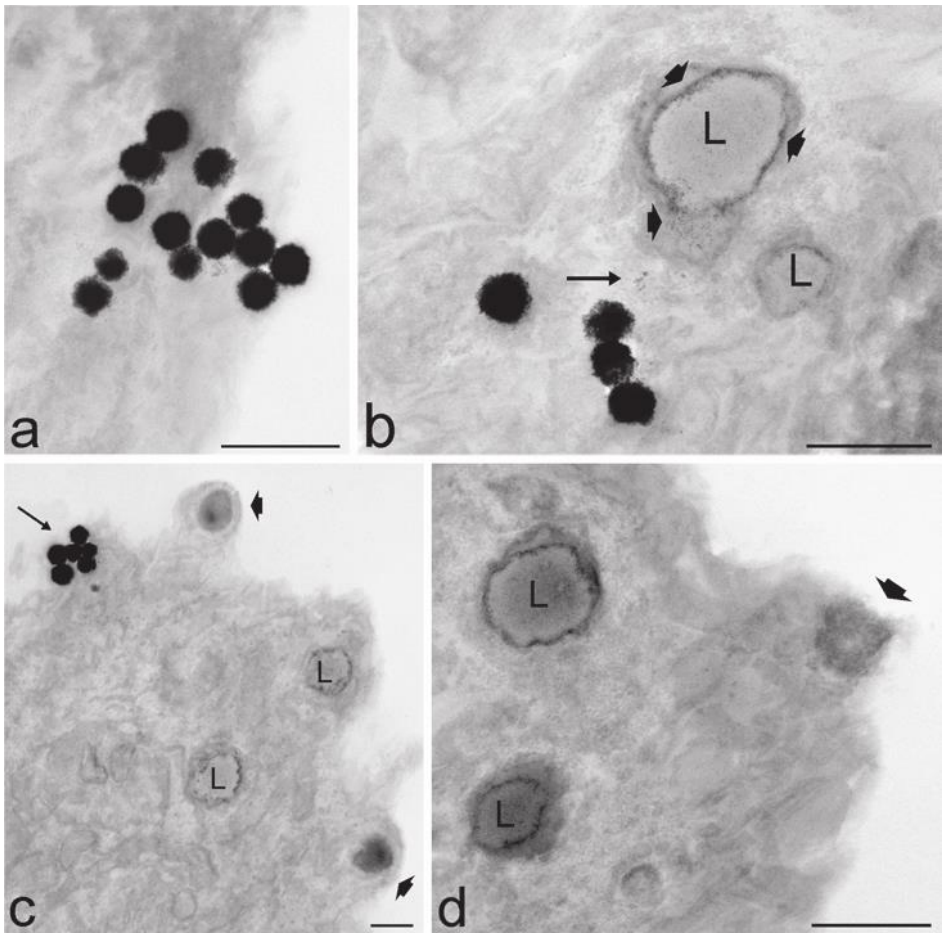

Figure 5. Transmission electron microscopy analysis of liposomes intracellular distribution after 2 h (a, b) and 24 h (c, d) incubation. a) Several liposomes enter the cell apparently without endocytotic process and occur free in the cytoplasm. Note their loose filamentous periphery. b) Electron dense fine granular material (arrow) occurs in the cytosol in close proximity to liposomes and lipid droplets (L). Granular material appears distributed also at the periphery (arrowheads) of the lipid droplets (L). c) After 24 h incubation, while liposome uptake continue (arrow), nearly all lipid droplets (L) contain electron dense granular material and some of them bud from the cell surface (arrowheads). d) Detail of a peripheral cellular region: two lipid droplets (L) containing granular material approach the cell surface and one is extruded (arrowhead). Cell organelles appear hardly recognizable. Scale bars: 500 nm.

No contact between polymeric NPs and cytoplasmic organelles, nor indication of cell alteration or damage were ever observed at any incubation time.

MSN

Observation at conventional and confocal fluorescence microscopy revealed that, after 2 h incubation, many MSN were internalized by HeLa cells, and it was evident that their amount progressively increased up to 24 h (Figure 3a''-c''). MSN often occurred as clusters both at the cell surface and inside the cytoplasm; after 24 h incubation most of MSN were located around (but never inside) the nucleus (Figure 4c). At TEM the MSN were roundish and highly electron dense (Figure 7). According to the observations in fluorescence microscopy, many MSN were found to adhere to the cell surface, frequently as large aggregates (Figure 7a). Single or few MSN were internalized by endocytosis (Figure 7c), while the large clusters entered the cell *via* phagocytosis (Figure 7b). In the cytoplasm, MSN were always found inside vacuoles of various sizes that were ubiquitously distributed in the cytoplasm (sometimes very close to the nuclear envelope), but they were never found inside cell nuclei (Figure 7 d,e). After 24 h incubation, MSN were observed inside large vacuoles (probably secondary lysosomes or residual bodies) containing heterogeneous material (Figure 7f). MSN did not contact any

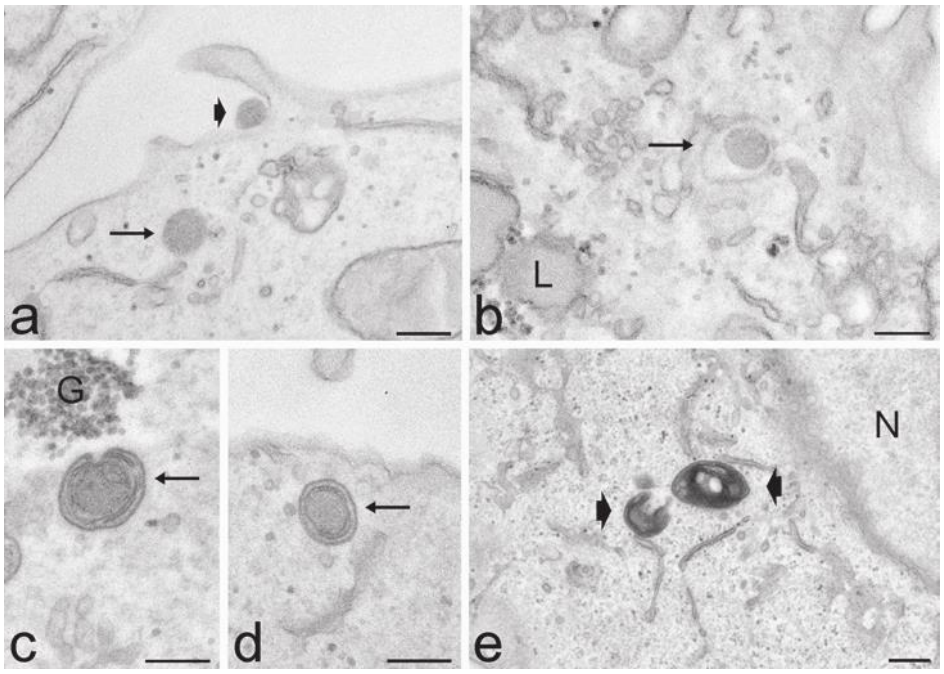

Figure 6. Transmission electron microscopy analysis of polymeric NPs intracellular distribution after 2 h (a-d) and 24 h (e) incubation. a) Two polymeric NPs occurs at the cell periphery: one adhering to the cell surface (arrowhead), the other freely distributed in the cytosol (arrow). b) A polymeric NP is enclosed in an endosome (arrow). Polymeric NPs are partially (c) and completely (d) enclosed by autophagic dual membranes (arrows). e) After 24 h incubation, the cytoplasm contains numerous small and strongly electron dense residual bodies (arrowheads). G, glycogen; L, lipid droplet; N, nucleus Scale bars: 200 nm.

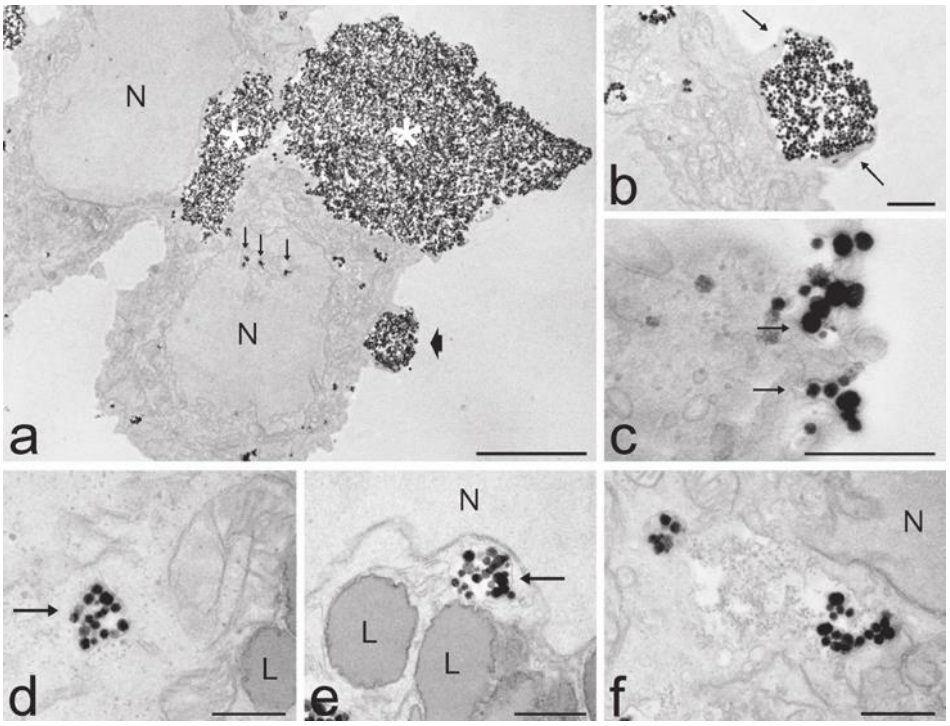

Figure 7. Transmission electron microscopy analysis of MSN intracellular distribution after 2 h (a-d) and 24 h (e, f) incubation. a) Large aggregates of MSN occurs at the cell surface (asterisks). Small clusters of MSN are visible inside the cytoplasm, even inside nuclear invaginations (arrows). The arrowhead indicates the detail showed in b. b) A MSN cluster is internalised via phagocytosis by the extrusion of pseudopodia (arrows). c) Small clusters of MSN enter the cells by endocytosis (arrows). d-e) Vacuoles containing MSN (arrows) are ubiquitously distributed in the cytoplasm, sometimes very close to the nucleus (N). f) MSN occur in large vacuoles containing heterogeneous material. L, lipid droplets; N, nucleus. Scale bars: a) 5 µm; b-f) 500 nm.

particular organelle, and there was never sign of subcellular alteration or damage at any incubation time.

Discussion

Biocompatibility and non-toxicity are essential prerequisites for nanocarriers to avoid adverse effects in the patient's organism, and are especially important when NPs are aimed at delivering therapeutic agents to restore the normal physiological functions in diseased cells which are to be preserved: this is the case with highly differentiated non-cycling cells such as myofibres and neurons.

In our experimental model, cell death was apparently unaffected by the exposure to the various NPs, consistently with previously published data by our group[4,14] and others.[25] However, hyaluronic acid-coated liposomes were found to significantly reduce cell population after both 24 h and 48 h, while uncoated liposomes induced a decrease after 48 h only. The slowdown of cell proliferation demonstrated after 48 h incubation with hyaluronic acid-coated liposomes partially explains such a cell number reduction, but it is likely that also cell death contributes to the population decline. This is only apparently in contrast with the results obtained by the Trypan blue exclusion test; in fact, it should be considered that dead cells, after detaching from the substrate, may undergo rapid degradation thus becoming undetectable: this may cause their underestimation especially at long incubation times.

Our experimental model seems therefore more sensitive to the treatment with liposomes in comparison to other previously investigated cell lines.[4] The stronger effect of hyaluronic-acid-coated liposomes is probably due to the capability of hyaluronic acid to increase the uptake efficiency by cells bearing CD44 receptors[24,27] as HeLa cells,[28] although the rapid disaggregation of these NPs does not allow to observe any difference in their intracellular accumulation. This observation confirms and extends previous data demonstrating that NP biocompatibility may depend -at least in part- on the cell type.[29]

Polymeric NPs were found to slow down cell proliferation after 48 h incubation, although the total cell number remained unaffected. This phenomenon has been already observed in cultured epithelial cells incubated with polymeric NPs for 1-3 days[30] and may be due to the intracellular overload of NPs and/or their remnants after long incubation times. The long-term effect of polymeric NP internalization certainly deserves further investigation since a significant reduction in cell proliferation may represent a predictive sign of cell death.

Conversely, cell proliferation was increased after brief (2 h) exposure to MSN: this is consistent with previous observations by Christen *et al.*[31] and our group (unpublished results), and could be related to the silica-NP-induced activation of MAPK signaling and the down-regulation of *p53*, which in turn inhibit apoptosis and induce cell proliferation.

Fluorescence microscopy demonstrated that cell uptake is quite rapid and efficient for all the NPs tested, although evident differences have been found in their intracellular distribution. TEM allowed monitoring the fine structural relationships between NPs and cell components, clarifying the uptake mechanisms and the intracellular fate of internalized NPs.

MSN enter cells in large amounts *via* both endocytosis and phagocytosis; once internalized, they always occur inside vacuoles, thus remaining segregated from the cytosol and cytoplasmic organelles. MSN were never found free in the cytosol and this suggests they are unable to escape endosomes (contrary to other NP types[32-35]). MSN do follow the intracellular lytic pathway, as suggested by the presence of residual bodies containing numerous NPs and heterogeneous cellular remnants (this was especially clear after 24 h incubation). Such an intracellular behavior must be taken into consideration when using MSN for drug delivery *in vivo*: in this case, the therapeutic agents to be targeted by MSN should be carefully selected to be able to cope with the lytic action of lysosomal enzymes, and to be capable of passing through the vacuole membrane before diffusing in the cytoplasm. Interestingly, MSN did not show any sign of morphological degradation even inside residual bodies; this demonstrates their long intracellular persistence and points to MSN as especially suitable nanovectors for sustained drug release. In addition, since MSN accumulate very close to the nuclear envelope, they could profitably be used to release drugs directed to nuclear targets. It is worth noting that, despite the large number of internalized MSN, the cells did not show any sign of organelle alteration or damage after 24 h exposure. Consistently, no ultrastructural alteration was found in a murine myoblast cell line after 7 days from MSN exposure,[36] thus confirming the good biocompatibility of these nanovectors. The same study[36] demonstrated that MSN uptake enhances differentiation into myotubes, opening interesting perspectives for their use in low renewing differentiated tissues.

Polymeric NPs enter the cell individually probably *via* endocytosis, and diffuse in the whole cytoplasm, accumulating in perinuclear position after long incubation times. They occur in the cytoplasm either inside endosomes or free in the cytosol, thus suggesting that these NPs can escape endosomes, as previously observed for other polymeric NPs.[21,33,35] Nevertheless, many polymeric NPs re-enter the lytic pathway due to the autophagic process, thus undergoing enzymatic degradation and giving rise to the numerous residual bodies observed after 24 h incubation. TEM observations therefore suggest that many of the fluorescing spots visible in the cytoplasm at fluorescence microscopy after long incubation times might correspond to the remnants of polymeric NPs inside residual bodies. The short intracellular permanence of polymeric NPs suggests that they may be especially suitable for rapid drug release. According to previous observations,[37,38] polymeric NPs have never been found inside cell nuclei.

The uncoated and hyaluronic acid-coated liposomes show a similar intracellular distribution pattern: they enter massively the cell, probably mainly by fusion with the plasma membrane[39,40] (although a receptor-mediated internalization cannot be excluded), and undergo rapid degradation in the peripheral region of the cytoplasm (no liposomes have ever been found in the inner part of the cytoplasm or in the nucleus). The presence of granular electron dense material in close proximity of liposomes and inside the adjacent lipid droplets suggests that liposome components are released and migrate into the cytosol to accumulate, probably due to chemical affinity, into the lipid deposits. At present, we cannot establish the reason for liposome degradation, which could be due to either intracellular lipases or intrinsic characteristics of the nanocarriers. In any case, this phenomenon should be taken into consideration when using liposomes as drug carriers; in fact, their rapid degradation could be exploited to allow a rapid and massive release of the therapeutic agent. The accumulation and extrusion of lipid droplets, observed in HeLa cells only after liposome internalization, likely represent different steps of the compartmentalization and elimination process of exogenous material due to excessive NP uptake. Accordingly, signs of cytological alteration are evident, especially after internalization of liposomes coated with hyaluronic acid, which increases uptake efficiency.[24,27,28] However, no necrotic or apoptotic cells were found in the slides incubated with liposomes, probably due to detachment from the substrate and/or degradation of dead cells. It should be underlined that the observation at fluorescence microscopy did not reveal any significant alteration in liposome-treated cells and only the high resolution of TEM demonstrated the actual occurrence of subcellular damages.

Interestingly, no one of the tested nanocarriers was found to enter the nucleus, even after long incubation times, thus demonstrating that they are unable not only to pass

through the nuclear pores but also to be entrapped by the nuclear envelope when it reforms after each mitotic cycle.[25,41] Entering cell nuclei might be considered as an advantage for drug-loaded NPs to reach intranuclear targets; however, it is worth noting that this may indubitably represent a risk because of the possible interactions between NPs *per se* and nucleic acids and/or nuclear factors, which could unpredictably alter cell function, irrespective of the drug action. In addition, it is well known that NP-mediated delivery of drugs or oligonucleotides to nuclear targets does not require that the nanocarrier enters the nucleus,[42,43] but essentially depends on the chemical nature of the therapeutic agents.

The biocompatible nanocarriers designed for drug delivery that have been tested in this study are ultimately intended for *in vivo* administration and further investigations on the complex interactions with the whole organism are mandatory to plan their therapeutic utilization. However, a nanocarrier-based therapeutic strategy cannot disregard basic knowledge and this study provides essential information on the structural and functional interactions of NPs with the cell components, further proving that microscopy techniques (and especially TEM) are irreplaceable in the attempt to describe the biological behavior of nanovectors.

References

1. Wicki A, Witzigmann D, Balasubramanian V, Huwyler J. Nanomedicine in cancer therapy: challenges, opportunities, and clinical applications. J Control Rel 2015; 200:138-57.
2. Yohan D, Chithrani BD. Applications of nanoparticles in nanomedicine. J Biomed Nanotechnol 2014;10:2371-92.
3. Estanqueiro M, Amaral MH, Conceição J, Sousa Lobo JM. Nanotechnological carriers for cancer chemotherapy: the state of the art. Colloids Surf B Biointerfaces 2015;126:631-48.
4. Arpicco S, Lerda C, Dalla Pozza E, Costanzo C, Tsapis N, Stella B, et al. Hyaluronic acid-coated liposomes for active targeting of gemcitabine. Eur J Pharm Biopharm 2013;85:373-80.
5. Pedrini I, Gazzano E, Chegaev K, Rolando B, Marengo A, Kopecka J, et al. Liposomal nitrooxy-doxorubicin: one step over Caelyx® in drug-resistant human cancer cells. Mol Pharm 2014;11:3068-79.
6. Arpicco S, Canevari S, Ceruti M, Galmozzi E, Rocco F, Cattel L. Synthesis, characterization and transfection activity of new saturated and unsaturated cationic lipids. Il Farmaco 2004;59:869-78.
7. De Rosa G, De Stefano D, Laguardia V, Arpicco S, Simeon V, Carnuccio R, et al. Novel cationic liposome formulation for the delivery of an oligonucleotide decoy to NF-B in to activated macrophages. Eur J Pharm Biopharm 2008;70:7-18.
8. Taetz S, Bochot A, Surace C, Arpicco S, Renoir JM, Schaefer UF, et al. Hyaluronic acid-modified DOTAP/DOPE liposomes for the targeted delivery of antitelomerase siRNA to CD44-expressing lung cancer cells. Oligonucleotides 2009;19:103-15.
9. Surace C, Arpicco S, Dufay-Wojcicki A, Marsaud V, Bouclier C, Clay D, et al. Lipoplexes targeting the CD44 hyaluronic acid receptor for efficient transfection of breast cancer cells. Mol Pharm 2009;6: 1062-73.
10. Nascimento TL, Hillaireau H, Noiray M, Bourgaux V, Arpicco S, Pehau-Arnaudet G, et al. Supramolecular organization and siRNA binding of hyaluronic acid-coated lipoplexes for targeted delivery to the CD44 receptor. Langmuir 2015;31:11186-94.
11. Grottkau BE, Cai X, Wang J, Yang X, Lin Y. Polymeric nanoparticles for a drug delivery system. Curr Drug Metab 2013;14:840-6.
12. Stella B, Arpicco S, Peracchia MT, Desmaële D, Hoebeke J, Renoir JM, et al. Design of folic acid-conjugated nanoparticles for drug targeting. J Pharm Sci 2000;89:1452-64.
13. Stella B, Arpicco S, Rocco F, Marsaud V, Renoir JM, Cattel L, et al. Encapsulation of gemcitabine lipophilic derivatives into polycyanoacrylate nanospheres and nanocapsules. Int J Pharm 2007;344:71-7.
14. Stella B, Marsaud V, Arpicco S, Géraud G, Cattel L, Couvreur P, et al. Biological characterization of folic acid-conjugated poly(H2NPEGCA-co-HDCA) nanoparticles in cellular models. J Drug Target 2007;15: 146-53.
15. Lince F, Bolognesi S, Stella B, Marchisio DL, Dosio F. Preparation of polymer nanoparticles loaded with doxorubicin for controlled drug delivery. Chem Eng Res Des 2011;89:2410-9.
16. Chen Y, Chen H, Shi J. Drug delivery/imaging multifunctionality of mesoporous silica-based composite nanostructures. Expert Opin Drug Deliv 2014;11:917-30.
17. Sapino S, Ugazio E, Gastaldi L, Miletto I, Berlier G, Zonari D, et al. Mesoporous silica as topical nanocarriers for quercetin: characterization and in vitro studies. Eur J Pharm Biopharm 2015;89:116-25.
18. Peng J, He X, Wang K, Tan W, Li H, Xing X, et al. An antisense oligonucleotide carrier based on amino silica nanoparticles for antisense inhibition of cancer cells. Nanomedicine 2006;2:113-20.
19. Panyam J, Zhou WZ, Prabha S, Sahoo SK, Labhasetwar V. Rapid endolysosomal escape of poly(DL-lactide-coglycolide) nanoparticles: implications for drug and gene delivery. FASEB J 2002;16:1217-26.
20. Watson P, Jones AT, Stephens DJ. Intracellular trafficking pathways and drug delivery: fluorescence imaging of living and fixed cells. Adv Drug Deliv Rev 2005; 57:43-61.
21. Malatesta M, Pellicciari C, Cisterna B, Costanzo M, Galimberti V, Biggiogera M, et al. Tracing nanoparticles and photosensitizing molecules at transmission electron microscopy by diaminobenzidine photooxidation. Micron 2014;59C:44-51.
22. Lince F, Bolognesi S, Marchisio DL, Stella B, Dosio F, Barresi A, Cattel L. Preparation of poly(MePEGCA-co-HDCA) nanoparticles with confined impinging jets reactor: experimental and modeling study. J Pharm Sci 2011b;100:2391-405.
23. Fessi H, Puisieux F, Devissaguet JPh, Ammoury N, Benita S. Nanocapsule formation by interfacial polymer deposition following solvent displacement. Int J Pharm 1989;55:R1–R4.
24. Yu M, Jambhrunkar S, Thorn P, Chen J, Gu W, Yu C. Hyaluronic acid modified mesoporous silica nanoparticles for target drug delivery to CD44-overexpressing cancer cells. Nanoscale 2013;5:178-83.
25. Guan M, Zhu Q, Liu Y, Bei Y-Y, Gu Z-L, Zhang X-N, et al. Uptake and transport of a novel anticancer drug-delivery system: lactosyl-norcantharidin-associated N-trimethyl chitosan nanoparticles across intestinal Caco-2 cell monolayers. Int J Nanomedicine 2012;7:1921-30.
26. Hahn AT, Jones JT, Meyer T. Quantitative analysis of cell cycle phase durations and PC12 differentiation using fluorescent biosensors. Cell Cycle 2009;8:1044-52.
27. Li J, Hu Y, Yang J, Wei P, Sun W, Shen M, et al. Hyaluronic acid-modified Fe_3O_4@Au core/shell nanostars for multimodal imaging and photothermal therapy of tumors. Biomaterials 2015;38:10-21.
28. Bruno S, Fabbi M, Tiso M, Santamaria B, Ghiotto F, Saverino D, et al. Cell activation via CD44 occurs in advanced stages of squamous cell carcinogenesis. Carcinogenesis 2000;21:893-900.
29. Chang JS, Chang KL, Hwang DF, Kong ZL. In vitro cytotoxicitiy of silica nanoparticles at high concentrations strongly depends on the metabolic activity type of the cell line. Environ Sci Technol 2007;41:2064-8.
30. Hussien R, Rihn BH, Eidi H, Ronzani C, Joubert O, Ferrari L, et al. Unique growth pattern of human mammary epithelial cells induced by polymeric nanoparticles. Physiol Rep 2013;1:e00027.

31. Christen V, Camenzind M, Fent K. Silica nanoparticles induce endoplasmic reticulum stress response, oxidative stress and activate the mitogen-activated protein kinase (MAPK) signaling pathway. Toxicology Reports 2014;1:1143-51.
32. Serda RE, Mack A, van de Ven AL, Ferrati S, Dunner K Jr, Godin B, et al. Logic-embedded vectors for intracellular partitioning, endosomal escape, and exocytosis of nanoparticles. Small 2010;6:2691-700.
33. Varkouhi AK, Scholte M, Storm G, Haisma HJ. Endosomal escape pathways for delivery of biologicals. J Control Release 2011; 151:220-8.
34. Zaki NM, Nasti A, Tirelli N. Nanocarriers for cytoplasmic delivery: cellular uptake and intracellular fate of chitosan and hyaluronic acid-coated chitosan nanoparticles in a phagocytic cell model. Macromol Biosci 2011;11:1747-60.
35. Malatesta M, Giagnacovo M, Costanzo M, Conti B, Genta I, Dorati R, et al. Diaminobenzidine photoconversion is a suitable tool for tracking the intracellular location of fluorescently labelled nanoparticles at transmission electron microscopy. Eur J Histochem 2012;56:e20.
36. Poussard S, Decossas M, Le Bihan O, Mornet S, Naudin G, Lambert O. Internalization and fate of silica nanoparticles in C2C12 skeletal muscle cells: evidence of a beneficial effect on myoblast fusion. Int J Nanomedicine 2015;10:1479-92.
37. Kim HR, Gil S, Andrieux K, Nicolas V, Appel M, Chacun H, et al. Low-density lipoprotein receptor-mediated endocytosis of PEGylated nanoparticles in rat brain endothelial cells. Cell Mol Life Sci 2007;64: 356-64.
38. Brambilla D, Nicolas J, Le Droumaguet B, Andrieux K, Marsaud V, Couraud PO, et al. Design of fluorescently tagged poly(alkyl cyanoacrylate) nanoparticles for human brain endothelial cell imaging. Chem Commun (Camb) 2010;46:2602-4.
39. Verma A, Stellacci F. Effect of surface properties on nanoparticle-cell interactions. Small 2010;6:12-21.
40. Nazarenus M, Zhang Q, Soliman MG, del Pino P, Pelaz B, Carregal-Romero S, et al. In vitro interaction of colloidal nanoparticles with mammalian cells: What have we learned thus far? Beilstein J Nanotechnol 2014;5:1477-90.
41. Malatesta M, Grecchi S, Chiesa E, Cisterna B, Costanzo M, Zancanaro C. Internalized chitosan nanoparticles persist for long time in cultured cells. Eur J Histochem 2015;59:2492.
42. Zhao F, Zhao Y, Liu Y, Chang X, Chen C, Zhao Y. Cellular uptake, intracellular trafficking, and cytotoxicity of nanomaterials. Small 2011;7:1322-37.
43. Yameen B, Choi WI, Vilos C, Swami A, Shi J, Farokhzad OC. Insight into nanoparticle cellular uptake and intracellular targeting. J Control Rel 2014;190:485-99.

M. Costanzo, F. Carton, M. Malatesta (2017a). Monitoring the uptake and intracellular fate of nanovectors by microscopical technique. In: Small is beautiful: nanovectors for biomedical research and therapy. Istituto Lombardo - Accademia di Scienze e Lettere. Incontri di studio 91:51-70, http://www.ilasl.org/index.php/Incontri/article/view/269.

MONITORING THE UPTAKE AND INTRACELLULAR FATE OF NANOVECTORS BY MICROSCOPICAL TECHNIQUES

MANUELA COSTANZO, FLAVIA CARTON, MANUELA MALATESTA (*)

SUNTO. – I nanovettori rivestono grande interesse per le loro potenzialità in campo terapeutico e diagnostico, come sistemi per veicolare farmaci e per l'*imaging* medicale. Le loro particolari caratteristiche ne consentono il passaggio attraverso le barriere biologiche e l'accumulo nei siti bersaglio, garantendo inoltre la protezione delle molecole caricate e la modulazione del loro rilascio. Per somministrare nanovettori in maniera efficace e sicura è ovviamente necessario valutarne il possibile effetto citotossico, ma è anche essenziale chiarire i meccanismi di internalizzazione, il traffico intracellulare, le relazioni con gli organuli e la persistenza all'interno della cellula dei nanoparticolati, con particolare attenzione alle loro vie degradative. La microscopia è particolarmente idonea per descrivere le interazioni dei nanovettori con la membrana cellulare e il loro destino intracellulare dopo l'internalizzazione. Nanoparticelle legate a fluorocromi possono essere osservate in microscopia a fluorescenza convenzionale e confocale, mentre l'elevata risoluzione della microscopia elettronica a trasmissione consente di rivelare le fini relazioni dei nanovettori con le strutture subcellulari. In questo articolo sono riassunti alcuni studi condotti utilizzando tecniche microscopiche per valutare le proprietà di nanoparticelle destinate a scopi terapeutici e diagnostici.

***

ABSTRACT. – Nanovectors are receiving great attention for their potential in therapeutic and diagnostic applications as innovative systems for drug delivery and medical imaging. Their unique features allow them to pass through the biological barriers, to accumulate at the target sites, to protect the loaded drugs from enzymatic degradation and to modulate their release. To design effective and safe administration procedures of nanovectors it is obviously mandatory to assess their possible cytotoxicity, but it is also essential to elucidate the uptake mechanism(s), the intracellular trafficking pathway, the interactions with cell organelles and the intracellular persistence of nanovectors, paying

(*) Department of Neuroscience, Biomedicine and Movement, Anatomy and Histology Section, University of Verona, Italy. E-mail: manuela.malatesta@univr.it

particular attention to their degradation routes. Microscopy is especially suitable to describe the interaction of nanocarriers with the cell surface and their intracellular fate following internalization. Fluorochrome-labelled nanoparticles may be observed by conventional and confocal fluorescence microscopy, while the higher resolution of transmission electron microscopy allows to reveal the specific relationships of nanocomposites with the subcellular constituents. This work summarizes some studies performed by different microscopical techniques to evaluate the properties of nanoparticles intended for therapeutic and diagnostic purposes.

INTRODUCTION

Nanovectors are receiving great attention for their potential in therapeutic and diagnostic applications as innovative drug delivery and medical imaging systems. Their unique properties (*e.g.* small size, large and functionalizable surface area) allow them to pass through the biological barriers (cell membrane, capillary wall, blood brain barrier) and to accumulate at the target sites. Moreover, nanovectors may protect the loaded molecules from enzymatic degradation, prolonging their permanence in the living organism; in addition, the release of the loaded drugs may be modulated, thus improving their sustainability and availability.

Biocompatibility and biodegradability are the basic features of nanovectors designed for biomedical use; it is therefore mandatory to test the behavior of nanovectors in the biological environment. Although nanovectors are intended for administration *in vivo*, the first step of their evaluation is generally performed in *in vitro* systems. Evaluating the safety and efficacy of a newly synthesized nanovectors *in vitro* represents, in fact, a necessary pre-requisite for *in vivo* experimentation: cultured cells are relatively simple experimental models that enable the analysis of the effects of nanocomposites under strictly controlled conditions, avoiding the complex systemic responses occurring in a living organism; moreover, *in vitro* experimentation is less expensive than *in vivo* tests, and allows a remarkable reduction of laboratory animals needed for the following systemic studies.

To design effective and safe administration procedures of nanovectors for therapeutic and diagnostic applications, it is obviously mandatory to assess their possible cytotoxicity after both short and long post-treatment times; in fact, cell necrosis or apoptosis may trigger an inflammatory response in tissues and organs of the patient receiving the

nanoparticulate system (Rock and Kono, 2008; Kono *et al.*, 2014). However, it is also essential to elucidate the uptake mechanism(s), the intracellular trafficking pathway, the interactions with cell organelles and the intracellular persistence of nanovectors, paying particular attention to their degradation route. The intracellular degradation pathway of nanoparticles (NPs) is crucial for estimating the efficacy of a nanocarrier since its entrapment into endosomes may imply a sequestration and a rapid inactivation of the loaded molecules by the lysosomal enzymes (Panyam *et al.*, 2002).

Microscopy is especially suitable to describe the interaction of NPs with the cell surface and their intracellular fate following internalization. Fluorochrome-labelled NPs may be observed by conventional and confocal fluorescence microscopy, while the higher resolution of transmission electron microscopy allows to reveal the specific relationships of nanocomposites with the subcellular constituents.

Recently, we have also demonstrated that diaminobenzidine photo-oxidation (Maranto, 1982) is especially suitable for unambiguously visualizing fluorescently-labelled NPs at transmission electron microscopy (Malatesta *et al.*, 2012; 2013b; 2014), thus allowing to overcome the limit due to the moderate electron density of many nanovectors (which makes them hardly distinguishable from the intracellular milieu), and to detect their remnants after lytic degradation.

The following chapters describe the information obtained by applying microscopical techniques to evaluate the suitability of different NPs for specific therapeutic and diagnostic purposes.

CHITOSAN NANOPARTICLES FOR THE DELIVERY OF HYPOMETABOLIZING OPIOIDS

D-Ala(2)-D-Leu(5)-enkephalin (DADLE) is a synthetic hypometabolizing opioid (Oeltgen *et al.*, 1988) of potential biomedical interest (Malatesta *et al.*, 2007). In fact, DADLE is able to significantly prolong the preservation of explanted organs (Oeltgen *et al.*, 1996; Bolling *et al.*, 1997; Su, 2000; Inuo *et al.*, 2007; Tisherman *et al.*, 2013), to improve cardioprotection (Romano *et al.*, 2004; Yao *et al.*, 2007; Forster *et al.*, 2007; 2010) and neuroprotection (Borlongan *et al.*, 2004; 2009; Su *et al.*, 2007; Wang *et al.*, 2011; Arrich *et al.*, 2012) under ischemic conditions, and to act as anti-tumour agent (Fichna and Janecka, 2004;

Debruyne *et al.*, 2010; Tsai *et al.*, 2010). Targeting DADLE to the brain would be instrumental to assess its hypometabolising effects *in vivo* with a consequent decrease in body temperature, which could improve the surgical procedures that imply hypothermy (such as in aortic arch surgery: Yan *et al.*, 2013). The use *in vivo* of DADLE is, however, problematic since this molecule is degraded by plasmatic enkephalinases in a few minutes (Shibanoki *et al.*, 1991) and cannot cross the blood brain barrier; encapsulating DADLE into NPs could make its systemic administration more efficient.

Chitosan is a natural cationic polysaccharide widely investigated for the development of drug delivery systems due to its peculiar features such as low immunogenicity and toxicity, easy functionalizability, availability, sustainability and biodegradability (Kumar *et al.*, 2004; Hu *et al.*, 2013; El Kadib *et al.*, 2014; Luo and Wang, 2014). Chitosan NPs are considered as good carriers for the sustained intracellular delivery of specific molecules since they are able to protect the loaded drugs from lysosomal degradation (Koping-Hoggard *et al.*, 2004; Douglas and Tabrizian, 2005; Serda *et al.*, 2010; Zaki *et al.*, 2011) and to cross diverse biological barriers (Schipper *et al.*, 1997; Peppas and Huang, 2004), including the blood brain barrier (Karatas *et al.*, 2009; Songjiang and Lixiang, 2009; Wang *et al.*, 2010; Jaruszewski *et al.*, 2012). These characteristics make chitosan NPs especially promising for DADLE delivery.

With this aim, we investigated the behavior of chitosan NPs inside cultured neuronal cells, and we monitored the intracellular drug release by DADLE-loaded NPs (Malatesta *et al.*, 2012; 2013a). According to previous observations in other cell types (*e.g.* Huang *et al.*, 2002; Ma and Lim, 2003; Harush-Frenkel *et al.*, 2007; Park *et al.*, 2010; Zaki *et al.*, 2011), chitosan NPs proved to be efficiently internalized by endocytosis (*Fig. 1a*), to distribute in the cytoplasm accumulating in the perinuclear region (*Fig. 1b*), and to escape endosomal degradation as they occur free in the cytosol (*Fig. 1c*). However, many NPs were also found inside secondary lysosomes and residual bodies, demonstrating that they finally enter the lytic pathway (*Fig. 1d*). When loaded with DADLE, chitosan NPs efficiently release the opioid in the intracellular milieu inducing a fully reversible hypometabolic state which is significantly longer than that observed when DADLE had directly been administered as free molecules in the culture medium. Chitosan NPs were found to persist for weeks inside both the cytoplasm and nucleus (Malatesta *et al.*, 2015); since their size does not

allow them to pass through the nuclear pore complex (Allen *et al.*, 2000; Labokha and Fassati, 2013), it is likely that they are entrapped into the nucleus at the end of mitosis, when the nuclear envelope reassembles (Guan *et al.*, 2012). Although chitosan NPs were never found to make preferential contact with any nuclear component, they could interfere with the overall nuclear functions (*e.g.* by establishing electrostatic interactions with the nucleic acids, Lai and Lin, 2009). Therefore, despite the absence of cell death or damage up to two weeks after internalization, further investigation is mandatory on the possible long-term effects of chitosan NP.

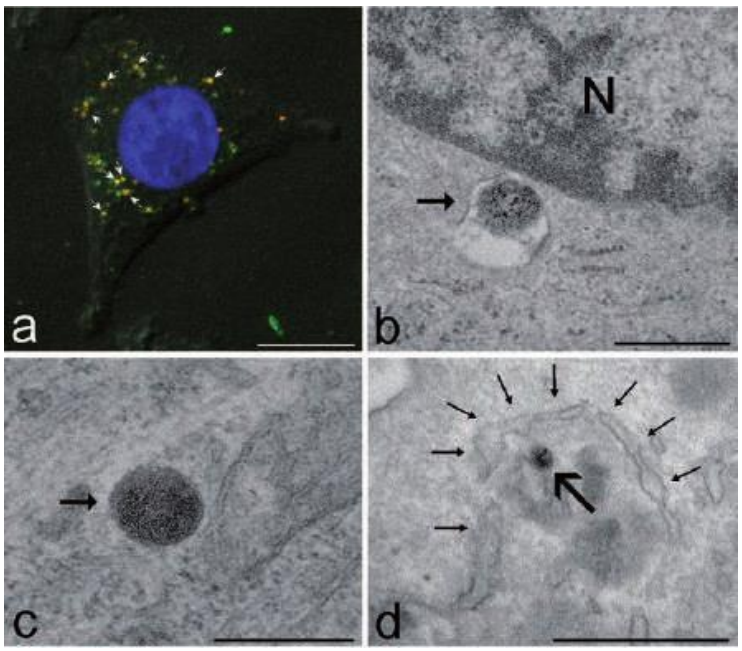

Fig. 1. a. Confocal micrograph of a cell after incubation with fluorescein 5(6)-isothiocyanate labelled chitosan NPs; the cells were previously incubated with the red-fluorescing dye, PKH26 to label the plasma membrane. For several NPs (arrows), green and red fluorescence co-locate, as the result of the endocytotic internalization of part of the plasma membrane. Bar, 10 µm. b-d. Transmission electron micrographs of cells incubated with chitosan NPs; the fine granular, dark reaction product of diaminobenzidine photo-oxidation makes the NPs clearly detectable. b) A NP enclosed in an endosome (arrow) is located very close to the nuclear envelope. N, nucleus. c) A NP (arrow) occurs free in the cytoplasm. d) A dual membrane (thin arrows) partially surrounds a NP (arrow). Bars, 500 nm. (a-c, from Malatesta et al.*, 2012; d, from Malatesta* et al.*, 2015).*

LIPOSOMES, POLYMERIC NANOPARTICLES AND MESOPOROUS SILICA NANOPARTICLES AS DRUG DELIVERY SYSTEMS FOR MUSCLE CELLS

Myotonic dystrophies (DM) are genetically heterogeneous neuromuscular disorders with autosomal dominant inheritance characterized by a variety of pathological features, especially concerning motor functions (Harper, 2001; Meola and Cardani, 2015). Currently, no disease-modifying therapies are available, and treatments are administered to only manage symptoms. Promising results have been obtained with experimental therapies based on either antisense oligomers or drugs such as pentamidine or actinomycin D (*e.g.* Lee *et al.*, 2009; Warf *et al.*, 2009; Wong *et al.*, 2011; Childs-Disney *et al.*, 2012; Lee *et al.*, 2012; Parkesh *et al.*, 2012; Wheeler *et al.*, 2012; Coonrod *et al.*, 2013; Nguyen *et al.*, 2014; 2015; Pandey *et al.*, 2015; Siboni *et al.*, 2016). However, these molecules have scarce therapeutic applicability in humans because of their low bioavailability due to enzymatic degradation or their high systemic toxicity. Nanocarriers are able to protect the encapsulated agents from lysis and to allow its sustained release inside the cells: they may, therefore, represent a suitable approach to improve the administration of these therapeutic agents. The nanocarriers must obviously be biocompatible and biodegradable to safely play their action without damaging patient's organism, and this is especially important when they are aimed at delivering therapeutic agents to restore the normal physiological functions in diseased cells that are to be preserved (as the highly differentiated non-cycling cells of skeletal muscles, heart or the central nervous system).

In the attempt to set up an innovative therapeutic strategy based on biocompatible nanocarriers, we tested in cultured cells different biocompatible NPs already known to act as efficient drug-delivery systems. We focused on liposomes, mesoporous silica NPs and polymeric NPs.

Liposomes are attractive vehicles for drug delivery: they are composed of natural phospholipids, consequently being biologically inert and weakly immunogenic, and possess low intrinsic toxicity, high biocompatibility and biodegradability. Further, drugs with different lipophilicities can be encapsulated into liposomes: lipophilic drugs are entrapped in the lipid bilayer while hydrophilic drugs in the aqueous compartment, and the amphiphilic agents are encapsulated

both in the lipid bilayer and in the aqueous core (Arpicco *et al.*, 2013; Pedrini *et al.*, 2014). In our study, we used unconjugated and hyaluronic-acid-conjugated liposomes in order to compare their internalization capability (it is known that hyaluronic acid may increase the uptake efficiency by cells bearing the CD44 receptors, Yu *et al.*, 2013; Li *et al.*, 2015).

Mesoporous silica NPs have attracted increasing attention due to their peculiar features: they can be easily synthesized and functionalized, show an excellent chemical stability, and are able to load large amounts of molecules whose release can be modulated by varying the size of the pores; moreover, they proved to be highly biocompatible (Chen *et al.*, 2014; Sapino *et al.*, 2015). Interestingly, both small molecules and oligonucleotides may be encapsulated in mesoporous silica NPs (Peng *et al.*, 2006). In our study we used amino-mesoporous silica NPs.

Polymeric NPs are made of either natural or synthetic polymers that may be structured as nanospheres (where the loaded drugs are homogeneously dispersed in the matrix) and nanocapsules (where the drug is restricted to the aqueous or oily hollow enclosed in a thin polymeric layer) (Grottkau *et al.*, 2013). Polymeric NPs are able to improve the solubility and stability of hydrophobic drugs thus reducing their toxicity; this allows a controlled and sustainable release at relatively low doses. Moreover, they demonstrated a high stability in plasma (Stella *et al.*, 2000; 2007a; b; Lince *et al.*, 2011). In our study we used poly(methoxypolyethyleneglycol cyanoacrylate-co-hexadecyl cyanoacrylate)-based polymeric NPs.

We first investigated the uptake and intracellular fate of the three nanocarrier types using a human cell line commonly used for basic research as a standardised *in vitro* system (HeLa cells) (Costanzo *et al.*, 2016b). All nanocarriers were rapidly internalized by the cells, although the uptake mechanisms and intracellular distribution were characteristic of each nanovector type. Liposomes enter massively the cell, probably by fusion with the plasma membrane (Nazarenus *et al.*, 2014) (although a receptor-mediated internalization cannot be excluded), and they undergo rapid degradation at the cell periphery (*Fig. 2a*).

Liposomic constituents diffuse into the cytosol and accumulate in lipidic droplets (*Fig. 2a'*), that are then extruded from the cell surface (a process likely due to excessive uptake of exogenous material).

The rapid intracellular disaggregation of liposomes suggests that they may be suitable for carrying drugs to be rapidly and massively released.

Polymeric NPs enter the cell individually *via* endocytosis, and occur in the cytoplasm either inside vacuoles or free (*Fig. 2b, b'*), demonstrating their ability to escape endosomes. However, most of polymeric NPs re-enter the lytic pathway due to the autophagic process, thus undergoing enzymatic degradation in a few hours. The short intracellular permanence suggests the utilization of these NPs for rapid drug release.

Mesoporous silica NPs are internalized as large clusters via endocytosis and phagocytosis, and remain always enclosed in vacuoles (first endosomes, then secondary lysosomes and finally residual bodies), thus following the intracellular lytic route (*Fig. 2c, c'*). However, they persist for long time inside the cell, suggesting their utilization for sustained release of drugs able to cope with the enzymatic degradation and then cross the vacuole membrane.

Based on these promising results, we investigated the effect of these NPs in an established myoblast cell line (C2C12) (Costanzo, 2016a). In these myoblasts, liposomes and amine-mesoporous silica NPs showed similar results as in HeLa cells, but the cyanoacrylate-based polymeric NPs were found to induce a dramatic increase of cell death and damage.

This strongly suggests that the biological effects of a nanovector may strictly be related to the cell type. Cyanoacrylate-based polymeric NPs were then replaced by poly(lactic-co-glycolic acid) (PLGA) NPs, which proved to be safe (unpublished results). PLGA is, in fact, one of the most successfully used biodegradable polymers because its hydrolysis leads to metabolite monomers (lactic acid and glycolic acid) which are endogenous and easily metabolized via the Krebs cycle, thus leading to a minimal systemic toxicity. Consistently, PLGA is approved by the US FDA and the European Medicine Agency (EMA) in various drug delivery systems for humans (Danhier *et al.*, 2012).

We are presently investigating liposomes, amine-mesoporous silica NPs and PLGA NPs on primary human myoblasts from skeletal muscle biopsies of healthy and dystrophic subjects, with very encouraging results.

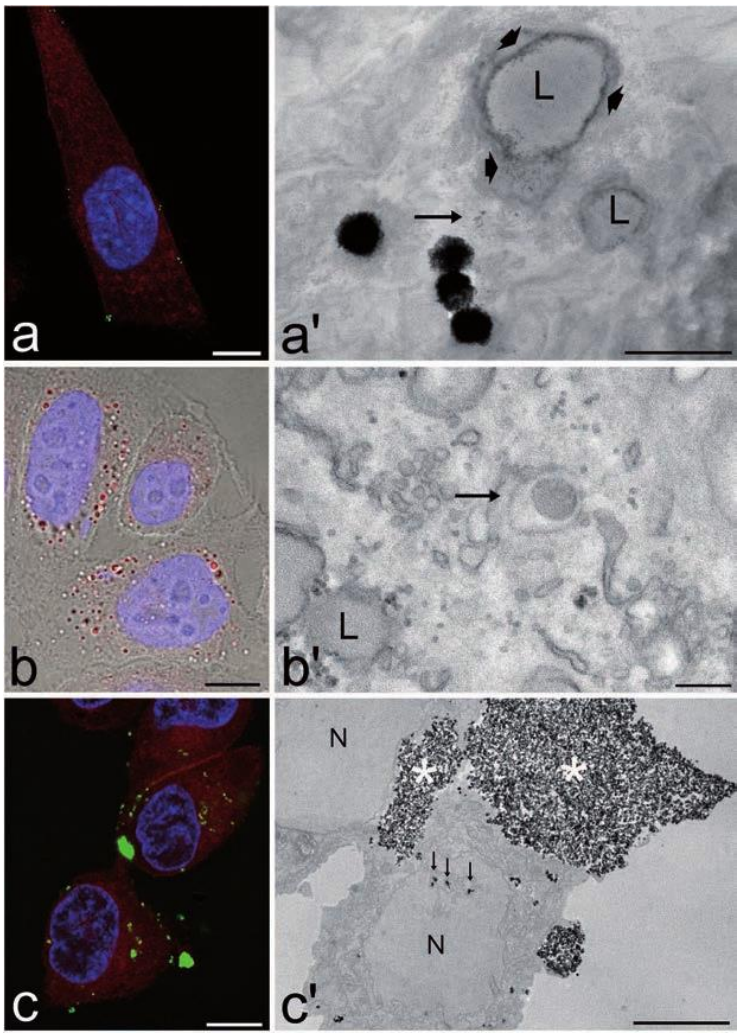

Fig. 2. a-c. Confocal micrographs of cells incubated with liposomes (green fluorescence, a), polymeric NPs (red fluorescence, b) and mesoporous silica NPs (green fluorescence, c). All the nanovectors are distributed in the cytoplasm but are absent from the nucleus; note the peripheral location of liposomes. DNA is stained with Hoechst 33342 (blue fluorescence). In a and c the cytoplasm is counterstained with trypan blue (red fluorescence); in b the red fluorescent signal of polymeric NPs has been merged with the brighfield image. Bars: 20 µm. a'-c'. Transmission electron microscopy analysis of the intracellular distribution of liposomes (a'), polymeric NPs (b') and mesoporous silica NPs (c'). a') Liposomes occur free in the cytoplasm and show a loose filamentous periphery. Electron dense fine granular material (arrow) occurs in the cytosol in close proximity to liposomes and lipid droplets (L). Granular material appears distributed also at the periphery (arrowheads) of the lipid droplets (L). b') A polymeric NP is enclosed in an endosome (arrow). c') Large aggregates of mesoporous silica NPs occur at the cell surface (asterisks). Small clusters of NPs are visible inside the cytoplasm, even inside nuclear invaginations (arrows). N, nucleus. Bars, 500 nm (a', b'); 5 µm (c'). (from Costanzo et al., 2016a).

MANGANESE-CONTAINING NPS AS A NOVEL CONTRAST AGENT FOR MAGNETIC RESONANCE IMAGING

Magnetic resonance imaging (MRI) is powerful diagnostic technique that exploits the properties of atom nuclei inside a living body (Cleary and Peters, 2010). It is a current non-invasive tool in daily clinics, allowing diagnosis to be performed in real time. An intrinsic limitation of MRI is its low sensitivity, which often compromises diagnostic quality. To overcome this disadvantage, different types of contrast agents, which are effective in shortening relaxation times of nearby protons, have been developed and used (Chopra *et al.*, 2012); among them, gadolinium (Gd) is currently used in the clinics as MRI contrast agent. Gd-based agents must always be used in chelated form due to the high toxicity of free Gd, although they are not completely free of serious risk (*e.g.*, nephrogenic systemic fibrosis may be induced; Kaewlai and Abujudeh, 2012). A promising alternative to Gd is represented by manganese (Mn) and its derivatives.

Mn is a trace element physiologically present in the human organism since it is indispensable for several metabolic pathways (*e.g.*, blood coagulation and hemostasis, blood glucose regulation, bone growth, nervous tissue function) (Wedler and Denman, 1984; Patchett *et al.*, 1991; Zwingmann *et al.*, 2004; Miao and St Clair, 2009; Horning *et al.*, 2015). Mn^{2+} is characterized by paramagnetic properties that cause a reduction in T1 relaxation times of water resulting in positive contrast enhancement *i.e.*, a 'bright' signal in T1-weighted MRI images of tissues where Mn^{2+} has accumulated. Accordingly, many Mn complexes have been investigated as alternative contrast agents for MRI (Mendonça-Dias *et al.*, 1983; Fornasiero *et al.*, 1987; Nordhoy *et al.*, 2004; Lelyveld *et al.*, 2011). Further, commercial Mn-based MRI contrast agents have been developed such as, mangafodipir trisodium (Mn-DPDP). However, Mn-based complexes easily dissociate after administration with the formation of free Mn^{2+}; exposure to excess Mn is neurotoxic, and Mn^{2+} accumulates most notably in the striatum resulting in the Mn poisoning referred to as 'manganism' (Santamaria, 2008). This suggests the need for biocompatible and thermodynamically stable Mn compounds.

Thanks to the progress in nanotechnology, Mn can be encapsulated in different types of NPs made of biocompatible materials which are expected to both limit Mn toxicity and become potential positive

contrast agents for T1-weighted MRI (Na *et al.*, 2007; Shin *et al.*, 2009; Howell *et al.*, 2013; Lee *et al.*, 2014). However, the research on Mn-based nano-contrast agents is still at a relatively early stage, and there is a paucity of investigations on *in vivo* and *in vitro* toxicity of Mn-based NPs (Li *et al.*, 2013; Xiao *et al.*, 2013; Bellusci *et al.*, 2014; Katsnelson *et al.*, 2015; Yu *et al.*, 2015).

Our group focused on NPs obtained by thermal decomposition of Mn-oleate complex and then encapsulated in a phospholipidic shell containing also a small amount of polyethylene glycol, thus improving their water solubility, stability, bioavailability and biocompatibility. These NPs are especially interesting since they gave promising results as MRI contrast agents and drug carriers (Howell *et al.*, 2013). By combining flow cytometry, confocal microscopy and transmission electron microscopy, we explored *in vitro* their cytotoxicity, internalization kinetics, intracellular distribution and degradation (Costanzo *et al.*, 2016c).

Our results confirmed the safety of these Mn-containing NPs since the viability assay did not detect alterations after both short (one hour) and long (two days) incubation times. Flow cytometry allowed monitoring the internalization kinetics of NPs: they entered the cells in a few minutes and reached the maximum internalization after one hour exposure, thus demonstrating an excellent uptake efficiency. Fluorescence microscopy and transmission electron microscopy demonstrated that Mn-containing NPs enter the cell probably by fusion with the plasma membrane (*Fig. 3a, b*), and remain free in the cytosol, without making contact with cell organelles (*Fig. 3c*). It is in fact known that the uptake of hydrophobic nanocomposite may occur by lipid raft-mediated endocytosis, a process that allows to bypass the endolytic pathway thus facilitating the intracellular permanence of the NPs (Lanza *et al.*, 2011). Interestingly, lipid rafts are typical of numerous tumor cells (Mollinedo and Gajate, 2015; Nicolson, 2015), thus opening promising perspectives for the use of Mn-containing NPs for diagnostic and therapeutic purposes.

Despite the long intracellular permanence of free Mn-containing NPs, no structural damage of cell components was detected, suggesting that the organic shell is not degraded by the cytosolic enzymes. Finally, the Mn-containing NPs undergo autophagic process, thus entering the lysosomal route and being degraded through a physiological pathway. The long-lasting intracellular per-

manence of Mn-containing NPs must be taken into account as a potential risk in the case of multiple administrations as contrast agent, but it may represent an advantage for their use as drug delivery system since it may ensure a sustained release.

Taken together, our *in vitro* data suggest that Mn-containing NPs may be promisingly considered for therapeutic and diagnostic applications *in vivo*, as drug carriers or contrast agent for MRI.

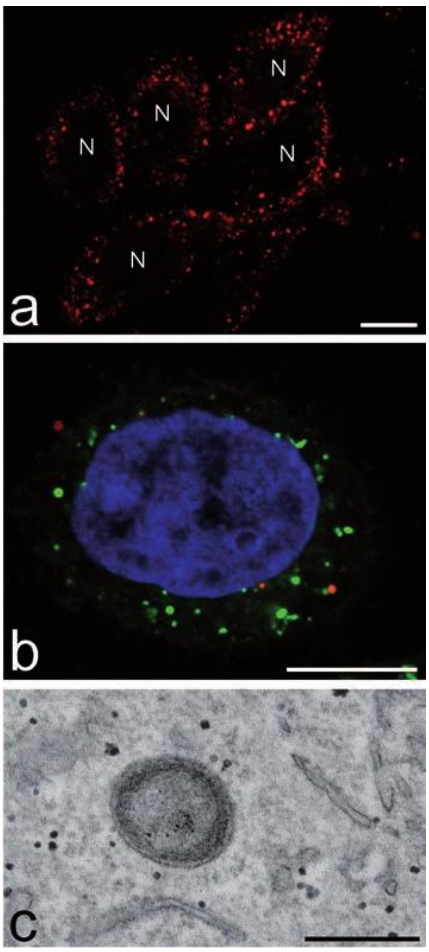

Fig. 3. a,b. Confocal fluorescence microscopy. a) Red fluorescent MnO containing-NPs are distributed in the whole cytoplasm, especially in the perinuclear region, but are absent from nudei (N). b) Cells pre-incubated with the PKH67 green-fluorescing dye to label the plasma membrane and endocytotic vesicles: the red fluorescing NPs never co-locate with green fluorescent endosomes. DNA is stained with Hoechst 33258 (blue fluorescence). Bars, 10 µm. c. Transmission electron micrograph of a MnO containing NPs showing the fine electron dense granular reaction product of diaminobenzidine photo-oxidation. Bar, 500 nm.

CONCLUSIONS

Microscopical techniques proved to be a powerful approach to investigate *in vitro* the effects of nanovectors on cell components. By brightfield and fluorescence microscopy, the uptake and distribution of NPs in the whole cell population may be described, while transmission electron microscopy provides highly-resolved images of the NP interaction with the plasma membrane and the subcellular organelles, and of the induced ultrastructural cell damage undetectable at light microscopy. Microscopical analyses are not limited to morphological observation, since the NPs can be detected in association with single molecular components visualized by cytochemical staining or immunocytochemical labelling.

It may be envisaged that this approach *in situ* will be increasingly applied to precisely elucidate the spatial and functional relationships of nanovectors with specific cell constituents in the attempt to fully understand the interaction mechanisms and the potential risks of NP administration.

ACKNOWLEDGEMENTS

We thank Prof. S. Arpicco for kindly providing us with a confocal image of MnO containing nanoparticles. F.C. is a PhD student in receipt of fellowships from the Doctoral Program in "Nanoscience and advanced technologies" of the University of Verona.

REFERENCES

Allen TD, Cronshaw JM, Bagley S, Kiseleva E, Goldberg MW. *The nuclear pore complex: mediator of translocation between nucleus and cytoplasm*. J Cell Sci 2000;113:1651-9.

Arpicco S, Lerda C, Dalla Pozza E, Costanzo C, Tsapis N, Stella B, *et al. Hyaluronic acid-coated liposomes for active targeting of gemcitabine*. Eur J Pharm Biopharm 2013;85:373-80.

Arrich J, Holzer M, Havel C, Müllner M, Herkner H. *Hypothermia for neuroprotection in adults after cardiopulmonary resuscitation.* Cochrane Database Syst Rev 2012;9:CD004128.

Bellusci M, La Barbera A, Padella F, Mancuso M, Pasquo A, Grollino MG, *et al. Biodistribution and acute toxicity of a nanofluid containing manganese iron oxide*

nanoparticles produced by a mechanochemical process. Int J Nanomedicine 2014;9:1919-29.

Bolling SF, Su TP, Childs KF, Ning XH, Horton N, Kilgore K, *et al. The use of hibernation induction triggers for cardiac transplant preservation*. Transplantation 1997;63:326-9.

Borlongan CV, Hayashi T, Oeltgen PR, Su TP, Wang Y. *Hibernation-like state induced by an opioid peptide protects against experimental stroke*. BMC Biol 2009;7:31.

Borlongan CV, Wang Y, Su TP. *Delta opioid peptide (D-Ala 2, D-Leu 5) enkephalin: linking hibernation and neuroprotection*. Front Biosci 2004;9:3392-8.

Chen Y, Chen H, Shi J. *Drug delivery/imaging multifunctionality of mesoporous silica-based composite nanostructures*. Expert Opin Drug Deliv 2014;11:917-30.

Childs-Disney JL, Hoskins J, Rzuczek SG, Thornton CA, Disney MD. *Rationally designed small molecules targeting the RNA that causes myotonic dystrophy type 1 are potently bioactive*. ACS ChemBiol 2012;7:856-62.

Chopra A, Shan L, Eckelman WC, Leung K, Latterner M, Bryant SH, *et al. Molecular Imaging and Contrast Agent Database (MICAD): evolution and progress*. Mol Imaging Biol 2012;14:4-13.

Cleary K, Peters TM. *Image-guided interventions: technology review and clinical applications*. Annu Rev Biomed Eng 2010;12:119-42.

Coonrod LA, Nakamori M, Wang W, Carrell S, Hilton CL, Bodner MJ, *et al. Reducing levels of toxic RNA with small molecules*. ACS ChemBiol 2013;8:2528-37.

Costanzo M. *Pilot studies for the treatment of sarcopenia and myotonic dystrophy: a multimodal approach.* 2016a. PhD thesis.

Costanzo M, Carton F, Marengo A, Berlier G, Stella B, Arpicco S, *et al. Fluorescence and electron microscopy to visualize the intracellular fate of nanoparticles for drug delivery*. Eur J Histochem 2016b;60:2640.

Costanzo M, Scolaro L, Berlier G, Marengo A, Grecchi S, Zancanaro C, *et al. Cell uptake and intracellular fate of phospholipidic manganese-based nanoparticles*. Int J Pharm 2016c;508:83-91.

Danhier F, Ansorena E, Silva JM, Coco R, Le Breton A, Préat V. *PLGA-based nanoparticles: An overview of biomedical applications*. J Control Release 2012;161:505-22.

Debruyne D, Leroy A, De Wever O, Vakaet L, Mareel M, Bracke M. *Direct effects of delta opioid receptor agonists on invasion-associated activities of HCT-8/E11 colon cancer cells*. Anticancer Res 2010;30:9-18.

Dougla, KL, Tabrizian M. *Effect of experimental parameters on the formation of alginate-chitosan nanoparticles and evaluation of their potential application as DNA carrier*. J Biomater Sci Polym Ed 2005;16:43-56.

El Kadib A, Bousmina M, Brunel D. *Recent progress in chitosan bio-based soft nanomaterials*. J Nanosci Nanotechnol 2014;14:308-31.

Fichna J, Janecka A. *Opioid peptides in cancer*. Cancer Metastasis Rev 2004;23:351-66.

Fornasiero D, Bellen JC, Baker RJ, Chatterton BE. *Paramagnetic complexes of manganese(II), iron(III), and gadolinium(III) as contrast agents for magnetic resonance imaging. The influence of stability constants on the biodistribution of radioactive aminopolycarboxylate complexes*. Invest Radiol 1987;22:322-7.

Förster K, Kuno A, Solenkova N, Felix SB, Krieg T. *The delta-opioid receptor agonist DADLE at reperfusion protects the heart through activation of pro-survival kinases via EGF receptor transactivation*. Am J Physiol Heart Circ Physiol 2007;293: H1604-8.

Förster K, Richter H, Alexeyev MF, Rosskopf D, Felix SB, Krieg T. *Inhibition of glycogen synthase kinase 3beta prevents peroxide-induced collapse of mitochondrial membrane potential in rat ventricular myocytes*. Clin Exp Pharmacol Physiol 2010;37:684-8.

Grottkau BE, Cai X, Wang J, Yang X, Lin Y. *Polymeric nanoparticles for a drug delivery system*. Curr Drug Metab 2013;14:840-6.

Guan M, Zhu Q, Liu Y, Bei Y-Y, Gu Z-L, Zhang X-N, *et al. Uptake and transport of a novel anticancer drug-delivery system: lactosyl-norcantharidin-associated N-trimethyl chitosan nanoparticles across intestinal Caco-2 cell monolayers*. Int J Nanomedicine 2012;7:1921-30.

Harper PS. Myotonic Dystrophy. London: WB Saunders 2001.

Harush-Frenkel O, Debotton N, Benita S, Altschuler Y. *Targeting of nanoparticles to the clathrin-mediated endocytic pathway*. Biochem Biophys Res Commun 2007;353:26-32.

Horning KJ, Caito SW, Tipps KG, Bowman AB, Aschner M. *Manganese is essential for neuronal health*. Annu Rev Nutr 2015;35:71-108.

Howell M, Mallela MJ, Wang C, Ravi S, Dixit S, Garapati U, *et al. Manganese-loaded lipid-micellar theranostics for simultaneous drug and gene delivery to lungs*. J Control Release 2013;167:210-8.

Hu L, Sun Y, Wu Y. *Advances in chitosan-based drug delivery vehicles*. Nanoscale 2013;5:3103-11.

Huang M, Ma Z, Khor E, Lim L-Y. *Uptake of FITC-chitosan nanoparticles by A549 cells*. Pharm Res 2002;19:1488-94.

Inuo H, Eguchi S, Yanaga K, Hamada T, Yamanouchi K, Okudaira S, *et al. Protective effects of a hibernation-inducer on hepatocyte injury induced by hypothermic preservation*. J Hepatobiliary Pancreat Surg 2007;14:509-13.

Jaruszewski KM, Ramakrishnan S, Poduslo JF, Kandimalla KK. *Chitosan enhances the stability and targeting of immuno-nanovehicles to cerebro-vascular deposits of Alzheimer's disease amyloid protein*. Nanomedicine 2012;8:250-60.

Kaewlai R, Abujudeh H. *Nephrogenic systemic fibrosis*. AJR Am J Roentgenol 2012;199: W17-23.

Karatas H, Aktas Y, Gursoy-Ozdemir Y, Bodur E, Yemisci M, Caban S, *et al. A nanomedicine transports a peptide caspase-3 inhibitor across the blood-brain barrier and provides neuroprotection.* J Neurosci 2009;29:13761-9.

Katsnelson BA, Minigaliyeva IA, Panov VG, Privalova LI, Varaksin AN, Gurvich VB, *et al. Some patterns of metallic nanoparticles' combined subchronic toxicity as exemplified by a combination of nickel and manganese oxide nanoparticles*. Food Chem Toxicol 2015;86:351-64.

Kono H, Kimura Y, Latz, E. *Inflammasome activation in response to dead cells and their metabolites*. Curr Opin Immunol 2014;30:91-8.

Koping-Hoggard M, Varum KM, Issa M, Danielsen S, Christensen BE, Stokke BT, *et al. Improved chitosan-mediated gene delivery based on easily dissociated chitosan polyplexes of highly defined chitosan oligomers*. Gene Ther 2004;11:1441-52.

Kumar MNVR, Muzzarelli RAA, Muzzarelli C, Sashiwa H, Domb AJ. *Chitosan chemistry and pharmaceutical perspectives*. Chem Rev 2004;104:6017-84.

Labokha AA, Fassati A. *Viruses challenge selectivity barrier of nuclear pores*. Viruses 2013;5:2410-23.

Lai WF, Lin MC. *Nucleic acid delivery with chitosan and its derivatives*. J Control Release 2009;134:158-68.

Lanza R, Langer R, Vacanti JP. Principles of tissue engineering. New York: Academic Press 2011.

Lee JE, Bennett CF, Cooper TA. *RNase H-mediated degradation of toxic RNA in myotonic dystrophy type 1.* Proc Natl Acad Sci U S A 2012;109:4221-6.

Lee MM, Pushechnikov A, Disney MD. *Rational and modular design of potent ligands targeting the RNA that causes myotonic dystrophy 2*. ACS Chem Biol 2009;4:345-55.

Lee SH, Kim BH, Na HB, Hyeon T. *Paramagnetic inorganic nanoparticles as T-1 MRI contrast agents*. WIRES Nanomed Nanobi 2014;6:196-209.

Lelyveld VS, Brustad E, Arnold FH, Jasanoff A. *Metal-substituted protein MRI contrast agents engineered for enhanced relaxivity and ligand sensitivity*. J Am Chem Soc 2011;133:649-51.

Li J, Hu Y, Yang J, Wei P, Sun W, Shen M, *et al. Hyaluronic acid-modified Fe3O4@Au core/shell nanostars for multimodal imaging and photothermal therapy of tumors*. Biomaterials 2015;38:10-21.

Li J, Zhao Z, Feng J, Gao J, Chen Z. *Understanding the metabolic fate and assessing the biosafety of MnO nanoparticles by metabonomic analysis*. Nanotechnology 2013;24:455102.

Lince F, Bolognesi S, Stella B, Marchisio DL, Dosio F. *Preparation of polymer nanoparticles loaded with doxorubicin for controlled drug delivery*. Chem Eng Res Des 2011;89:2410-9.

Luo Y, Wang Q. *Recent development of chitosan-based polyelectrolyte complexes with natural polysaccharides for drug delivery*. Int J Biol Macromol 2014;64:353-67.

Ma Z, Lim L-Y. *Uptake of chitosan and associated insulin in Caco-2 cell monolayers: a comparison between chitosan molecules and chitosan nanoparticles*. Pharm Res 2003;20:1812-9.

Malatesta M, Biggiogera M, Zancanaro C. *Hypometabolic induced state: a potential tool in biomedicine and space exploration*. Rev Environ Sci Biotechnol 2007;6:47-60.

Malatesta M, Galimberti V, Cisterna B, Costanzo M, Biggiogera M, Zancanaro C. *Chitosan nanoparticles are efficient carriers for delivering biodegradable drugs to neuronal cells*. Histochem Cell Biol 2013a;141:551-8.

Malatesta M, Giagnacovo M, Costanzo M, Conti B, Genta I, Dorati R, *et al. Diaminobenzidine photoconversion is a suitable tool for tracking the intracellular location of fluorescently labelled nanoparticles at transmission electron microscopy*. Eur J Histochem 2012;56:e20.

Malatesta M, Grecchi S, Chiesa E, Cisterna B, Costanzo M, Zancanaro C. *Internalized*

chitosan nanoparticles persist for long time in cultured cells. Eur J Histochem 2015;59:2492.

Malatesta M, Pellicciari C, Cisterna B, Costanzo M, Galimberti V, Biggiogera M, *et al. Tracing nanoparticles and photosensitizing molecules at transmission electron microscopy by diaminobenzidine photo-oxidation*. Micron 2014;59C:44-51.

Malatesta M, Zancanaro C, Costanzo M, Cisterna B, Pellicciari C. *Simultaneous ultrastructural analysis of fluorochrome-photoconverted diaminobenzidine and gold immunolabelling in cultured cells*. Eur J Histochem 2013b;57:e26.

Maranto AR. *Neuronal mapping: a photooxidation reaction makes Lucifer yellow useful for electron microscopy*. Science 1982;217:953-5.

Mendonça-Dias MH, Gaggelli E, Lauterbur PC. *Paramagnetic contrast agents in nuclear magnetic resonance medical imaging*. Semin Nucl Med 1983;13:364-76.

Meola G, Cardani R. *Myotonic dystrophies: An update on clinical aspects, genetic, pathology, and molecular pathomechanisms*. Biochim Biophys Acta 2015;1852:594-606.

Miao L, St Clair DK. *Regulation of superoxide dismutase genes: implications in disease*. Free Radical Bio Med 2009;47:344-56.

Mollinedo F, Gajate C. *Lipid rafts as major platforms for signaling regulation in cancer*. Adv Biol Regul 2015;57:130-46.

Na HB, Lee J, An HK, Park YI, Park M, Lee IS, *et al. Development of a T1 contrast agent for magnetic resonance imaging using MnO nanoparticles*. Angew Chem Int Ed Engl 2007;46:5397-5401.

Nazarenus M, Zhang Q, Soliman MG, del Pino P, Pelaz B, Carregal-Romero S, *et al. In vitro* interaction of colloidal nanoparticles with mammalian cells: What have we learned thus far? Beilstein J Nanotechnol 2014;5:1477-90.

Nguyen L, Lee JY, Wong CH, Zimmerman SC. *Small Molecules that Target the Toxic RNA in Myotonic Dystrophy Type 2.* Chem Med Chem 2014;9:2455-62.

Nguyen L, Luu LM, Peng S, Serrano JF, Edwin Chan HY, Zimmerman SC. *Rationally designed small molecules that target both the dna and rna causing myotonic dystrophy type 1*. J Am Chem Soc 2015;137:14180-9.

Nicolson GL. *Cell membrane fluid-mosaic structure and cancer metastasis*. Cancer Res 2015;75:1169-76.

Nordhoy W, Anthonsen HW, Bruvold M, Brurok H, Skarra S, Krane J, *et al. Intracellular manganese ions provide strong T1 relaxation in rat myocardium*. Magn Reson Med 2004;52:506-14.

Oeltgen PR, Horton ND, Bolling SF, Su TP. *Extended lung preservation with the use of hibernation trigger factors*. Ann Thorac Surg 1996;61:1488-93.

Oeltgen PR, Nuchols PA, Nilekani WA, Spurrier WA, Su TP. *Further studies on opioids and hibernation: delta opioid receptor ligand selectively induced hibernation in summer active ground squirrels*. Life Sci 1988;43:1565-74.

Pandey SK, Wheeler TM, Justice SL, Kim A, Younis HS, Gattis D, *et al. Identification and characterization of modified antisense oligonucleotides targeting DMPK in mice and nonhuman primates for the treatment of myotonic dystrophy type 1.* J Pharmacol Exp Ther 2015;355:329-40.

Panyam J, Zhou WZ, Prabha S, Sahoo SK, Labhasetwar V. *Rapid endolysosomal escape*

of poly(DL-lactide-coglycolide) nanoparticles: implications for drug and gene delivery. FASEB J 2002;16:1217-26.

Park S, Lee SJ, Chung H, Her S, Choi Y, Kim K, *et al. Cellular uptake pathway and drug release characteristics of drug-encapsulated glycol chitosan nanoparticles in live cells*. Microsc Res Tech 2010;73:857-65.

Parkesh R, Childs-Disney JL, Nakamori M, Kumar A, Wang E, Wang T, *et al. Design of a bioactive small molecule that targets the myotonic dystrophy type 1 RNA via an RNA motif-ligand database and chemical similarity searching*. J Am Chem Soc 2012;134:4731-42.

Patchett ML, Daniel RM, Morgan HW. *Characterisation of arginase from the extreme thermophile Bacillus caldovelox*. Biochim Biophys Acta 1991;1077:291-8.

Pedrini I, Gazzano E, Chegaev K, Rolando B, Marengo A, Kopecka J, *et al. Liposomal nitrooxy-doxorubicin: one step over Caelyx® in drug-resistant human cancer cells*. Mol Pharm 2014;11:3068-79.

Peng J, He X, Wang K, Tan W, Li H, Xing X, *et al. An antisense oligonudeotide carrier based on amino silica nanoparticles for antisense inhibition of cancer cells*. Nanomedicine 2006;2:113-20.

Peppas NA, Huang Y. *Nanoscale technology of mucoadhesive interactions*. Adv Drug Deliv Rev 2004;56:1675-87.

Rock KL, Kono H. *The inflammatory response to cell death*. Annu. Rev. Pathol. 2008;3:99-126.

Romano MA, McNish R, Seymour EM, Traynor JR, Bolling SF. *Differential effects of opioid peptides on myocardial ischemic tolerance*. J Surg Res 2004;119:46-50.

Santamaria AB. *Manganese exposure, essentiality and toxicity*. Indian J Med Res 2008;128:484-500.

Sapino S, Ugazio E, Gastaldi L, Miletto I, Berlier G, Zonari D, *et al. Mesoporous silica as topical nanocarriers for quercetin: characterization and in vitro studies*. Eur J Pharm Biopharm 2015;89:116-25.

Schipper NGM, Olsson S, Hoogstraate JA, deBoer AG, Varum KM, Artursson P. *Chitosans as absorption enhancers for poorly absorbable drugs 2: mechanism of absorption enhancement*. Pharm Res 1997;14:923-9.

Serda RE, Mack A, van de Ven AL, Ferrati S, Dunner K Jr, Godin B, *et al. Logic-embedded vectors for intracellular partitioning, endosomal escape, and exocytosis of nanoparticles*. Small 2010;6:2691-700.

Shibanoki S, Weinberger SB, Beniston D, Nudelman KA, Schulteis G, Bennett EL, *et al. Hydrolysis of [Leu]enkephalin by chick plasma in vitro*. J Pharmacol Exp Ther 1991;256:650-5.

Shin J, Anisur RM, Ko MK, Im GH, Lee JH, Lee IS. *Hollow manganese oxide nanoparticles as multifunctional agents for magnetic resonance imaging and drug delivery.* Angew Chem Int Ed Engl 2009;48:321-4.

Siboni RB, Nakamori M, Wagner SD, Daniel MC, Matthew KT, Berglund JA. *Actinomycin D specifically reduces expanded CUG repeat RNA in myotonic dystrophy models*. Cell Rep 2015;13:2386-94.

Songjiang Z, Lixiang W. *Amyloid-Beta associated with chitosan nano-carrier has favor-*

able immunogenicity and permeates the BBB. AAPS PharmSciTech 2009; 10:900-5.

Stella B, Arpicco S, Peracchia MT, Desmaële D, Hoebeke J, Renoir JM, *et al. Design of folic acid-conjugated nanoparticles for drug targeting*. J Pharm Sci 2000;89:1452-64.

Stella B, Arpicco S, Rocco F, Marsaud V, Renoir JM, Cattel L, *et al. Encapsulation of gemcitabine lipophilic derivatives into polycyanoacrylate nanospheres and nanocapsules*. Int J Pharm 2007a;344:71-7.

Stella B, Marsaud V, Arpicco S, Géraud G, Cattel L, Couvreur P, *et al. Biological characterization of folic acid-conjugated poly(H2NPEGCA-co-HDCA) nanoparticles in cellular models*. J Drug Target 2007b;15:146-53.

Su DS, Wang ZH, Zheng YJ, Zhao YH, Wang XR. *Dose-dependent neuroprotection of delta opioid peptide [D-Ala2, D-Leu5] enkephalin in neuronal death and retarded behavior induced by forebrain ischemia in rats*. Neurosci Lett 2007;423:113-7.

Su TP. *Delta opioid peptide[D-Ala(2),D- Leu(5)]enkephalin promotes cell survival.* J Biomed Sci 2000;7:195-9.

Tisherman SA (Moderator); Ornato JP, Peberdy MN, Tisherman SA (Participants). *Managing hypothermia during organ transplantation and cardiac arrest*. Ther Hypothermia Temp Manag 2013;3:7-10.

Tsai SY, Lee CT, Hayashi T, Freed WJ, Su TP. *Delta opioid peptide DADLE and naltrexone cause cell cycle arrest and differentiation in a CNS neural progenitor cell line*. Synapse 2010;64:267-73.

Wang S, Duan Y, Su D, Li W, Tan J, Yang D, *et al. Delta opioid peptide [d-Ala2, d-Leu5] enkephalin (DADLE) triggers postconditioning against transient forebrain ischemia*. Eur J Pharmacol 2011;658:140-4.

Wang ZH, Wang ZY, Sun CS, Wang CY, Jiang TY, Wang SL. *Trimethylated chitosan-conjugated PLGA nanoparticles for the delivery of drugs to the brain.* Biomaterials 2010;31:908-15.

Warf MB, Nakamori M, Matthys CM, Thornton CA, Berglund JA. *Pentamidine reverses the splicing defects associated with myotonic dystrophy*. Proc Natl Acad Sci USA 2009;106:18551-6.

Wedler FC, Denman RB. *Glutamine synthetase: the major Mn(II) enzyme in mammalian brain*. Curr Top Cell Regul 1984;24:153-69.

Wheeler TM, Leger AJ, Pandey SK, MacLeod AR, Nakamori M, Cheng SH, *et al. Targeting nuclear RNA for in vivo correction of myotonic dystrophy*. Nature 2012;488:111-5.

Wong CH, Fu Y, Ramisetty SR, Baranger AM, Zimmerman SC. *Selective inhibition of MBNL1-CCUG interaction by small molecules toward potential therapeutic agents for myotonic dystrophy type 2 (DM2).* Nucleic Acids Res 2011;39:8881-90.

Xiao J, Tian XM, Yang C, Liu P, Luo NQ, Liang Y, *et al. Ultrahigh relaxivity and safe probes of manganese oxide nanoparticles for in vivo imaging*. Sci Rep 2013; 3:3424.

Yan TD, Bannon PG, Bavaria J, Coselli JS, Elefteriades JA, Griepp RB, *et al. Consensus on hypothermia in aortic arch surgery*. Ann Cardiothorac Surg 2013;2:163-8.

Yao LL, Wang YG, Cai WJ, Yao T, Zhu YC. *Survivin mediates the anti-apoptotic effect*

of delta-opioid receptor stimulation in cardiomyocytes. J Cell Sci 2007;120(Pt 5):895-907.

Yu C, Zhou Z, Wang J, Sun J, Liu W, Sun Y, *et al. In depth analysis of apoptosis induced by silica coated manganese oxide nanoparticles in vitro.* J Hazard Mater 2015; 283:519-28.

Yu M, Jambhrunkar S, Thorn P, Chen J, Gu W, Yu C. *Hyaluronic acid modified mesoporous silica nanoparticles for target drug delivery to CD44-overexpressing cancer cells*. Nanoscale 2013;5:178-83.

Zaki NM, Nasti A, Tirelli N. *Nanocarriers for cytoplasmic delivery: cellular uptake and intracellular fate of chitosan and hyaluronic acid-coated chitosan nanoparticles in a phagocytic cell model*. Macromol Biosci 2011;11:1747-60.

Zwingmann C, Leibfritz D, Hazell AS. *Brain energy metabolism in a sub-acute rat model of manganese neurotoxicity: an ex vivo nuclear magnetic resonance study using [1-13C]glucose*. Neurotoxicology 2004;25:573-87.

M. Costanzo, F. Carton, M. Malatesta (2017b): Microscopy techniques in nanomedical research. Microscopie 27:66-71, DOI: 10.4081/microscopie.2017.6732.

Microscopy techniques in nanomedical research

Manuela Costanzo, Flavia Carton, Manuela Malatesta

Department of Neurosciences, Biomedicine and Movement Sciences, Section of Anatomy and Histology, University of Verona, Italy

Corresponding author: Manuela Malatesta
Department of Neurosciences, Biomedicine and Movement Sciences, Section of Anatomy and Histology, University of Verona
Strada Le Grazie 8, I-37134 Verona, Italy
Tel. +39.045.8027569
E-mail: manuela.malatesta@univr.it

Summary
In recent years, the application of nanotechnology to biomedicine has been exponentially increasing. The physical and chemical properties, quality and safety of nanomaterials designed for biomedical application need to be accurately evaluated by means of reliable and robust techniques. Among the methods used, microscopy techniques play a primary role. This paper presents a brief overview of the contribution of different microscopy techniques to the study of the structural and functional aspects of nanoconstructs and their relationships with the biological milieu, demonstrating the great impact that microscopy sciences have in nanomedical research and applications.

Key words: electron microscopy, fluorescence microscopy, nanomedicine, nanoparticles.

Introduction

In recent years, the application of nanotechnology to biomedicine for the development of e.g. new drug delivery systems, diagnostic tools, sorting systems, scaffold components (Lim *et al.*, 2010; Bobo *et al.*, 2016; Fernandes *et al.*, 2016; Soica *et al.*, 2016) has been exponentially increasing. Understanding the structure of nanocomposites is crucial to elucidate their physical and chemical properties, quality and safety, as well as their distribution and behavior *in vivo*. All these features, in fact, strongly affect the efficiency of nanoconstructs in the living organism, from the molecular to the systemic level. It is therefore essential to perform accurate studies by means of reliable and robust techniques. Among the methods used for evaluating the structural and functional aspects of nanoconstructs and their relationships with the biological milieu, microscopy techniques play a primary role. This paper presents a brief overview of the contribution of different microscopy techniques to the development of nanomedicine.

Microscopy to characterize nanoconstructs for biomedical application

A wide variety of analytical methods have been used for evaluating the physico-chemical characteristics of manufactured nanomaterials (for a review, see Lin *et al.*, 2014): these include chromatography, electrophoresis, magnetic resonance, X-ray scattering and spectroscopy, mass spectrometry, circular dichroism spectroscopy, zeta-potential measurements, as well as techniques of microscopy on which the present article will especially be focused.

In fact, transmission electron microscopy (TEM) is one of the most efficient tools for the characterization of nanomaterials. TEM provides high resolution of minute structural details, which is essential, for instance, to obtain information about the crystalline structure and granularity of the nanoparticles (Williams and Carter, 2009). Through TEM it is also possible to detect alterations in nanoparticle morphology due to the incorporation of drugs at different concentrations, thus representing an indispensable technique for the development of drug delivery systems (Govender *et al.*, 2000). To be suitable for observation at TEM, nanomaterials usually need to be dehydrated, but it is also possible to freeze them (cryo-TEM), thus better preserving their original morphology (Williams and Carter, 2009). Although TEM provide 2D images, the technique of electron tomography can be used to create 3D images using a sequence of micrographs taken at different tilts (Williams and Carter, 2009).

Scanning electron microscopy (SEM) uses electrons for high resolution imaging of the sample surface (Reimer, 2000), and represents a valid tool to investigate some nanomaterials (Bogner *et al.*, 2005). The topography of the nanostructured samples can be preserved using special techniques that avoid any manipulation (environmental or wet SEM) or pre-

serve their morphology by rapid freezing (cryo-SEM). The environmental SEM, allowing analyses on hydrated materials without fixing, drying, freezing or coating the specimen (Bogner *et al.*, 2005), is especially suitable to characterize microspheres and microcapsules (Xiong *et al.* 2012). Cryo-SEM method has been applied for the characterization of microspheres (Allan-Wojtas *et al.*, 2008) and nanoemulsions (Hoesli *et al.*, 2012).

Polarized light microscopy (PLM) may be used for the preliminary identification of many liquid-crystalline structures (Gaisin *et al.*, 2010). The anisotropic systems cause a deviation in the plane of polarized light and show typical black and white or colored textures. Based on this texture, liquid-crystalline structures can be classified in: (i) lamellar liquid crystalline phase which reveals oily streaks with inserted "maltese crosses" in the micrograph; (ii) hexagonal liquid-crystalline structure which is indicated by a fanlike texture (Müller-Goymann, 2004; Carvalho *et al.*, 2010; Rissi *et al.*, 2014). However, PLM can be applied to particles whose size approaches the wavelength of visible light (400 to 700 nm); for liquid crystal particles presenting smaller dimensions, TEM is necessary to resolve them (Müller-Goymann, 2004).

Atomic force microscopy (AFM) is one of the most popular scanning probe microscopy methods (Binning *et al.*, 1986) and the interaction of nanoparticles with the AFM probe has been extensively studied from different experimental points of view (AFM tip modification, nanoparticle manipulation, substrate influence) (Theil Hansen *et al.* 1998; Lee *et al.*, 1998; Klapetek *et al.*, 2011; Henry, 2005). AFM allows detection and imaging of nanoparticles from 0.5 nm in diameter and, although it has been mostly applied to inorganic nanoconstructs, it is also suitable to characterize hydrated nanomaterials.

Microscopy for visualizing nanoconstructs in living organisms

To be used in nanobiology and nanomedicine, nanoconstructs need to be tested in living organisms. Cells cultured *in vitro*, which ensures simple and controlled conditions, represent the experimental model of choice. The preliminary utilization of *in vitro* systems also allows short experimental times and reduction of the number of laboratory animals for the following *in vivo* studies, thus implying a significant decrease of the research costs.

Light microscopy has been largely applied for the safety assessment of nanomaterials and for designing efficient administration strategies for biomedical use. Microscopy techniques proved to be useful to study the interaction of nanoparticles with the cells and to visualize their intracellular fate, while allowing to simultaneously evaluate signs of cell damage or death (for a review, see Ostrowski *et al.*, 2015).

By definition, nanoparticle are less than 100 nm in size and cannot be resolved as single entities even at the highest magnification in conventional light microscopy. Thus, only nanoparticulates that form clusters or aggregates of more than 200 nm in size can directly be visualized in single cells or tissues. Depending on their chemical composition, some nanoconstructs (e.g., carbon nanotubes, iron oxide or titanium dioxide nanoparticles) can be directly observed as naturally colored deposits (Porter *et al.*, 2010; van Landeghem *et al.*, 2009; Adachi *et al.*, 2010). Enhanced darkfield microscopy has also been used to detect metal oxide nanoparticles in histological samples (Roth *et al.*, 2015). In addition, some histochemical techniques are suitable to stain either inorganic or organic nanoparticles; Prussian blue may be used to stain iron containing nanoconstructs (Bumb *et al.*, 2011 and Figure 1a) while nanoparticles con-

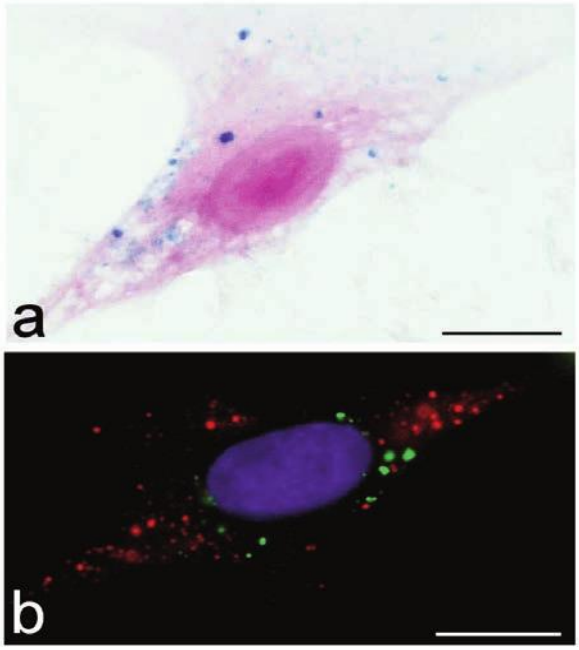

Figure 1. a) Brightfield microscopy. Iron oxide nanoparticles (Prussian blue staining) inside a murine fibroblast (hematoxylin countestaining). b) Fluorescence microscopy. Chitosan nanoparticles (green) inside a human epithelial cell; lysosomes (red) are visualized by specific immunostaining; DNA (blue) is stained with Hoechst 33258. Bars: 20 μm.

taining polysaccharide with negatively charged sulfate groups have been successfully visualized by Alcian blue staining (Holzhausen *et al.*, 2013).

No doubt, fluorescence microscopy is the most widely used approach to investigate the biodistribution and the intracellular localization of nanoconstructs at light microscopy. To this purpose, nanoparticles are usually labelled with fluorochromes (Figure 1b), which must be selected for their structure, molecular weight and charge not to alter the physicochemical characteristics of nanoconstructs.

The interaction of fluorochrome-conjugated nanoparticles with specific cells or intracellular organelles may be visualized by the simultaneous immunofluorescence labelling of marker proteins (Cho *et al.*, 2009; Malatesta *et al.*, 2015 and Figure 1b). A more precise spatial localization of nanoparticles in their interactions with cells may be obtained by confocal laser scanning microscopy: by this technique, serial optical sectioning of the sample are obtained, which allows 3D reconstructions of single cells or tissues sections. However, confocal microscopy is diffraction-limited as much as conventional fluorescence microscopy, so that the X-Y resolution is restricted to about 200 nm, substantially larger than the <100 nm size of nanoparticles. Techniques of super-resolution light microscopy may overcome this limitation, allowing to significantly increase X-Y resolution up to about 30 nm (Willig *et al.*, 2006; Sonnefraud *et al.*, 2014; Guggenheim *et al.*, 2016).

TEM, thanks to its higher resolution, is however the most appropriate approach to obtain detailed and unequivocal information on each step of nanoconstruct interactions with the cell components, from their uptake at the cell surface to their intracellular degradation (Figure 2). A clear analysis of nanoparticle internalization mechanism(s) can be

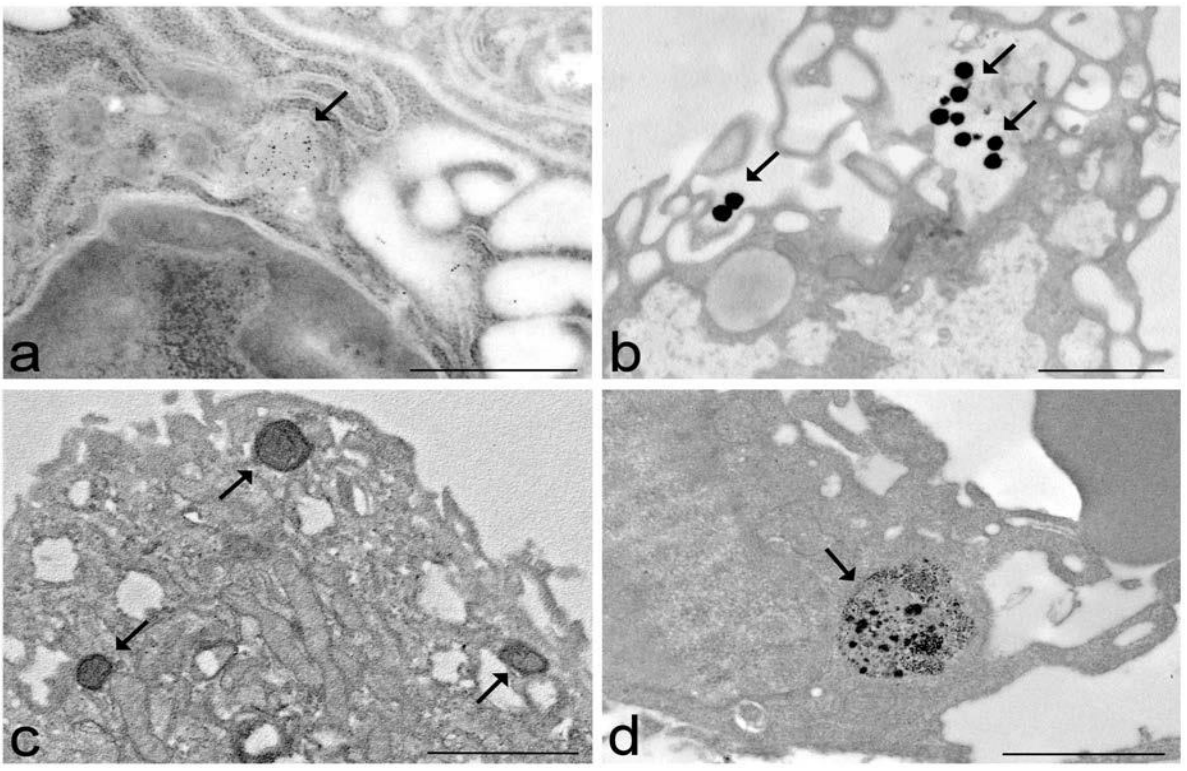

Figure 2. Transmission electron microscopy. a) Gold nanoparticles (arrow) internalized in a human macrophage. b) Lipid nanoparticles (arrows) entering a human epithelial cell. c) Polymeric nanoparticles (arrows) in a human myoblast. d) Quantum dots (arrow) inside a murine macrophage. Bars: a,c 200 nm; b,d 1000 nm.

obtained, visualizing the contact with the plasma membrane and the passage into the cell by endocytosis, phagocytosis or membrane fusion (as in the case of nanoconstructs of lipid nature) (e.g., Zhang *et al.*, 2011; Malatesta *et al.*, 2012; Costanzo *et al.*, 2016a,b; Boyles *et al.*, 2015; Poussard *et al.*, 2015; Lopes *et al.*, 2016; Messerschmidt *et al.*, 2016; Zielinska *et al.*, 2016). The distribution of the nanoparticulates in the cellular compartments provides information on their fate: the entrapment into endosomes or phagosomes prefigures their rapid degradation in the lysosomal compartment, while their free (organelle-unbound) occurrence in the cytosol indicates their ability to escape endosomes and, consequently, the enzymatic lysis (Panyam *et al.*, 2002; Varkouhi *et al.* 2011). However, TEM observations revealed that these free nanoparticles may re-enter the lytic pathway by autophagosomal processes (Costanzo *et al.*, 2016a,b). Importantly, TEM allows to distinguish the presence of intact nanoparticles or their remnants after enzymatic lysis, thus providing unequivocal information on their biodegradability. TEM can also provide clear evidence for the distribution of nanoparticulates inside the cell nucleus: some nanoparticles may, in fact, enter the nucleus by passing through the nuclear pores or being entrapped therein at the end of mitosis (Nabiev *et al.*, 2007; Colonna *et al.*, 2011; Guan *et al.*, 2012; Malatesta *et al.*, 2013, 2015; Zhang *et al.*, 2015). This is a crucial information for evaluating the safety of nanoconstructs, since the persistence of exogenous materials in close proximity of nucleic acids may have unpredictable consequences on whole cell activity.

An important contribution to nanomedical research has been given also by correlative microscopy. Light (especially fluorescence) microscopy was combined with advanced TEM methods (conventional, immuno and energy-filtered electron microscopy, and electron tomography) to analyze the biodistribution of different types of nanoparticles (Mühlfeld *et al.*, 2007). Quantum dots were identified in *in vitro* and *ex vivo* samples by combining fluorescence microscopy, TEM and scanning transmission electron microscopy (STEM) (Dukes *et al.*, 2010; Killingsworth and Bobryshev, 2016), and the combination of TEM and Serial Block Face SEM allowed to quantify their intracellular uptake (Hondow *et al.*, 2016). The intracellular distribution of gold nanoparticles was investigated by using interferometric photo-activated localization microscopy and electron microscopy (Shtengel *et al.*, 2014), while their identification inside tumor masses was performed by combining optical microscopy and SEM (Kempen *et al.*, 2015). The uptake and intracellular fate of ZnO-based nanoparticles were analyzed combining dynamic confocal imaging, low resolution bright field TEM and dark field STEM (Othman *et al.*, 2016). Cryo-soft X-ray tomography was used to obtain three-dimensional information on the interaction of super-paramagnetic iron oxide nanoparticles with cancer cells (Chiappi *et al.*, 2016). Fluorescence microscopy and SEM were combined to investigate macrophage uptake of cylindrical nanoparticles (Tscheka *et al.*, 2015).

Concluding remarks

In the last 15 years, more than 190,000 articles have been published in qualified journals on nanoparticles, (source: Scopus database, https://www.scopus.com), and in about 57,000 papers of these, microscopy techniques were used among the experimental methods. This clearly indicates the great impact that microscopy sciences have in nanomedical research and applications. It is easy to foresee that this will even increase in the years to come, thanks to the continuous progress in microscopy technology and instrumentation. TEM still is the most informative approach for investigating the interaction of nanoconstructs with cells and intracellular organelles, but super-resolution light microscopy may be envisaged as the future in the field: multicolor histochemical techniques will allow to simultaneously detect the interactions of nanoparticles with several subcellular components at the nanodimension of super-resolved fluorescence microscopy.

Acknowledgements

We thank Prof. A. Sbarbati for kindly providing us with an image of iron oxide nanoparticles. F.C. is a PhD student in receipt of fellowship from the Doctoral Program in "Nanoscience and advanced technologies" of the University of Verona.

References

Adachi K, Yamada N, Yamamoto K, Yoshida Y, Yamamoto O. In vivo effect of industrial titanium dioxide nanoparticles experimentally exposed to hairless rat skin. Nanotoxicology 2010;4:296-306.

Allan-Wojtas P, Hansen LT, Paulson AT. Microstructural studies of probiotic bacteria-loaded alginate microcapsules using standard electron microscopy techniques and anhydrous fixation. LWT-Food Sci Technol 2008;41:101-8.

Binning G, Quate CF, Gerber C. Atomic force microscope. Phys Rev Lett 1986;56:930-3.

Bobo D, Robinson KJ, Islam J, Thurecht KJ, Corrie SR. Nanoparticle-based medicines: a review of FDA-approved materials and clinical trials to date. Pharm Res 2016;33:2373-87.

Bogner A, Thollet G, Basset D, Jouneau PH, Gauthier C. Wet STEM: A new development in environmental SEM for imaging nano-objects included in a liquid phase. Ultramicroscopy 2005;104:290-301.

Boyles MS, Kristl T, Andosch A, Zimmermann M, Tran N, Casals E, et al. Chitosan functionalisation of gold nanoparticles encourages particle uptake and induces cytotoxicity and pro-inflammatory conditions in phagocytic cells, as well as enhancing particle interactions with serum components. J Nanobiotechnology 2015;13:84.

Bumb A, Regino CA, Egen JG, Bernardo M, Dobson PJ, Germain RN, et al. Trafficking of a dual-modality magnetic resonance and fluorescence imaging superparamagnetic iron oxide-based nanoprobe to lymph nodes. Mol Imaging Biol 2011;13:1163-72.

Carvalho FC, Sarmento VHV, Chiavacci LA, Barbi MS, Gremião MPD. Development and in vitro evaluation of surfactant systems for controlled release of zidovudine. J Pharm Sci 2010;99:2367-74.

Chiappi M, Conesa JJ, Pereiro E, Sorzano CO, Rodríguez MJ, Henzler K, et al. Cryo-soft X-ray tomography as a quantitative three-dimensional tool to model nanoparticle:cell interaction. J Nanobiotechnology 2016;14:15.

Cho M, Cho WS, Choi M, Kim SJ, Han BS, Kim SH, et al. The impact of size on tissue distribution and elimination by single intravenous injection of silica nanoparticles. Toxicol Lett 2009;189:177-83.

Colonna C, Dorati R, Conti B, Modena T, Biggiogera M, Spedito A, et al. Induction of an in vitro reversible hypometabolism through chitosan-based nanoparticles. J Microencapsul 2011;28:229-39.

Costanzo M, Carton F, Marengo A, Berlier G, Stella B, Arpicco S, et al. Fluorescence and electron microscopy to visualize the intracellular fate of nanoparticles for drug delivery. Eur J Histochem 2016a;60:2640.

Costanzo M, Scolaro L, Berlier G, Marengo A, Grecchi S, Zancanaro C, et al. Cell uptake and intracellular fate of phospholipidic manganese-based nanoparticles. Int J Pharm 2016b;508:83-91.

Dukes MJ, Peckys DB, de Jonge N. Correlative fluorescence microscopy and scanning transmission electron microscopy of quantum-dot-labeled proteins in whole cells in liquid. ACS Nano 2010;4:4110-6.

Fernandes RS, Dos Santos Ferreira D, de Aguiar Ferreira C, Giammarile F, Rubello D, de Barros AL. Development of imaging probes for bone cancer in animal models. A systematic review. Biomed Pharmacother 2016;83:1253-64.

Gaisin N, Gnezdilov O, Pashirova T, Zhil'tsova EP, Lukashenko SS, Zakharova LYa, et al. Micellar and liquid-crystalline properties of bicyclic fragment-containing cationic surfactant. Colloid J 2010;72:764-70.

Govender T, Riley T, Ehtezazi T, Garnett MC, Stolnik S, Illum L, et al. Defining the drug incorporation properties of PLA–PEG nanoparticles. Int J Pharm 2000;199:95-110.

Guan M, Zhu Q, Liu Y, Bei Y-Y, Gu Z-L, Zhang X-N, et al. Uptake and transport of a novel anticancer drug-delivery system: lactosyl-norcantharidin-associated N-trimethyl chitosan nanoparticles across intestinal Caco-2 cell monolayers. Int J Nanomedicine 2012;7:1921-30.

Guggenheim EJ, Khan A, Pike J, Chang L, Lynch I, Rappoport JZ. Comparison of confocal and super-resolution reflectance imaging of metal oxide nanoparticles. PLoS One 2016;11:e0159980.

Henry CR. Morphology of supported nanoparticles. Prog Surf Sci 2005;80:92.

Hoesli CA, Kiang RLJ, Mocinecová D, Speck M, Mošková DJ, Donald-Hague C, et al. Reversal of diabetes by βTC3 cells encapsulated in alginate beads generated by emulsion and internal gelation. J Biomed Mater Res B Appl Biomater 2012;100:1017-28.

Holzhausen C, Gröger D, Mundhenk L, Welker P, Haag R, Gruber AD. Tissue and cellular localization of nanoparticles using ^{35}S labeling and light microscopic autoradiography. Nanomedicine 2013;9:465-8

Hondow N, Brown MR, Starborg T, Monteith AG, Brydson R, Summers HD, et al. Quantifying the cellular uptake of semiconductor quantum dot nanoparticles by analytical electron microscopy. J Microsc 2016;261:167-76.

Kempen PJ, Kircher MF, de la Zerda A, Zavaleta CL, Jokerst JV, Mellinghoff IK, et al. A correlative optical microscopy and scanning electron microscopy approach to locating nanoparticles in brain tumors. Micron 2015;68:70-6.

Killingsworth MC, Bobryshev YV. Correlative light- and electron microscopy using quantum dot nanoparticles. J Vis Exp 2016:114.

Klapetek P, Valtr M, Nečas D, Salyk O, Dzik P. Atomic force microscopy analysis of nanoparticles in non-ideal conditions. Nanoscale Res Lett. 2011;6:514.

Lee I, Chan KY, Phillips DL. Atomic force microscopy of platinum nanoparticles prepared on highly oriented pyrolytic graphite. Ultramicroscopy 1998;75:69.

Lim CT, Han J, Guck J, Espinosa H. Micro and nanotechnology for biological and biomedical applications. Med Biol Eng Comput 2010;48:941-3.

Lin PC, Lin S, Wang PC, Sridhar R. Techniques for physicochemical characterization of nanomaterials. Biotechnol Adv 2014;32:711-26.

Lopes VR, Loitto V, Audinot JN, Bayat N, Gutleb AC, Cristobal

S. Dose-dependent autophagic effect of titanium dioxide nanoparticles in human HaCaT cells at non-cytotoxic levels. J Nanobiotechnology 2016;14:22.
Malatesta M, Galimberti V, Cisterna B, Costanzo M, Biggiogera M, Zancanaro C. Chitosan nanoparticles are efficient carriers for delivering biodegradable drugs to neuronal cells. Histochem Cell Biol 2013;141:551-8.
Malatesta M, Giagnacovo M, Costanzo M, Conti B, Genta I, Dorati R, et al. Diaminobenzidine photoconversion is a suitable tool for tracking the intracellular location of fluorescently labelled nanoparticles at transmission electron microscopy. Eur J Histochem 2012;56:e20.
Malatesta M, Grecchi S, Chiesa E, Cisterna B, Costanzo M, Zancanaro C. Internalized chitosan nanoparticles persist for long time in cultured cells. Eur J Histochem 2015;59:2492.
Messerschmidt C, Hofmann D, Kroeger A, Landfester K, Mailänder V, Lieberwirth I. On the pathway of cellular uptake: new insight into the interaction between the cell membrane and very small nanoparticles. Beilstein J Nanotechnol 2016;7:1296-1311.
Mühlfeld C, Rothen-Rutishauser B, Vanhecke D, Blank F, Gehr P, Ochs M. Visualization and quantitative analysis of nanoparticles in the respiratory tract by transmission electron microscopy. Part Fibre Toxicol 2007;4:11.
Müller-Goymann CC. Physicochemical characterization of colloidal drug delivery systems such as reverse micelles, vesicles, liquid crystals and nanoparticles for topical administration. Eur J Pharm Biopharm 2004;58:343-56.
Nabiev I, Mitchell S, Davies A, Williams Y, Kelleher D, Moore R, et al. Nonfunctionalized nanocrystals can exploit a cell's active transport machinery delivering them to specific nuclear and cytoplasmic compartments. Nano Lett 2007;7:3452-61.
Ostrowski A, Nordmeyer D, Boreham A, Holzhausen C, Mundhenk L, Graf C, et al. Overview about the localization of nanoparticles in tissue and cellular context by different imaging techniques. Beilstein J Nanotechnol 2015;6:263-80.
Othman BA, Greenwood C, Abuelela AF, Bharath AA, Chen S, Theodorou I, et al. Correlative light-electron microscopy shows RGD-targeted ZnO nanoparticles dissolve in the intracellular environment of triple negative breast cancer cells and cause apoptosis with intratumor heterogeneity. Adv Healthc Mater 2016;5:1310-25.
Panyam J, Zhou WZ, Prabha S, Sahoo SK, Labhasetwar V. Rapid endolysosomal escape of poly(DL-lactide-coglycolide) nanoparticles: implications for drug and gene delivery. FASEB J 2002;16:1217-26.
Porter DW, Hubbs AF, Mercer RR, Wu N, Wolfarth MG, Sriram K, et al. Mouse pulmonary dose- and time course-responses induced by exposure to multi-walled carbon nanotubes. Toxicology 2010;269:136-47.
Poussard S, Decossas M, Le Bihan O, Mornet S, Naudin G, Lambert O. Internalization and fate of silica nanoparticles in C2C12 skeletal muscle cells: evidence of a beneficial effect on myoblast fusion. Int J Nanomedicine 2015;10:1479-92.
Reimer L. Scanning electron microscopy: physics of image formation and microanalysis. 2nd ed. Heidelberg: Springer-Verlag Berlin Heidelberg; 2000.
Rissi NC, Guglielmi DAS, Corrêa MA, Chiavacci LA. Relationship between composition and organizational levels of nanostructured systems formed by Oleth 10 and PPG-5-Ceteth-20 for potential drug delivery. BJPS 2014;50:653-61.
Roth GA, Sosa Peña MdP, Neu-Baker NM, Tahiliani S, Brenner SA. Identification of metal oxide nanoparticles in histological samples by enhanced darkfield microscopy and hyperspectral mapping. J Vis Exp 2015;(106):e53317.
Shtengel G, Wang Y, Zhang Z, Goh WI, Hess HF, Kanchanawong P. Imaging cellular ultrastructure by PALM, iPALM, and correlative iPALM-EM. Methods Cell Biol 2014;123:273-94.
Soica C, Coricovac D, Dehelean C, Pinzaru I, Mioc M, Danciu C, et al. Nanocarriers as tools in delivering active compounds for immune system related pathologies. Recent Pat Nanotechno 2016;10:128-45.
Sonnefraud Y, Sinclair HG, Sivan Y, Foreman MR, Dunsby CW, Neil MA, et al. Experimental proof of concept of nanoparticle-assisted STED. Nano Lett 2014;14:4449-53.
Theil Hansen L, Kühle A, Sørensen AH, Bohr J, Lindelof PE. A technique for positioning nanoparticles using an atomic force microscope. Nanotechnology 1998;9:337.
Tscheka C, Hittinger M, Lehr CM, Schneider-Daum N, Schneider M. Macrophage uptake of cylindrical microparticles investigated with correlative microscopy. Eur J Pharm Biopharm 2015;95:151-5.
van Landeghem FK, Maier-Hauff K, Jordan A, Hoffmann KT, Gneveckow U, Scholz R, et al. Post-mortem studies in glioblastoma patients treated with thermotherapy using magnetic nanoparticles. Biomaterials 2009;30:52-7.
Varkouhi AK, Scholte M, Storm G, Haisma HJ. Endosomal escape pathways for delivery of biologicals. J Control Release 2011;151:220-8.
Williams DB, Carter CB. Transmission Electron Microscopy A Textbook for Materials Science, 2nd ed. New York: Springer; 2009.
Willig KI, Keller J, Bossi M, Hell SW. STED microscopy resolves nanoparticle assemblies. New Journal of Physics 2006;8:106.
Xiong X, Wang Y, Zou W, Duan J, Chen Y. Preparation and characterization of magnetic chitosan microcapsules. J Chem 2012;2013:1-8.
Zhang LW, Bäumer W, Monteiro-Riviere NA. Cellular uptake mechanisms and toxicity of quantum dots in dendritic cells. Nanomedicine (Lond) 2011;6:777-91.
Zhang X, Shastry S, Bradforth SE, Nadeau JL. Nuclear uptake of ultrasmall gold-doxorubicin conjugates imaged by fluorescence lifetime imaging microscopy (FLIM) and electron microscopy. Nanoscale 2015;7:240-51.
Zielinska E, Tukaj C, Radomski MW, Inkielewicz-Stepniak I. Molecular mechanism of silver nanoparticles-induced human osteoblast cell death: protective effect of inducible nitric oxide synthase inhibitor. PLoS One 2016;11:e0164137.

V. Guglielmi, F. Carton, G. Vattemi, S. Arpicco, B. Stella, G. Berlier, A. Marengo, F. Boschi, M. Malatesta (2018): Uptake and intracellular distribution of different types of nanoparticles in primary human myoblasts and myotubes. (submitted to the International Journal of Pharmaceutics, presently under revision).

UPTAKE AND INTRACELLULAR DISTRIBUTION OF DIFFERENT TYPES OF NANOPARTICLES IN PRIMARY HUMAN MYOBLASTS AND MYOTUBES

Guglielmi V.[a], Carton F.[a], Vattemi G.[b], Arpicco S.[c], Stella B.[c], Berlier G.[d], Marengo A.[c], Boschi F.[e], Malatesta M.[a]

[a] Department of Neurosciences, Biomedicine and Movement Sciences, Section of Anatomy and Histology, University of Verona, Strada Le Grazie, 8 – 37134 Verona, Italy

[b] Department of Neurosciences, Biomedicine and Movement Sciences, Section of Clinical Neurology, University of Verona, P.Le L.A. Scuro 10 – 37134 Verona, Italy

[c] Department of Drug Science and Technology, University of Torino, Via P. Giuria, 9 - 10125 Torino, Italy

[d] Department of Chemistry and NIS Centre, University of Torino, Via P. Giuria, 7 - 10125 Torino, Italy

[e] Department of Computer Science, University of Verona, Strada Le Grazie 15-37134 Verona, Italy

Send correspondence to:

Manuela Malatesta

Department of Neuroscience, Biomedicine and Movement Sciences, Anatomy and Histology Section, University of Verona, Strada Le Grazie 8, 37134 Verona, Italy.

Phone +39.045.8027569.

e-mail : manuela.malatesta@univr.it

ABSTRACT

The use of NPs as drug carriers in the field of skeletal muscle diseases has been poorly addressed and the interaction of NPs with skeletal muscle cells has been investigated almost exclusively on C2C12 murine myoblasts. In this study we investigated the effects poly(lactide-*co*-glycolide) (PLGA) nanoparticles (NPs), mesoporous silica nanoparticles (MSNs) and liposomes, on the viability of primary human myoblasts and analyzed their cellular uptake and intracellular distribution in both primary human myoblasts and myotubes. Our data demonstrate that PLGA NPs do not negatively affect myoblasts viability, contrarily to MSNs and liposomes that induce a decrease in cell viability at the highest doses and longest incubation time. PLGA NPs and MSNs are internalized by endocytosis, PLGA NPs undergo endosomal escape whereas MSNs

always occur within vacuoles. Liposomes were rarely observed within the cells. The uptake of all tested NPs was less prominent in primary human myotubes as compared to myoblasts.
Our findings represent the first step toward the characterization of the interaction between NPs and primary human muscle cells and suggest that PLGA NPs might find an application for drug delivery to skeletal muscle.

Key words: primary human myoblast; primary human myotube; nanoparticle; fluorescence microscopy; electron microscopy.

Abbreviations: nanoparticles (NPs); poly(lactide-co-glycolide) (PLGA); mesoporous silica nanoparticles (MSNs); tetraethyl orthosilicate (TEOS); cetyltrimethylammonium bromide (CTAB); Structure Directing Agent (SDA); fluorescein isothiocyanate (FITC); 1,2-distearoyl-sn-glycero-3-phosphocholine (DSPC); 1,2-distearoyl-sn-glycero-phosphoethanolamine-N-[amino(polyethylene glycol)-2000] (DSPE-PEG); polydispersity index (PI); quasi-elastic light scattering (QELS); transmission electron microscopy (TEM).

Funding: This research did not receive any specific grant from funding agencies in the public, commercial, or not-for-profit sectors.

Declaration of interest: none.

1. INTRODUCTION

The continuous expansion of nanotechnology has led to a great interest in the potential applications of nanomaterials in the biomedical field. Nanomaterials are, by definition, materials with size ranging between 1 and 100 nm, at least in one dimension (Su et al. 2017). The interest in nanotechnology is due to the unique properties that the matter acquires at the nano-scale size that allow to overcome some limitations displayed by the corresponding material in its larger state (Su et al. 2017). Several nanodevices have been designed for different biomedical purposes including drug delivery, gene therapy, disease diagnosis and for the design of advanced protheses and implants (Su et al. 2017; Kunzmann et al. 2011). Nanomedicine is intensively exploring the use of nanoparticles (NPs) for drug delivery because it provides many advantages compared to the administration of the free drug including increased bioavailability, reduced toxicity and side effects as well as prolonged half-life

and efficacy of the drug (Su et al. 2017). Moreover, NPs can be modified to target specific cells or tissues allowing to control the delivery of therapeutics at the site of action while reducing the dosage and unwanted side effects due to the interaction of the pharmacological agent with off-targets (Su et al. 2017).

When NPs are to be used for medical purposes it is mandatory to characterize their physicochemical properties, to exclude their intrinsic toxicity, and to elucidate their interactions with the biological systems (e.g., their ability to be internalized, persist and be degraded by the cell) (Kunzmann et al. 2011). Evaluating the effects of NPs on *in vitro* cell systems represents the first step to assess the biosafety and biocompatibility of nanoconstructs (Schrand et al. 2012).

Poly(lactide-*co*-glycolide) (PLGA) NPs, mesoporous silica nanoparticles (MSNs) and liposomes have been widely investigated in many *in vitro* and *in vivo* experimental systems. These studies demonstrated that PLGA NPs, MSNs and liposomes are biodegradable and biocompatible, creating the basis for their current use in the biomedical, pre-clinical or clinical setting (Wang et al. 2015; Danhier et al. 2012; Sercombe et al. 2015).

PLGA NPs are particularly attractive for biomedical uses because PLGA polymer is approved for medical application by both FDA and EMA, is biodegradable and is already widely employed in the biomedical field for sutures, drug delivery and tissue engineering (Ulery et al. 2011; Danhier et al. 2012).

MSNs have been drawing the attention in many fields including the medical one due to their unique honeycomb-like porous structure that allows to carry relatively high amount of molecules and to their unique properties such as tunable size, shape and pore dimension, large surface area and high reactive surface which makes their functionalization easy (Slowing et al. 2008; Asefa and Tao 2012).

Liposomes are vesicles constituted of a bilayer of phospholipids and an internal aqueous cavity (Sercombe et al. 2015). They offer many advantages including high-loading capacity, biocompatibility, low toxicity and a great versatility allowing the incorporation of both hydrophobic and hydrophilic drugs, that are entrapped in the membrane bilayer or in the aqueous cavity, respectively (Sercombe et al. 2015; Abu Lila and Ishida 2017). Liposomes have a long history of successful applications in the medical field, specifically in drug delivery, that testify their ability to prevent early degradation of the encapsulated compound, to reduce toxicity and improve biodistribution and drug delivery (Bulbake et al. 2017; Sercombe et al. 2015).

In the present study, we report the effects on cell viability, cellular uptake and intracellular distribution of PLGA NPs, MSNs and liposomes in primary human myoblasts and myotubes, which

have been used as an *in vitro* model of skeletal muscle tissue. Skeletal muscle accounts for about 45% of total body weight and has high blood flow: these features make this tissue highly exposed to circulating drugs, and explain why skeletal muscle is one of the main target of drug adverse reactions (Klopstock 2008). Therefore, understanding the interaction between NPs and skeletal muscle is important to identify suitable nanocarriers for drug delivery and to define the impact of NPs on this abundant tissue.

2. MATERIALS AND METHODS

2.1 Preparation and characterization of nanoparticles

For the preparation of PLGA (50:50 - Resomer® RG 502 H - or 75:25 - Resomer® RG 752 H, Sigma-Aldrich)) NPs, the nanoprecipitation technique was employed (Fessi et al. 1989). Practically, for each preparation, 12 mg of PLGA 50:50 or 75:25 were dissolved in 2 ml of acetone. This organic solution was then poured into 4 ml of MilliQ® water under magnetic stirring. Precipitation of particles occurred spontaneously. After solvent evaporation under reduced pressure, an aqueous suspension of NPs was obtained. Fluorescently labelled PLGA NPs were prepared by nanoprecipitation of PLGA 50:50 or 75:25 (12 mg) in the presence of 16.8 µg of Nile red (9-diethylamino-5H-benzo[α]phenoxazine-5-one, Sigma-Aldrich) dissolved in acetone; this solution was then added to 4 ml of MilliQ® water under magnetic stirring, as previously described for non-labelled NPs. Fluorescent NPs were purified from non-incorporated dye by gel filtration on a Sepharose CL-4B column. MSNs were prepared by using tetraethyl orthosilicate (TEOS) as silica source and cetyltrimethylammonium bromide (CTAB) as Structure Directing Agent (SDA), in a basic aqueous solution (NaOH, Sigma-Aldrich) at 80 °C, as described elsewhere (Sapino et al. 2015; Musso et al. 2015). SDA was removed from the inner porosity by calcination at 550°C in nitrogen and oxygen, followed by surface functionalization using 3-aminopropyltriethoxysilane (APTS, Sigma-Aldrich) as grafting agent (Sapino et al. 2015). The resulting material, after drying, was suspended in MilliQ® water (1 mg MSNs in 150 µl) before adding 250 µl of fluorescein isothiocyanate (FITC) ethanol solution (0.3 mg/ml), adapting a previously proposed procedure (Yu et al. 2013). After 5 h under stirring in the dark, FITC labeled MSNs were centrifuged and washed with ethanol three times to obtain colorless supernatants. Liposomes were prepared by the thin lipid film hydration and extrusion method. Chloroform solution of 1,2-distearoyl-sn-glycero-3-phosphocholine (DSPC, Avanti Polar-Lipids), cholesterol (Chol, Avanti Polar-Lipids) and 1,2-distearoyl-sn-glycero-phosphoethanolamine-N-[amino(polyethylene glycol)-2000] (DSPE-PEG, ammonium salt, Avanti

Polar-Lipids) in a molar ratio 65:30:5 were mixed and evaporated under reduce pressure to obtain a thin lipid film. The resulting lipid film was hydrated with a 20 mM HEPES buffer (pH 7.4) and vortexed for 10 min to obtain a suspension of multilamellar liposomes. The resulting suspension was then extruded 10 times under nitrogen through 200 nm polycarbonate filter at 60°C. Fluorescently labeled liposomes were prepared as described above by adding 10 mM solution of fluorescein-5-(and-6)-sulfonic acid trisodium salts (Invitrogen) in HEPES buffer during the hydration of the lipid film. The unentrapped fluorescein was removed by gel filtration using Sepharose CL-4B column eluting with HEPES buffer.

The mean particle size and the polydispersity index (PI) of liposomes and PLGA NPs were determined at 25°C by quasi-elastic light scattering (QELS) using a nanosizer (Nanosizer Nano Z, Malvern Inst., Malvern, UK). The selected angle was 173° and the measurement was made after dilution of the nanoparticle suspension in MilliQ® water. Each measure was performed in triplicate.

2.2 Primary human myoblasts and myotubes cultures

Primary human myoblasts were established from a portion of diagnostic *vastus lateralis* of two different subjects who underwent muscle biopsy for diagnostic purpose and that, after all tests had been performed, were deemed to be free of muscle diseases (the samples were conventionally named ctr1 and ctr2). Myoblasts were isolated and grown in a cell culture incubator with saturating humidity in a mixture of 5% CO_2 and air at 37°C, as previously described (Askanas and Engel 1975). For the differentiation into myotubes, myoblasts were grown at confluence and then shifted to a medium without growth factors for 8 days (Guglielmi et al. 2017). The study was approved by the local ethical board.

2.3 Cell viability assay

The effect of two different formulations of PLGA NPs (PLGA 50:50 and PLGA75:25), MSNs and liposomes on the viability of primary human myoblasts was evaluated by the MTT assay (Mosmann 1983). Cells were seeded in flat-bottom 96 multiwell plates at the density of $3x10^3$ cells/well. Four wells for each condition were seeded. After 24 h, the medium was removed and replaced with medium containing the NPs. PLGA NPs and liposomes were administered at the final concentrations of 0.1, 0.2 or 0.4 mg/ml whereas MSNs were supplied at the final doses of 0.01, 0.05 or 0.1 mg/ml. MTT assay was performed after 2 h, 24 h and 72 h treatment, as previously reported (Denizot and Lang 1986). Briefly, after incubation with NPs, the medium was replaced with 100 µl of 0.5 mg/ml MTT in culture medium and incubated for 4 h at 37°C in a cell culture incubator. Then, MTT solution was

removed, formazan crystals were dissolved in 100 ul of DMSO and the absorbance was measured at 570 nm. Statistically significant differences ($p<0.05$) in cell viability were determined by one-way ANOVA followed by Bonferroni's post-hoc test. Cell viability was expressed as percentage of control (sham-treated) cells (mean ± SE).

2.4 Uptake and intracellular distribution of nanoparticles

Uptake and intracellular distribution of NPs were investigated by confocal fluorescence microscopy and transmission electron microscopy (TEM) in both primary human myoblasts and myotubes.
Cells were seeded on glass coverslips in 24 multiwell plates. Twenty-four hours after seeding, the medium was replaced with fresh medium containing the NPs. Myotubes were treated after 8 days of differentiation. PLGA NPs and liposomes were administered at the final concentration of 0.2 mg/ml whereas MSNs were used at the final dose of 0.01 mg/ml. After 2 h incubation with NPs, cells were either fixed or moved to fresh medium without NPs and further grown for 24 h or 72 h.
For fluorescence microscopy, cells were fixed with 1% paraformaldehyde and 0.01% glutaraldehyde in PBS, pH 7.4, for 30 min at 4°C. Myoblasts and myotubes treated with Nile red labeled-PLGA NPs were permeabilized with 0.1% Triton X100 in PBS at room temperature (RT) for 8 min and incubated with phalloidin conjugated with Alexa488 (1:20 in PBS) for 1 h at RT. Myoblasts exposed to either FITC-labeled liposomes or FITC-labeled MSNs were counterstained with 0.004% Trypan Blue in PBS for 1 min at RT. Myotubes incubated with FITC-labeled liposomes or FITC-labeled MSNs were counterstained with phalloidin conjugated with Atto 594 (1:20 in PBS) for 1 h at RT. Cells nuclei were stained with Hoechst 33258 (1 mg/ml in PBS for 5 min). After washes with PBS, the samples were mounted in 50% glycerol in PBS. Imaging by confocal laser scanning microscopy was performed with a Leica TCS SP5 AOBS system (Leica Microsystems Italia). For fluorescence excitation, a diode laser at 405 nm for Hoechst 33342, an Ar laser at 488 nm for FITC and PKH67 Green Fluorescent Cell Linker, and a He/Ne laser at 543 nm for Trypan blue, Nile Red, PHK26 Red Fluorescent Cell Linker and phalloidin conjugated with Atto 594 were employed. To access whether NPs enter the cells via endocytosis, myoblasts were incubated with either the PKH67 Green Fluorescent Cell Linker or the PHK26 Red Fluorescent Cell Linker at the final concentration of 2 uM for 5 min in the incubator, to stain the plasma membrane, and then treated with Nile red-labeled or FITC-labeled NPs, respectively. This allowed to track the endocytic vesicles originated for the plasma membrane, and to detect their possible co-localization with the fluorescent NPs internalized by the cell. Then myoblasts were fixed, stained for DNA with Hoechst 33258, and analyzed by confocal fluorescence microscopy as described above.

For TEM, cells were fixed with 2.5% glutaraldehyde and 2% paraformaldehyde in 0.1 M phosphate buffer, pH 7.4, at 4°C for 1 h, post-fixed with 1% osmium tetroxide and 1.5% potassium ferrocyanide at RT for 1 h, dehydrated with acetone and embedded in Epon. Ultrathin sections were observed with a Philips Morgagni transmission electron microscope (FEI Company Italia Srl, Milan, Italy) operating at 80 kV and equipped with a Megaview II camera for digital image acquisition.

3. RESULTS

3.1 Characterization of NPs

NPs mean particle size and zeta potential values are reported in Table 1. In particular, all the systems showed a mean diameter under 200 nm. The zeta potential was negative for PLGA NPs and liposomes while for MSNs a positive value was observed in relation to the functionalization with aminopropyl groups (Musso et al. 2015) necessary for preparation of FITC labeled MSNs through a covalent link. Fluorescent labeling did not appreciably affect both particle size and zeta potential.

3.2 Cell viability

A statistically significant increase in cell viability was observed after 24 h of treatment with 0.4 mg/ml PLGA 50:50 NPs in ctr1 myoblasts and after 24 h incubation with 0.4 mg/ml PLGA 75:25 NPs in both ctr1 and ctr2 myoblasts (Fig. 1).

A statistically significant decrease in cell viability was reported after 72 h treatment with MSNs at the final concentration of 0.1 mg/ml in both ctr1 and ctr2 myoblasts (Fig. 1).

A statistically significant decrease in cell viability was observed after 24 h and 72 h incubation with 0.4 mg/ml liposomes in ctr2 myoblasts and after 72 h treatment with 0.2 mg/ml and 0.4 mg/ml liposomes in ctr1 myoblasts (Fig. 1).

Statistically significant differences were not observed for any of the other tested conditions.

3.3 Uptake and intracellular distribution of nanoparticles

NPs uptake and intracellular distribution were investigated in primary human myoblasts and myotubes treated with fluorescent or unlabeled NPs using confocal fluorescence microscopy and TEM, respectively.

3.3.1 PLGA NPs

By confocal fluorescence microscopy and TEM, the two formulations of PLGA NPs, i.e. PLGA 50:50 and PLGA 75:25, did not display any difference in term of cellular uptake, intracellular localization and ultrastructural features in both primary human myoblasts and myotubes. By confocal fluorescence microscopy PLGA NPs were found in the cytoplasm and close to cell nuclei in cells treated for 2 h, 24 h and 72 h (Fig. 2a-c, g-i). A partial co-localization between PLGA NPs and fluorescent-labeled membrane derived vesicles was observed in proximity of cell surface and in the cytoplasm of a few treated myoblasts (Fig. 2d-f). The uptake of PLGA NPs was less prominent in primary human myotubes as compared to myoblasts (Fig. 2a-c, g-i). At TEM, PLGA NPs showed a regular round shape and a moderate electron density (Fig. 2j-m). In myoblasts, after 2 h incubation, single NPs were rarely found adhering to the plasma membrane or inside endosomes, whereas they mostly occurred free in the cytosol (Fig. 2j-l). Accordingly, some PLGA NPs were found escaping from endosomes (Fig. 2k). Some PLGA NPs occurring free in the cytosol were partially surrounded by a double membrane as typical of autophagy (Fig. 2l). After 24 h incubation, a high number of small vacuoles containing roundish electron dense structures accumulated in the cytoplasm (Fig. 2m); these particular residual bodies were never found in untreated cells or in samples treated with MSNs or liposomes. In myotubes, PLGA NPs were less frequent than in myoblasts, but their intracellular distribution was similar (not shown). No contact between PLGA NPs and cytoplasmic organelles was observed; moreover, NPs never occurred inside the nucleus. Neither myoblasts nor myotubes showed alteration or damage of their structural components at any incubation time.

3.3.2 MSNs

Confocal fluorescence microscopy revealed MSNs aggregates in the cytoplasm of a few myoblasts and myotubes that were treated for 24 h and 72 h (Fig. 3a-g). MSNs co-localizing with fluorescent-labeled membrane derived vesicles were occasionally observed (Fig. 3e).

At TEM, MSNs appeared roundish and showed a finely granular highly electron dense content (Fig. 3h-i). In myoblasts, clusters of MSNs were found to adhere to the cell surface and to be internalized by endocytosis (Fig. 3i). In the cytoplasm, MSNs always occurred inside heterogeneous vacuoles ubiquitously distributed in the cytoplasm at all analyzed incubation times (Fig. 3h). In myotubes, MSNs were less frequent than in myoblasts and were usually enclosed in vacuoles (Fig. 3i). MSNs neither get in contact with organelles nor enter the cell nucleus. No signs of subcellular alteration or damage were observed in both myoblasts and myotubes at short incubation time (2 h, Fig. 3h, i),

whereas starting form 24 h incubation the cells contained large amounts of vesicular and membranous structures while organelles were morphologically unrecognizable (not shown).

3.3.3 Liposomes

By confocal fluorescence microscopy, liposomes were rarely observed inside primary human myoblasts and myotubes (Fig. 4a-d). A co-localization between liposomes and fluorescent-labeled membrane derived vesicles was never observed (Fig. 4a, b). A few myotubes displayed liposomes in their cytoplasm after 24 h and 72 h treatment (Fig. 4c, d).

At TEM, liposomes showed a roundish shape with a fine irregular profile and strong electron density (likely due to the lipid staining by osmium tetroxide, Fig. 4e, f). A few liposomes were found inside myoblasts and they were even scarcer in myotubes. In both cell types, liposomes were found adhering to the cell surface and in the peripheral region of the cytoplasm but never occurred inside the cell nuclei (Fig. 4e, f). No internalization processes such as endocytosis or phagocytosis, and no contact with any cell organelles were observed. No evident structural alterations were observed in myoblasts at short and long incubation time and in myotubes after 2 h incubation, whereas in myotubes incubated with liposomes for longer times the organelles were morphologically unrecognizable (not shown).

4. DISCUSSION

In the last decades, many efforts have been directed to develop NPs-based drug formulations for treating cancer and other pathologies but, so far, the use of NPs has been poorly investigated in the field of skeletal muscle diseases (Su et al. 2017). Only recently NPs have been explored as a possible drug delivery system for antisense oligonucleotides (AONs) in the exon-skipping treatment of Duchenne muscular dystrophy (DMD) (Falzarano et al. 2014): these studies have been performed on the murine model of DMD (*mdx* mice) and aimed at improving the delivery of AONs and reducing the effective therapeutic dose (Falzarano et al. 2014). However, the interaction between NPs and skeletal muscle cells has been poorly investigated and the current knowledge is limited to *in vitro* studies performed almost exclusively on C2C12 immortalized murine myoblasts and only a few papers described the impact of NPs on human primary myoblasts and myotubes (Nie et al. 2012; Leite et al. 2015; Lojk et al. 2015; Poussard et al. 2015; Ramachandran et al. 2017).

It has been demonstrated that the extent of the NPs cellular uptake depends on the intrinsic chemical and physical properties of the NPs as well as on the target cell type (Akinc and Battaglia 2013; Sahay et al. 2010; Frohlich et al. 2012). NPs size and shape as well as the chemical properties of their surface

dictate the ability of the NPs to interact with the cell membrane, the extent and pathway of internalization and, once inside the cells, their intracellular fate (Akinc and Battaglia 2013). On the other hand, cell type, proliferation rate and cell-membrane characteristics have a major influence on the effect that a certain type of NPs might have on a cell (Lojk et al. 2015; Kim et al. 2011; Tang et al. 2015; Wang et al. 2016; Kettler et al. 2014; Frohlich et al. 2012). Therefore, it is of extreme importance to study the impact of NPs on the appropriate *in vitro* cellular model especially when the final goal is to translate the findings to the medical field (Kunzmann et al. 2011).

In the present study, the effects of PLGA NPs, MSNs and liposomes have been investigated on primary human myoblasts and myotubes that have been used as an *in vitro* model of human skeletal muscle. PLGA NPs, MSNs and liposomes have been chosen because they are biodegradable and biocompatible, as previously demonstrated in several studies performed on other cell types, and already have a biomedical, pre-clinical or clinical application (Wang et al. 2015; Danhier et al. 2012; Sercombe et al. 2015). Two formulations of PLGA NPs with a different composition of lactic acid and glycolic acid (50:50 *vs* 75:25) have been synthetized and applied to primary human muscle cells; indeed, PLGA composition affects some properties of the copolymer such as degradation time that increases with increasing lactide:glycolide ratio (Ulery et al. 2011). We reported that PLGA NPs do not negatively affect myoblasts viability at any of the tested doses and duration of treatment, contrarily to MSNs and liposomes, which both reduce cell viability when administered at the highest tested doses for long incubation time. A slight but statistically significant increase in cell viability was observed after 24 h incubation at the highest tested dose (i.e. 0.4 mg/ml) with both PLGA NPs formulations. This data could be due to an increased mitochondrial dehydrogenase activity, measured by MTT assay, due to high levels of glycolic acid and lactic acid resulting from PLGA degradation that enter the Krebs cycle bursting oxidative metabolism in the mitochondria (Danhier et al. 2012). Interestingly, the effect of PLGA 50:50 NPs and MSNs on cell viability was similar in myoblasts from different donors, namely increasing (24 h with 0.4 mg/ml) *vs* decreasing (72 h with 0.1 mg/ml) cell viability, respectively. Similarly, a reduction in cells viability after 72 h incubation with 0.4 mg/ml liposomes was reported in myoblasts derived from both donors. On the contrary, treatment with 0.4 mg/ml liposomes for 24 h negatively affected the viability of cells derived from only one of the two healthy subjects. Moreover, the increase in cell viability after 24 h of incubation with 0.4 mg/ml PLGA 75:25 was found only in myoblasts derived from ctr1 donor whereas PLGA 75:25 did not influence the viability of ctr2 myoblasts. These findings demonstrate that NPs might have a variable effect on the viability of cells derived from different subjects, and indicate that, despite the

difficult access to human material and requirement of appropriate expertise, primary human cultures offer the important advantage to better reproduce the *in vivo* physiological conditions and variability between donors, highlighting the importance of using primary human cells to test the biocompatibility of NPs for biomedical applications.

Subsequently, the intracellular distribution of NPs was analyzed by confocal fluorescence microscopy and TEM. For this purpose, PLGA NPs, MSNs and liposomes were used at concentrations that did not show a negative effect on myoblasts viability. The two formulations of PLGA NPs did not display any remarkable difference in term of cell uptake and intracellular localization: PLGA NPs were observed in the cytoplasm inside membrane-derived vesicles (suggesting they enter the cell by endocytosis) and undergoing endosomal escape, in agreement with previous observations (Panyam et al. 2002; Danhier et al. 2012). Free PLGA NPs were observed close to the nuclei in both myoblasts and myotubes but were never found within the nuclear compartment, making unlikely their interaction with genetic material. Autophagic processes led PLGA NPs inside the lysosome pathway, as demonstrated by the residual bodies likely made of PLGA NPs remnants starting from 24 h incubation. In agreement with data from the literature demonstrating their biocompatibility and biosafety, PLGA NPs did not affect the structural components of the cells neither in myoblasts nor in myotubes, and in PLGA NPs-treated cells all organelles appeared to be well preserved. Previous studies investigated the use of PLGA polymer in the production of scaffolds and matrices for myoblasts culture and differentiation as well as for the development of microcarriers for successful expansion of myoblasts *in vitro* and enhanced engraftment and survival of myoblasts after transplantation (Gu et al. 2013; Parmar and Day 2015; Shin et al. 2015). However, for the first-time, we focused on the interaction between PLGA NPs and primary human myoblasts and provided data supporting the biocompatibility of nanostructured PLGA with this cell type, opening the way to future studies on biomedical applications involving skeletal muscle tissue.

As regard MSNs, after 24 h from the treatment, both myoblasts and myotubes displayed numerous cytoplasmic vesicular and membranous structures, pointing to the over-activation of the lysosome pathway, and morphologically altered organelles even after exposure to NPs concentrations found to be safe by the viability assay. This highlights the key role of morphological studies in evaluating the biological impact of nanoconstructs, and suggests a poor biocompatibility of MSNs with primary human myoblasts and myotubes. MSNs clusters were observed on the cell surface as well as in large cytoplasmic vacuoles in both primary human myoblasts and myotubes, a distribution closely resembling the one reported in C2C12 myoblasts after treatment with silica-based NPs (Poussard et

al. 2015). To our knowledge, the present study is the first investigating the interaction between MSNs and human myoblasts. Indeed, MSNs have been used to develop scaffolds for the delivery of γ-secretase inhibitors of Notch pathway to promote the differentiation of C2C12 myoblasts, but data on the effects of MSNs on cell viability and intracellular distribution have not been reported in primary human muscle cells (Bocking et al. 2014).

Even if treatment with liposomes did not affect the structural integrity of myoblasts, morphological alterations of organelles were detected in myotubes starting at 24 h from liposome exposure, suggesting that myotubes might be more sensitive to liposomes as compared to myoblasts. It is possible that the degradation of the internalized liposomes may cause an overload of lipid components that these highly differentiated non-cycling cells are unable to metabolize. Despite this difference, in both myoblasts and myotubes, liposomes were observed in the cytoplasm of only a few cells, pointing to their poor cellular uptake. The negative effect of PEGylation on liposome internalization by C2C12 reported in a previous study may provide another explanation of the poor uptake of our liposomes, which also harbor PEG on their surface, by primary human myoblasts and myotubes (Teo et al. 2013). Alternatively, liposomes might have a short half-life within the cell and be subjected to rapid cytosolic degradation, as documented by the presence of liposomes with irregular profiles and undergoing dissolution, as previously observed in HeLa cells (Costanzo et al. 2016).

Even though, in the past, liposomes have been tested on C2C12 myoblasts and on primary human myoblasts and myotubes, most of these studies evaluated liposomes prepared with cationic lipids to deliver nucleic acid to these low transfectable cells (Helbling-Leclerc et al. 1999; Vitiello et al. 1998; Dodds et al. 1998; Neuhuber et al. 2002; Pampinella et al. 2002). Up to now, data on the interaction of liposomes and primary human myoblasts and myotubes were missing; indeed, only a few other studies assessed the interaction between liposomes and murine myoblasts (Jeong and Conboy 2011; van der Westen et al. 2012; Teo et al. 2013). Our liposomes contain DSPC, a derivative of phosphatidylcholine (PC). It has been reported that PC-liposomes decrease primary murine myoblasts fusion and myotube elongation; however the uptake and the intracellular distribution of PC-liposomes were not evaluated (Jeong and Conboy 2011). The internalization of liposomes has been demonstrated also in C2C12 by flow cytometry and an increased uptake/association with the cells was reported for polydopamine (PDA)-coated liposomes (van der Westen et al. 2012). We report a poor internalization of PEGylated liposomes by primary human myoblasts and myotubes and their negative effect on cell viability, suggesting that PEGylated liposomes might not be suitable for drug delivery to this cell type.

5. CONCLUSIONS

The present study provides novel data about the interaction between PLGA NPs, MSNs and liposomes and primary human muscle cells, and suggests that nanocarriers previously demonstrated to be safe in various cell lines can pose biocompatibility issue in this cell type, as supported by the cell viability assay and by the ultrastructural analysis of MSNs and liposome treated myoblasts/myotubes. This further highlights the importance to use the appropriate cell type for biocompatibility studies. Our findings suggest that, among the tested NPs, PLGA NPs are the most promising nanocarriers for skeletal muscle cells, as they do not affect cell viability and structural organization; future *in vivo* experiments will allow to better understand the interaction between PLGA NPs and the skeletal muscle, and to develop functionalized nanocarriers for drug delivery to this specific tissue. The investigation *in vivo* will be crucial, since we also observed a difference in the uptake of all NPs investigated between myoblasts and myotubes. Even if we did not perform a quantitative evaluation, myotubes appeared to be less prone to internalize NPs suggesting that the interaction and uptake of NPs might differ between cycling and post-mitotic cells, probably because of modifications of cell membrane and cytoskeleton composition and dynamics occurring during the differentiation process (Le Bihan et al. 2015). Elucidating *in vivo* the actual interaction of NPs with the myofibers will be crucial to design the most appropriate approach for the NP-mediated administration of therapeutic agents to a diseased muscle tissue.

REFERENCES

Abu Lila AS, Ishida T (2017) Liposomal Delivery Systems: Design Optimization and Current Applications. Biol Pharm Bull 40 (1):1-10

Akinc A, Battaglia G (2013) Exploiting endocytosis for nanomedicines. Cold Spring Harb Perspect Biol 5 (11):a016980

Asefa T, Tao Z (2012) Biocompatibility of mesoporous silica nanoparticles. Chem Res Toxicol 25 (11):2265-2284

Askanas V, Engel WK (1975) A new program for investigating adult human skeletal muscle grown aneurally in tissue culture. Neurology 25 (1):58-67

Bocking D, Wiltschka O, Niinimaki J, Shokry H, Brenner R, Linden M, Sahlgren C (2014) Mesoporous silica nanoparticle-based substrates for cell directed delivery of Notch signalling modulators to control myoblast differentiation. Nanoscale 6 (3):1490-1498

Bulbake U, Doppalapudi S, Kommineni N, Khan W (2017) Liposomal Formulations in Clinical Use: An Updated Review. Pharmaceutics 9 (2)

Costanzo M, Carton F, Marengo A, Berlier G, Stella B, Arpicco S, Malatesta M (2016) Fluorescence and electron microscopy to visualize the intracellular fate of nanoparticles for drug delivery. Eur J Histochem 60 (2):2640

Danhier F, Ansorena E, Silva JM, Coco R, Le Breton A, Preat V (2012) PLGA-based nanoparticles: an overview of biomedical applications. J Control Release 161 (2):505-522

Denizot F, Lang R (1986) Rapid colorimetric assay for cell growth and survival. Modifications to the tetrazolium dye procedure giving improved sensitivity and reliability. J Immunol Methods 89 (2):271-277

Dodds E, Dunckley MG, Naujoks K, Michaelis U, Dickson G (1998) Lipofection of cultured mouse muscle cells: a direct comparison of Lipofectamine and DOSPER. Gene Ther 5 (4):542-551

Falzarano MS, Passarelli C, Ferlini A (2014) Nanoparticle delivery of antisense oligonucleotides and their application in the exon skipping strategy for Duchenne muscular dystrophy. Nucleic Acid Ther 24 (1):87-100

Fessi H, Puisieux F, Devissaguet JP, Ammoury N, Benita S (1989) Nanocapsule formation by interfacial polymer deposition following solvent displacement. International Journal of Pharmaceutics 55 (1):R1-R4. doi:https://doi.org/10.1016/0378-5173(89)90281-0

Frohlich E, Meindl C, Roblegg E, Griesbacher A, Pieber TR (2012) Cytotoxity of nanoparticles is influenced by size, proliferation and embryonic origin of the cells used for testing. Nanotoxicology 6 (4):424-439

Gu Y, Chen P, Yang Y, Shi K, Wang Y, Zhu W, Zhu G (2013) Chondrogenesis of myoblasts in biodegradable poly-lactide-co-glycolide scaffolds. Mol Med Rep 7 (3):1003-1009

Guglielmi V, Nowis D, Tinelli M, Malatesta M, Paoli L, Marini M, Manganotti P, Sadowski R, Wilczynski GM, Meneghini V, Tomelleri G, Vattemi G (2017) Bortezomib-Induced Muscle Toxicity in Multiple Myeloma. J Neuropathol Exp Neurol 76 (7):620-630

Helbling-Leclerc A, Scherman D, Wils P (1999) Cellular uptake of cationic lipid/DNA complexes by cultured myoblasts and myotubes. Biochim Biophys Acta 1418 (1):165-175

Jeong J, Conboy IM (2011) Phosphatidylserine directly and positively regulates fusion of myoblasts into myotubes. Biochem Biophys Res Commun 414 (1):9-13

Kettler K, Veltman K, van de Meent D, van Wezel A, Hendriks AJ (2014) Cellular uptake of nanoparticles as determined by particle properties, experimental conditions, and cell type. Environ Toxicol Chem 33 (3):481-492

Kim JA, Aberg C, Salvati A, Dawson KA (2011) Role of cell cycle on the cellular uptake and dilution of nanoparticles in a cell population. Nat Nanotechnol 7 (1):62-68

Klopstock T (2008) Drug-induced myopathies. Curr Opin Neurol 21 (5):590-595

Kunzmann A, Andersson B, Thurnherr T, Krug H, Scheynius A, Fadeel B (2011) Toxicology of engineered nanomaterials: focus on biocompatibility, biodistribution and biodegradation. Biochim Biophys Acta 1810 (3):361-373

Le Bihan MC, Barrio-Hernandez I, Mortensen TP, Henningsen J, Jensen SS, Bigot A, Blagoev B, Butler-Browne G, Kratchmarova I (2015) Cellular Proteome Dynamics during Differentiation of Human Primary Myoblasts. J Proteome Res 14 (8):3348-3361

Leite PE, Pereira MR, do Nascimento Santos CA, Campos AP, Esteves TM, Granjeiro JM (2015) Gold nanoparticles do not induce myotube cytotoxicity but increase the susceptibility to cell death. Toxicol In Vitro 29 (5):819-827

Lojk J, Bregar VB, Rajh M, Mis K, Kreft ME, Pirkmajer S, Veranic P, Pavlin M (2015) Cell type-specific response to high intracellular loading of polyacrylic acid-coated magnetic nanoparticles. Int J Nanomedicine 10:1449-1462

Mosmann T (1983) Rapid colorimetric assay for cellular growth and survival: application to proliferation and cytotoxicity assays. J Immunol Methods 65 (1-2):55-63

Musso GE, Bottinelli E, Celi L, Magnacca G, Berlier G (2015) Influence of surface functionalization on the hydrophilic character of mesoporous silica nanoparticles. Phys Chem Chem Phys 17 (21):13882-13894

Neuhuber B, Huang DI, Daniels MP, Torgan CE (2002) High efficiency transfection of primary skeletal muscle cells with lipid-based reagents. Muscle Nerve 26 (1):136-140

Nie Y, Zhang ZR, He B, Gu Z (2012) Investigation of PEG-PLGA-PEG nanoparticles-based multipolyplexes for IL-18 gene delivery. J Biomater Appl 26 (8):893-916

Pampinella F, Lechardeur D, Zanetti E, MacLachlan I, Benharouga M, Lukacs GL, Vitiello L (2002) Analysis of differential lipofection efficiency in primary and established myoblasts. Mol Ther 5 (2):161-169

Panyam J, Zhou WZ, Prabha S, Sahoo SK, Labhasetwar V (2002) Rapid endo-lysosomal escape of poly(DL-lactide-co-glycolide) nanoparticles: implications for drug and gene delivery. Faseb J 16 (10):1217-1226

Parmar N, Day RM (2015) TIPS to manipulate myogenesis: retention of myoblast differentiation capacity using microsphere culture. Eur Cell Mater 30:41-49; discussion 49-50

Poussard S, Decossas M, Le Bihan O, Mornet S, Naudin G, Lambert O (2015) Internalization and fate of silica nanoparticles in C2C12 skeletal muscle cells: evidence of a beneficial effect on myoblast fusion. Int J Nanomedicine 10:1479-1492

Ramachandran R, Krishnaraj C, Sivakumar AS, Prasannakumar P, Abhay Kumar VK, Shim KS, Song CG, Yun SI (2017) Anticancer activity of biologically synthesized silver and gold nanoparticles on mouse myoblast cancer cells and their toxicity against embryonic zebrafish. Mater Sci Eng C Mater Biol Appl 73:674-683

Sahay G, Alakhova DY, Kabanov AV (2010) Endocytosis of nanomedicines. J Control Release 145 (3):182-195

Sapino S, Ugazio E, Gastaldi L, Miletto I, Berlier G, Zonari D, Oliaro-Bosso S (2015) Mesoporous silica as topical nanocarriers for quercetin: characterization and in vitro studies. Eur J Pharm Biopharm 89:116-125

Schrand AM, Dai L, Schlager JJ, Hussain SM (2012) Toxicity testing of nanomaterials. Adv Exp Med Biol 745:58-75

Sercombe L, Veerati T, Moheimani F, Wu SY, Sood AK, Hua S (2015) Advances and Challenges of Liposome Assisted Drug Delivery. Front Pharmacol 6 (286):286

Shin YC, Lee JH, Kim MJ, Hong SW, Kim B, Hyun JK, Choi YS, Park JC, Han DW (2015) Stimulating effect of graphene oxide on myogenesis of C2C12 myoblasts on RGD peptide-decorated PLGA nanofiber matrices. J Biol Eng 9 (22):22

Slowing, II, Vivero-Escoto JL, Wu CW, Lin VS (2008) Mesoporous silica nanoparticles as controlled release drug delivery and gene transfection carriers. Adv Drug Deliv Rev 60 (11):1278-1288

Su H, Wang Y, Gu Y, Bowman L, Zhao J, Ding M (2017) Potential applications and human biosafety of nanomaterials used in nanomedicine. J Appl Toxicol 6 (10)

Tang J, Liu Z, Ji F, Li Y, Liu J, Song J, Li J, Zhou J (2015) The role of the cell cycle in the cellular uptake of folate-modified poly(L-amino acid) micelles in a cell population. Nanoscale 7 (48):20397-20404

Teo BM, van der Westen R, Hosta-Rigau L, Stadler B (2013) Cell response to PEGylated poly(dopamine) coated liposomes considering shear stress. Biochim Biophys Acta 1830 (10):4838-4847

Ulery BD, Nair LS, Laurencin CT (2011) Biomedical Applications of Biodegradable Polymers. J Polym Sci B Polym Phys 49 (12):832-864

van der Westen R, Hosta-Rigau L, Sutherland DS, Goldie KN, Albericio F, Postma A, Stadler B (2012) Myoblast cell interaction with polydopamine coated liposomes. Biointerphases 7 (1-4):8

Vitiello L, Bockhold K, Joshi PB, Worton RG (1998) Transfection of cultured myoblasts in high serum concentration with DODAC:DOPE liposomes. Gene Ther 5 (10):1306-1313

Wang X, Hu X, Li J, Russe AC, Kawazoe N, Yang Y, Chen G (2016) Influence of cell size on cellular uptake of gold nanoparticles. Biomater Sci 4 (6):970-978

Wang Y, Zhao Q, Han N, Bai L, Li J, Liu J, Che E, Hu L, Zhang Q, Jiang T, Wang S (2015) Mesoporous silica nanoparticles in drug delivery and biomedical applications. Nanomedicine 11 (2):313-327

Yu M, Jambhrunkar S, Thorn P, Chen J, Gu W, Yu C (2013) Hyaluronic acid modified mesoporous silica nanoparticles for targeted drug delivery to CD44-overexpressing cancer cells. Nanoscale 5 (1):178-183

TABLES

Table 1. Characteristics of NPs (*n*=3)

	mean diameter (nm±S.E.)	**polydispersity index**	**zeta potential (mV±S.E.)**
Liposomes	155±12	0.09	-10±2.10
Fluorescent liposomes	160±8	0.08	-11±1.75
MSNs	94±23[a]	-	+35±0.90
Fluorescent MSNs	105±24[a]	-	+22±0.60
PLGA 50:50 NPs	117±8	0.07	-31±0.92
PLGA 75:25 NPs	128±4	0.06	-27±0.84
Fluorescent PLGA 50:50 NPs	121±6	0.08	-29±1.18
Fluorescent PLGA 75:25 NPs	132±4	0.06	-25±2.01

[a] determined by TEM analysis

FIGURES

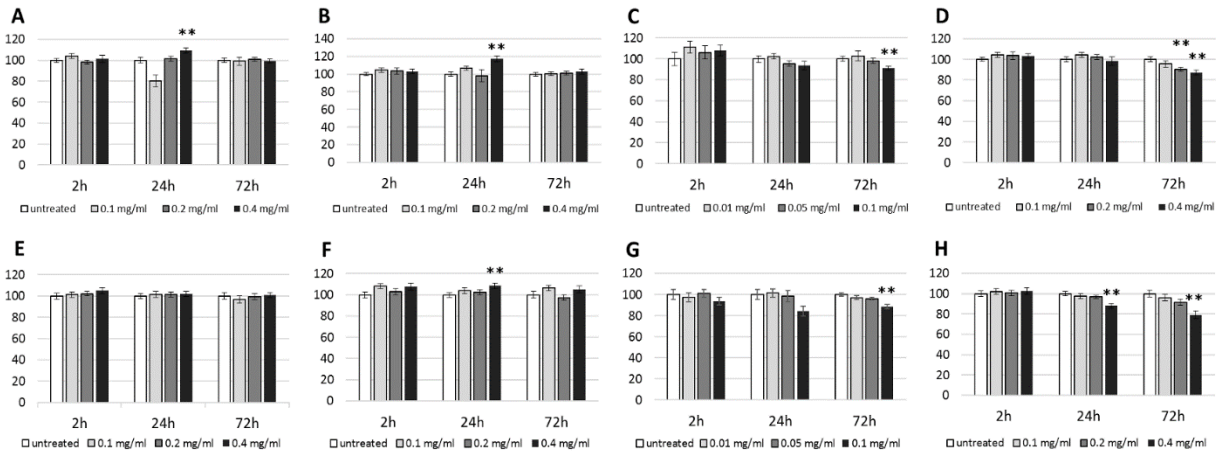

Fig. 1 Effect of NPs on cell viability of primary human myoblasts

Primary human myoblasts were obtained from two healthy subjects (Ctr1: a-d, Ctr2: e-h). The effect of PLGA 75:25 NPs (a, e), PLGA 50:50 NPs (b, f), MSNs (c, g) and liposomes (d, h) on cell viability was measured by MTT assay. Box-plots show the mean value±S.E. of percentage of cell viability after 2 h, 24 h and 72 h of incubation with NPs at different concentrations. *p<0.05; **p<0.01

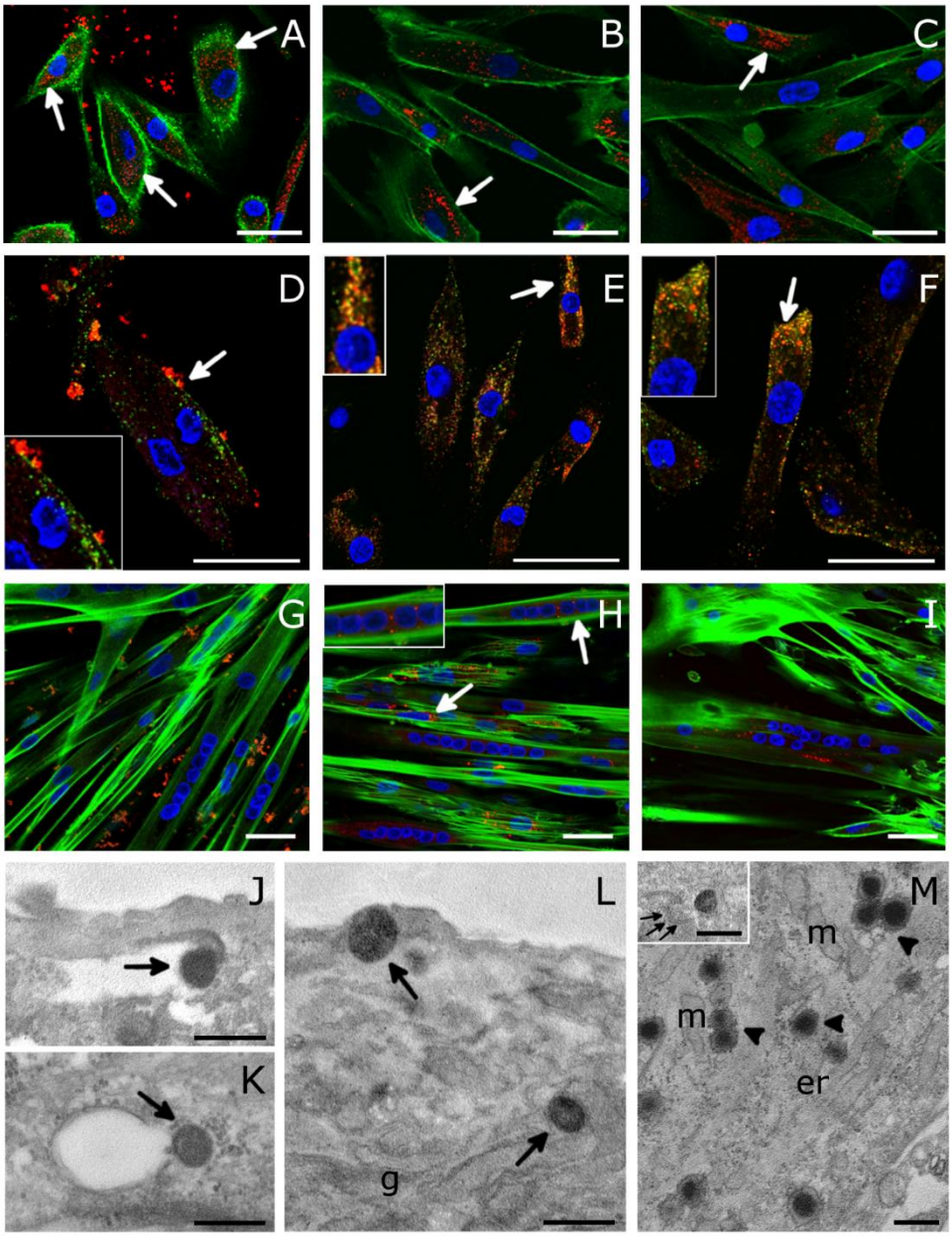

Fig. 2 Intracellular distribution of PLGA NPs in primary human myoblasts and myotubes

Confocal fluorescence microscopy analysis of myoblasts (a-f) and myotubes (g-i) that have been incubated with PLGA NPs at the concentration of 0.2 mg/ml for 2 h, 24 h and 72 h. PLGA NPs are loaded with Nile red (red fluorescence) and cells are counterstained with either phalloidin conjugate with Alexa488 (green fluorescence) to highlight actin filaments (a-c, g-i) or PKH67 Green Fluorescent Cell Linker (green fluorescence, d-f) to label cell-membrane derived vesicles. Hoechst 33258 (blue fluorescence) staining depicts cell nuclei. Confocal fluorescence microscopy analysis revealed PLGA NPs in the cytoplasm after 2 h (a, arrows), 24 h (b, arrow) and 72 h treatment (c, arrow). PLGA NPs partially co-localizing with fluorescent-labelled membrane derived vesicles were

visible on the surface of myoblasts that have been treated for 2 h (D, arrow) and on the cell surface and cytoplasm of myoblasts after 24 h (e, arrow) and 72 h (f, arrow) incubation. The insets in d, e and f show the partial co-localization between the green fluorescent cell membrane stain PKH67 and PLGA NPs. In myotubes, PLGA NPs were observed near the cell surface but not in the cytoplasm after 2 h incubation (g). PLGA NPs were detected in the cytoplasm in myotubes that have been treated for 24 h (h) and 72 h (i). PLGA NPs near cell nuclei were visible after 24 h (h, arrows and inset) incubation. Scale bars: 50 um. TEM analysis of PLGA NPs intracellular distribution after 2 h (j-l) and 24 h (m) incubation in myoblasts. A PLGA NP enclosed in an endosome (j, arrow) occurs just beneath the cell surface. A PLGA NP (k, arrow) is escaping from an endosome. Two PLGA NPs (l, arrows) occur free in the cytosol. After 24 h incubation (m), the cytoplasm contains large amounts of peculiar vacuoles containing NPs remnants (arrowhead). The inset shows a NPs partially enclosed by autophagic double-membranes (small arrows). Mitochondria (m), endoplasmic reticulum (er), Golgi complex (g). Bars: 250 nm

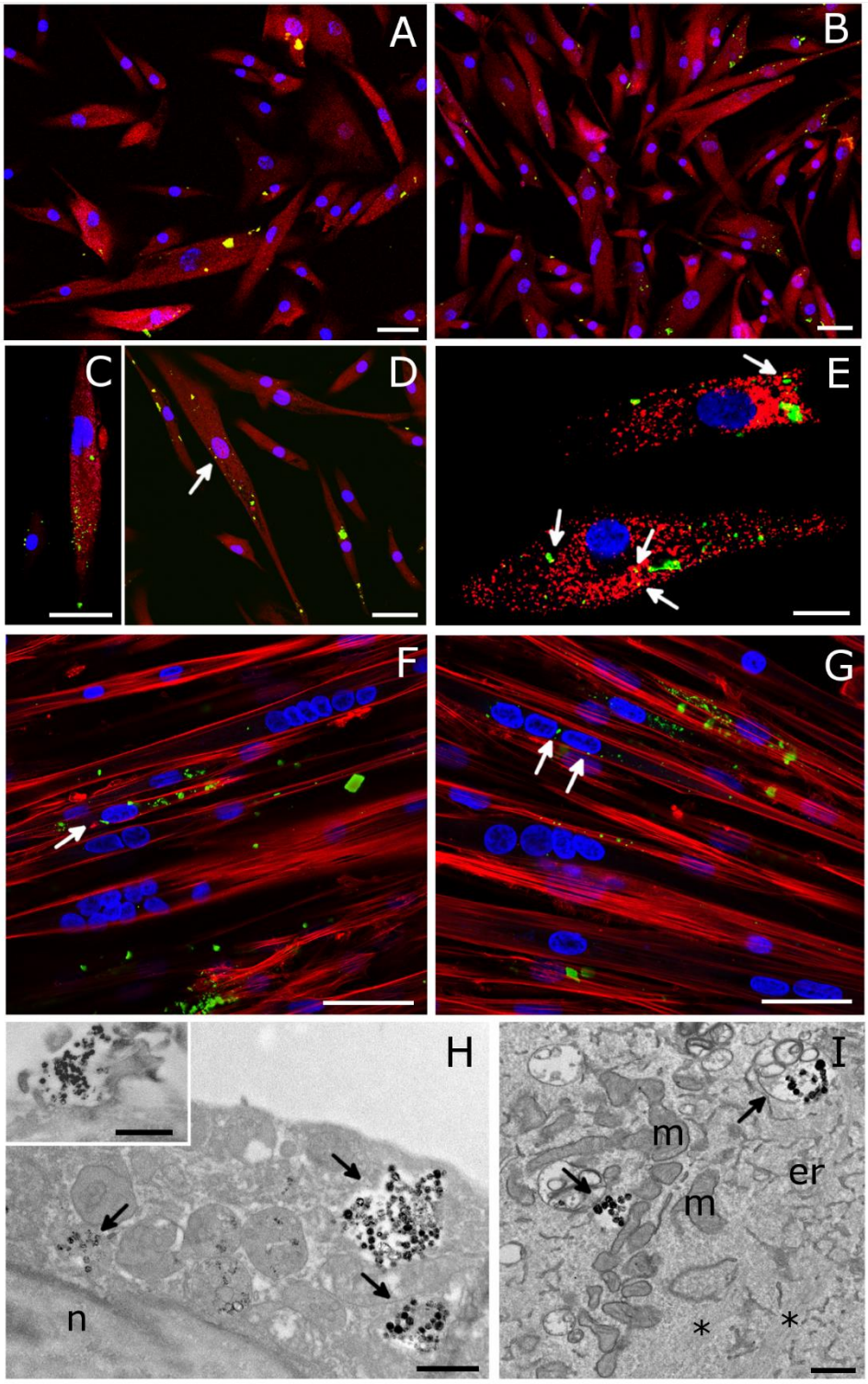

Fig. 3 Intracellular distribution of MSNs in primary human myoblasts and myotubes

Conventional (a, b) and confocal (c-g) fluorescence microscopy analysis of myoblasts (a-e) and myotubes (f and g) that have been incubated with MSNs at the final dose of 0.01 mg/ml for 24 h (a, c, e and f) and 72 h (b, d and g). MSNs are labelled with FITC (green fluorescence) whereas myoblasts and myotubes are counterstained with Trypan blue (red fluorescence, a-d) or with PHK26 Red

Fluorescent Cell Linker (red fluorescence, e) or phalloidin conjugate with Atto 594 (red fluorescence, f, g), respectively. Hoechst 33258 (blue fluorescence) staining has been used to depict cell nuclei. MSNs aggregates occurred in the cytoplasm of a few myoblasts that have been treated with for 24 h (a, c) and 72 h (b, d). A partial co-localization between the red fluorescent cell membrane stain PKH26 and MSNs was observed in myoblasts (e, arrows). MSNs occurred in the cytoplasm of some myotubes that have been treated for 24 h (e) and 72 h (f). MSNs near cell nuclei have also been observed in both myoblasts (d, arrow) and myotubes (e and f, arrows). TEM analysis of MSNs intracellular distribution after 2 h incubation in myoblasts (h) and myotubes (i). Internalized MSNs occur inside various vacuoles (h, arrows), sometimes located very close to the nucleus. Inset: A cluster of MSNs at the cell surface. In myotubes (i), MSNs accumulate in vacuoles (arrows) without perturbing the structural organization: bundles of myofibrils (asterisks), mitochondria (m), endoplasmic reticulum (er), nucleus (n). Bars: 250 nm

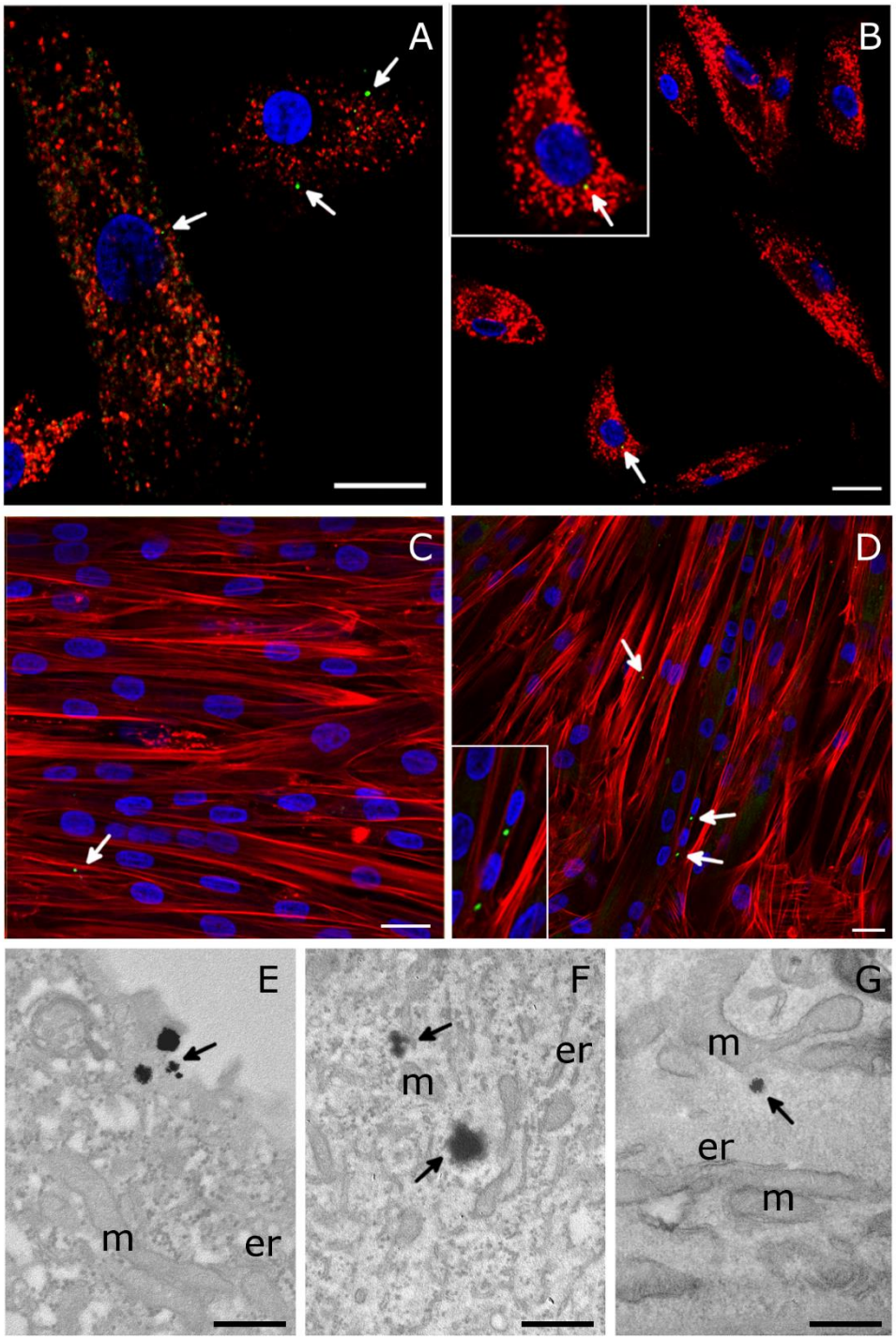

Fig. 4 Intracellular distribution of liposomes in primary human myoblasts and myotubes

Confocal fluorescence microscopy analysis of myoblasts (a, b) and myotubes (c, d) that have been incubated with liposomes at the concentration of 0.2 mg/ml for 24 h (a, c) and 72 h (b, d). Liposomes are labelled with FITC (green fluorescence) whereas myoblasts and myotubes are counterstained PKH26 Red Fluorescent Cell Linker (red fluorescence), to label cell-membrane derived vesicles, or

with phalloidin conjugated with Atto 594, respectively. Hoechst 33258 (blue fluorescence) staining has been used to depict cell nuclei.

Confocal fluorescence microscopy revealed rare liposomes inside primary human myoblasts located close but not within cell nuclei (a, b, arrows). A co-localization between liposomes and fluorescent-labelled membrane derived vesicles was never observed (a, b). A few myotubes displayed liposomes in their cytoplasm after 24 h (c) and 72 h (d) treatment. Scale bars 25 um. TEM analysis of liposome intracellular distribution in myoblasts after 2 h (e) and 24 h (f) incubation, and in myotubes (g) after 2 h incubation. Some liposomes (e, arrow) occur free in the cytoplasm at the cell periphery. The internalized liposomes (f, g, arrows) show fine irregular profiles. Mitochondria (m), endoplasmic reticulum (er). Bars: 250 nm

A. Preliminary results I

Once the biocompatibility of PLGA NPs had been verified for healthy human myoblasts and myotubes, we tested their suitability as nanocarriers for PTM. Two formulations of PLGA NPs (50:50 and 75:25) were synthesized and characterized by Prof. B. Stella and S. Arpicco and loaded with PTM-B. Briefly, both PLGA NPs formulations were synthesized by the nanoprecipitation method (Fessi et al., 1989) starting from PLGA 50:50 (Resomer® RG 502 H, mw 7000-17000 Da) or PLGA 75:25 (Resomer® RG 752 H, mw 4000-15000 Da). For *in vitro* tests, PLGA NPs containing 6 mg/ml polymer and 180 µg/ml PTM-B were used: they showed a diameter ranging from 89.56 to 154.4 nm, a Z potential of -19.3±0.27 mV, an encapsulation efficiency of about 80% and a good stability up to three weeks (unpublished results). Anyways, for the *in vitro* test on DM1 myoblasts freshly prepared NPs were used.

Myoblasts obtained from diagnostic muscle biopsies of a DM1 patient were treated with either PTM-loaded PLGA NPs (75:25 or 50:50) or free PTM-B at different concentrations, according to the literature data on the efficacy of this drug in limiting missplicing (Warf et al, 2009). We found that administration of PTM-loaded PLGA NPs resulted in a statistically significant higher cell viability (3-(4,5-dimethylthiazol-2-yl)-2,5-diphenyltetrazolium bromide, MTT test) as compared to cells treated with the free molecule, suggesting that the delivery of PTM through PLGA NPs reduces the intrinsic drug toxicity (Figure 15).

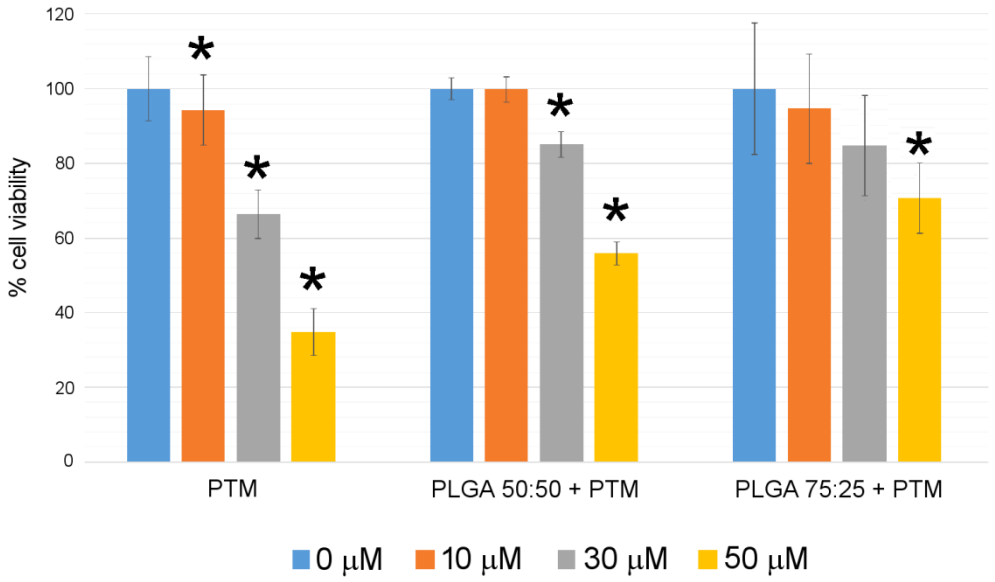

Figure 15. Mean±SD of cell viability of primary human myoblasts obtained from a patient affected by DM1. The effect of free PTM-B, and PLGA 50:50 and 75:25 NPs loaded with PTM-B was measured by the MTT assay 24 h after treatment at different PTM-B concentrations. Asterisks indicate values significantly different from 0μM PTM-B samples (control) (*$p<0.05$, one-way Anova test).

Subsequently, we used primary human myoblasts to evaluate the ability of PTM-loaded PLGA NPs to reduce specific cytopathological features of DM1. Based on the results shown in Figure 1 (Guglielmi et al.), PLGA 75:25 NPs and a concentration of 30 μM PTM-B were selected. In detail, we evaluated the number of intranuclear foci labelled with anti-MBNL1 antibody (one of the pathological markers of DM: Miller et al., 2000; Meola and Cardani, 2009): myoblasts were fixed with 4% paraformaldehyde in PBS for 15 min at 4°C, washed in PBS, and incubated overnight at 4°C with a rabbit polyclonal anti-MBNL1 antibody (kind gift of Prof. C. A. Thornton, University of Rochester, NY) at a dilution of 1:1000 in PBS containing 0.1% bovine serum albumin and 0.05% Tween-20, then incubated for 1h at room temperature with an Alexafluor 488-labelled goat anti-rabbit antibody diluted 1:200 in PBS. The cells were finally stained for DNA with Hoechst 33258, and mounted in PBS-glycerol 1:1. As negative controls, some slides were processed as described above, but omitting the incubation with the

primary antibody. The samples were observed with an Olympus BX51 microscope equipped with a 100W mercury lamp under the following conditions: 450-480 nm excitation (excf) filter, 500 nm dichroic mirror (dm), and 515-550 nm band-pass filter, for Alexafluor 488; 330-385 nm excf filter, 400 nm dm, and 420 nm barrier filter, for Hoechst 33258. For quantitative assessment, the ImageJ software (NIH) was used: the area of the nucleus was measured, the foci were counted, and the results were expressed as the number of foci per square micrometer of nuclear area. As shown in Figure 16 a-b), a significant reduction in the number of MBNL1-posive foci was found after treatment with 30 µM PTM-loaded PLGA 75:25 NPs.

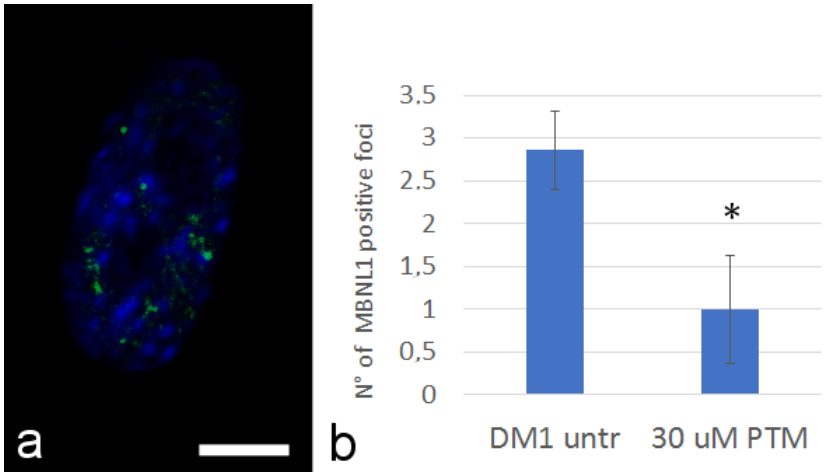

Figure 16. (a) Conventional fluorescence micrograph of a myoblast nucleus immunolabelled with anti-MBNL1 antibody (green fluorescence) and counterstained for DNA with Hoechst 33342 (blue fluorescence); note the green spots (foci). Bar: 10 µm. (b) Quantitative evaluation of foci in myoblast nuclei of a DM1 patient: their number is significantly decreased (asterisk) after incubation with 30 µM PTM-loaded PLGA 75:25 NPs in comparison to untreated (untr) samples (n=25, one-way Anova test).

F. Carton, Y. Chevalier, L. Nicoletti, M Tarnowska, B. Stella, S. Arpicco, M. Malatesta, LP. Jordheim, S. Briançon, and G. Lollo: Hyaluronic acid-based nano-complexes for hydrophilic drug encapsulation (in preparation).

Hyaluronic acid-based nano-complexes for hydrophilic drug encapsulation

Flavia Carton[1,2], Yves Chevalier[1], Letizia Nicoletti[1,3], Małgorzata Tarnowska[1], Barbara Stella[3], Silvia Arpicco[3], Manuela Malatesta[2], Lars Petter Jordheim[4], Stephanie Briançon[1], and Giovanna Lollo[1]*

[1]University of Lyon, Université Claude Bernard Lyon 1, CNRS, LAGEP UMR 5007, 43 bd 11 Novembre 1918, 69622, Villeurbanne, France.

[2]Department of Neurosciences, Biomedicine and Movement Sciences, Anatomy and Histology Section, University of Verona, Strada le Grazie 8, Verona, Italy.

[3]Department of Drug Science and Technology, University of Torino, Via P. Giuria 9, Torino, Italy.

[4]University of Lyon, Université Claude Bernard Lyon 1, INSERM 1052, CNRS 5286, Centre Léon Bérard, Centre de Recherche en Cancérologie de Lyon, 69008 Lyon, France.

* corresponding author

Keywords: hyaluronic acid, polyarginine, pentamidine, biomaterials, polymer-drug complexes, nanoparticles.

Abstract

In this work, nanoparticles of polymeric complexes made of hyaluronic acid and polyarginine were investigated for the encapsulation of the cationic hydrophilic drug pentamidine isethionate. To study the interaction between the anionic hyaluronic acid and the cationic pentamidine, the formation of polyelectrolyte complexes of hyaluronic acid and pentamidine were firstly investigated by mixing them at different mole ratio. Then, nanoparticles made of hyaluronic acid and polyarginine loaded with pentamidine were developed as drug delivery systems of enhanced stability. Pentamidine-loaded nanoparticles formed monodisperse population with a negative zeta potential able to encapsulate pentamidine (80%). Such high encapsulation efficiency was confirmed by measurements of the counterion isethionate released from pentamidine during nanoparticles formation. Besides, freeze-dried pentamidine-loaded nanoparticles kept their integrity after their reconstitution in water. *In vitro* studies on lung (A549) and human breast (MDA-MB-231) cancer cell lines showed that pentamidine-loaded nanoparticles were more cytotoxic in comparison to the free drug, suggesting an enhanced internalization of encapsulated drug by cancer cells.

Introduction

Over the last decades, the development of pharmaceutical nanocarriers based on natural polysaccharides has led to a growing interest in drug delivery technologies.[1] Natural polysaccharides present interesting properties as biocompatibility, biodegradability and low toxicity suitable for biomedical application.[2,3,4] Besides, they have a large number of reactive groups, a wide range of molar masses (M_W), varying chemical composition and origin, which make them a promising biomaterial for the preparation of nanometric carriers.[5]

Among the different natural polysaccharides, hyaluronic acid (HA) has been extensively used in the pharmaceutical field because of its interesting physicochemical and biological properties.[6,7]

HA belongs to the class of anionic glycosaminoglycans (GAGs) formed by several identical subunits (D-glucuronic acid and N-acetyl-D-glucosamine disaccharide) bound together by glycosidic bonds.[8,9] HA is an important component of the extracellular matrix (ECM) highly distributed throughout connective, epithelial, and neural tissues in which plays essential physiological roles.[6] HA backbone itself is endowed with targeting moieties that specifically recognize and interact with different cell surface proteins like stabilin-2, CD44 and other membrane-integrated glycoproteins overexpressed on various cancer cells.[10] Therefore, specific targeting of these receptors has been exploited as an effective strategy for increasing the accumulation of associated drug in the target site.[11,12] In addition, HA bears carboxylic group in each glucuronic unit (p*K*a 3–4) which behaves as an acidic polyelectrolyte enabling interactions with cationic polymers or molecules holding an appropriate basic group which results in the formation of complexes.[13]

So far, in attempts to exploit HA properties, polymeric conjugates, liposomes, microparticles, and nanoparticles (NP) have been developed. They are generally obtained through the formation of self-assembling micelles, chemical conjugation via cross-linking approaches or by polyelectrolyte complexation.[13-16] Among these techniques, polyelectrolyte complexation represents the most widely used method to tailor HA-based drug delivery systems, because of the mild process conditions, absence of organic solvents and wide range of cationic polymers proper for HA interaction.[17] Several previous works provided instances showing the ability of HA-based polyelectrolyte nanostructures to associate active compounds such as genetic materials or positive charged drugs.[7] Contreras-Ruiz et al. described NP made of HA complexed with chitosan (CS) oligomers for pDNA delivery. HA-CS complexes entered cells and yielded significant transfection of pDNA into the corneal and conjunctival cells.[18] Recently, a novel ionic metal complex based on HA and an oxaliplatin derivative, dichloro(1,2-diaminocyclohexane) platinum(II) (DACHPt), has been patented. Compared to the DACHPt aqueous solution, once injected intravenously, DACHPt-loaded nano-complexes were able

to protect the associated drug from enzymatic degradation enhancing plasmatic concentration while lowering drug elimination rate.[19] Also, Battistini et al. reported a doxorubicin-HA ionic complex as a tumor targeting drug delivery system. *In vitro* studies on tumor cells overexpressing CD44 receptors demonstrated the improved internalization of the complexes in comparison to the free drug.[11]

Based on this background information, the present work deals with an extensive physicochemical characterization of polyelectrolyte complexes (PEC) made of HA and a cationic molecule, pentamidine isethionate (PTM) as model drug. PTM is well known for its antiprotozoal, antifungal and anticancer activity.[20,21] It is a water-soluble molecule with two terminal amidine groups, protonated in a wide pH range (pK_a = 12-13) including physiological/neutral conditions. To stabilize PTM-HA PEC and to maximize the amount of PTM associated to the system, polyarginine (PArg) was used to crosslink HA and form NP. PArg is a biocompatible cationic polyaminoacid belonging to the cell penetrating peptide polymers able to improve the intracellular delivery of the therapeutic agent.[22] At neutral pH, the amine groups of PArg are protonated and are able to interact with carboxylic moieties of HA leading to the formation of NP. The formation of PEC and NP was investigated studying size, zeta potential evolution and quantifying the amount of isethionate, the PTM counterion, released during the formation process. Lyophilization studies were also carried out in order to preserve PTM-loaded NP. The morphology of the formed systems was analyzed by transmission electron microscopy (TEM) and cryogenic-transmission electron microscopy (Cryo-TEM). Finally, *in vitro* studies were performed on lung and breast human cell lines (A549 and MDA–MB 231) to assess the anticancer activity of encapsulated PTM.

Experimental section

Materials

Sodium hyaluronate (HA) (Molar mass, M_w = 20 kDa) was purchased from LifeCore® Biomedical (Chaska, Minnesota, USA). Poly(L-arginine hydrochloride) (PArg) (Molar mass, M_w = 5.8 kDa) was purchased from Alamanda® Polymers (Huntsville, Alabama, USA) and pentamidine isethionate (PTM) (Molar mass, M_W = 592.679 Da) from Sigma-Aldrich® (St Quentin-Fallavier, France). Milli-Q water was obtained using a milli-Q Academic System (Merck Millipore®, St Quentin-Fallavier, France). For transmission electron microscopy (TEM) silicotungstate was supplied from Agar Scientific® (Parsonage Lane, Stansted, UK*).* Dulbecco's Modified Eagle Medium (DMEM) without glucose, glutamine, phenol red and sodium pyruvate was bought from Gibco® (Thermo Fisher Scientific®, Waltham, Massachusetts, USA) and used to evaluate the stability in physiological medium. Human lung carcinoma cells (A549) and human breast adenocarcinoma cells (MDA-MB-231) were from ATCC and grown in complete Dulbecco's Modified Eagle Medium (DMEM), Gibco, Thermo Fisher Scientific, Inc) supplemented with 10% fetal bovine serum, 100 U/mL penicillin, 100 mg/mL streptomycin, 1% L-glutamine, all were purchased from Life Technologies® (Carlsbad, California, USA). 3-(4,5-dimethylthiazol-2-yl)-2,5-diphenyltetrazolium bromide (MTT) purchased from Sigma-Aldrich (St Quentin-Fallavier, France).

Solubility study of pentamidine

Saturated solutions of PTM at different pH solution (pH 7.4, 9, 10, 12) and in phosphate buffer saline (PBS, pH 7.4) were prepared. The solutions were stirred for 2 h at room temperature and left overnight to reach equilibrium. Then, all samples were centrifuged (62,000 g, 30 min, 20 °C) and the supernatant was analyzed for PTM by measuring its UV absorbance at $\lambda = 270$ nm (UV-1280, Shimadzu, Marne-la-Vallée, France).

Preparation of pentamidine-hyaluronic acid polyelectrolyte complexes

Pentamidine-hyaluronic acid polyelectrolyte complexes (PTM-HA PEC) were prepared by mixing aqueous solutions of PTM and HA at different mole ratio PTM/HA ranging between 0.2 and 2.4. Seven different PTM-HA PEC were obtained by adding 500 µL of HA aqueous solution (2.5 $mg \cdot mL^{-1}$) over 500 µL of PTM solution in water (concentration from 0.6 to 9 $mg \cdot mL^{-1}$). Size, polydispersity index, zeta potential and pH of PEC were studied.

Preparation of blank and pentamidine-loaded nanoparticles

Blank nanoparticles (HA-PArg NP) were prepared by polyelectrolyte complexation using a similar methodology of ionic gelation technique.[23] Briefly, 0.5 mL of an anionic solution containing HA at different concentration (ranging from 0.5 to 5 $mg \cdot mL^{-1}$) were added to an equal volume of cationic solution containing polyarginine (PArg) (0.27 $mg \cdot mL^{-1}$). Nine different formulations with mole ratio HA/PArg between 0.82 to 8.25 were prepared.

Pentamidine-loaded nanoparticles (PTM-loaded NP) were prepared by mixing 0.5 mL of different amounts of PTM dissolved in water (ranging from 0.50 to 0.17 $mg \cdot mL^{-1}$) and 0.5 mL of cationic PArg solution at 0.18 $mg \cdot mL^{-1}$. This premix was left under agitation during 10 min, and 0.5 mL of HA solution (ranging from 0.83 to 3.3 $mg \cdot mL^{-1}$) were added. The mole ratio between HA (negatively charged) and PArg, PTM (positively charged) was ranging between 1.13 and 4.51. HA-PArg NP and PTM-loaded NP were characterized in terms of pH, size, polydispersity index, zeta potential and encapsulation efficiency. The main characteristics of all the compounds used to obtain PEC and NP are listed in Table 1.

Table 1. Chemical characteristics of the compounds used to obtain polyelectrolyte complexes and nanoparticles.

Compound	Molecular formula	Molecular structure	p*Ka*	M_W (g·mol^{-1})
Pentamidine isethionate	$C_{23}H_{36}N_4O_{10}S_2$	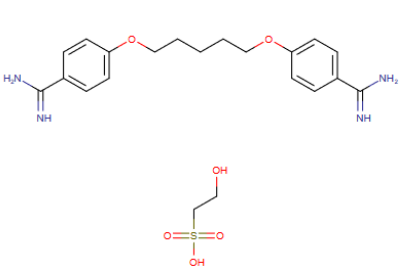	12.13	592.679
Sodium Hyaluronate	$(C_{14}H_{20}NO_{11}Na)_n$	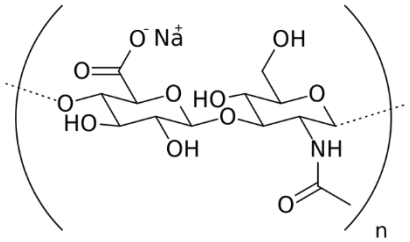	2.87	401.3
Poly(L-arginine hydrochloride)	$(C_6H_{14}N_4O_2)_n$	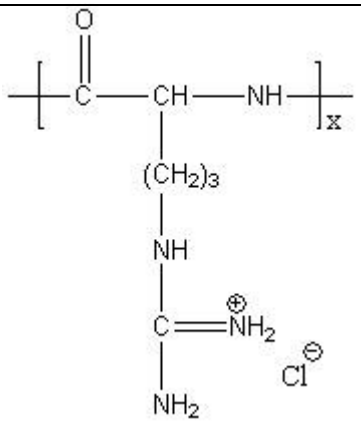	12.42	174.201

Physicochemical characterization of polyelectrolyte complexes, blank and pentamidine-loaded nanoparticles

Size distribution and surface potential of the prepared particles (PEC and NP) were analyzed using a Malvern Zetasizer® (model Nano ZS, Malvern Panalytical, Malvern, UK). Particle size distributions were determined by Dynamic Light Scattering (DLS) of samples diluted with milli-Q water. Analyses were carried out at 25 °C with an angle of detection of 173°. Particle size distribution was determined

using the cumulants method that provides the *z*-average diameter and the polydispersity index (*PdI*). The zeta potential (ζ) was determined from the electrophoretic mobility (u_E). For all measurements, samples were diluted in milli-Q water and placed in a U-tube shaped electrophoresis cell DTS1070 from Malvern. ζ was calculated according to the Henry equation under the Smoluchowski approximation of the Henry factor $f(\kappa a)$:

$$u_E = \frac{2}{3}\frac{\varepsilon_0 \varepsilon\, \zeta}{\eta} f(\kappa a)$$

where η is the viscosity of water (η = 0.887 mPa·s at 25 °C), κ is the inverse Debye length, a is the radius of particles, and $f(\kappa a)$ = 3/2.

Turbidity of PEC was monitored by absorbance measurements at 600 nm using an UV spectrometer (UV-1280 from Shimadzu, Marne-la-Vallée, France) equipped with a cuvette with an optical path of 10 mm. The turbidity (τ) was calculated from the absorbance (*Abs*) reading as τ = ln (10) *Abs* = 2.3 *Abs*.

Ion-exchange chromatography

Isethionate ions released due to association of positively charged PTM to negatively charged HA were quantified using ion exchange chromatography (IC) (930 Compact IC Flex, Metrohm, Switzerland) equipped with a chemical suppressor and conductivity detection. PTM-loaded NP were centrifuged (7,000 g, 30 min, 25 °C) using Amicon® filter (Amicon Ultra-0.5, 30,000 NMWL, Millipore, Spain), supernatants were recovered and injected at the IC. The analyses were conducted using Metrosep a Supp 5 250/4.0 column with an adequate pre-column at the temperature of 30 °C. For the detection of anions, the mobile phase used was 8 mmol·L^{-1} solution of Na_2CO_3 (Fischer Scientific, France) prepared in ultrapure water (resistivity > 18 MΩ·cm), filtered at 0.45 µm and

degassed in an ultrasonic bath prior to use with a flow rate of 0.7 $mL \cdot min^{-1}$. Such conditions ensured linearity of calibration curve ranging from 0.005 to 5 $mmol \cdot L^{-1}$ of isethionate.

Morphological analysis of blank and loaded nanoparticles using transmission and cryogenic electron microscopy

Transmission electron microscopy (TEM) was performed with a Philips CM120 microscope at "Centre Technologique des Microstructures" (CTμ) at the University of Lyon 1 (Villeurbanne, France). A small drop of suspension (5 μL) was deposited on a carbon/formvar microscope grid (Delta Microscopies, Saint-Ybars, France), negatively stained with a 1% w/w sodium silicotungstate aqueous solution, and slowly dried in open air. The dry samples were observed by TEM under 120 kV acceleration voltage.

Regarding cryogenic-transmission electron microscopy (Cryo-TEM), diluted samples of HA-PArg NP and PTM-loaded NP were dropped onto 300 mesh holey carbon films (Quantifoil R2/1) and quench-frozen in liquid ethane using a cryo-plunge workstation (made at Laboratoire de Physique des Solides-LPS Orsay, France). The specimens were then mounted on a precooled Gatan 626 specimen holder, transferred in the microscope (Phillips CM120) and observed at an accelerating voltage of 120 kV at the "Centre Technologique des Microstructures" (CTμ) at the University of Lyon 1 (Villeurbanne, France).

Encapsulation efficiency of pentamidine into complexes and nanoparticles

The association efficiency (*AE*) of PTM into PEC and the encapsulation efficiency (*EE*) of PTM into loaded NP was determined by measurements of the concentration of free PTM in the aqueous phase. PTM-HA PEC and PTM-loaded NP were centrifuged (7,000 g, 30 min, 25 °C) using Amicon® filter (Amicon Ultra-0.5, 30.000 NMWL, Merck Millipore®, Burlington, Massachusetts, USA),

supernatants were recovered and analyzed for free PTM using UV absorbance at 270 nm wavelength. Calibration was performed using PTM solutions at different concentrations from 2.5 µg·mL^{-1} to 30 µg·mL^{-1}. AE and *EE* were calculated using the following equation:

$$AE/EE(\%) = \frac{Total\ drug - Free\ drug\ in\ supernatant}{Total\ drug} \times 100$$

All measurements were performed at least in triplicate using PTM aqueous solution as control.

Stability studies of blank and pentamidine-loaded nanoparticles

Colloidal stability of HA-PArg NP and PTM-loaded NP was evaluated over 4 weeks under storage condition at 4 °C. Size, polydispersity index and ζ were analyzed every week. Leakage of the drug was also evaluated at the end of the storage period.

The stability in DMEM without glucose, glutamine, phenol red and sodium pyruvate was also tested in order to study the effect of protein factors on NP aggregation.

***In vitro* release study of pentamidine-loaded nanoparticles**

In vitro release behavior of PTM-loaded NP in simulated physiological conditions (PBS at 37 °C) was performed using a bicompartmental diffusion device (Franz-type static glass diffusion cells) mounted with a semi-synthetic cellulose membrane (6-8 kDa MWDO from Spectra/Por, Spectrum Laboratories, The Netherlands). To assure sink condition 2 mL of PTM-loaded NP prepared using 2.3 and 3.3 mg·mL^{-1} of HA and 0.50 mg·mL^{-1} of PTM were placed in the upper part of the cell (donor chamber). The lower part of the cell (receptor chamber) was filled with 10 mL of release media (PBS, pH 7.4 at 37 °C) with a horizontal shaking. At different time points (15 min, 30 min, 1 h, 2 h, 3 h, 4 h, 6 h, 8 h, 24 h,48 h, 72 h), 1 mL of each sample was collected and analyzed using UV spectra (λ = 270 nm). The amount of drug released over the time was calculated indirectly by the difference

between the initial total amount of the drug present in PTM-loaded NP and the amount of PTM present in the receptor chamber. The experiment was performed for both NP in triplicate.

Freeze-drying studies of blank and loaded pentamidine nanoparticles

Once the development of NP has been completed, HA-PArg NP and PTM-loaded NP were freeze-dried using CRYONEXT pilot freeze dryer. During the formulation step, the bulking agent mannitol was added to the formulations at different concentration (5%, 10% w/v). The freeze-drying program consisted of an initial freezing at -20 °C in a freezer for 12 h. After that, the freeze dryer was pre-cooled to -20 °C and the samples were introduced therein. Then, the temperature was decreased to -50 °C at a rate of 1 °C·min^{-1} and this temperature was kept for 12 h. The sublimation step was carried out at a temperature between -35 °C and 5 °C and a pressure between 0.100 and 0.3000 mbar according to the recipe. Finally, the secondary drying step is carried out at 35 °C and 0.010 mbar. After freeze-drying, HA-PArg NP and PTM-loaded NP were resuspended by adding 1 mL of milli-Q water and left under magnetic stirring for 30 min. Size, polydispersity, AE of PEC and EE of NP were measured before and after resuspension. Also, morphological observations using TEM form were performed.

***In vitro* cell viability studies**

Human lung carcinoma cells (A549) and human breast adenocarcinoma cells (MDA-MB-231) were used to evaluate the cell viability. Cells (3000 cells/well) were seeded in 96 well plates in 100 µL media and left to adhere for 24 hours. Then, the medium was replaced with a fresh one containing different concentrations (0.01- 100 µM) of free PTM, HA-PArg NP and PTM-loaded NP. After 72 h of exposure, metabolically active cells were quantified by 3-(4,5-dimethylthiazol-2-yl)-2,5-diphenyltetrazolium bromide (MTT) assay according to the supplier's instructions. Briefly, 20 µL of

MTT reagent (5 mg·mL^{-1}) was added in each well and the plate was incubated at 37 °C for 2 h. After that the supernatant was replaced by 100 µL of isopropanol/HCl/H_2O (90/1/9 v/v/v) and the optical density was measured using Ascent Software for Multiskan at 570-690 nm. Cell viability from the absorbance values was calculated using the following equation:

$$Cell\ viability\ (\%) = \frac{Abs_{treated}}{Abs_{untreated}} \times 100$$

IC50 values were determined using the CompuSyn software. Results are expressed as mean values of IC50 ± SD (µM) of three independent experiments.

Results and discussion

Solubility of pentamidine at different pH

PTM is a synthetic amidine derivative, highly soluble in water (> 30 mg·mL^{-1}) having a p*K*a of 12.5. [20,21] In the range of pH from 3 to 10, is it free soluble (values above 50 mg·mL^{-1}) due to the ionization of amidine groups, while at pH values higher than 12 the solubility was drastically reduced (6.5 mg·mL^{-1}) (Figure 1). Solubility also depends on ionic strength, in fact at pH 7.4 in PBS, PTM highly precipitated being the solubility of around 6.9 mg·mL^{-1}.

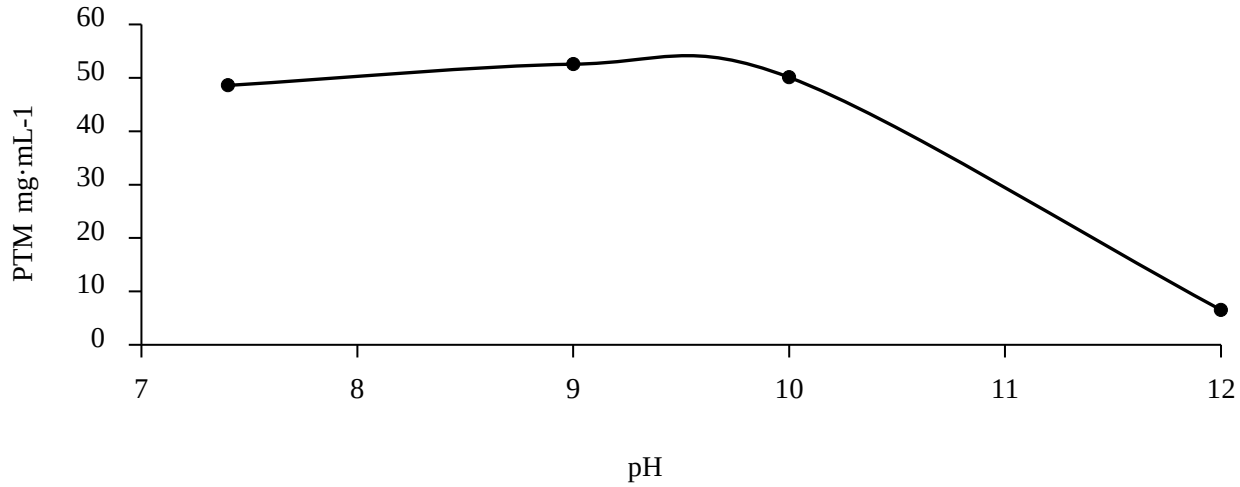

Figure 1. Solubility of PTM at different pH values.

Preparation and physicochemical characterization of pentamidine-hyaluronic acid polyelectrolyte complexes

Polyelectrolyte complexes (PEC) are defined as complexes formed through electrostatic interactions between oppositely charged structures. The formation of PTM-HA PEC was based on the electrostatic interaction between the positively charged drug (PTM), containing two amino groups and the negatively charged polysaccharide (HA) which contains one carboxylic unit for each repeat unit. The stoichiometry of the complex was defined as the PTM/HA mole ratio of the HA repeated unit to the PTM molecules. The repeated unit of HA contains two sugar residues, neutral N-acetyl-D-glucosamine and negatively charged sodium salt of D-glucuronic acid acid (Table 1). The PTM/HA charge ratio is half the mole ratio since PTM is a divalent cationic compound. Different PTM-HA PEC having a mole ratio PTM/HA between 0.2 and 2.4 (from PEC A to PEC G) (Table 2). Briefly, HA solution was added to an equal volume of PTM at different concentration under magnetic stirring. Since the concentration of the low molecular electrolyte strongly affects the formation of the complexes, only the amount of PTM was varied.[24] All the formulations were prepared at pH values around 6-7 in order to obtain an optimal charge density that generates attractive interactions between the cationic amine groups of PTM and the carboxylate groups of HA.

Table 2. Formulation code for PTM-HA PEC developed. Mole ratio HA/PTM and PTM/HA, mass ratio, and pH values are represented.

Complexes	Mole ratio PTM/HA	Mass ratio PTM/HA	pH
PEC A	0.2	2.5: 0.6	6.75
PEC B	0.3	2.5: 1.25	6.79
PEC C	0.7	2.5: 2.5	6.71
PEC D	0.9	2.5: 3.7	6.86
PEC E	1.5	2.5: 5.5	6.74
PEC F	2.0	2.5: 7.5	6.76
PEC G	2.4	2.5: 9.0	6.74

Size measurements of PTM-HA PEC were carried out using DLS. Two different size populations were identified for all the PTM-HA PEC: one having a hydrodynamic diameter of around 10 nm, and another one of around 150 nm (Figure 2). As shown in Figure 2, the increase of PTM concentration, from PEC A (purple line) to PEC G (black line), is correlated to an increase of the peak at 10 nm and a simultaneous decrease of the peak at 150 nm. Thus, the two different populations were attributed to the formation of soluble complexes of size around 10 nm, and insoluble complexes of size around 150 nm. The increase of PTM concentration caused the larger binding of PTM to HA, increasing its hydrophobic character and decreasing its charge, so that precipitation took place above a given PTM concentration. To confirm this hypothesis, the presence of soluble complexes in the supernatant after ultracentrifugation using Amicon® filter was detected for PEC A and PEC B by means of size measurements. Both complexes (PEC A and PEC B) presented only the peak at 10 nm, relative to the presence of the soluble complex while the population having a size around 150 nm has been retained by the filter (Figure 3).

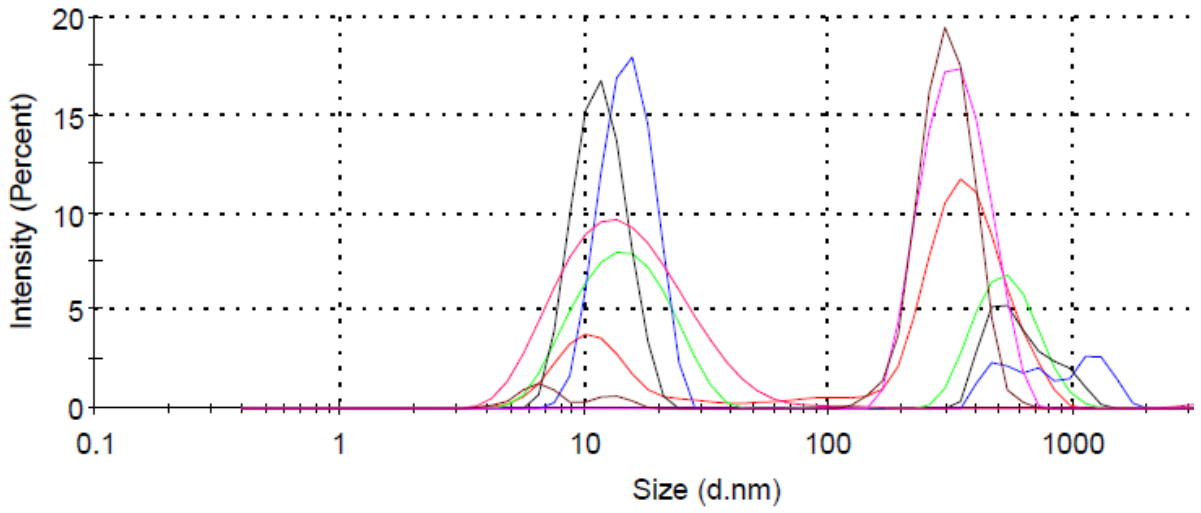

Figure 2. Size distribution of PTM-HA PEC. PEC A: mole ratio PTM/HA 0.2 (purple), PEC B: mole ratio 0.3 (brown), PEC C: mole ratio 0.7 (pink), PEC D: mole ratio 0.9 (red), PEC E: mole ratio 1.5 (green), PEC F: mole ratio 2.0 (blue), PEC G: mole ratio 2.4 (black). Distributions are given as mean ± SD (n = 3)

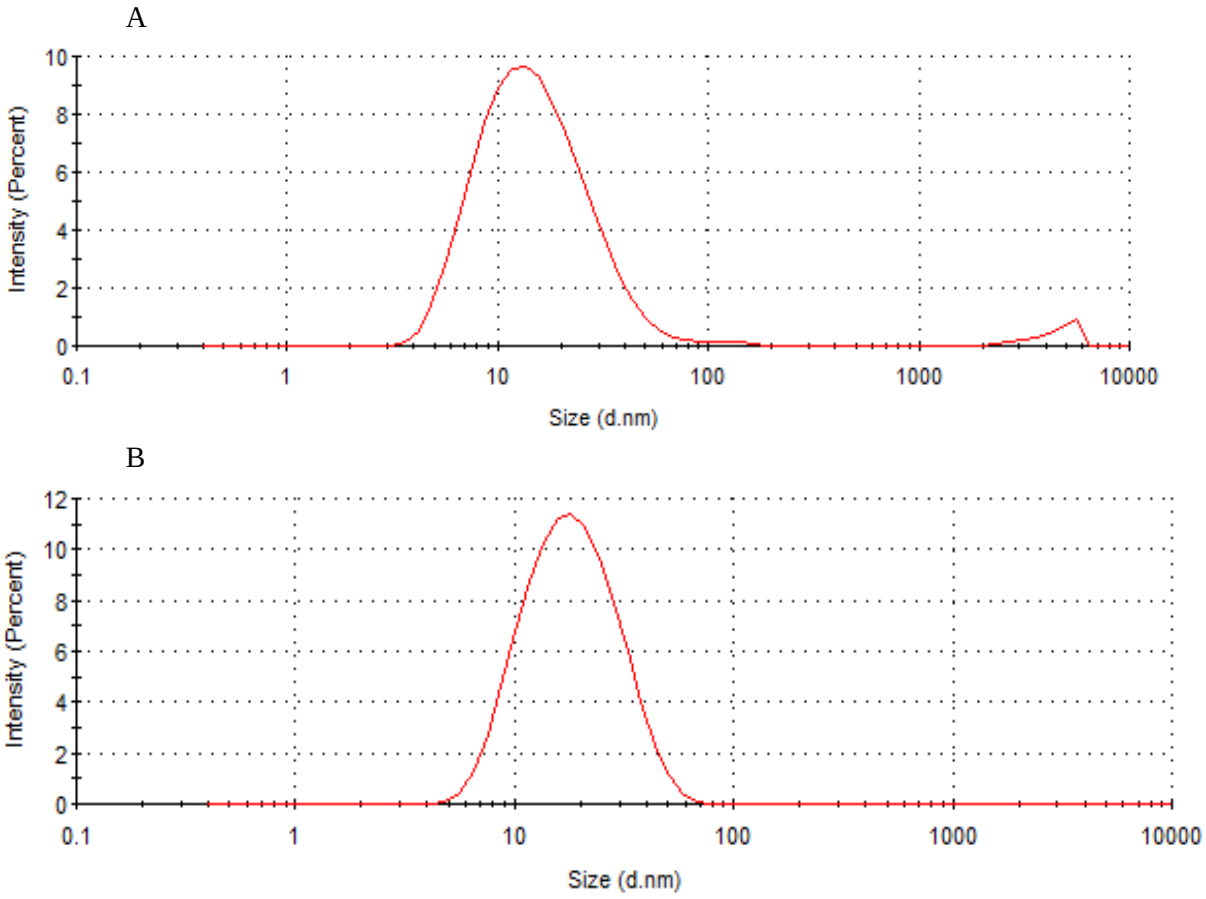

Figure 3. Size distribution (nm) of soluble complexes (PEC A and PEC B) detected in the supernatant.

Turbidity measurements of PTM-HA PEC provide a confirmation of the conclusions drawn from DLS. The interaction between HA and PTM was accompanied by an increase in turbidity (Figure 4). A slight increase of turbidity was first observed as PTM was added to HA. Then a sharp increase of turbidity took place between PTM/HA ratios of 1.5 and 2.4, indicating precipitation of insoluble species. This data confirmed the formation of insoluble particles upon increasing PTM concentration. Moreover, turbidity data disclosed precipitation occurring in a narrow concentration domain. As an outcome, combination of DLS and turbidity revealed that the solubility of the complex progressively decreased as more PTM bound to HA.

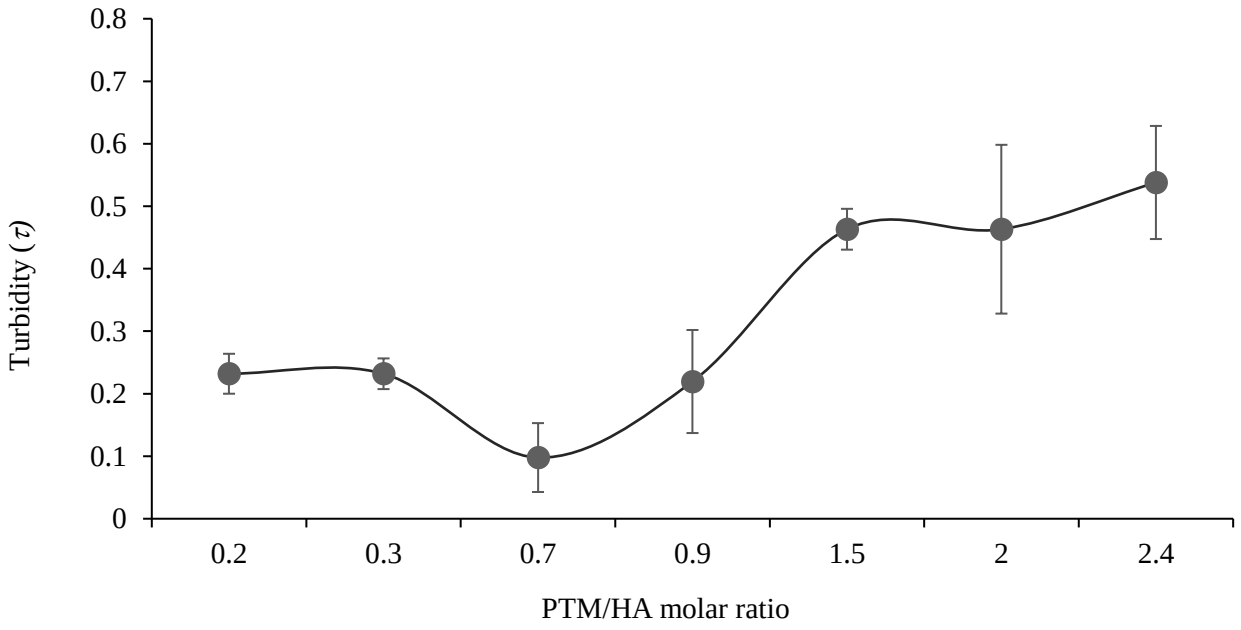

Figure 4. Turbidity (Abs = 600 nm) of PTM-HA PEC as a function of PTM/HA mole ratio. PEC A mole ratio 6.61, PEC B mole ratio 2.98, PEC C mole ratio 1.49, PEC D mole ratio 1.06, PEC E mole ratio 0.68, PEC F mole ratio 0.50, PEC G mole ratio 0.41. Values are given as mean ± *Sem* (*n* = 3).

The assignment of the low- and large-sized species to soluble complexes and insoluble particles respectively is in accordance with similar cases of mixed polyelectrolytes of opposite charges reported in the framework of complex coacervation.[25-27] The presence of soluble complexes as function of mixing ratio and supramolecular order of polymeric chains has already been disclosed in such previous works.[25-27] Electrostatic interaction between the negatively charged carboxylate groups of HA and positively charged groups of PTM shifts the complexation equilibria towards formation of both complexes. The complexes formed in this way are soluble when the charge is low. Higher concentration of PTM makes the complex species more hydrophobic and decreases the negative charge of HA. Both effects act together to decrease the solubility of the complex. Precipitation occurs when the solubility becomes lower than the HA concentration. A coacervate phase separates as nanoparticles.

DLS disclosed the presence of nanoparticles of 150 nm and there was a slight turbidity for PTM/HA < 1.5 where the complexes were claimed soluble. Both results showed that there were few nanoparticles formed below this ratio. Indeed, such nanoparticles were few as their contribution to the "intensity" size distribution inferred from DLS should be viewed considering that large particles scatter light stronger than the small soluble species, so that their contribution to the "volume" size distribution was weaker than that the "intensity" size distribution shown in Figure 2. Such few precipitated nanoparticles might come from the smaller solubility of complexes formed with the sodium hyaluronate macromolecules of the largest molar masses in the broad molar mass distribution of HA.

ζ measurements gave more insight into the mechanism of precipitation above PTM/HA = 1.5. (Table 3). ζ was negative over the whole concentration range studied, showing that binding of PTM to HA did not allow for compensation of the negative charge of HA. Binding of PTM was sub-stoichiometric with respect to electrical charges. ζ assumed less negative values as the concentration of PTM was increased, indicating a neutralization of the charge at high PTM/HA mole ratio. The same behavior occurred with electrophoretic mobility measurement (Figure 5). Therefore, the highly charged complex species at low PTM content were soluble; precipitation occurred when the negative charge has been reduced such that weakened electrostatic repulsions between charged complex species allowed for aggregation and precipitation as colloidal particles. Precipitation occurred when repulsive electrostatic forces between complex species become weaker than attractive forces of hydrophobic and dispersion (van der Waals) origins.[28,29] It is worth noticing that the complex is more hydrophobic than free HA because PTM is a more hydrophobic molecule than HA; indeed, PTM has the structure of a bolaform surfactant.[30] Such behavior as the same features as the adsorption of polyelectrolytes to colloidal particles of opposite charge where weakening the charge by adsorption

cause the interparticle interactions to turn from repulsive to attractive upon increasing the PE/NP ratio.[31]

The association efficiency (*AE*) of PTM was measured by centrifugation and titration of the supernatant. *AE* was quite low in all instances (Table 3). The PTM/HA mole ratio is twice the PTM/HA mole ratio since PTM is a divalent cationic species whereas the repeat unit of HA is singly charged. The mole ratio increased with respect to PTM concentration and approached the value of one corresponding to charge compensation when extensive precipitation of nanoparticles occurred (samples PEC F and PEC G). It is presumed that PEC had a neutral central core containing the main part of PTM and a negatively charged shell richer in HA that generate electrostatic repulsions allowing the formation of nanoparticles.

Table 3: Physicochemical characteristics of PTM-HA PEC (PEC A - PEC G). EE (%): encapsulation efficiency. Values are given as mean ± Sem ($n > 3$).

Complexes	**Mole ratio PTM/HA**	**pH**	**Zeta potential (mV)**	**AE (%)**
PEC A	0.2	7.17	- 21.7 ± 1.6	42 ± 9
PEC B	0.3	7.07	- 15.7 ± 2.8	32 ± 6
PEC C	0.7	6.78	- 12.3 ± 2.8	33 ± 4
PEC D	0.9	6.76	- 10.4 ± 1.7	19 ± 8
PEC E	1.5	6.79	- 9.4 ± 2.3	22 ± 5
PEC F	2.0	6.65	- 4.8 ± 1.6	22 ± 2
PEC G	2.4	6.22	- 3.1 ± 1.3	15 ± 1

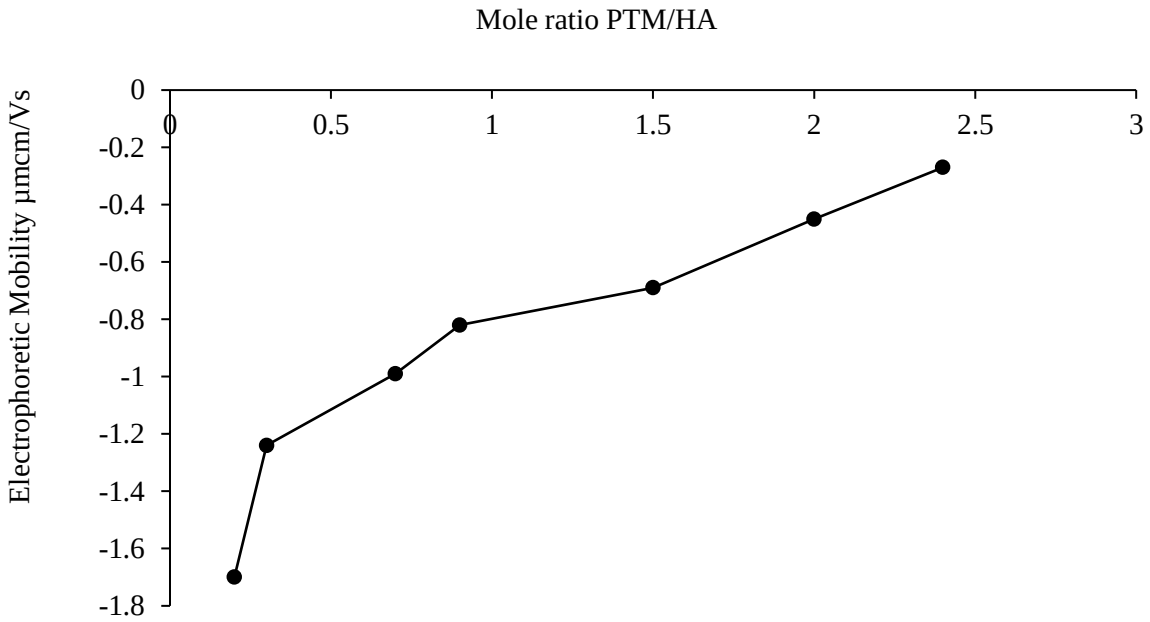

Figure 5. Electrophoretic mobility of PTM-HA PEC in function of mole ratio PTM/HA (from 0.2 to 2.4). Values are given as mean ± SD (n > 3).

As an overall outcome, complexation of PTM by HA takes place and it causes the formation of NP. But soluble complex species form at low PTM/HA ratio; formation of NP requires PTM/HA mole ratio above 1.5. Under such conditions, the low association efficiency (less than 40%) is an issue. Electrostatic binding of PTM to HA is weak because the PTM cation is only divalent. Since the association of polyelectrolytes of opposite charges is usually quite strong, a cationic polyelectrolyte (polyarginine, PArg) will be added in order to help precipitation and improve the encapsulation of PTM.

Preparation and physicochemical characterization of the blank hyaluronic acid-polyarginine nanoparticles

To stabilize the insoluble form of PEC and to obtain a delivery system able to associate a high amount of PTM, NP made of HA and the cationic polyaminoacid PArg were prepared. PArg was selected as a cationic polymer able to crosslink HA and allowing the formation of nanoparticles. HA-PArg NP were prepared by polyelectrolyte complexation in a similar manner described by Yadav et al.[23] Briefly, 0.5 mL of a solution containing HA at different concentration (from 0.5 to 5 $mg \cdot mL^{-1}$) were added to an aqueous solution of PArg (0.27 $mg \cdot mL^{-1}$) under magnetic stirring at room temperature for 30 min. The formation of NP was ensured by the electrostatic interaction between the positively charged groups of PArg and the negatively charged carboxylate groups of HA.

HA-PArg NP (Blank A - Blank I) containing different amounts of HA (from 0.5 to 5 $mg \cdot mL^{-1}$) with a mole ratio HA/PArg between 0.82 and 8.25 were studied for their size, polydispersity index (*PdI*) and ζ (Table 4).

The average size of the resulting blank NP ranged between 112 and 244 nm with a low polydispersity index (< 0.2). ζ values ranged from +33 to -22 mV. When the charge ratio HA/PArg was lower than 1.24, NP had a size around 120 nm with a positive ζ values (+33 mV) indicating that the charge brought about by PArg was larger than that of HA. At mole ratio higher than 1.24, NP size increased from 166 to 244 nm, and an inversion of the ζ to -31 mV occurred. The increase in the hydrodynamic size was correlated to the amount of HA used to obtain the NP. Besides, inversion of surface potential indicated a conformational change which exposes carboxylic groups of HA in excess with respect to cationic groups of PArg towards the external surface of NP. The HA/PArg system is interesting as it allows the preparation of NP of 100-250 nm size with a narrow size distribution and reversal of the electrical charge according to the HA/PArg ratio. It is worth to notice that NP sizes did not vary much although the chemical composition and the overall charge of them varied in a wide range.

It is presumed that the precipitation mechanism of NP was the same whatever the HA/PArg ratio. So, neutral nanoparticles precipitated as a first step and an outer shell rich in the majority polymer further adsorbed on the surface and set the final electrical charge.

Table 4. Physicochemical characteristics of HA-PArg NP. *PdI*: Polydispersity index. Values are given as mean ± Sem ($n \geq 3$).

	Mass ratio [HA/PArg]	**Mole ratio [HA/PArg]**	**Size (nm)**	***PdI***	**Zeta potential (mV)**
Blank A	0.50: 0.27	0.82	112 ± 6	< 0.2	+ 33 ± 5
Blank B	0.75: 0.27	1.24	129 ± 1	< 0.2	+ 32 ± 3
Blank C	1.25: 0.27	2.06	166 ± 7	< 0.2	- 31 ± 0
Blank D	1.5: 0.27	2.47	158 ± 4	< 0.2	- 38 ± 2
Blank E	2.0: 0.27	3.30	167 ± 3	< 0.1	- 33 ± 2
Blank F	2.5: 0.27	4.12	180 ± 14	< 0.1	- 29 ± 3
Blank G	3: 0.27	4.95	201 ± 14	< 0.1	- 31 ± 3
Blank H	3.5: 0.27	5.77	222 ± 11	< 0.2	- 30 ± 4
Blank I	5: 0.27	8.25	244 ± 5	< 0.1	- 22 ± 3

Development and physicochemical characterization of pentamidine-loaded hyaluronic acid-polyarginine nanoparticles

PTM-loaded NP were prepared following the protocol described for blank NP. Different concentrations of HA (0.83 $mg \cdot mL^{-1}$ to 3.3 $mg \cdot mL^{-1}$) were added to an aqueous solution containing PArg (0.18 $mg \cdot mL^{-1}$) and PTM (concentration ranging from 0.5 to 0.17 $mg \cdot mL^{-1}$) (Figure 6).

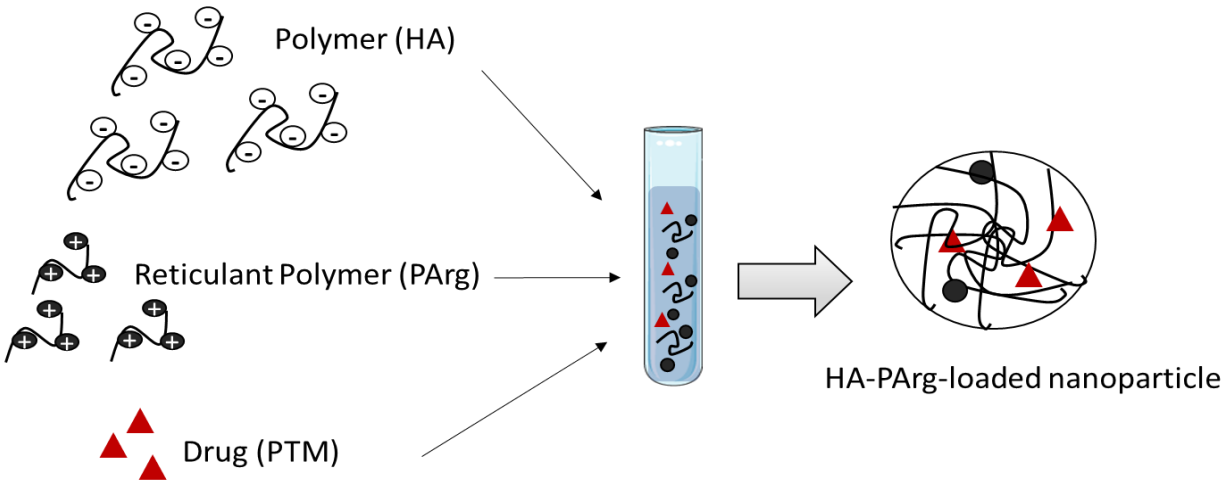

Figure 6. Preparation of PTM loaded NP by polyelectrolyte association.

In Table 5 the physicochemical characterization of NP obtained using a PTM solution at 0.5 mg·mL^{-1} was presented. All the NP showed an average size between 155 and 203 nm with a low *PdI* (< 0.1) and a negative ζ ranging from -24 to -18 mV. Interestingly, the incorporation of the drug in the NP involved a reduction of the NP size compared to the blank ones (Table 4). The balance between negative (HA) and positive charge (PTM and PArg) was reduced in the case of PTM-loaded NP as compared to the HA-PArg NP. Therefore, the attractive force that modulates electrostatic interactions within the complexes determined a "condensation phenomenon" responsible of the reduction of the complex particle size.[32,33] The ζ decreased from -24 to -76 mV for Loaded A to Loaded F, and then increased to -18 mV for Loaded G. The effect of NP size reduction has been observed also for other particles suggesting the strong interaction between the drug and the polymeric chains.[14] Table 5 also shows the results of the encapsulation efficiency of PTM. The amounts of encapsulated PTM varied from 26% (Loaded A) to 82% (Loaded G). The increase in the mole ratio, due to an increasing amount of HA, was correlated to the EE and to the strong interaction between HA and PTM. Also, the loading capacity varied from 33 to 12%. Taking together all these results, we can suggest that PTM was

efficiently encapsulated in a HA-PArg NP at a mole ratio above 2.25 and with a loading capacity ranging from 20 to 10%.

Table 5. Physicochemical properties of PTM-loaded NP. *PdI*: polydispersity index; *EE* (%): encapsulation efficiency. Values are given as mean ± Sem ($n \geq 3$).

	Mass ratio [PArg+PTM/HA]	**Mole ratio [PArg+PTM/HA]**	**Size (nm)**	***PdI***	**Zeta potential (mV)**	**Load (%)**	***EE* (%)**
Loaded A	1.25:0.27:0.75	1.13	155 ±3	< 0.1	-24 ±3	33	26 ±3
Loaded B	1.5:0.27:0.75	1.35	159 ±4	< 0.1	-25 ±2	30	31 ±4
Loaded C	2:0.27:0.75	1.80	191 ±20	< 0.1	-27 ±2	25	46 ±5
Loaded D	2.5:0.27:0.75	2.25	157 ±6	< 0.1	-25 ±5	21	61 ±5
Loaded E	3:0.27:0.75	2.70	172 ±14	< 0.1	-29 ±4	19	65 ±1
Loaded F	3.5:0.27: 0.75	3.15	179 ±4	< 0.1	-26 ±1	17	76 ±1
Loaded G	5: 0. 27: 0.75	4.51	203 ± 9	< 0.1	-18 ±1	12	82 ±1

Then, to study the influence of HA and PTM concentration on the association efficiency of the NP, nanosystems prepared with different amounts of HA and PTM (ranging from 0.17 to 0.5 $mg \cdot mL^{-1}$) were obtained. In Figure 7, the mass of PTM associated to the nanosystems in function of the mass of HA for the systems developed (from Loaded A to Loaded G) was represented. The highest PTM binding efficiency was obtained for the Loaded F (containing 2.3 $mg \cdot mL^{-1}$ of HA) and Loaded G (containing 3.3 $mg \cdot mL^{-1}$ of HA) being the amount of PTM associated of 0.55 mg and 0.59 mg, respectively. These results confirmed the excellent ability of PTM-loaded NP to associate a high quantity of PTM by electrostatic interaction in comparison to another HA based systems. The formulations having the ability to associate the highest amount of the drug, Loaded F and Loaded G,

were hence retained for the *in vitro* studies. PTM has been encapsulated into liposomes, however due to its hydrophilic character the encapsulation efficiency remained below 50%.[34] PLGA NP synthesized by double emulsion/solvent evaporation methodology were used to encapsulate PTM. As described for the liposomal formulation, the amount of PTM loaded into PLGA NP was very low (2.9% loading efficiency).[21] Micale et al. also developed a synthetic method to obtain PTM-HA bioconjugates as drug and targeting delivery platform. The drug loading in this case ranged from 20 to 30%, however the use of chemical reactions and organic solvents make this system less exploitable for drug delivery applications.[32]

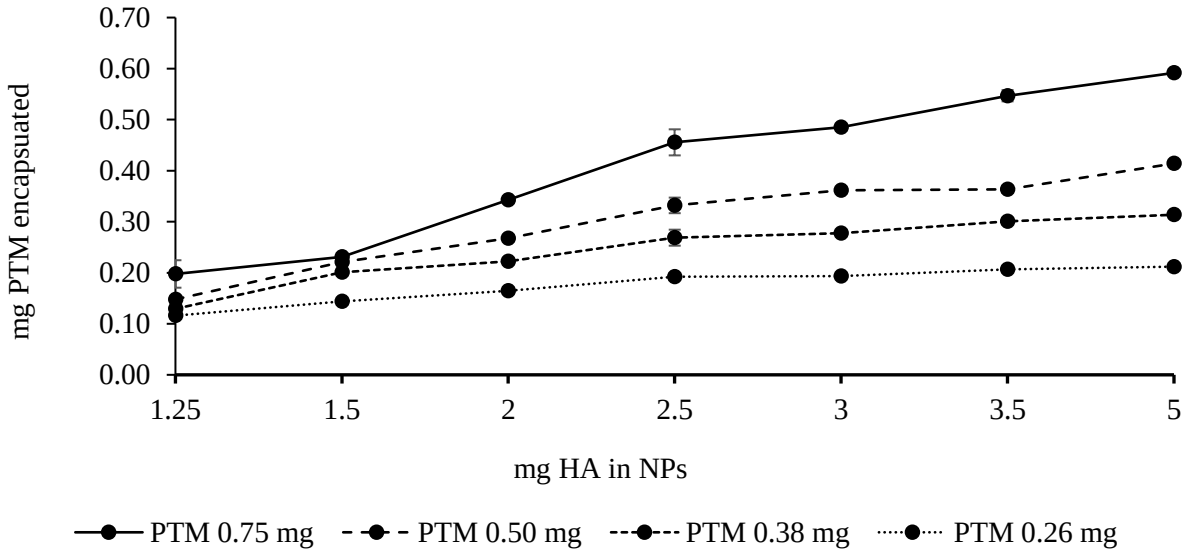

Figure 7. Amount of PTM (mg) associated to PTM-loaded NP in function of the amount of HA present in the formulation (from 0.83 mg·mL^{-1} to 3.33 mg·mL^{-1}). Values are given as mean ± Sem (n ≥ 3).

Quantification of isethionate ions using ion-exchange chromatography

As previous reported, at low ionic strength, the ion concentration in the counterion cloud that surrounded the charged molecules is significantly higher than that in the solution. When two opposite charged macro-ions form a complex, as in the case of HA with PTM and PArg, this double layer is

perturbed and counterions are released in the solutions.[28] To assess the influence of HA concentration on the formation of PTM-loaded NP, the release of isethionate, the counterion of PTM, was quantified using ion exchange chromatography. As shown in Figure 8, no significant difference in term of isethionate ions release was observed for the formulations prepared using different amounts of HA and PTM (dotted lines). While, in the case of the formulations obtained using 0.26 mg pf PTM (0.5 mg·mL^{-1}), there was an increased release of isethionate (full line). Above 3.5 mg of HA (2.3 mg·mL^{-1}), the amount of isethionate released did not change. These results are consistent with the encapsulation efficiency (Table 5) values. In fact, encapsulation efficiency for Loaded F and Loaded G was around 76 and 82%, respectively.

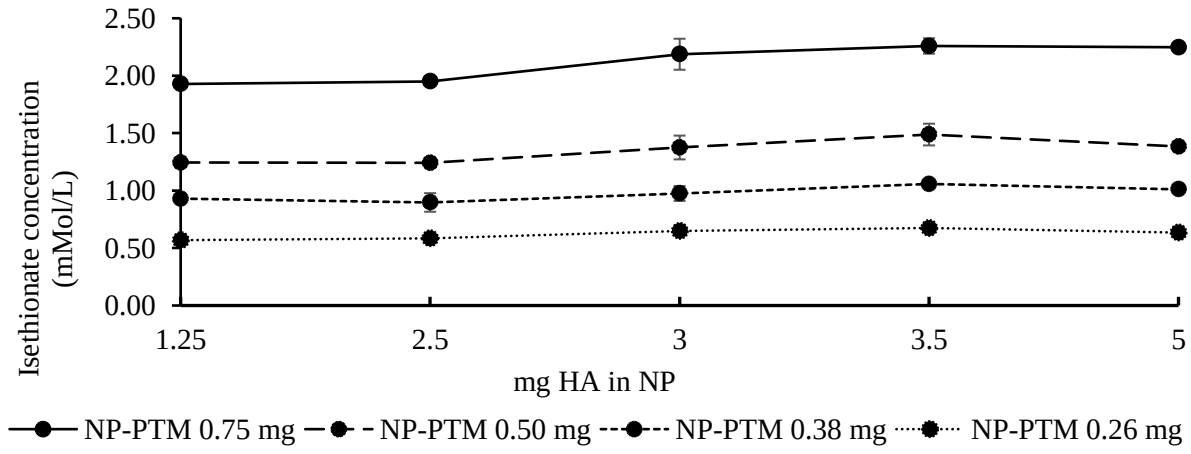

Figure 8. Isethionate ions (mmol·L^{-1}) released after the formation of PTM-loaded NP in function of HA concentration in the NP. Values are given as mean ± Sem ($n \geq 3$).

Morphological analysis of blank and pentamidine-loaded nanoparticles

The morphological analysis of HA-PArg NP and PTM-loaded NP was carried out using TEM and CryoTEM. As showed in Figure 9, HA-PArg NP and PTM-loaded NP presented a regular round shape and formed monodispersed population as observed by DLS measurement. In addition, to

observe PTM-loaded NP in their native state and to confirm the spherical structure of the system, Cryo-TEM observations were also presented (Figure 10).

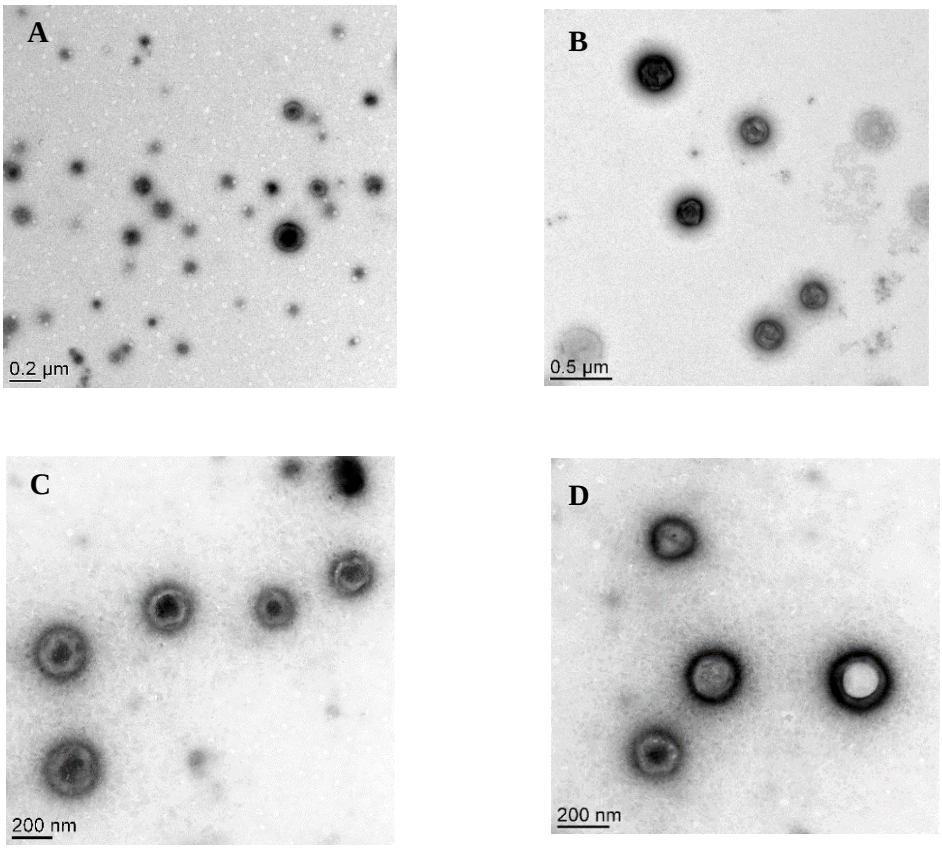

Figure 9. TEM images of blank H with 3.5 mg·mL^{-1} of HA (A); blank I with 5 mg·mL^{-1} of HA (B); loaded F with 2.3 mg·mL^{-1} of HA (C) and loaded G with 3.3 mg·mL^{-1} of HA (D).

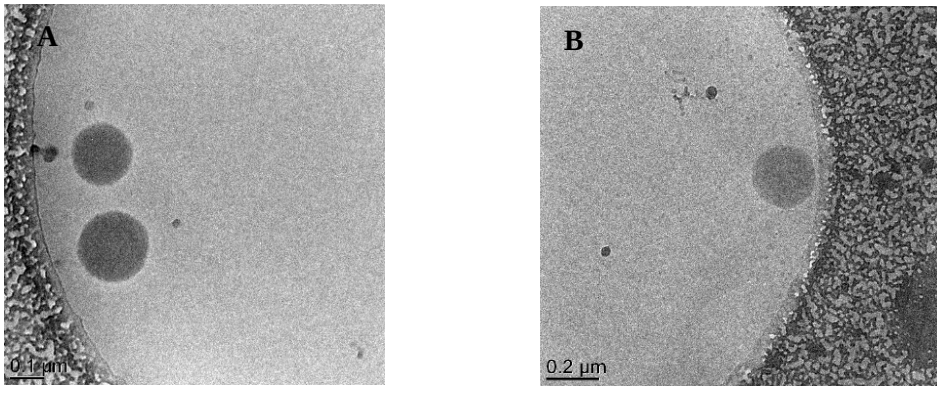

Figure 10. Cryo-TEM images of loaded F with 2.3 mg·mL^{-1} of HA (A) and loaded G with 3.3 mg·mL^{-1} of HA (B).

In vitro release study of pentamidine-loaded nanoparticles

The *in vitro* release study of PTM from HA-PArg NP (Loaded F and Loaded G) was studied upon incubation with PBS at 37 °C using vertical diffusion Franz cells. Sink conditions were ensured by the high-water solubility of PTM (> 30 mg·mL^{-1}, https://cameochemicals.noaa.gov/chemical/20859). For both formulations tested a biphasic profile characterized by an initial burst PTM release (60%) in the first 10 h, followed by a constant release was observed (Figure 11). This behavior has been described also for PLGA NP and liposomes[21,35] and a model mechanism has been proposed.[13] According to the authors the release towards water as receptor medium occurs through diffusion of the neutral species, since diffusion of charged ones is prevented by the electrostatic gradient produced by the polyanion (HA in our case).[13] Moreover, as we used PBS from to study the release behavior, we can suggest that the saline composition of the biological simulated fluid promotes PTM release from the carrier.

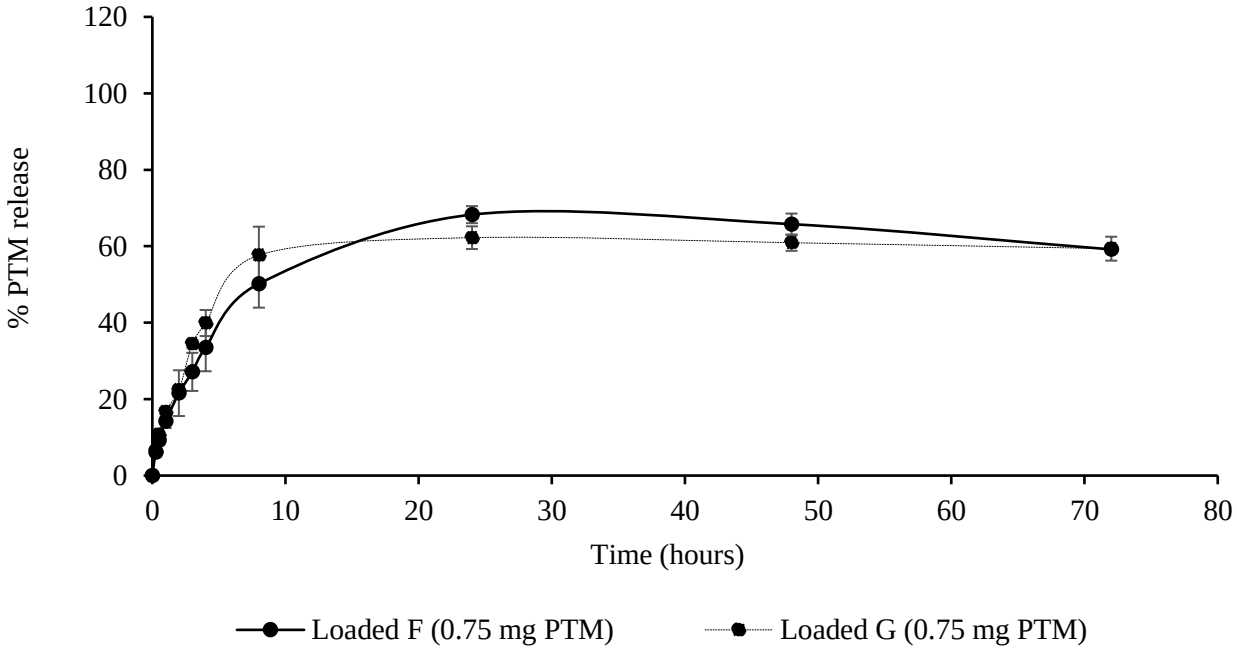

Figure 11. Release profile of PTM from Loaded F (2.3 mg·mL^{-1} of HA, 0.5 mg·mL^{-1} PTM) and Loaded G (3.3 mg·mL^{-1} of HA, 0.5 mg·mL^{-1} PTM) in PBS medium. The diffusion cells were thermoregulated with a water jacket a 37 °C. (Mean ± Sem n = 3).

Stability studies of blank and pentamidine-loaded nanoparticles

The stability studies of colloidal suspension of Blank H and I (Figure 12-A) and Loaded F and G (Figure 12-B) NP at 4 °C was evaluated over 1 month of storage. Size, polydispersity index and leakage of the drug were evaluated every week. As reported in Figure 12-A size and *PdI* of Blank H and I increased over time. While, the corresponding loaded formulations Loaded F and G were more stable, their size and *PdI* vary less in comparison to the empty formulations (Figure 12-B). Moreover, no leakage of the drug was observed, for both formulations demonstrating the ability of NP to encapsulate PTM in an efficient manner. In addition, Blank H and PTM-Loaded F did not aggregate in DMEM (data not show).

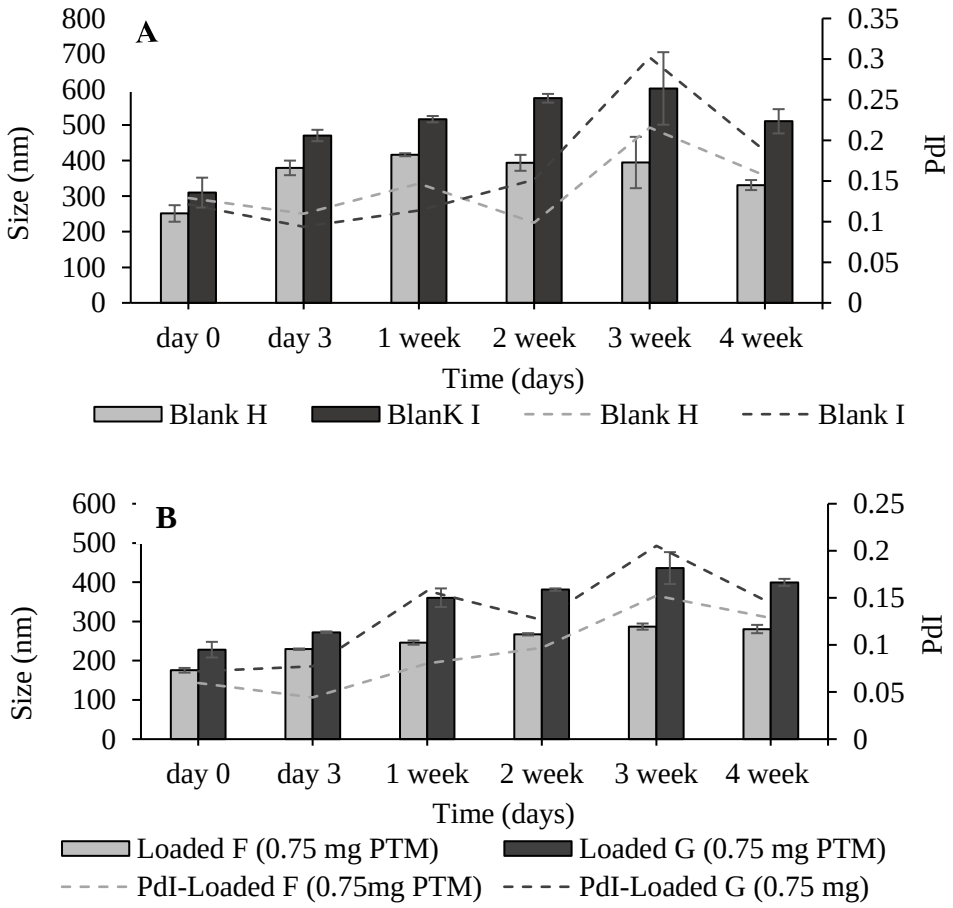

Figure 12. Stability studies, size and *PdI*, upon storage condition for 4 weeks at 4 °C in aqueous solution of Blank H with 3.5 mg·mL^{-1} of HA, Blank I with 5 mg·mL^{-1} of HA (A) and Loaded F with 2.3 mg·mL^{-1} of HA, Loaded G with 3.3 mg·mL^{-1} of HA (B). *PdI*: polydispersity index. (Mean ± *Sem.*; *n* = 3).

Freeze-drying studies of blank and pentamidine-loaded nanoparticles

To provide long-term stability to the formulations developed, the optimal freeze-dry conditions to convert the aqueous suspension into powder were set up. Blank H, Blank I, Loaded F and Loaded G were freeze-dried using different amount of mannitol (5%, 10% w/v). Mannitol was chosen as bulking and isotonic agent. The aim was to obtain isotonic values close to the physiological condition (280-300 $mOsm \cdot L^{-1}$). Tables 6 and 7 show the physiochemical characteristics (size, *PdI* and osmolarity) of HA-PArg NP and PTM-loaded NP formulations prepared with different mannitol concentration, before and after resuspension in water. Also, stability after resuspension was evaluated over 16 days at 4 °C. All the formulations, HA-PArg NP and PTM-loaded NP, were successfully resuspended in water irrespective of the amount of mannitol used. However, to obtain isotonic formulation mannitol at 5% was needed. Following reconstitution in water, the size of HA-PArg NP increased from ~150 nm to ~210 nm. Moreover, the size continued to increase during the storage period (Table 6). The size of PTM-loaded NP, following reconstitution in water, increased from ~150 to ~220 nm and a slightly increased at day 16 following reconstitution in water was observed (Table 6). However, the population remained monodispersed (*PdI* > 0.1) and no leakage of the drug during the time was observed. Figure 13 confirms that both Blank H and Loaded F recovered the initial morphology characteristics upon freeze-drying and reconstitution in water. Both formulations formed monodispersed population showing a regular round shape and no aggregation was detected.

Table 6. Physicochemical characterization of Blank H before and after freeze-drying. *PdI*: polydispersity index. (Mean ± *Sem*.; *n* = 3).

	5% mannitol			10% mannitol		
Days	**Size (nm)**	***PdI***	**Osmol. (mOsm·L^{-1})**	**Size (nm)**	***PdI***	**Osmol. (mOsm·L^{-1})**
0	151 ± 5	< 0.1	-	148 ± 6	-	-
0	218 ± 5	< 0.1	665	210 ± 8	< 0.1	305
8	233 ± 7	< 0.1	665	254 ± 11	< 0.2	305
16	315 ± 45	< 0.1	665	383 ± 42	< 0.2	305

Table 7. Physicochemical characterization of Loaded F after freeze-drying. *PdI*: polydispersity index. *EE* (%) encapsulation efficiency. (Mean ± *Sem*.; *n* = 3).

	5% mannitol				10% mannitol			
Days	**Size (nm)**	***PdI***	***EE* (%)**	**Osmol. (mOsm·L^{-1})**	**Size (nm)**	***PdI***	***EE* (%)**	**Osmol. (mOsm·L^{-1})**
0	149 ± 1	< 0.1	79 ± 0.5	-	157 ± 6	-	64 ± 2	-
0	234 ± 12	< 0.2	76 ± 0.05	669	204 ± 12	< 0.1	64 ± 4	297
8	287 ± 13	< 0.1	-	669	265 ± 3	< 0.1	-	297
16	353 ± 6	< 0.1	78 ± 0.4	669	321 ±10	< 0.2	75 ± 0.15	297

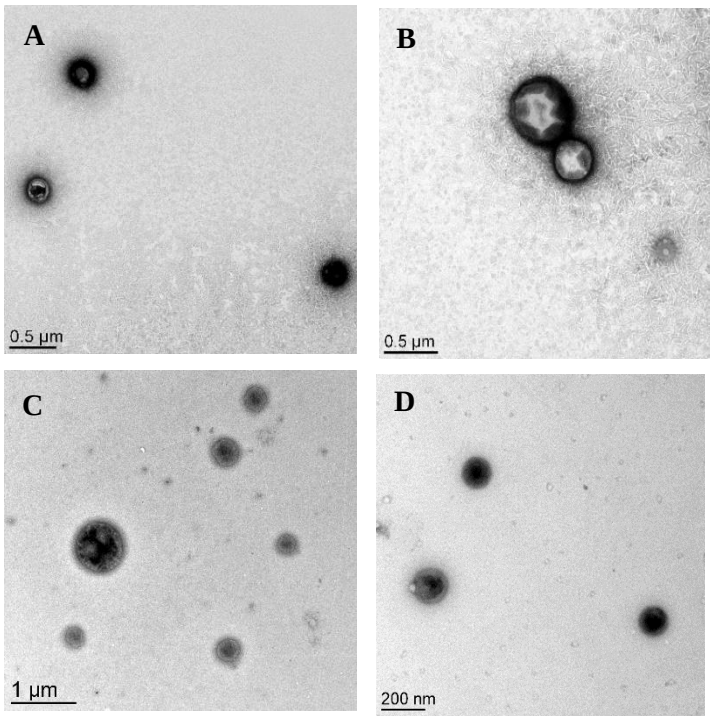

Figure 13. TEM pictures of Blank H (A-B) and Loaded F nanoparticles after freeze-drying and reconstitution in 1 mL of water.

In vitro cell viability studies of pentamidine-loaded nanoparticles

The antiproliferative activity of free and encapsulated PTM into loaded F was assessed using the MTT assay. Lung (A549) and human breast cancer (MDA-MB-231) cell lines were selected based on their sensitivity to PTM.[20,35] The viability of A549 and MDA-MB-231 was monitored after incubation with different concertation of free PTM and PTM-loaded NP for 72 h. HA-PArg NP were used as a control to evaluate the biocompatibility of the nanocarrier. As shown in Table 8, the use of PTM-loaded NP was associated with a better activity than free PTM both on lung (IC50 = 0.21 ± 0.08 µM vs 1.2 ± 0.8 µM) and breast cancer cells (IC50 = 2.2 ± 1.8 µM vs 4.6 ± 3.7 µM). Blank I showed very low toxicity (IC50 >40 µM) highlighting the biocompatibility of the nanocarrier. These data confirmed that the PTM activity *in vitro* was significantly optimized when the drug was incorporated inside nanoparticles formulation (Figure 14). Battistini et al. observed that in A549 cells, cytotoxicity

of HA-doxorubicin complexes was 3-fold higher than that of the reference free drug. These results indicated an increased cellular uptake of doxorubicin when it was complexed with HA due to the presence of overexpressed CD44 membrane receptors.[11] Targeting CD44 using HA moieties has also been demonstrated *in vivo* in CD44-positive human breast tumor xenografts. HA based micelles loaded with paclitaxel exhibit a remarkably high accumulation and retention in the CD44 receptor-overexpressing tumor following i.v. injection in comparison to the free drug.[12] We can hence expect a similar behavior for PTM-loaded NP. Further studies will demonstrate the *in vivo* activity of the developed nanosystem.

Table 8. IC50 values of studied compounds on A549 and MDA-MB-231 cells. Results are expressed as mean values of IC50 ± SD (µM) of three independent experiments.

Cell line	**Formulations**	**IC50 (µM)**
A549	PTM	1.2 ± 0.8
	PTM-loaded NP	0.21 ± 0.08
	Blank HA NP	42 ± 16
MDA-MB-231	PTM	4.6 ± 3.7
	PTM-loaded NP	2.2 ± 1.8
	Blank HA NP	66 ± 47

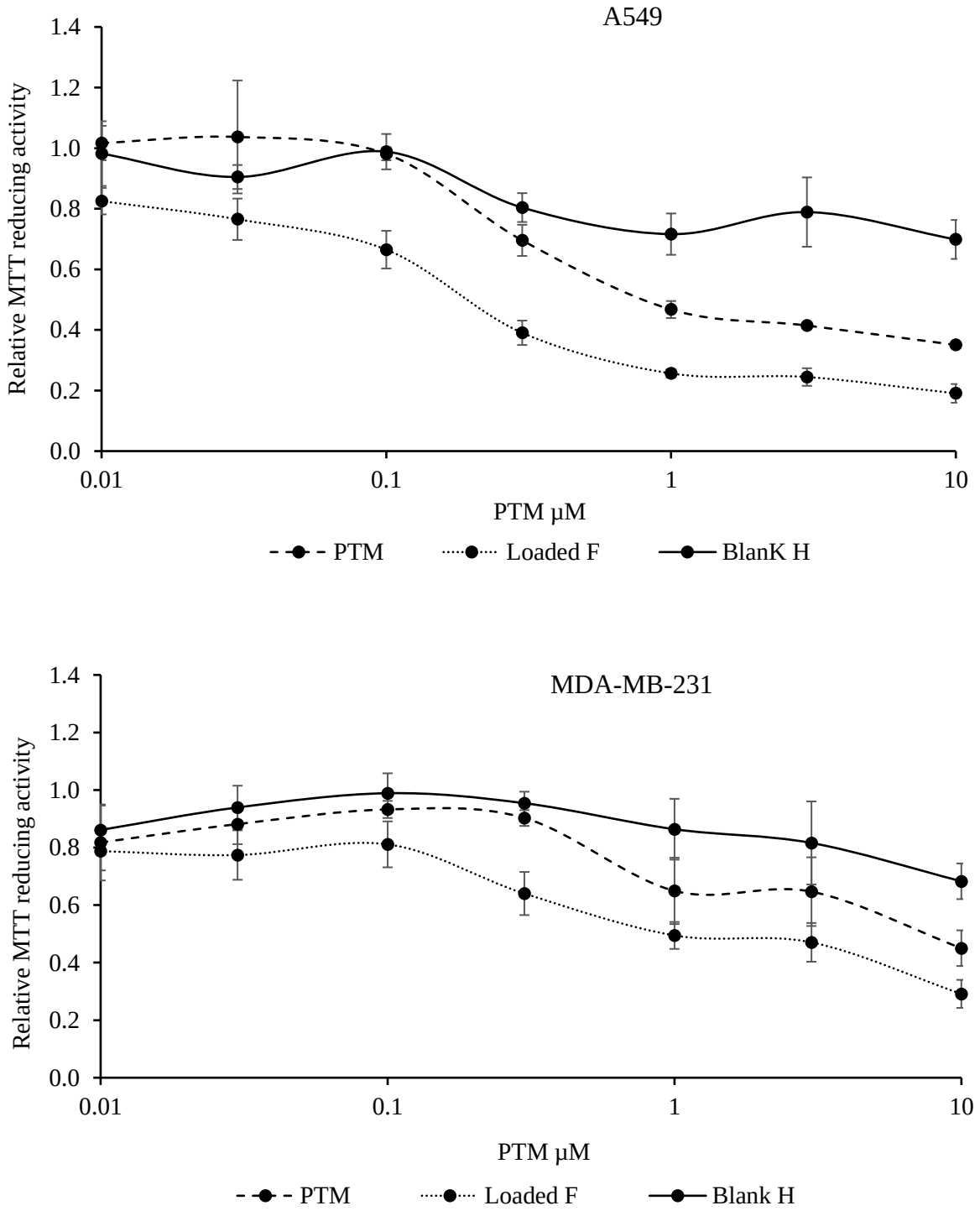

Figure 14. Drug sensitivity curves for A549 cells (A) and MDA-MB-231 cells (B) exposed to PTM (black lines), Loaded F 1 (dashed lines) and Blank H (dotted lines) for 72 h. Graphs are of mean values from three independent experiments and error bars are standard deviations.

Conclusions

The present study provides insight over a new HA based nanocomplex, namely nanoparticles, for positive hydrophilic drug encapsulation. In a first set of experiments, HA-PTM complexes were studied. The complexes obtained were not stable, highly polydispersed, showing a low PTM association efficiency. To stabilize the complex and to maximize the amount of the drug associated to the system, HA-PArg NPs were developed using ionotropic gelation technique. NPs were kinetically stabilized by the excess charge, which prevents their aggregation and ensure high encapsulation efficiency of PTM. Also, high encapsulation efficiency was associated to the release of the isethionate counterion in the solution quantified by IC. *In vitro* release behavior shows that the system was able to retain by ensuring a slow release of the drug during the time. Following *in vitro* studies, PTM-loaded NP were more effective in reducing cell viability as compared with free drug suggesting enhanced efficacy and cell internalization via CD44 receptor. Moreover, their optimum pharmaceutical properties, namely easy production using mild conditions, stability and possibility to obtain a ready-to-use dry powders, highlight the potential of HA-PArg nanoparticles as novel drug delivery system for nanomedicine applications.

Funding Sources

This work has been carried out within the research program RESOLVE, financially supported by EuroNanoMed-III (8^{th} call). Flavia Carton had a fellowship from the Ministry of Education of Italy.

Acknowledgements

Authors are thankful to Geraldine Agusti, Sébastien Urbaniak from Université of Lyon 1, CNRS, LAGEP UMR 5007, for their kind help with TEM images and lyophilization studies. We would like to acknowledge Pierre-Yves Dugas (Université of Lyon 1, C2P2 UMR 5265) for cryo-TEM

observations at the “Centre Technologique des Microstructures” (CTμ - University of Lyon 1). Émeline Cros and Zineb Bousfiha from Université of Lyon 1, INSERM 1052, CNRS 5286, Centre Léon Bérard, Centre de Recherche en Cancérologie de Lyon, are here gratefully acknowledged for cell culture. The research leading to these results has received funding from Italian Ministry for University and Research (MIUR)-University of Torino, “Fondi Ricerca Locale (ex-60%)”.

References

1. Joshi JR, Patel RP. Role of biodegradable polymers in drug delivery. *Int J Curr Pharm Res*. 2012;4(4):74-81.

2. Goycoolea FM, Lollo G, Remuñán-López C, Quaglia F, Alonso MJ. Chitosan-alginate blended nanoparticles as carriers for the transmucosal delivery of macromolecules. *Biomacromolecules*. 2009;10(7):1736-1743.

3. Pistone S, Goycoolea FM, Young A, Smistad G, Hiorth M. Formulation of polysaccharide-based nanoparticles for local administration into the oral cavity. *Eur J Pharm Sci*. 2017;96:381-389.

4. Weber C, Drogoz A, David L, Domard A, Charles MH, Verrier B, Delair T. Polysaccharide-based vaccine delivery systems: Macromolecular assembly, interactions with antigen presenting cells, and in vivo immunomonitoring. *J Biomed Mater Res - Part A*. 2010;93(4):1322-1334.

5. Liu Z, Jiao Y, Wang Y, Zhou C, Zhang Z. Polysaccharides-based nanoparticles as drug delivery systems. *Adv Drug Deliv Rev*. 2008;60(15):1650-1662.

6. Morra M. Engineering of biomaterials surfaces by hyaluronan. *Biomacromolecules.* 2005;6:1205-1223.

7. Dosio F, Arpicco S, Stella B, Fattal E. Hyaluronic acid for anticancer drug and nucleic acid delivery. *Adv Drug Deliv Rev*. 2016;97:204-236.

8. Chen B, Miller RJ, Dhal PK. Hyaluronic acid-based drug conjugates: State-of-the-art and perspectives. *J Biomed Nanotechnol*. 2014;10(1):4-16.

9. Cadete A. Targeting cancer with hyaluronic acid-based nanocarriers: recent advances and translational perspectives. *Nanomedicine*. 2016;11:2341-2357.

10. Lee GY, Kim J-H, Choi KY, Yoon HY, Kim K, Kwon IC, Choi K, Lee B-H, Park JH, Kim I-S. Hyaluronic acid nanoparticles for active targeting atherosclerosis. *Biomaterials*. 2015;53:341-348.

11. Battistini FD, Flores-Martin J, Olivera ME, Genti-Raimondi S, Manzo RH. Hyaluronan as drug carrier. The in vitro efficacy and selectivity of Hyaluronan-Doxorubicin complexes to affect the viability of overexpressing CD44 receptor cells. *Eur J Pharm Sci*. 2014;65:122-129.

12. Zhong Y, Goltsche K, Cheng L, et al. Hyaluronic acid-shelled acid-activatable paclitaxel prodrug micelles effectively target and treat CD44-overexpressing human breast tumor xenografts in vivo. *Biomaterials*. 2016;84:250-261.

13. Battistini FD, Olivera ME, Manzo RH. Equilibrium and release properties of hyaluronic acid-drug complexes. *Eur J Pharm Sci*. 2013;49(4):588-594.

14. Thomas RG, Moon MJ, Lee SJ, Jeong YY. Paclitaxel loaded hyaluronic acid nanoparticles for targeted cancer therapy: In vitro and in vivo analysis. *Int J Biol Macromol*. 2014;72:510-518.

15. Choi KY, Chung H, Min KH, Yoon HY, Kim K, Park JH, Kwon IC, Jeong SY. Self-assembled hyaluronic acid nanoparticles for active tumor targeting. Biomaterials. 2010;31(1):106-114.

16. Lin C, Kim SB, Yon J-M, Park SG, Gwon LW, Lee J-G, Baek I-J, Lee BJ, Yun YW, Nam S-Y. Temporal and subcellular distributions of Cy5.5-labeled hyaluronic acid nanoparticles in mouse organs during 28 days as a drug carrier. *Korean J Vet Res*. 2017;57(4):215-222.

17. Nagavarma BVN, Yadav HKS, Ayaz A, Vasudha LS, Shivakumar HG. Different techniques for preparation of polymeric nanoparticles - A review. Asian J Pharm Clin Res. 2012;5(Suppl. 3):16-23.

18. Contreras-Ruiz L, de la Fuente M, Párraga JE, López-García A, Fernández I, Seijo B, Sánchez A, Calonge M, Diebold Y. Intracellular trafficking of hyaluronic acid-chitosan oligomer-based nanoparticles in cultured human ocular surface cells. Mol Vis. 2011;17(1):279-290.

19. Lollo G, et al. Platinium drug cancer. 2018, S155_EP_INSERM_BR78507/KLP/SLC/sb.

20. Jung HJ, Suh S Il, Suh MH, Baek WK, Park JW. Pentamidine reduces expression of hypoxia-inducible factor-1α in DU145 and MDA-MB-231 cancer cells. *Cancer Lett*. 2011;303(1):39-46.

21. Arias JL, Unciti-Broceta JD, Maceira J, del Castillo T, Hernández-Quero J, Magez S, Soriano M, García-Salcedo JA. Nanobody conjugated PLGA nanoparticles for active targeting of African Trypanosomiasis. *J Control Release*. 2015;197:190-198.

22. Lollo G, Gonzalez-Paredes A, Garcia-Fuentes M, Calvo P, Torres D, Alonso MJ. Polyarginine nanocapsules as a potential oral peptide delivery carrier. *J Pharm Sci*. 2017;106(2):611-618.

23. Oyarzun-Ampuero FA, Goycoolea FM, Torres D, Alonso MJ. A new drug nanocarrier consisting of polyarginine and hyaluronic acid. *Eur J Pharm Biopharm*. 2011;79(1):54-57.

24. Dautzenberg H. Polyelectrolyte complex formation in highly aggregating systems. 1. Effect of salt: Polyelectrolyte complex formation in the presence of NaCl. *Macromolecules*. 1997;30(25):7810-7815.

25. Weinbreck F, de Vries R, Schrooyen P, de Kruif CG. *Biomacromolecules* .2003; 4:293-303.

26. Espinosa-Andrews H, Ba JG, Cruz-sosa F, Vernon-Carter EJ. Gum arabic - Chitosan complex coacervation. *Biomacromolecules*. 2007;8(4):1313-1318.

27. Vinayahan T, Williams PA, Phillips GO. Electrostatic interaction and complex formation between gum arabic and bovine serum albumin. *Biomacromolecules*. 2010;11:3367-3374.

28. van der Gucht J, Spruijt E, Lemmers M, Cohen Stuart MA. Polyelectrolyte complexes: Bulk phases and colloidal systems. *J Colloid Interface Sci*. 2011;361(2):407-422.

29. Tsuchida E. Formation of polyelectrolyte complexes and their structures. *J Macromol Sci Part A*. 1994;31(1):1-15.

30. Menger FM, Wrenn S. Interfacial and micellar properties of bolaform electrolytes. J Phys Chem. 1974;78:1387-1390.

31. Truzzolillo D, Bordi F, Sciortino F, Sennato S. Interaction between like-charged polyelectrolyte-colloid complexes in electrolyte solutions: A Monte Carlo simulation study in the Debye-Hückel approximation. *J Chem Phys*. 2010;133(2):024901.

32. Micale N, Piperno A, Mahfoudh N, Schurigt U, Schultheis M, Mineo PG, Schirmeister T, Scala A, Grassi G. A hyaluronic acid-pentamidine bioconjugate as a macrophage mediated drug targeting delivery system for the treatment of leishmaniasis. *RSC Adv*. 2015;5(116):95545-95550.

33. Paul M, Durand R, Boulard Y, Fusai T, Fernandez C, Rivollet D, Deniau M, Astier A. Physicochemical characteristics of pentamidine-loaded polymethacrylate nanoparticles: Implication in the intracellular drug release in Leishmania major infected mice. *J Drug Target*. 1998;5(6):481-490.

34. Mérian J, De Souza R, Dou Y, Ekdawi SN, Ravenelle F, Allen C. Development of a liposome formulation for improved biodistribution and tumor accumulation of pentamidine for oncology applications. *Int J Pharm*. 2015;488(1-2):154-164.

35. Lee MS, Johansen L, Zhang Y, Wilson A, Keegan M, Avery W, Elliott P, Borisy AA, Keith CT. The novel combination of chlorpromazine and pentamidine exerts synergistic antiproliferative effects through dual mitotic action. *Cancer Res*. 2007;(25):11359-11368.

B. Preliminary results II

C2C12 myoblasts, a spontaneously immortalised cell line (ECACC) were grown in 25 cm^2 plastic flasks (1-2x10^3 cells/cm^2) in Dulbecco's modified Eagle medium with 10% (v/v) foetal bovine serum (FBS), 1% (w/v) glutamine, 0.5% (v/v) amphotericin B, 100 units/ml of penicillin and 100µg/mL of streptomycin (Gibco), at 37°C in a 5% CO_2 humidified atmosphere. Under these culture conditions, myoblasts adhered to the substrate and, in 24h, took the form of a spindle.

Cells were trypsinized (0.25% trypsin in Phosphate-buffered saline (PBS) containing 0.05% Ethylenediamine Tetraacetic Acid; buffered solution (EDTA)) when subconfluent (about 70%) and seeded on 96 multi-well plastic microplates (2x10^3 cells/well) for cell viability evaluation. The experiments were performed using cells at passage 7-10.

Myoblasts were treated with blank NPs (HA-Parg NPs) or NPs loaded with PTM-S as well as with free PTM-S one day post-seeding: the medium was replaced with a fresh one containing the nanocarriers or the drug, and the cells were incubated for 2h (as a short exposure time), 24h (a time sufficient for C2C12 to complete one cell cycle (https://www.dsmz.de/catalogues/details/culture/ACC-565.html?tx_dsmzresources_pi5%5BreturnPid%5D=192), and 72h (as a long-term incubation time); untreated cells at the same culture times were used as controls.

To estimate the effect on cell viability, different concentrations of HA-Parg NPs, PTM-loaded NPs, and free PTM-S were tested, based on our preliminary results with PLGA NPs on DM1 myoblasts. At the end of each incubation time, the cells were stained for 2 min with 0.01% Trypan blue in the culture medium: the cells found to be permeable to Trypan blue were considered as non-viable. Cell samples not exposed to NPs were considered as controls. Briefly, four randomly selected fields/well were imaged using a 10x objective in a LEICA DM IL inverted microscope; in each field, the total cell number and the number of non-viable cells were counted, and the percentage of dead cells was calculated. Results were expressed as the mean ± standard deviation (SD) of three independent experiments, and statistical significance was evaluated by Kruskal Wallis test.

Figure 17 shows that no cell death was found at each time point in samples treated with blank NPs, thus demonstrating the high biocompatibility of these NPs for murine myoblasts. As for cells treated with PTM-loaded NPs or free PTM-S, no cell death was found after 2h; after 24h all samples treated with PTM-loaded NPs showed a significant increase in their death rate in comparison to control, while only samples treated with 30 µM free PTM-S had significantly higher values; after 72h, only cells treated with NPs loaded with 10 µM PTM-S showed a death rate similar to control, while all the other samples underwent a significant increase in death rate.

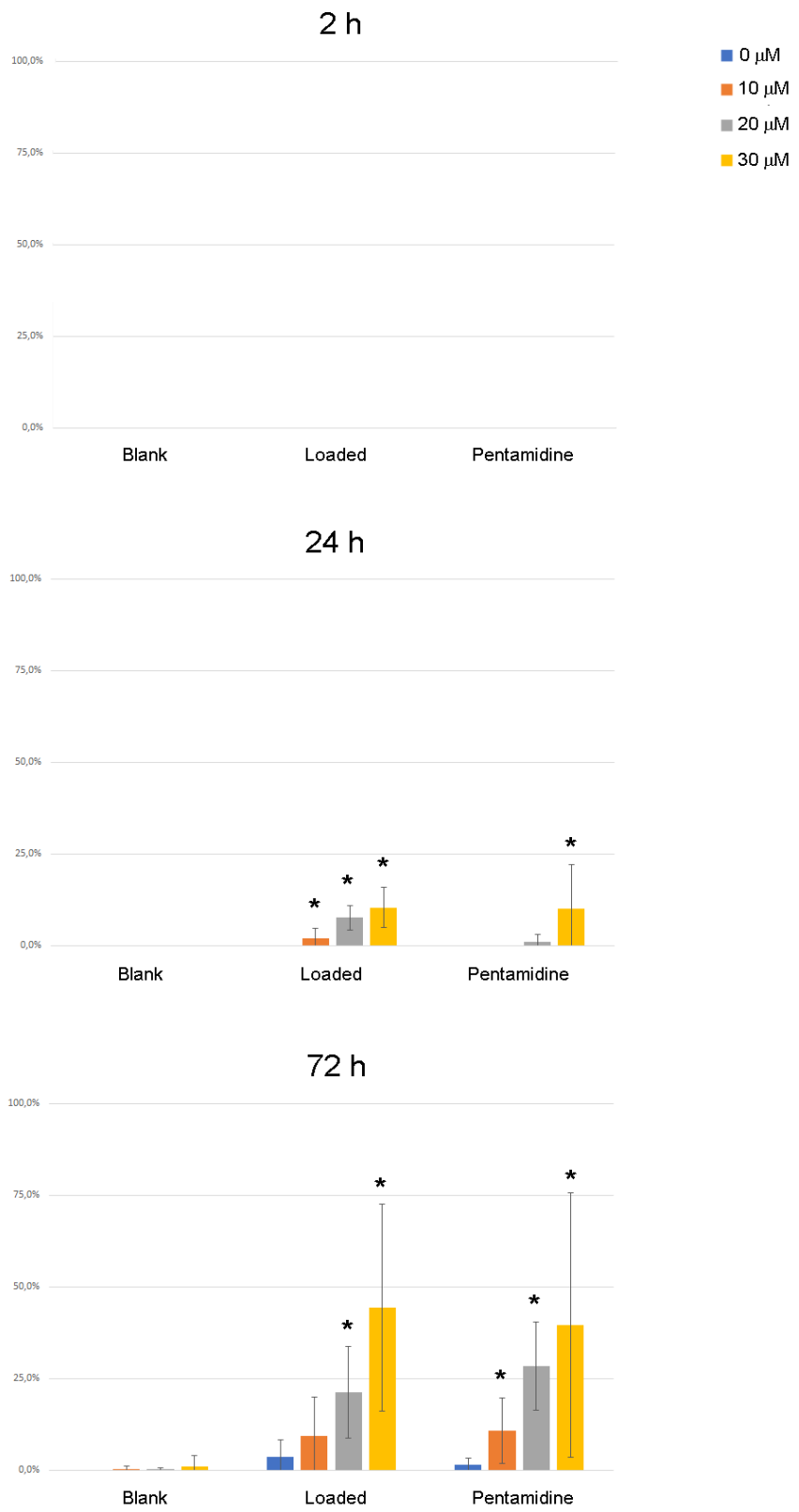

Figure 17. Mean±SD percentage of dead C2C12 cells. The effect of HA-Parg NPs, NPs loaded with PTM-S and free PTM-S was assessed by the Trypan blue test 2h, 24h and 72h after treatment at different PTM-S concentrations. Asterisks indicate values significantly different from 0µM PTM samples (control) (*p<0.05, Kruskal Wallis test).

These preliminary results seem to indicate that NPs loaded with PTM-S are more toxic that the free drug at 24h, whereas a similarly higher toxicity for PTM-loaded NPs and the free drug occurs after prolonged incubation. Since we have so far, no data on the uptake mechanisms and the intracellular fate of these NPs in C2C12 cells, we may only hypothesize that NPs easily entered the cells thus facilitating PTM internalisation. We are presently synthesising fluorescently-labelled NPs that will allow to elucidate their interactions with the cells.

F. Carton, L. Calderan, M. Malatesta (2017): Incubation under fluid dynamic conditions markedly improves the structural preservation in vitro of explanted skeletal muscles. Eur J Histochem 61:2862, DOI: 10.4081/ejh.2017.2862.

Incubation under fluid dynamic conditions markedly improves the structural preservation *in vitro* of explanted skeletal muscles

Flavia Carton, Laura Calderan, Manuela Malatesta

Department of Neurosciences, Biomedicine and Movement Sciences, Anatomy and Histology Section, University of Verona, Italy

Abstract

Explanted organs and tissues represent suitable experimental systems mimicking the functional and structural complexity of the living organism, with positive ethical and economic impact on research activities. However, their preservation in culture is generally limited, thus hindering their application as experimental models for biomedical research. In the present study, we investigated the potential of an innovative fluid dynamic culture system to improve the structural preservation *in vitro* of explanted mouse skeletal muscles (soleus). We used light and transmission electron microscopy to compare the morphological features of muscles maintained either in multiwell plates under conventional conditions or in a bioreactor mimicking the flow of physiological fluids. Our results demonstrate that fluid dynamic conditions markedly slowed the progressive structural deterioration of the muscle tissue occurring during the permanence in the culture medium, prolonging the preservation of some organelles such as mitochondria up to 48 h.

Introduction

During the last decades, the adoption by scientists of the "3 Rs" principles (Replacement, Reduction and Refinement)[1] has led to progressive reduction of animals used for scientific experimentation. In fact, this set of ethical principles proposes that every effort should be made to *Replace* animals with non-sentient alternatives, to *Reduce* to a minimum the number of animals used in experiments, and to *Refine* the experiments so as to cause the least pain and distress. However, research aimed at setting up novel therapeutic and/or diagnostic strategies in human or veterinary medicine, or at performing efficacy/safety evaluations of new drugs or materials requires experimental models able to mimic efficiently the complex structural and functional features of living organisms or organs. Unfortunately, the currently available *in vitro* systems, from the conventional 2D cell cultures to the 3D co-cultures, can be suitably used only in basic or early-phase applied research because they are not able to reproduce the systemic milieu. On the other hand, the promising technology of microfluidic organs-on-chips, intended to simulate levels of tissue and organ functionality not possible with 2D or 3D culture systems,[2] is still far from reliably mimicking tissue and organ physiology.

It is therefore necessary to develop alternative experimental models characterized by a functional and structural complexity similar to the living organism. In this view, explanted organs and tissues could represent a suitable and relatively easy solution: surgical and bioptic explants from human or animal subjects could be used for scientific purposes thus drastically reducing tests on laboratory animals. However, the preservation in culture of explanted organs and tissues is generally limited, thus hindering their application as experimental models for biomedical research, especially for long-term studies.

Skeletal muscle is a highly differentiated organ with a complex cytoarchitecture whose maintenance *in vitro* has been scarcely explored. In the present study, we investigated the potential of an innovative fluid dynamic *in vitro* system to improve the structural preservation of explanted mouse skeletal muscles. We used light and transmission electron microscopy to compare the morphological features of muscles maintained either in multiwell plates under conventional conditions or in a bioreactor mimicking the flow of physiological fluids.

Correspondence: Manuela Malatesta, Department of Neurosciences, Biomedicine and Movement Sciences, Anatomy and Histology Section, University of Verona, Strada Le Grazie 8, 37134 Verona, Italy.
Tel. +39.045.8027569.
E-mail: manuela.malatesta@univr.it

Keywords: Skeletal muscle; organ culture; bioreactor; morphology; ultrastructure.

Acknowledgments: This work was supported by I-Care Foundation. F.C. is a PhD student in receipt of a fellowship from the Doctoral Program "Nanoscience and Advanced Technologies" of the University of Verona.

Received for publication: 14 October 2017.
Accepted for publication: 14 November 2017.

European Journal of Histochemistry 2017; 61:2862
doi:10.4081/ejh.2017.2862

Materials and Methods

Muscle isolation and incubation

Soleus muscles were explanted from healthy 3-month-old male Balb/c mice sacrificed in the frame of a research project approved by the Italian Ministry of Health (protocol code: ZA/14/18). The mice were previously anaesthetized with an overdose of isoflurane using a pre-anesthesia chamber and then we proceeded with the cervical dislocation. The soleus muscle was isolated and excised from each paw, and four muscles per experimental group were used (see Figure 1 for the experimental plan).

Freshly excised muscles were rapidly washed in pre-warmed culture medium (see below) at 37°C and then maintained in an incubator at 37°C in a 5% CO_2 humidified atmosphere for 6 h, 24 h and 48 h, under either conventional or fluid dynamic condition (the bioreactor can be maintained into the incubator). The culture medium was composed of medium 199 (Gibco, Waltham, MA, USA) supplemented with 5.5 mM glucose, 2.54 mM $CaCl_2$ (Merk, Kenilworth, NJ, USA), 25 mM NaHCO3, 0.6 nM insulin (Sigma-Aldrich, St. Louis, MO, USA), 0.1% BSA (Gibco), 200 uU/mL penicillin-streptomycin (Gibco) and 0.5% Amphotericin B (Gibco), according to.[3]

For conventional culture condition, muscles were incubated in 12-multiwell plastic plates containing 2 mL of medium each: during the first incubation day, the medium was replaced every 6 h while in the following days it was changed every 4 h; in addition, the plates were gently shaken manually every 30 min, with the exclusion of the overnight incubation.

For fluid dynamic culture condition, a LiveFlow bioreactor compatible with the incubator environment (IV-Tech, Massarosa, LU, Italy) was used. In detail, muscles were placed in cell culture chambers (LiveBox1) containing 1.5 mL of the same medium used for conventional condition; four chambers were joined in series in a fluidic circuit connected to a 15 mL-mixing chamber; a flow rate of 300 µL/min was applied. Similar to conventional condition,

the first day of incubation the medium was replaced every 6 h, while for the following days it was changed every 4 h.

As controls for time 0, some muscle samples were processed for light and transmission electron microscopy (see below) immediately after excision.

Tissue processing for microscopy analysis

To evaluate the integrity of the explanted muscles at each incubation times, the samples were processed for light and transmission electron microscopy. For light microscopy, the muscles were immersed in isopentane precooled in liquid nitrogen for 30 s to allow the complete freezing, then they were kept at -80°C. For sectioning, the samples were embedded in OCT, and 10 µm-thick sections were cut in a cryostat and collected on glass slides. For morphological observations, cryosections were hydrated for 5 min in PBS, dipped in Mayer's hematoxylin (Sigma-Aldrich) for 90 s, rinsed with tap H_2O for 5 min, stained with eosin (Sigma-Aldrich) for 30 s, dehydrated in graded ethanols, cleared in xylene, and mounted with Entellan (Sigma-Aldrich). The sections were observed with an Olympus BX51 microscope equipped with a 40x objective lens; micrographs were taken with an Olympus Camedia 5050 digital camera.

For transmission electron microscopy, muscles were fixed with 2% (v/v) paraformaldehyde and 2,5% (v/v) glutaraldehyde in 0.1 M phosphate buffer, pH 7.4, at 4°C for 2 h, post-fixed with 1% OsO_4 and 1.5% potassium ferrocyanide at room temperature for 1h, dehydrated with acetone and embedded in Epon. Ultrathin sections were placed on copper grids, stained with lead citrate and observed in a Philips Morgagni transmission electron microscope operating at 80 KV and equipped with a Megaview II camera for digital image acquisition.

Results and Discussion

In this study, soleus muscles explanted from mice were maintained in culture under either conventional (multiwell plates) or fluid dynamic (bioreactor) conditions, and their structural preservation at increasing incubation times was compared by using light and transmission electron microscopy, in order to analyze both the histological organization and the fine morphology of myofibre components. Cryofixation was applied due to the potential of these samples

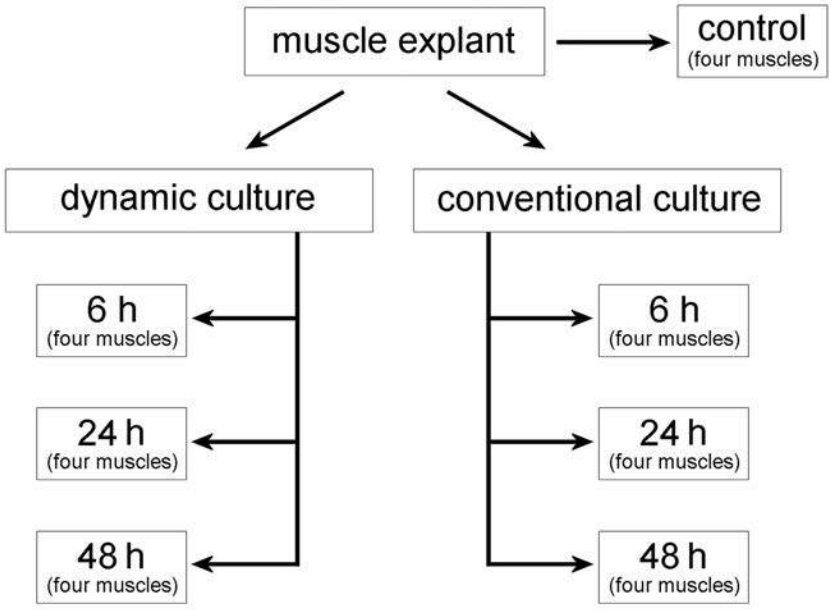

Figure 1. Graphical representation of the experimental plan.

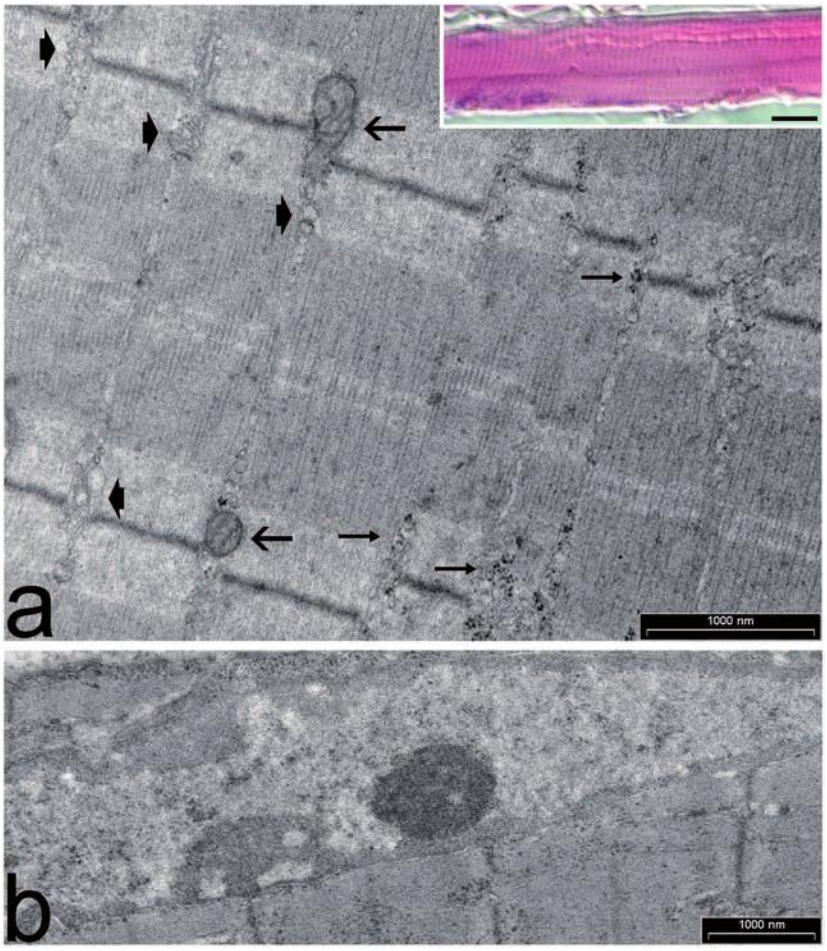

Figure 2. Soleus muscle, control samples. a) The myofibre shows the typical transverse banding and numerus subsarcolemmal nuclei (inset). In the sarcoplasm, the myofilaments are arranged to form sarcomeres, and mitochondria (arrows) and glycogen granules (thin arrows) occur between myofibrils; note the sarcoplasmic reticulum elements (arrowheads). Scale bars: 1000 nm; inset scale bar: 10 µm. b). The myonucleus shows condensed chromatin clumps mainly located at its periphery, and one condensed nucleolus.

to be used not only for morphological analyses (as in the present study), but also for histochemistry and immunohistochemistry at bright field and fluorescence microscopy; this represents an obvious advantage in experiments intended for *e.g.* localizing specific components *in situ* or tracking labelled molecules or nanoparticles. Conventional processing with aldehyde-osmium fixation and Epon embedding was applied since these samples allow a refined high-resolution visualization of all tissue/cell components, thus providing unequivocal information on their structural preservation.

Soleus muscle was selected due to its small size, allowing rapid diffusion of fluids and solutes from and to the culture medium; moreover, soleus can easily be isolated and dissected out without damaging the muscle belly since it originates from the head of the fibula by a slender tendon, and inserts onto the tuber calcanei (together with the gastrocnemius muscle) by the Achilles' tendon.

Control muscles where characterized by myofibres with their distinctive banding pattern and multiple myonuclei located in subsarcolemmal position (Figure 2). In detail, the sarcoplasm was mostly occupied by the longitudinally arrayed myofibrils, with myofilaments arranged in sarcomeres; ovoid mitochondria, membrane structures belonging to the sarcoplasmic reticulum

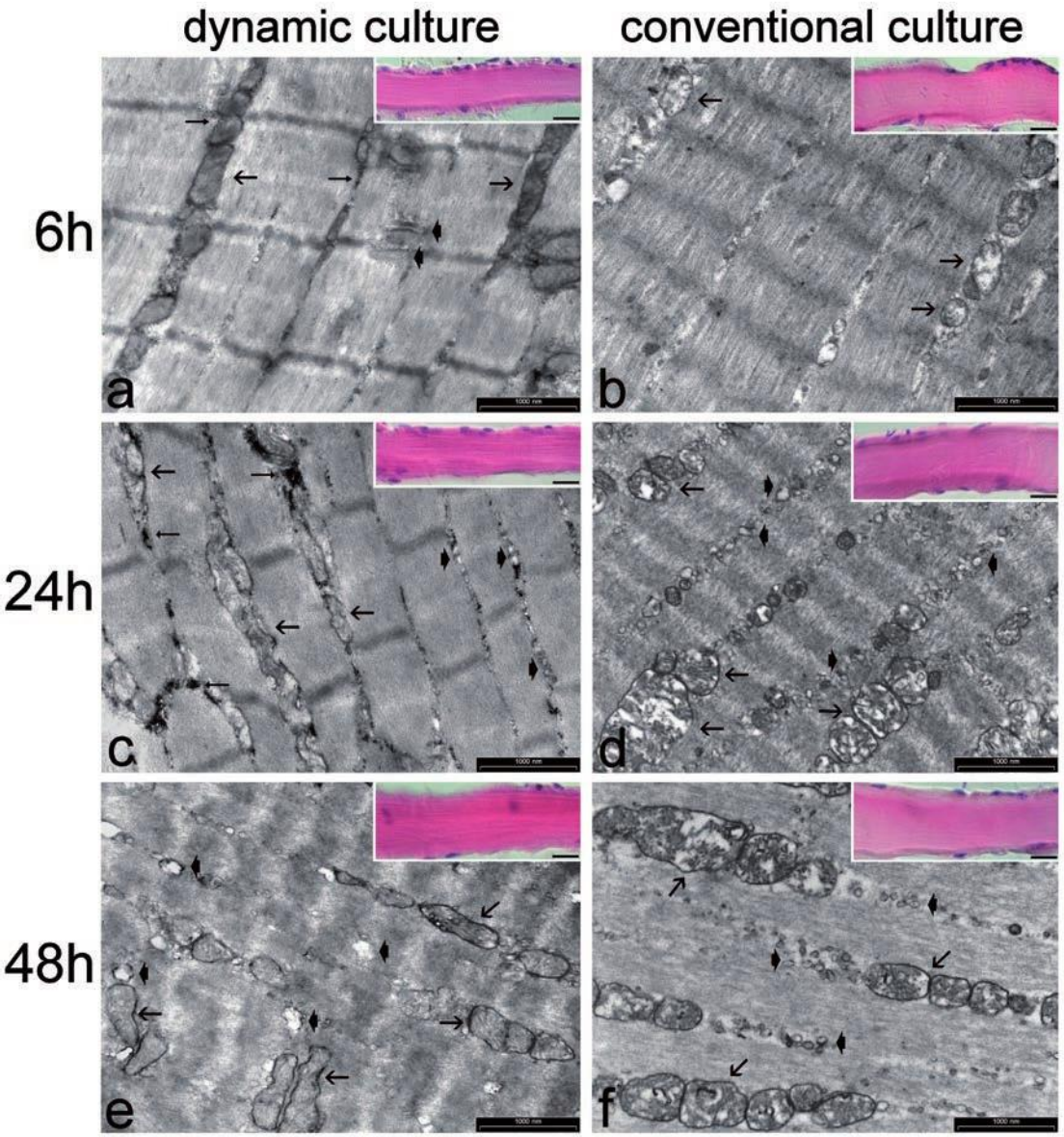

Figure 3. Soleus muscle samples maintained in culture under fluid dynamic (a,c,e) or conventional (b,d,f) conditions. After 6 h incubation in the bioreactor (a), sarcomere organization is preserved, as well as mitochondria (arrows), sarcoplasmic reticulum (arrowheads) and glycogen (thin arrows); under conventional culture condition (b), cytoskeleton is loosened, mitochondria (arrows) are swollen and glycogen is quite scarce. After 24 h incubation in the bioreactor (c), cytoskeletal organization is still recognizable, and mitochondria (arrows), sarcoplasmic reticulum (arrowheads) and glycogen (thin arrows) are well preserved; under conventional condition (d) the cytoskeletal architecture is loosened, mitochondria (arrows) and sarcoplasmic reticulum (arrowheads) are swollen and glycogen is lost. After 48 h in the bioreactor (e), sarcomere organization is hardly recognizable, sarcoplasmic reticulum (arrowheads) is swollen, but mitochondria (arrows) are still preserved; under conventional condition (f), the cytoskeletal organization is definitely lost, and mitochondria (arrows) and sarcoplasmic reticulum (arrowheads) are strongly damaged. Scale bars: 1000 nm. Insets scale bars: 10 µm.

and glycogen granules occurred between the myofibrils (Figure 2a); the myonuclei showed small condensed chromatin clumps at both the nuclear and nucleolar periphery, and one or two roundish nucleoli (Figure 2b).

Explanted muscles maintained under *in vitro* conditions underwent a progressive structural deterioration during their permanence in the culture medium; however, both light and electron microscopy observations demonstrated that fluid dynamic conditions markedly slowed this process (Figure 3).

After 6 h in the bioreactor, the general appearance of the muscle tissue was almost comparable to the one of samples immediately fixed after dissection (Figure 3a): in the sarcoplasm, the spatial arrangement of myofilaments and the sarcomere architecture were clearly recognizable, ovoid shaped mitochondria with well-preserved cristae were lined between the myofibrils, the sarcoplasmic reticulum did not show any enlargement, and glycogen clusters were present; myonuclei did not show morphological alterations (not shown). On the contrary, after 6 h under conventional condition, the cytoskeletal organization showed some loosening and mitochondria were often swollen; moreover, glycogen deposits were very scarce (Figure 3b). It is known that glycogen is markedly affected by *post mortem* processes, undergoing significant decrease, de-location and even disappearance.[4,5] In myonuclei no structural alteration was observed (*not shown*).

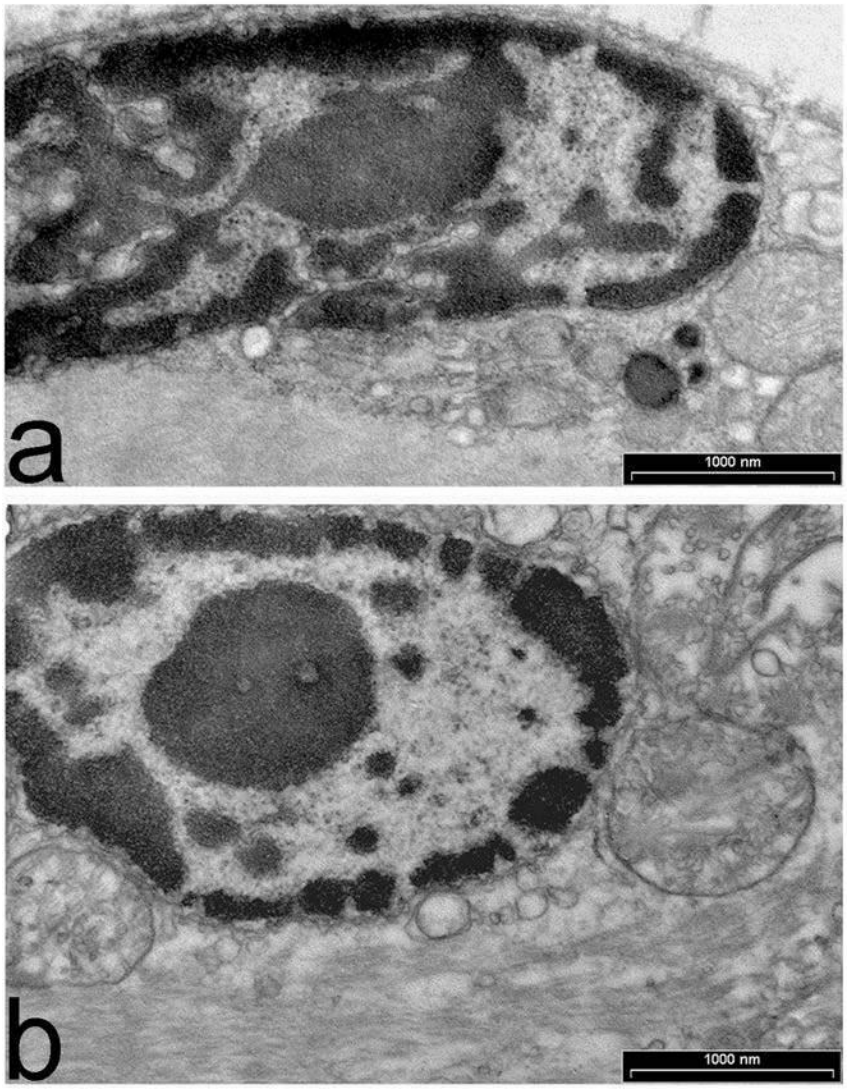

Figure 4. Soleus muscle; samples maintained in culture for 48 h under fluid dynamic (a) or conventional (b) conditions. Both myonuclei show clumps of condensed chromatin at their periphery and one condensed nucleolus. In conventional conditions (b), the nuclear envelope is wrinkled and the perinuclear space is enlarged.

After 24 h of permanence in culture, the difference in structural preservation became even more marked: under fluid dynamic conditions, the histological and ultrastructural features of the muscle were still preserved and detectable, despite some loosening (Figure 3c), whereas muscles cultured under conventional conditions underwent dramatic cytological damage, with sarcomere disorganization, swelling of the mitochondria and sarcoplasmic structures, and massive glycogen loss (Figure 3d), although cell nuclei still preserved a good morphology (*not shown*).

After 48 h, the muscles maintained under fluid dynamic conditions underwent important cytoskeletal disorganization, although some sarcomere remnants were still appreciable even at light microscopy (Figure 3e); the sarcoplasmic reticulum underwent swelling and glycogen was lost, while most of the mitochondria maintained their typical morphology. Myonuclei seemed to undergo some condensation of the peripheral chromatin, but both nucleoli and nucleoplasmic structural constituents maintained their usual morphological features, and no evidence of necrosis or apoptosis was observed (Figure 4a). The muscles cultured under conventional condition definitely lost the ordered myofibril arrangement, while the cytoplasmic organelles underwent morphological alterations typical of necrosis (Figure 3f). In myonuclei, chromatin condensation was more evident than in samples maintained under fluid dynamic conditions, the nuclear envelope appeared as wrinkled and the perinuclear space as enlarged (Figure 4b); in some cases, massive autolytic artefacts were observed (*not shown*).

These results, obtained by both light and transmission electron microscopy, demonstrate that fluid dynamic culture is suitable to prolong the structural preservation of explanted skeletal muscle in comparison to conventional conditions. The bioreactor used in the present study was found to stimulate metabolism in hepatocytes, epithelial cells and adipocytes,[6-8] and to ameliorate permeability in cultured enterocytes,[9,10] in both 2D and 3D cultures. The metabolism of skeletal muscles is known to be especially sensitive to variations in flow rate,[11] and the fluid dynamic environment probably stimulates cell activity by facilitating molecular turnover through an increased oxygen/nutrient supply and faster catabolite removal.

Interestingly, myofibrillar organization seems to be more affected by the culture condition than the mitochondria, although these organelles are known to be highly sen-

sitive to environmental alterations. It is likely that the structural preservation of the sarcomeric arrangement is related also to mechanoreceptor stimulation[12,13] which was obviously lost in the bioreactor too.

Previously reported culture methods of isolated skeletal muscles were based on the incubation in a shaking water bath at 35°C with O_2/CO_2 insufflation: the muscles were maintained under such conditions until 18 h and then submitted to biochemical analysis.[3,14-17] The bioreactor used for the present study seems to be more efficient as it may be directly placed inside the incubator, thus allowing to maintain steady levels of temperature, humidity, O_2 and CO_2, which are essential factors to improve cell survival under *in vitro* conditions. In addition, this fluid dynamic system may ensure a culture environment more similar to the physiological one than other previously proposed incubation methods: in our experiment, the flow rate in the bioreactor was set at 300 µL/min, to reproduce the blood flow values in skeletal muscle,[18] but the fluid flow may be finely modulated, to mimic metabolic changes for functional studies. We cannot exclude that an increase in the flow rate could further ameliorate muscle preservation by improving metabolite/ catabolite turnover. A concomitant temperature decrease of a few degrees would possibly prolong the *in vitro* preservation, but this would obviously make the tissue differently responsive to the experimental stimuli.

It is worth noting that the availability of reliable systems for organ preservation and culture will have a positive ethical and economic impact on research activities allowing to effectively reduce the experimentation on animals. Prolonging the preservation of explanted organs under *in vitro* conditions expands their potential as experimental systems suitable for basic research as well as for efficacy/safety tests on chemicals, pharmaceuticals, nanocomposites and food/feed components.

References

1. Russell WMS, Burch RL. The principles of humane experimental technique. London: Methuen; 1959.
2. Bhatia SN, Ingber E. Microfluidic organs-on-chips. Nat Biotechnol 2014; 32:760-72.
3. Cieniewski-Bernard C, Montel V, Berthoin S, Bastide B. Increasing O-GlcNAcylation level on organ culture of soleus modulates the calcium activation parameters of muscle fibers. PLoS One 2012;7:e48218.
4. Lefaucheur L, Buche P, Ecolan P, Lemoing M. Classification of pig myofibres and assessment of post-mortem glycogen depletion according to fibre type by computerized image analysis. Meat Sci 1992;32:267-78.
5. Ertbjerg P, Puolanne E. Muscle structure, sarcomere length and influences on meat quality: A review. Meat Sci 2017;132:139-52.
6. Vinci B, Murphy E, Iori E, Marescotti MC, Avogaro A, Ahluwalia A. Flow-regulated glucose and lipid metabolism in adipose tissue, endothelial cell and hepatocyte cultures in a modular bioreactor. Biotechnol J 2010;5:618-26.
7. Vinci B, Duret C, Klieber S, Gerbal-Chaloin S, Sa-Cunha A, Laporte S, et al. Modular bioreactor for primary human hepatocyte culture: medium flow stimulates expression and activity of detoxification genes. Biotechnol J 2011;6:554-64.
8. Vinci B, Murphy E, Iori E, Meduri F, Fattori S, Marescotti MC, et al. An in vitro model of glucose and lipid metabolism in a multicompartmental bioreac tor. Biotechnol J 2012;7:117-26.
9. Iori E, Vinci B, Murphy E, Marescotti MC, Avogaro A, Ahluwalia A. Glucose and fatty acid metabolism in a 3 tissue in-vitro model challenged with normo- and hyperglycaemia. PLoS One 2012; 7:e34704.
10. Giusti S, Sbrana T, La Marca M, Di Patria V, Martinucci V, Tirella A, et al. A novel dual-flow bioreactor simulates increased fluorescein permeability in epithelial tissue barriers. Biotechnol J 2014;9:1175-84.
11. Korthuis RJ. Skeletal muscle circulation. 1st ed. San Rafael: Morgan & Claypool Life Sciences; 2011.
12. Rindom E, Vissing K. Mechanosensitive molecular networks involved in transducing resistance exercise-signals into muscle protein accretion. Front Physiol 2016;7:547.
13. Franchi MV, Reeves ND, Narici MV. Skeletal muscle remodeling in response to eccentric vs. concentric loading: morphological, molecular, and metabolic adaptations. Front Physiol 2017;8:447.
14. Stace PB, Marchington DR, Kerbey AL, Randle PJ. Long term culture of rat soleus muscle in vitro. Its effects on glucose utilization and insulin sensitivity. FEBS Lett 1990;273:91-4.
15. Ojuka EO, Nolte LA, Holloszy JO. Increased expression of GLUT-4 and hexokinase in rat epitrochlearis muscles exposed to AICAR in vitro. J Appl Physiol 2000;88:1072-5.
16. Ojuka EO, Jones TE, Nolte LA, Chen M, Wamhoff BR, Sturek M, et al. Regulation of GLUT4 biogenesis in muscle: evidence for involvement of AMPK and Ca2+. Am J Physiol Endo Metab 2002;282:E1008-13.
17. Arias EB, Kim J, Cartee GD. Prolonged incubation in PUGNAc results in increased protein O-Linked glycosylation and insulin resistance in rat skeletal muscle. Diabetes 2004;53:921-30.
18. Klabunde RE. Cardiovascular physiology concepts. 2nd ed. Philadelphia: Lippincott Williams & Wilkins/Wolters Kluwer; 2012.

C. Priminary results III

The distribution of PLGA NPs successfully tested on cultured muscle cells was evaluated in the target organ *i.e.*, the skeletal muscle, using the *in vitro* fluid dynamic system set up by our group (Carton et al., 2017).

Soleus muscles were explanted from the mouse hind limbs, maintained under fluid dynamic conditions, and treated with fluorescent Nile-red-labelled PLGA NPs either administered by post-explant intramuscular (i.m.) injection or directly suspended in the culture medium. For i.m. administration, 0.4 mg/mL of fluorescent PLGA NPs were injected into freshly excised mouse soleus muscles using a Hamilton syringe, and then incubated into Livebox chambers joined in series for 1 to 24h. For NP administration in suspension, 0.4 mg/mL of PLGA NPs were put into the LiveFlow fluidic circuit and explanted muscles were placed in chambers joined in parallel for 6 to 24h. At each time point, muscles were immersed in isopentane precooled in liquid nitrogen, embedded in OCT compound, and cut in a cryostat. Sections were stained for proteins with Fluorescein isothiocyanate (FITC) and for DNA with 33342 and observed in fluorescence with an Olympus BX51 microscope under the appropriate filter conditions.

Our preliminary data demonstrated that, whatever the administration way, the PLGA NPs hardly enter the myofibers in the whole muscle since most of them remained confined into the connective tissue (Figure 18 et Figure 19). Modifications of PLGA NPs surface are in progress to improve targeting to the muscle fibers.

This result demonstrates that *in vitro* tissue/organ testing under dynamic condition provides essential information to set up efficient drug nanocarriers.

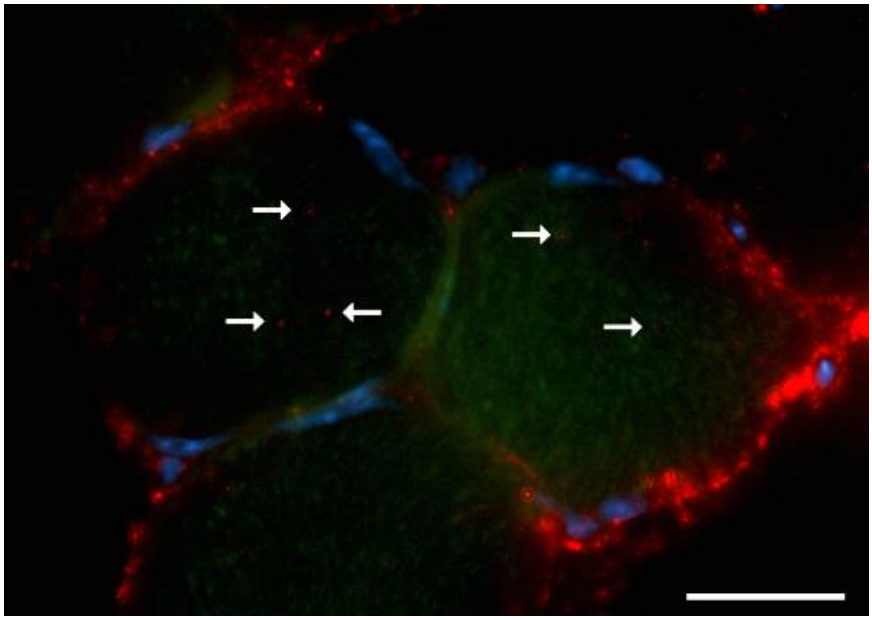

Figure 18. Cross-section of soleus muscle, conventional fluorescence microscopy. After 3h incubation post-i.m. injection, Nile red-labeled PLGA NPs (red fluorescence) mostly accumulate in the endomysium and perimysium. Arrows indicate the few NPs inside the muscle fibers. Green fluorescence, sarcoplasm; blue fluorescence, cell nuclei. Bar: 30 µm.

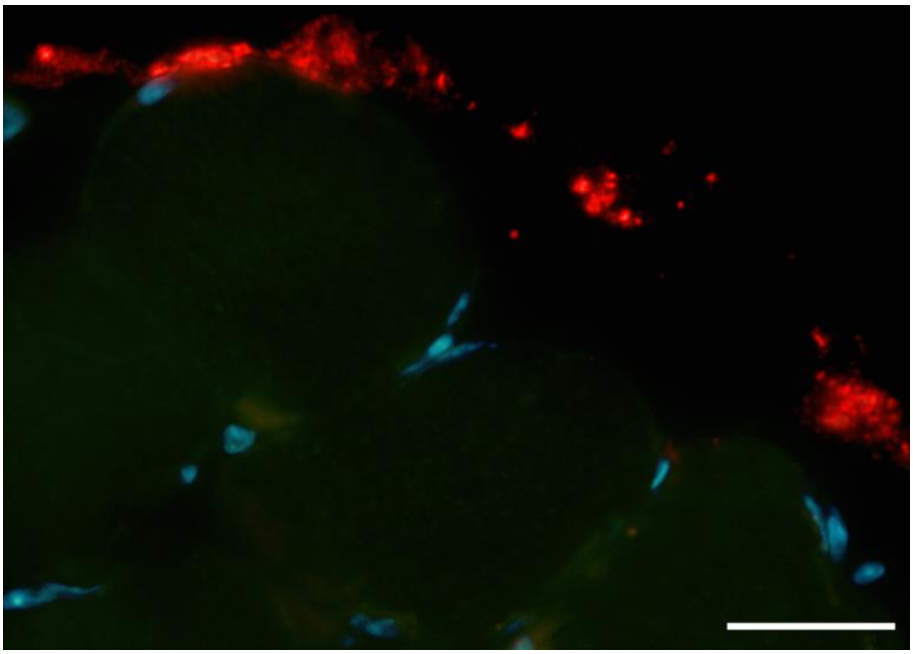

Figure 19. Cross-section of soleus muscle, conventional fluorescence microscopy. After 6h incubation post-administration in the medium, most of the PLGA NPs (red fluorescence) accumulate in the epimysium. Green fluorescence, sarcoplasm; blue fluorescence, cell nuclei. Bar: 30 µm.

III. DISCUSSION

Nanocarriers have great potential in therapeutic applications as innovative drug delivery systems. They take advantage from their unique properties, such as small size and large and functionalizable surface area, to go through the biological barriers and accumulate at the target sites; in addition, they may protect the loaded molecules from the enzymatic degradation, thus improving their sustainability and availability.

Browsing the scientific literature, most of the nanocarriers so far designed for drug delivery have been intended to treat tumours, whereas less attention has been paid to cure and preserve differentiated diseased cells, such as muscle or neuronal cells. At present, many neuromuscular diseases, chiefly those of genetic origin, still lack effective therapy; even when promising therapeutic molecules have been identified, their clinical application is often prevented by their low bioavailability or high systemic toxicity. In this view, nanocarriers can be envisaged as a suitable tool that can couple therapeutic efficacy and reduction of adverse side effects.

The research activity of my Doctoral program was aimed at identifying appropriate nanocarriers for skeletal muscle cells, as potential vectors of therapeutic agents for treating missplicing in DM, a neuromuscular disease of genetic origin still lacking specific treatment.

There are two main differences between selecting nanocarriers suitable for treating cancer cells or for delivering active molecules to skeletal muscle: 1) treating cancer means to kill the diseased cells while muscle treatment implies to cure the cells in order to restore the physiological conditions or, at least, limit the pathological features; 2) cancer cells are highly proliferating cells while muscle is composed of terminally differentiated cells unable to proliferate (myofibres), and quiescent cells (satellite cells) that can be activated (myoblasts) thus undergoing proliferation and differentiation. These special needs oriented my efforts towards nanocarriers that had already been demonstrated to be biocompatible and biodegradable in different biological systems.

The aim of the first study was to monitor by fluorescence and transmission electron microscopy techniques the uptake and intracellular fate of different biocompatible nanocarriers which already proved to be efficient drug delivery systems for cancer cell lines. NPs were synthesised and characterised at the

University of Torino by Prof. Arpicco's, Prof. Berlier's, and Prof. Stella's groups; my task was to investigate their relationships with cultured cells. Microscopical techniques were a powerful approach to elucidate the precise spatial and functional relationships of nanocarriers with cell constituents, especially in relation to the internalization and degradation pathways, thus clarifying the interaction mechanisms and the potential risks of NPs administration: fluorescence microscopy provided information on the uptake and distribution of NPs in the whole cell population, while transmission electron microscopy allowed to visualize at high resolution the intracellular location of NPs, and to detect ultrastructural cell damages undetectable at light microscopy or by cytotoxicity assays (Costanzo et al., 2016, 2017a,b).

Based on the results obtained in this first study, selected nanocarriers (LPs, MSNs and PLGA NPs) were tested on primary human myoblasts and myotubes obtained from skeletal muscle biopsies and their derived myotubes (Guglielmi et al., submitted). It should be underlined that these cells are quite difficult to obtain and grow *in vitro*, hence the results of our work may contribute to the progress of knowledge in this field. Table 5 summarizes the results obtained in these primary cell cultures.

Table 5. Mechanisms of internalization and cell viability of different types of NPs into primary human myoblasts

<table>
<tr><th>Type of NPs</th><th colspan="2">Mechanism of internalization on primary human myoblasts</th><th>Myoblast viability</th></tr>
<tr><td>Polymeric NPs (PLGA)</td><td rowspan="3">• Rapid uptake (within 2 h)
• Cytoplasmatic distribution
• No subcellular alteration
• Never inside cell nucleai</td><td>• Enter the cell individually
• Endocytosis internalization
• Endosomal escape process
• Degradation by lysosome pathway starting from 24 h incubation</td><td>• Not negatively affect myoblasts viability at any of tested doses and duration of treatment</td></tr>
<tr><td>Liposomes (LPs)</td><td>• Poor cellular uptake
• Entering probably by fusion with plasma membrane
• Rapid degradation into the cytoplasm – short half life
• Accumulation into lipid droplets extruded from cells after 24h</td><td rowspan="2">• Statistically reduction in cell viability at high concentration and long incubation times</td></tr>
<tr><td>Silica NPs (MSNs)</td><td>• Internalization as large clusters
• Endocytosis internalization
• Numerous cytoplasmatic vesicular and membrane structures</td></tr>
</table>

We confirmed that the chosen NPs are biocompatible for muscle cells, although at lower concentrations than those reported as safe for some cancer cell lines (*e.g.* Slowing et al., 2006; Arpicco et al., 2013; Jonderian and Maalouf, 2016; Quagliariello et al., 2017). In particular, we found that LPs and MSNs induced a significant increase in cell death at the highest NPs concentrations tested (0.1 mg/ml and 0.4 mg/ml, respectively) and at the longest incubation times (72h). It may be hypothesized that LPs, which rapidly disassemble in the cytoplasm (as demonstrated in Costanzo et al., 2016), may cause a lipid overloading thus interfering with cell metabolism. MSNs were found to accumulate inside the cell for long time (up to 4 days) without undergoing evident degradation or inducing cell damage (Costanzo et al., 2016), even in an immortalized murine myoblast cell line (Poussard et al., 2015). However, primary myoblasts were found to be more

sensitive than established cell lines to the accumulation of MSNs, which maybe hinder cell functions in the long term (Guglielmi et al., submitted). On the other hand, PLGA NPs did not affect myoblast death at any concentration and time investigated and proved to undergo degradation *via* the lysosomal pathway thus avoiding long-term intracellular accumulation. In addition, in Guglielmi et al. (submitted) we evidenced that muscle-derived cells have lower internalization capability than cancer cells.

It is known that different cell types may differently react to nanocarrier administration; in particular, it has been demonstrated that myoblasts are much more sensitive (Nie et al., 2012) and internalize nanocarriers less efficiently than other cell types (Freichels et al., 2011; Pan et al., 2012). It may be hypothesized that these discrepancies are related to different metabolic rates or peculiar cell features, such as different membrane composition or endocytic capability. We also observed that the uptake of all NPs tested was less prominent in primary human myotubes than in myoblasts, according to a previous study reporting that some nanocarriers able to easily enter myoblasts are not internalized by myotubes (Salova et al., 2011). Several factors may be involved in this phenomenon: 1) cycling cells have higher metabolic rate than terminally differentiated resting cells (Chang et al., 2007); 2) myoblast differentiation into myotubes entails a differential expression of several membrane proteins and lipids (Kislinger et al., 2005; Briolay et al., 2013; Forterre et al., 2014); 3) the different composition of the culture media for myoblasts and myotubes may affect the adsorption of environmental proteins on NPs thus altering in turn their interactions with the cells (Mahmoudi, 2018).

The identification of PLGA 75:25 and 50:50 NPs as nanocarriers suitable for human muscle cells (Guglielmi et al., submitted) opened the way to preliminary tests *in vitro* on the therapeutic efficacy of PLGA NPs loaded with PTM-B on myoblasts from a DM1 patient. PTM was, in fact, identified as a promising agent to recover missplicing in DM1 (Warf et al., 2009) The synthesis and characterization of PTM -loaded PLGA NPs was performed at the University of Torino and I tested their effects on DM1 cultured primary myoblasts. Despite the considerable difficulties in treating these diseased cells, the results of this pilot experiment were promising because the NPs-mediated PTM administration proved

to limit the formation of nuclear foci (*i.e.*, one of the typical pathological features of DM: Miller et al., 2000; Meola and Cardani, 2009) while reducing the cell death rate due to drug toxicity. Moreover, the viability of cells treated with PLGA 75:25 NPs is higher than that of cells treated with PLGA 50:50 NPs, likely due to the higher hydrophilicity of the latter ones that speeds up polymer hydrolysis and drug release. These results are obviously very preliminary, and studies are currently ongoing at the University of Torino in order to better characterize and optimize PTM loading and release in PLGA NPs.

The preliminary results obtained with PLGA NPs loaded with PTM-B encouraged us to focus our research on the synthesis of a highly biocompatible nanocarrier for an even more efficient and safer delivery of this drug. During my stage at the University of Lyon, I succeeded to synthesize novel PNPs made of HA and polyarginine (HA-PArg NPs) (Carton et al., submitted). We selected HA as a natural polysaccharide with high biocompatibility and biodegradability. Chemically, HA is a linear polysaccharidic glycosaminoglycan (GAG) formed of identical subunits (D-glucuronic acid and N-acetyl-D-glucosamine disaccharides) bound together by glyosidic bonds. Biologically, it is an important component of the extracellular matrix (ECM) highly distributed throughout connective, epithelial, and neural tissues. The natural origin of HA ensures it to be non-toxic, non-immunogenic and highly biocompatible for human body. A number of authors have reported the potential of HA to form complexes, micelles, NPs, microparticles and hydrogels for gene- and drug-delivery application: their potential for anticancer treatments has been widely explored, especially as multifunctional carriers for a variety of drugs and nucleic acids in combination therapies, immunomodulation and theranostics (Cadete and Alonso, 2016; Dosio et al., 2016; Swierczewska et al., 2016; Eroglu et al., 2017). They have also been envisaged as efficient nanocarriers for intra-articular injection to treat knee osteoarthritis (He et al., 2017), or for oral drug administration to cure inflammatory bowel disease (Si et al., 2016; Sithole et al., 2017), or for successfully delivering antiphlogistic agents for the treatment of diverse ocular inflammations (Sharma et al., 2016). HA-based NPs have also been considered for delivering active molecules across the blood-brain barrier (Lalatsa and Barbu, 2016). Finally, decoration of nanocarriers of different chemical nature

with HA significantly improved their active cell targeting (*e.g.*, Pradhan et al., 2015; Wang et al., 2015; Cao et al., 2018; Ricci et al., 2018; Sang et al., 2018). Although to our knowledge no data on effects of HA-based NPs in muscle cells are available, Wang et al. (2009) demonstrated that scaffolds made of HA at appropriate concentration are well biocompatible for skeletal muscle cells and can promote their cell proliferation and growth. All these data make HA a favorable material for drug delivery systems to the skeletal muscle.

The delivery of PTM-S using NPs made of HA was investigated by Carton et al. (submitted) in human lung carcinoma cells and human breast adenocarcinoma cells (A549 and MDA-MB-231): we demonstrated that NPs-carried PTM-S was more toxic than PTM-S administered as a free molecule, probably due to an enhanced internalization of the encapsulated drug by cancer cells. The administration of PTM-loaded NPs is currently under investigation on cultured muscle cells. Our preliminary results indicate that, similarly to PLGA NPs, LPs and MSNs, HA-PArg NPs are well tolerated by cultured muscle cells, but lower concentrations must be used compared to cancer cells; moreover, as much as it occurs in cancer cells, PTM-loaded NPs induced a higher cell death rate than the free drug. Tests using fluorescently-labelled HA are ongoing to monitor the uptake, biodistribution and degradation NPs in skeletal muscle cells.

All the encouraging experimental work described above was performed using cells in culture; however, it should be kept in mind that nanocarriers are intended to be used in living organisms that are much more highly complex systems, and that the biological environment (the body fluids and intercellular milieu) submits nanoconstructs to multiple physicochemical interactions which can radically change their behaviour. Therefore, *in vivo* experiments are mandatory to determine the suitability of a nanoconstructs for biomedical use; however, this experimental phase implies several ethic and economic problems. In this view, the fluid dynamic *in vitro* system set up in the frame of my Doctoral project represents a suitable intermediate step between *in vitro* and *in vivo* experimentation (Carton et al., 2017). In fact, this system allowed us to utilize organs and tissues explanted from untreated laboratory animals from various experimental protocols and destined to be discarded. Moreover, it represents a relative simple solution to the problem of

mimicking under *in vitro* conditions the complexity of biological systems, which are composed of different tissues with peculiar cells and extracellular matrix and exist in dynamic environments where physiological fluids are constantly moving. These conditions are obviously hard to replicate in conventional 2D or 3D cell culture or co-cultures, and even the recent microfluidic organs-in-chip technology is far from reliably mimicking tissue and organ physiology (Sosa-Hernández et al., 2018; Weinhart et al., 2018).

The fluid dynamic conditions set up in our laboratory allowed a prolonged preservation of muscle tissue in comparison to previous methods (see references in Carton et al., 2017), as proved by the high-resolution analysis at transmission electron microscopy. Interestingly, although mitochondria are highly sensitive to environmental alterations, they maintained a good morphology up to 48 h whereas, at this time point, the myofibrils lost their typical organization in sarcomeres. These observations suggest a degradation of the cytoskeletal components rather than a generalized necrotic process. Accordingly, skeletal muscle is known to respond to mechanical stimuli and, in particular, disuse induces a loss of contractile proteins mainly due to the unbalanced regulation of protein catabolism and anabolism (Baldwin and Haddad, 2001; Kandarian and Stevenson, 2002). In this view, as a future development of our fluid dynamic *in vitro* system, an electric pulse stimulation *in vitro* (*e.g.* Evers-van Gogh et al., 2015) could be envisaged to further prolong skeletal muscle tissue preservation.

The maintenance of explanted murine soleus muscles in our fluid dynamic system allowed us to obtain essential information on the interaction between PLGA NPs and muscle tissue. In fact, the PLGA NPs, which proved to be easily internalized and well tolerated by cultured muscle cells, were found to be entrapped in the connective tissue and be unable to enter myofibers. The nanocarriers have to pass through the connective tissue before reaching and entering the myofibers, irrespective of the selected administration route for the DM therapeutic agent (by intramuscular injection, as in Lee et al., 2012; subcutaneously, as in Weeler et al., 2012 or in Pandey et al., 2015; intraperitoneally, as in Parkesh et al., 2012; intravenously as in Leger et al., 2013). Our fluid dynamic *in vitro* model will allow to rapidly and reliably explore the effect of surface modifications on the

intramuscular distribution of NPs; in particular, targeting strategies (such as carnitine conjugation) are under investigation (Ebner et al., 2015). This experimental phase will provide the scientific know-how to proceed in assessing the biodistribution *in vivo* of highly selected nanocarriers.

The application of the fluid dynamic conditions may be extended to organs and tissues other than the skeletal muscle, and also to biological material obtained by bioptic and surgery procedures in humans and animals. This opens interesting perspectives for the development of this fluid dynamic *in vitro* system for testing the effects of NPs and, more generally, active molecules, significantly reducing the number of animals and, consequently, the costs and the time required for the experimentation. At present, experimentation *in vivo* cannot be completely replaced by our fluid dynamic *in vitro* system, but the potential of our application of fluid dynamic culture for the preservation of explanted organs attracted the attention of the association I-CARE Europe Onlus, committed to the respect of the 3R principles, that offered us a financial support. Moreover, the interesting results obtained with the *in vitro* preservation of skeletal muscle provided a suitable experimental basis to plan the adaptation of the fluid dynamic *in vitro* system to laminar organs (*e.g.*, skin, gut, blood vessels) in order to investigate the interactions of NPs with various biological barriers. Recently our project obtained a financial support by the University of Verona in the frame of a call promoting the cooperation between Academia and Companies.

In conclusion, the application of nanotechnology to cure skeletal muscle is an intriguing challenge and the work performed during my Doctoral program may be considered as a step only in a long way to go.

In recent years, the evidence that most of the tested nanoconstructs could not actually find application in the clinical practice led to a moment of reflection in the scientific community (Mahmoudi, 2018), as to how nanotechnology may more affectively impact on therapy. In my opinion, based on the experience gained during my Doctoral program, chemists, pharmacologists, biologists and physicians should strictly cooperate to manufacture biocompatible nanoconstructs able to interact with tissues and cells in their natural environment, while being suitable for carrying therapeutic agents at their target sites; then the structural and physiological effects

of drug-loaded NPs on cells should carefully be monitored at high resolution by refined microscopical and imaging techniques. The future of nanomedical research may be probably found in such a wider multidisciplinary approach.

IV. APPENDIX

During my Doctoral program, besides my research on biocompatible nanocarriers for skeletal muscle, I gave my contribution to two collaborative studies:

- In the frame of a collaboration with Prof. Goria Berlier (Department of Chemistry and NIS Research Centre, University of Torino, Italy), MSNs were functionalized with HA to improve their active targeting to different tumor cell lines *in vitro* (Ricci et al., 2018). My task was to culture cells and apply fluorescence microscopy techniques.

- In the frame of a collaboration with Dr. Gabriele Tabaracci (San Rocco Clinic, Montichiari, BS, Italy), we explored the effects of the exposure to low ozone concentrations on adult stem cells derived from adipose tissue at various steps of the cell differentiation process (Costanzo et al., 2018). My task was to apply cytochemical and morphometrical techniques at light microscopy.

As a result of these collaborative researches, two scientific articles were published (the articles have been reproduced with the permission of the journals' Publishers).

V. Ricci, D. Zonari, S. Cannito, A. Marengo, Mt. Scupoli, M. Malatesta, F. Carton, F. Boschi, G. Belier, S. Arpicco (2018). Hyaluronated mesoporous silica nanoparticles for active targeting: influence of conjugation method and hyaluronic acid molecular weight on the nanovector properties. J. Colloid Interface Sci. 516:484-497, DOI: 10.1016/j.jcis.2018.01.072.

Journal of Colloid and Interface Science 516 (2018) 484–497

Contents lists available at ScienceDirect

Journal of Colloid and Interface Science

journal homepage: www.elsevier.com/locate/jcis

Regular Article

Hyaluronated mesoporous silica nanoparticles for active targeting: influence of conjugation method and hyaluronic acid molecular weight on the nanovector properties

Valentina Ricci [a], Daniele Zonari [b], Stefania Cannito [c], Alessandro Marengo [b], Maria Teresa Scupoli [d], Manuela Malatesta [e], Flavia Carton [e], Federico Boschi [f], Gloria Berlier [a,⇑], Silvia Arpicco [b,⇑]

[a] Department of Chemistry and NIS Centre, University of Torino, Via P. Giuria 7, Torino, Italy
[b] Department of Drug Science and Technology, University of Torino, Via P. Giuria 9, Torino, Italy
[c] Department of Clinical and Biological Sciences, University of Torino, Corso Raffaello 30, Torino, Italy
[d] Research Center LURM (University Laboratory of Medical Research), University of Verona, Piazzale L.A. Scuro 10, Verona, Italy
[e] Department of Neurosciences, Biomedicine and Movement Sciences, Anatomy and Histology Section, University of Verona, Strada le Grazie 8, Verona, Italy
[f] Department of Computer Science, University of Verona, Strada le Grazie 15, Verona, Italy

graphical abstract

Hyaluronated mesoporous silica nanoparticles (MSN/HA) are preferentially internalized in CD44+ tumor cells.

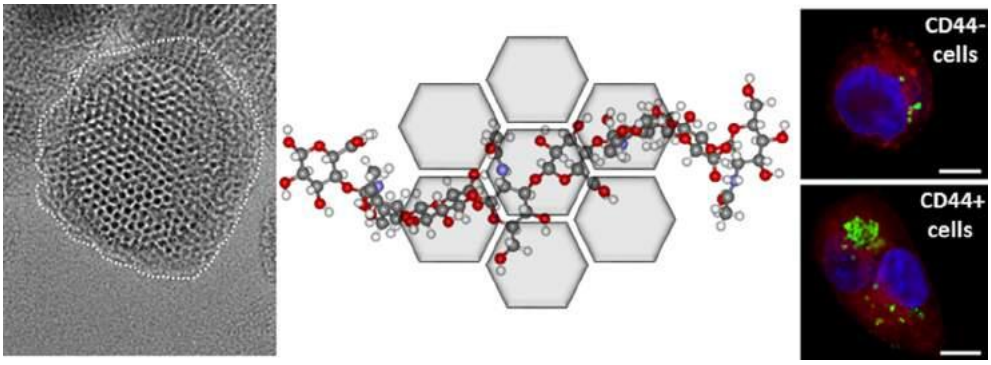

article info

Article history:
Received 25 October 2017
Revised 19 January 2018
Accepted 19 January 2018
Available online 31 January 2018

Keywords:
Hyaluronic acid
Mesoporous silica nanoparticles
CD44 receptor
Active targeting

abstract

We have prepared and evaluated the physico-chemical and biological properties of four different hyaluronated mesoporous silica nanoparticles (MSNs) samples (MSN/HA). Hyaluronic acid (HA) with two different molecular weights (200 and 6.4 kDa) was used for the conjugation of aminopropyl-functionalized MSN (NH_2-MSN), following two different procedures. Namely, samples HA200A and HA6.4A were prepared by reacting activated HA with NH_2-MSN (method A), while samples HA200B and HA6.4B were obtained carrying out HA activation in the presence of the nanoparticles (method B). The four samples showed similar hydrophilicity, but clear differences in the HA loading, textural properties, surface charge and stability of the suspensions. More in detail, conjugation using low molecular weight HA with method A resulted in low HA loading, with consequent scarce effects on dispersity and stability in physiological media. The highest yield and corresponding best performances were obtained with method B using high

⇑ Corresponding authors at: Department of Drug Science and Technology, University of Torino, Via P. Giuria 9, 10125 Torino, Italy (S. Arpicco); Department of Chemistry and NIS Centre, University of Torino, Via P. Giuria 7, 10125 Torino, Italy (G. Berlier).
E-mail addresses: gloria.berlier@unito.it (G. Berlier), silvia.arpicco@unito.it (S. Arpicco).

https://doi.org/10.1016/j.jcis.2018.01.072

Hydrophilicity
Infrared
Water adsorption
MSN

molecular weight HA. HA loading and molecular weight also inf uenced in a concerted way the biological response towards the MSNs of CD44 target cancer cells ($CD44^{+}$) and control cells (CD44): MDA-MB-231 and A2780, respectively. The absence of cytotoxicity was assessed. Moreover, the targeting ability of the best performing MSN/HA was conf rmed by cellular uptake studies.

1. Introduction

Nanoparticles-based targeted therapy has emerged in recent years as an innovative strategy to maintain a drug therapeutic dose at the target site, while reducing systemic drug toxicity and adverse side effects to healthy tissues [1–3]. This approach is particularly important in relation to cancer therapy, where the differences in biochemistry between cancerous and normal tissues can be exploited for the selective targeting of over-expressed tumor specif c receptors [4–7]. To this aim, nanomaterials are an ideal playground, thanks to their intrinsic properties such as high surface area, tuneable size and shape coupled to ease of synthesis and functionalization. Nanoparticles may be loaded with a plethora of bioactive molecules (e.g., small molecules, peptides, nucleic acids, etc.) to protect them from cleavage by external agents, thus the encapsulated drugs do not participate in the control over pharmacokinetic and biodistribution. Moreover, nanosize permits passive transport in biological f uids and to establish molecular interactions at the cellular and subcellular level [1].

Liposomes [8–10] and biodegradable polymeric nanoparticles [11–13] are among the most versatile biocompatible systems to encapsulate active ingredients. Mesoporous silica nanoparticles (MSNs) can be considered as their inorganic counterparts, with intrinsic features such as a huge available inner volume, inertness and chemical stability [14–17]. The ease of surface functionalization makes them ideal materials to develop "pharmaceutically adapted platforms" [18,19], with great potentiality in relation to stimuli responsive applications [20–26]. One of the major drawbacks for the systemic application of these nanosystems is their poor dispersity in biological f uids, which can be however improved by appropriate surface functionalization [19]. Functionalization (often carried out to optimize the interaction with the guest drug molecules) can be obtained with a variety of organosilanes [27]. This has important consequences on the surface properties, such as charge and hydrophilicity [28], which can profoundly inf uence cytotoxicity [29], cellular uptake, transport and/or fate in biological f uids of the nanoparticles [30,31].

Surface modif cation of nanocarriers through macromolecules is particularly relevant in the f eld of cancer treatment [32], where the conjugation of cytotoxic drugs with macromolecules is designed to improve their pharmacokinetic prof le, prolonging the distribution and elimination phases [33]. The most employed are N-(2-hydroxypropyl) methacrylamide (HPMA), polyglutamate, human serum albumin, dextrans, heparin, chitosan, dendrimers, multi-arm polyethylene glycol (PEG), and hyaluronic acid (HA) [32,33]. HA is a naturally-occurring glycosaminoglycan and a major component of the extracellular matrix. The HA receptor CD44 is overexpressed in many cancer cells, and in particular in tumor-initiating cells. HA has thus attracted considerable interest for the development of nanoplatforms for actively targeting drugs, genes, and diagnostic agents [34,35].

In recent years, HA-conjugated MSN systems have been proposed in the literature, with the double aim to improve dispersity and obtain a targeted delivery to CD44 overexpressing cancer cells [36–38]. Zhang et al. recently proposed biotin-modif ed HA coupled to MSN to enable controlled drug release at cancer cells expressing CD44 HA receptor [39]. Moreover, Chen et al. used HA as both capping and targeting agent. In their work, the entrapped guest molecules were released from the inner pores of MSNs upon HA degradation in response to hyaluronidase-1, after receptor-mediated endocytosis into targeted cancer cells [40]. The potentiality of HA-conjugated MSN systems was further investigated by developing dual-stimuli responsive systems. To this aim, the polysaccharide was conjugated to MSNs through a disulf de bond, which was cleaved in the presence of the high glutathione concentration characterizing cancer cells [23,24]. Additionally, multifunctional "theranostic" materials where developed, coupling the above-mentioned properties to those of a gadolinium based bovine serum albumin complex for simultaneous redox-responsive targeted drug delivery and magnetic resonance imaging [41].

In this work, hyaluronated MSNs (MSN/HA) have been developed with the double aim to improve their dispersion in physiological media and their targeting ability. For the f rst time we compare different synthetic approaches, and the use of HA of different molecular weights (6.4 kDa and 200 kDa), to identify the optimal strategy to obtain the better performances, both in terms of biological response and potential pharmaceutical application. A full physico-chemical description of the produced hybrid materials is given, including routine characterization, hydrophilicity assessment, molecular and quantitative analysis of the HA external shell. Finally, the biological effects in cultured cells were studied and the results correlated to the materials properties.

2. Experimental section

2.1. Materials

Cetyltrimethylammonium bromide (CTAB), tetraethyl orthosilicate (TEOS), sodium hydroxide (NaOH), (3-aminopropyl)-triethoxysilane (APTS) and all the other reagents and solvents were purchased from Sigma-Aldrich (Milan, Italy) and employed as received. Sodium hyaluronate (HA, of molecular weights MW 6.4 and 200 kDa) was purchased from Lifecore Biomedical (Chaska, MN). Fluorescein-5-isothiocyanate (FITC) was provided by Invitrogen (Life Technologies, Monza, Italy). MilliQ® water was used in all synthetic steps.

2.2. NH_2-MSN synthesis

MSN samples were prepared following a slightly modif ed literature procedure [42,43]. CTAB (1 g, 2.74 mmol) employed as Structure Directing Agent (SDA), was dissolved in 480 ml of water under stirring and heating. At the stable temperature of 80 °C, NaOH (2.0 M, 3.5 ml) was slowly added to the mixture. TEOS (5 ml, 22.4 mmol) was then added dropwise under vigorous stirring. After 2 h the milky reaction mixture was cooled to room temperature (RT) and the white precipitate was f ltered off and washed with abundant water and methanol. The SDA was removed from the as-synthesized material by calcination at 550 °C, heating to the desired temperature under N_2 f ow and switching to O_2 for a 6 h isotherm.

Aminopropyl-functionalized MSN (NH_2-MSN) sample was prepared with APTS by post-synthesis grafting with a procedure

modified from the literature [44,45]. Namely, 1 g of MSN (overnight dried at 100 °C) were suspended in 30 ml of anhydrous toluene. The particles suspension was heated at 130 °C under stirring. Next, 0.6 ml of APTS were added dropwise and the mixture was allowed to reflux for 17 h. The modified NH_2-MSNs were filtered off and washed with toluene, ethanol, water and finally methanol. Subsequently, the sample was dried at 110 °C for 3 h for curing, and at 80 °C overnight [46].

2.3. Hyaluronic acid conjugation: MSN/HA samples

Conjugation with HA was carried out starting from NH_2-MSN, to exploit the aminopropyl functionality for covalent linking of the targeting agent. We followed three different procedures proposed in the literature [36,37,40]. The protocol described in Ref. [40] was discarded since the prepared samples resulted in the lowest derivatization yield. This is probably ascribable to the low concentration of the coupling agent 1-ethyl-3-(3′-dimethylaminopropyl) carbodiimide (EDAC), notwithstanding the excess of HA with respect to MSN. The methodologies proposed by Yu et al. and by Ma et al. [36,37] briefly described below, are hereafter mentioned as method A and B, respectively. HA of MW of 6.4 and 200 kDa were used for both preparations.

2.3.1. Samples HA200A and HA6.4A

This approach requires activation of HA through N-hydroxysuccinimide (NHS) and EDAC as coupling agent, before nanoparticles conjugation [37]. To this aim, 56 mg of NHS and 30 mg of EDAC were separately dissolved in 1.5 ml water, each. 17 mg of HA were suspended in 9 ml water, before adding the NHS and EDAC solutions previously prepared. The mixture was left under magnetic stirring at RT for 1 h. 150 mg of NH_2-MSN were suspended by sonication in 15 ml of water, before adding the activated HA solution. pH was then adjusted to 9 with trimethylamine (TEA). The mixture was heated to 38 °C and left under stirring overnight. After cooling down to RT, the supernatant was separated by centrifugation (60 rpm, 20 min). The solid powdered product was washed thrice with water and suspended in few ml of water before freeze-drying. This procedure was carried out with HA 200 kDa and 6.4 kDa, resulting in samples HA200A and HA6.4A, respectively.

2.3.2. Samples HA200B and HA6.4B

Following method B, activation of HA was carried out directly in the presence of the nanoparticles. 150 mg of NH_2-MSN were sonicated in 30 ml of 2-(N-morpholino)ethanesulfonic acid (MES) buffer 0.01 M, at pH 6. 150 mg of HA were dissolved in 15 ml of MES and added to the nanoparticles suspension. 15 mg of EDAC and 15 mg of NHS, each dissolved in 7.5 ml of MES, were added to the MSN suspension. The reaction was kept under magnetic stirring at RT for 4 h and successively centrifuged (60 rpm, 20 min). After removal of the supernatant, the solid powdered product was washed thrice with water and re-suspended in few ml of water for freeze-drying [36]. The procedure was carried out with HA 200 kDa and 6.4 kDa, resulting in samples HA200B and HA6.4B, respectively.

2.3.3. Fluorescent labelling

FITC labelled NH_2-MSN and MSN/HA samples were prepared as reported in Ref. [37] with minor modifications. Briefly, 250 μl of FITC ethanol solution (0.3 mg/ml) were added to a suspension of 1 mg of MSN in 150 ml of water. The mixture was maintained at RT for 6 h under stirring in the dark and then the nanoparticles were centrifuged (60 rpm, 10 min) and washed with ethanol thrice until the supernatants were colorless.

2.4. Physico-chemical characterization

Transmission Electron Microscopy (TEM) measurements were carried out with a JEM 3010-UHR microscope (JEOL Ltd.) operating at 300 kV. Powders were dispersed on a copper grid coated with a perforated carbon film. The size distribution of the samples was obtained by measuring a statistically representative number of particles (ca. 250 particles). The results are indicated as mean particle diameter (dm) ± standard deviation (STD) (dm ± STD).

Specific surface area (SSA), cumulative pore volume and pore size distribution of samples were calculated by gas-volumetric analysis measuring N_2 adsorption-desorption isotherms at liquid nitrogen temperature (LNT) using an ASAP 2020 physisorption analyser (Micromeritics). The SSA was calculated by the Brunauer-Emmett-Teller (BET) method and the average pore size was determined by means of the Barrett-Joyner-Helenda (BJH) method, employing Kruk–Jaroniec–Sayari (KJS) equations on the adsorption branch of nitrogen isotherms. Before the measurement, the samples were outgassed at RT overnight.

Powder X Ray Diffraction (XRD) patterns were collected with a PW3050/60 X'Pert PRO MPD diffractometer (Panalytical) working in Bragg–Brentano geometry, using Cu Kα radiation (40 mA and 45 kV), with a scan speed of 0.0167° min^{-1} and a measurement time of 200 s/step. The measurement was carried out at low angles, in the range of 1.5–12°.

Thermogravimetric analysis (TGA) was carried out on a Q600 analyzer (TA Instruments) heating the samples at a rate of 10 °C/min from RT to 1000 °C in air flow. Before starting measurements, samples were equilibrated at 30 °C.

Fourier Transform Infrared (FTIR) spectra were recorded using an IFS28 spectrometer (Bruker Optics) equipped with a MCT detector, working with a resolution of 4 cm^{-1} over 64 scans. The spectra were obtained in transmission mode, with samples pressed in the form of self-supporting pellets, mechanically protected with a pure gold frame. Samples were placed in quartz cells equipped with KBr windows, allowing in situ activation and measurement. Before spectra measurement the samples were outgassed at RT for 4 h to remove adsorbed water and impurities. Spectra were normalized with respect to pellet thickness for direct comparison, by using the silica overtone modes in the 2100–1500 cm^{-1} interval.

Colorimetric carbazole test was carried following the procedure described in [47]. Briefly, a suspension of 4 mg/ml in water was prepared for each sample. Two aliquots (60 and 180 ml) were diluted to a final volume of 1 ml in water. 3 ml of a 0.025 M $Na_2B_4O_7$ in H_2SO_4 96% solution were added to each tube. The suspensions were then shaken and heated at 100 °C for 10 min. After cooling down, 100 ml of a carbazole solution 0.1% p/v in absolute ethanol was added, before mixing and heating again at 100 °C for 10 min. After cooling down, absorbance was measured at 530 nm using a DU-70 Beckman spectrophotometer.

Microgravimetric H_2O adsorption/desorption isotherms were measured with an intelligent gravimetric analyzer (IGA-002, Hiden Analytical), based on an ultrahigh-vacuum (UHV) microbalance (weighing resolution of 0.2 mg) with integrated temperature and pressure control. Temperature control was based on a thermostated water bath/circulator, while pressure control was achieved with a Baratron capacitance manometer (accuracy ± 0.05 mbar). Buoyancy corrections were carried out using the weights and densities of all the components of the sample (including adsorbed phase) and counterweight sides of the balance, and the measured temperature. The mass uptake was measured as a function of time, and the approach to equilibrium of the mass relaxation curve was monitored in real time using a computer algorithm (real time processor, RTP). For each isotherm point the time origin of real-time analysis was set at 75% of the pressure change, while the minimum and maximum data collection time

were set to 5 and 60 min, respectively. RTP uses last-squares regression of a linear driving force (LDF) model in order to extrapolate a value of the mass relaxation asymptote and assess the time-scale of interaction. The samples were loaded in a sealed stainless steel reactor, where they were outgassed at 50 °C overnight prior to H_2O dosage, in order to measure the sample dry weight. Two consecutive adsorption/desorption isotherms were measured varying the water equilibrium pressure in the 0–20 mbar interval (step of 3 mbar) at 28 °C. This corresponds to a maximum p/p^0 value around 0.55 (p^0 ffi 38 mbar at the measurement temperature).

The experimental isotherms were analyzed with a Langmuir model, which assumes a monolayer adsorption onto the surface and is expressed by the equation:

$$q = \frac{q_m K p}{1 + K p} \quad (1)$$

where q is the equilibrium water uptake, q_m is the adsorption capacity (corresponding to the monolayer saturation) and K the Langmuir constant, which corresponds to the adsorption equilibrium constant [48]. q_m and K were calculated via the linearization of the Langmuir equation, as follows:

$$\frac{p}{q} = \frac{1}{K q_m} + \frac{p}{q_m} \quad (2)$$

Calculations were carried out expressing the equilibrium pressure as p/p^0, so that the K values reported in Table 4 are dimensionless.

The mean hydrodynamic size was determined at 25 °C by Dynamic Light Scattering (DLS) using a nanosizer (Nanosizer Nano Z, Malvern Inst., Malvern, UK). The selected angle was 173° and the measurement was carried out after dilution of the nanoparticle suspensions in water and in phosphate buffered saline (PBS 0.1 M, pH = 7.4). The particle surface charge was investigated by f potential measurements at 25 °C in water and PBS solution applying the Smoluchowski equation and using the Zetasizer Nanoseries ZS 90 (Malvern Instruments). In both cases, measurements were carried out in triplicate by diluting 80 l l of a 1 mg/ml particles suspension in water with the selected medium, to reach a f nal volume of 1 ml.

For the dispersity test 2 mg of NH_2-MSN and MSN/HA samples were added to 1 ml of different medium [PBS 0.1 M or Dulbecco's Modif ed Eagle Medium (DMEM) supplemented with 10%of fetal bovine serum (FBS)] and bath sonicated for 30 min. The stability of the dispersions was evaluated after 0, 4, 8, 24 and 30 h.

2.5. Tumour cell lines culture

MDA-MB-231 (human breast adenocarcinoma) and A2780 (human ovarian carcinoma) cells were used. MDA-MB-231 cells were grown in DMEM supplemented with 10%of FBS, 0.03%of L-glutamine and 2%penicillin and streptomycin. A2780 cells were cultured in RPMI 1640 medium containing 10% FBS, 0.03% of L-glutamine, 2%penicillin and streptomycin, and 50g/ml of gentamicin sulfate. Cells were maintained in a humidif ed incubator at 37 °C in 5%CO_2.

2.6. Receptor expression analysis

Flow cytometry was used to determine the presence of CD44 on the cell surface by indirect immunof uorescence. Cells were washed twice with PBS and incubated 30 min in the dark at 4 °C with CD44 primary antibody, washed twice with PBS and then incubated 30 min in the dark at 4 °C with a phycoerythrin (PE) conjugated goat antibody (Dako Italia, Milan, Italy). Samples were analyzed on a f ow cytometer instrument (FACSCanto, Becton Dickinson, San Jose, CA). Dead cells and debris were excluded on the basis of forward-scatter and side-scatter. Flow cytometry data were analyzed using the FlowJo software (TreeStar, Ashland, OR). CD44 expression was measured by calculating the ratio between median f uorescence intensity of cells labelled with antibodies versus unlabelled cells (Relative Median Fluorescence Intensity, RMFI).

2.7. Incubation with MSN and cytotoxicity evaluation

MDA-MB-231 and A2780 cells were seeded at 1 x 10^4 cells/well in 96 wells microtiter plates and incubated overnight to allow cellular adhesion. Various dilutions of NH_2-MSN and MSN/HA samples (1.5–25 mg/ml) were added in triplicate, and incubated for 24, 48 and 72 h.

Cell growth inhibition was evaluated by sulforhodamine B (SRB) colorimetric proliferation assay, modif ed by Vichai and Kirtikara [49].

2.8. Confocal analysis of f uorescent MSN

After 24 h incubation with either FITC labelled NH_2-MSN or MSN/HA, MDA-MB-231 and A2780 cells were f xed for f uorescence microscopy with 4%(v/v) paraformaldehyde in PBS, pH 7.4, for 30 min at room temperature. The samples were stained for DNA with Hoechst 33342 (1 l g/ml in PBS for 5 min; Sigma), counterstained with 0.1%Trypan blue in PBS for 30 s to visualize the cytoplasm, rinsed in PBS, and mounted in a 1:1 mixture of glycerol:PBS (Calbiochem, Inalco, Milan, Italy). For confocal laser scanning microscopy (CLSM), a Leica TCS SP5 AOBS system (Leica Microsystems Italia, Milan, Italy) was used with a 40 oil immersion objective. For f uorescence excitation, a diode laser at 405 nm for Hochest, an Ar laser at 488 nm for FITC and a He/Ne laser at 543 for Trypan blue were employed. Z-stack of 1.5 nm step sized images (each image in the 1024 1024 pixel format) were collected and processed by the Leica confocal software. The RGB channels of the images presented here are the gray intensity images obtained with 405 nm (B), 488 nm (G) and 533 nm (R) excitation wavelengths respectively.

2.9. Cellular uptake

A quantitative determination of the cellular uptake was performed on a f uorescence-activated cell sorter (FACS). MDA-MB-231 and A2780 cells seeded in 6-well culture plates (5 10^5 cells/well), were exposed for different length of time (15 min, 30 min or 1 h) to FITC labelled NH_2-MSN and MSN/HA with equivalent f uorescence. After removal of the free FITC-NH_2-MSN and FITC-MSN/HA, cells were washed twice with PBS, collected by tripsynization and f nally re-suspended in 1 ml of PBS. Then the intracellular uptake of MSNs was analyzed using a FACScan. Detection of FITC-MSNs green f uorescence (FL-1) was performed on at least 5000 events per samples, using the CellQuest software (Becton-Dickinson, Milano, Italy). Cells incubated in the absence of MSN were used as control.

3. Results and discussion

The general properties of all samples, including textural and morphological features, were analyzed. Sample HA6.4A was discarded due to low derivatization yield and scarce dispersity (see later), and will thus not be described in detail in the following. The NH_2-MSN sample used for HA conjugation was measured for comparison. Corresponding results are hereafter discussed only when relevant.

3.1. Effect of conjugation on porous structure

MSN/HA samples are composed by spherical nanoparticles (particle size 94 ± 20 nm, see corresponding histogram as Fig. S1), which are characterized by an ordered pore structure with the typical hexagonal array of MCM-41-like materials. This can be appreciated in the high resolution TEM picture of sample NH_2-MSN, reported in Fig. 1a, showing two superimposed particles with pores parallel and perpendicular to the image plane (circle and hexagon shapes, respectively). The same particle size, morphology and ordered porosity are preserved after HA conjugation, as shown in Fig. 1b–d. However, in this case an amorphous-like external layer is clearly observed, which can be attributed to the formation of a shell of HA, covering the particles. The formation of a HA shell is supported by both qualitative and quantitative characterization results, described in the following.

The ordered pore structure of the materials is also reflected in the typical XRD pattern, characterized by low angle peaks at 2.3, 4.0 and 4.7° (Fig. S2). These can be labelled as (1 0 0), (1 1 0) and (2 0 0) in the P6mm symmetry group, corresponding to a hexagonal array of pores. After HA conjugation, the peaks decrease in intensity and move to slightly higher 2h values in all samples. The change is in the order HA200A < HA6.4B ffi HA200B. Both phenomena are usually observed in MCM-41-like materials after functionalization and/or drug encapsulation, and are interpreted in terms of molecules filling/lining the pores [50,51]. Particularly, the d_{100} parameter, which is the distance between planes passing through the pores centre (see Fig. S3), can be calculated from the Bragg equation, as resumed in Table 1. These data are further discussed hereafter in combination with results from gas-volumetric analysis.

The nitrogen adsorption/desorption isotherms of the three MSN/HA and parent NH_2-MSN materials are reported in Fig. 2 (top panel), with the corresponding pore size distribution calculated with the BJH method (bottom). Curves a) and b) corresponding to NH_2-MSN and HA200A, can be classified as type IV typical of mesoporous materials. Namely, a steep increase of the adsorbed amount is observed below $p/p^0 = 0.3$, which corresponds to the capillary condensation of the adsorbate inside the pores. The narrow hysteresis loop present in all samples at p/p^0 reaching 1 is instead related to condensation of nitrogen in the interparticle porosity. After conjugation, the adsorbed amount decreases in the order HA200A > HA6.4B ffi HA200B, and in the last two the capillary condensation related to mesopores filling is no more present. This is reflected in the corresponding pore size distribution curves (Fig. 2, bottom panel). Parent NH_2-MSN material shows an intense and relatively narrow peak centred around 30 Å, corresponding to the pores lined with aminopropyl groups. This peak is weaker and shifted to lower values for HA200A, very weak and not present in HA6.4B and HA200B.

The textural parameters obtained from these data are summarized in Table 1. On the whole, we observe a major effect of conjugation on samples prepared by method B, where Specific Surface Area (SSA), pore volume and diameter are sensibly decreased. This suggests that during this procedure (where HA activation is carried out directly in the presence of the nanoparticles) the polymer is not only forming an external layer but is also diffusing inside the pores. This is less likely in the case of high

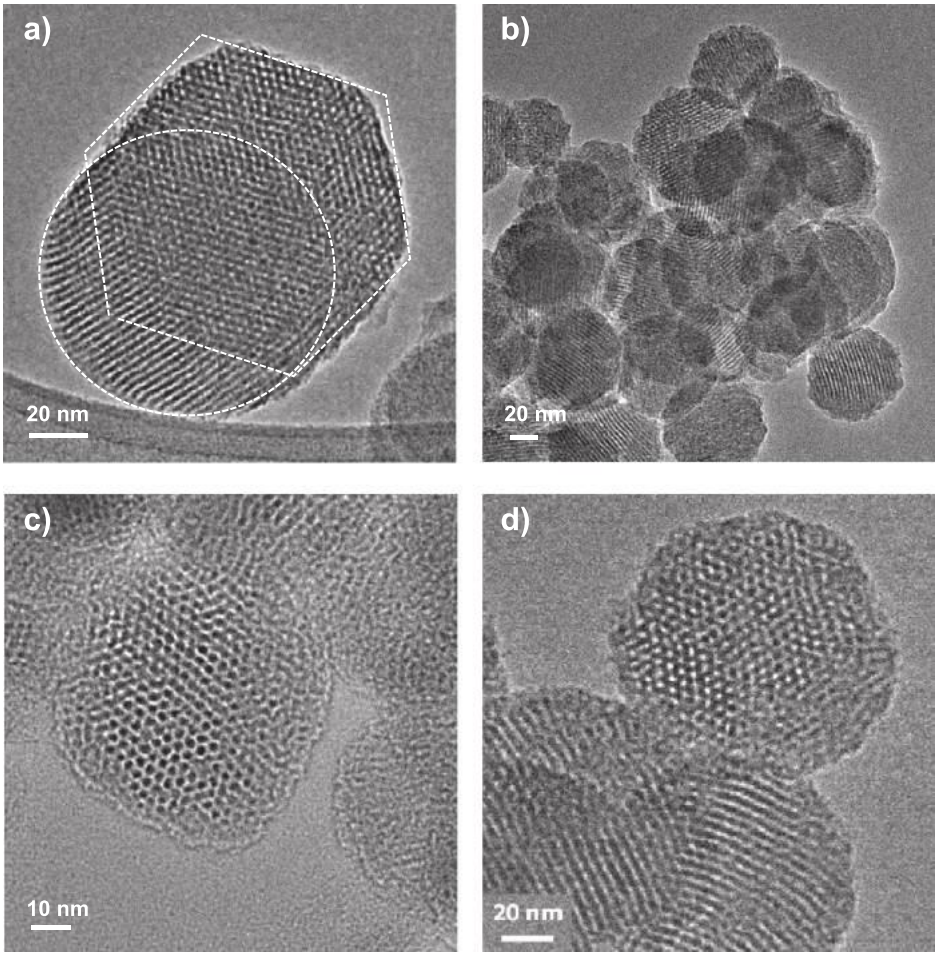

Fig. 1. TEM images of (a) NH_2-MSN; (b) HA200A; (c) HA200B and (d) HA6.4B.

Table 1
Textural and structural properties of the studied materials.

Samples	SSA (m^2/g)	Mesopores volume (cm^3/g)	Mean diameter (Å)	d_{100} (Å)	a (Å)	Wall thickness (Å)
NH_2-MSN	789	1.18	30	38.21	44.12	14
HA200A	494	0.91	26	37.88	43.74	18
HA200B	204	0.33	<20	36.32	41.94	>22
HA6.4B	222	0.60	22	36.78	42.47	20

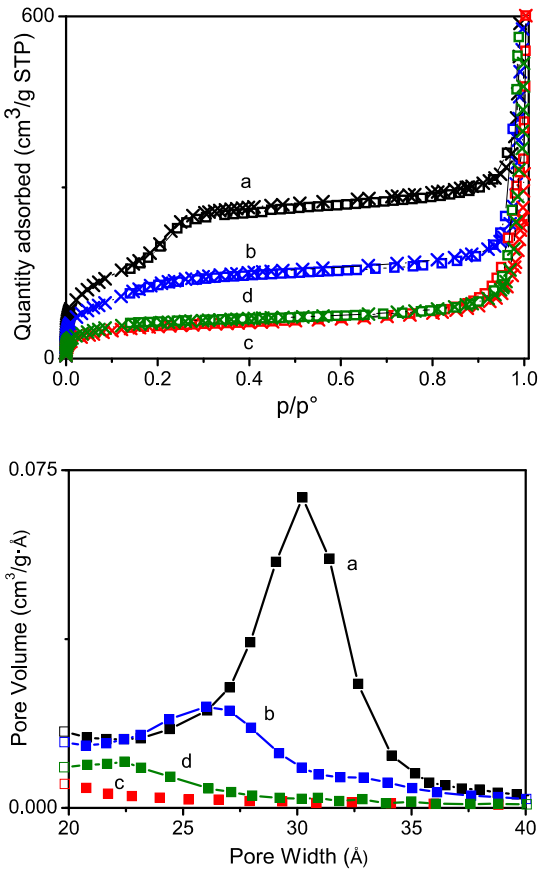

Fig. 2. Nitrogen gas-volumetric adsorption (crosses) and desorption (squares) isotherms (top) and pore size distributions (bottom) of (a) NH_2-MSN; (b) HA200A; (c) HA200B and (d) HA6.4B.

molecular weight HA, where the polymer could mainly block pores entrance not allowing nitrogen molecules to diffuse within during BET measurements. On the other hand, method A, where HA activation is carried out before reaction with NH_2-MSN, results in a minor diffusion inside the pores, which are less obstructed to the diffusion of the nitrogen adsorbate used for gas-volumetric analysis. These considerations are in very good agreement with XRD and TEM observations, showing an apparently thicker HA layer on sample HA200B with respect to the other two (compare Fig. 1b with c and d). Finally, the mean pore diameter calculated by BJH method was combined with the a parameter calculated from XRD (distance between centres of the pores, see Fig. S3), to calculate the apparent wall thickness. The values summarized in last column of Table 1, clearly show an increase in the order HA200A <HA6.4B ffi HA200B, in agreement with the above considerations.

3.2. Quantitative HA analysis

Quantif cation of HA covalently linked to the NH_2-MSN particles was carried out by two independent techniques, namely TGA and the carbazole colorimetric test.

TGA was carried out from 30 to 1000 °C in air f ow, in order to quantify the amount of organic groups anchored to the silica surface. This was calculated on the basis of the observed weight loss, normalized to the dry mass of the sample, i.e. after removal of physisorbed water around 100 °C (Fig. S4). All MSN/HA samples show a consistent weight loss between ca 180 and 650 °C, which is higher with respect to parent NH_2-MSN, in the order HA200A <HA200B ffiHA6.4B. The calculated amounts are summarized in Table 2. More details about the criteria used for quantif cation can be found in the Supplementary Material. In this context, it is suff cient to mention that samples HA200B and HA6.4B show very similar weight losses and curves slope, while HA200A has an intermediate prof le, both in terms of quantity and curve shape, in very good agreement with the trends observed with textural and structural techniques, as described above.

Carbazole colorimetric test was also employed for HA quantif - cation. As mentioned above, HA is a high molecular weight glycosaminoglycan, formed by a repeating disaccharide unit composed by D-glucuronic acid and N-acetyl-D-glucosamine. In this test HA is hydrolyzed in acid environment, so that monosaccharide units can form coloured adducts with carbazole through their glucuronic acid residues. This allows the quantif cation of HA through a simple optical measurement.

The values obtained with both techniques are resumed in Table 2, expressed as HA weight percentage. First of all, we underline the very good agreement between the two techniques. Secondly, the results show that a def nitely higher mass of HA has been linked to MSN with method B, irrespective of its molecular weight. Method A def nitely yields a materials with lower (around one third) HA loading. This could be explained by the fact that in the latter case HA activation was carried out before reaction with NH_2-MSN. On the basis of gas-volumetric and TEM results, we infer that this could result in a more diff cult diffusion inside the pores, so that mainly external aminopropyl groups were involved in the reaction. Finally, these results contribute to the interpretation of the structural and textural parameters of the MSN/HA samples, which appear to be mainly affected by the HA loading, irrespective of its molecular weight.

3.3. Qualitative HA analysis: infrared spectroscopy

Infrared spectroscopy is a powerful tool to investigate interface interactions in hybrid organic-inorganic materials. It can be used to assess the molecular structure of surface grafted functionalizing groups, and the weak interactions taking place between silica surface and adsorbed/encapsulated drug molecules [28,50–58]. The spectra of parent NH_2-MSN and HA conjugated samples are reported in Fig. 3, in the high and low frequency ranges (top and bottom panel, respectively). All samples were measured in transmission mode on self-supporting pellets, after RT evacuation necessary to remove adsorbed impurities and water, which would inf uence the spectral analysis (see for instance Refs. [28]; [57]). The spectrum of HA 200 kDa (measured in KBr) is reported for comparison in the Supplementary Material (Fig. S5). The bands assignment discussed in the following is resumed in Table 3.

The spectrum of parent NH_2-MSN sample, reported for comparison, is similar to what already reported and discussed in

Table 2
Quantitative analysis, f potential and mean hydrodynamic diameter.

Samples	HA loading (wt%)		f potential (mV)		Mean hydrodynamic diameter (nm)	
	TGA	Carbazole	Water	PBS[a]	Water	PBS[a]
NH_2-MSN	–	–	+35.0 ±0.9	+12.4 ±0.7	360.7 ±11.2	409.3 ±23.0
HA200A	6.6	8.1	+14.3 ±1.3	16.5 ±0.8	292.7 ±10.6	309.0 ±18.2
HA200B	17.4	19.9	19.8 ±1.9	15.7 ±0.9	253.1 ±10.5	265.9 ±20
HA6.4A	n. d.	3.1	+34.5 ±0.1	1.3 ±0.5	313.8 ±8.4	389.2 ±13.0
HA6.4B	19.0	18.9	8.8 ±0.7	16.8 ±0.8	301.9 ±12.1	354.7 ±16.1

n. d.: not determined.
[a] 0.1 M, pH =7.4.

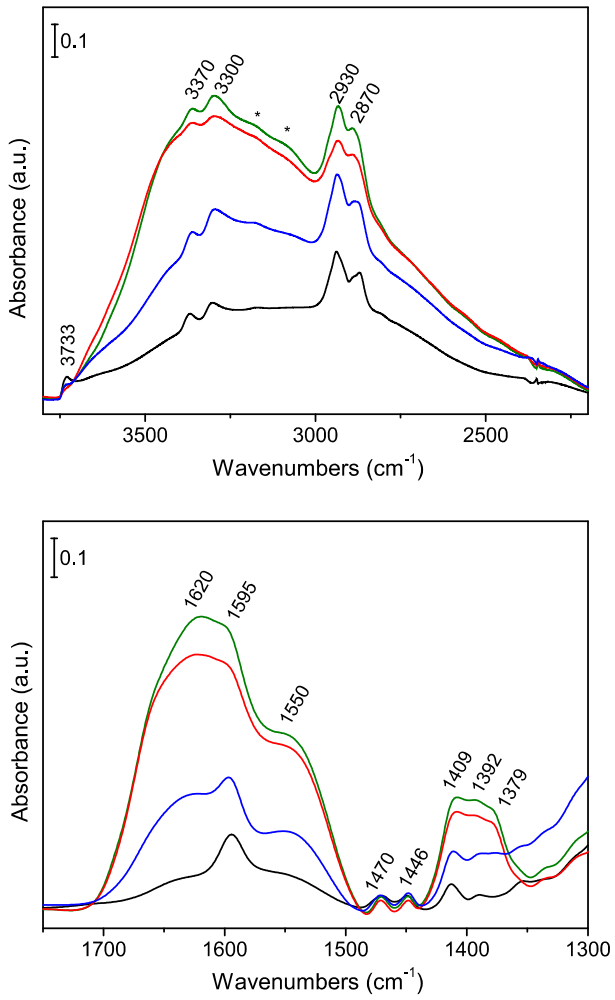

Fig. 3. Infrared spectra in the high and low frequency regions (top and bottom panels, respectively) of NH_2-MSN (black); HA200A (blue); HA200B (red) and HA6.4B (green). Spectra were measured on dehydrated samples and are normalized with respect to pellet thickness. (For interpretation of the references to colour in this f gure legend, the reader is referred to the web version of this article.)

Table 3
Main infrared assignments.

High frequency		Low frequency	
Position	Assignment	Position	Assignment
3370 cm ^{1}	masym NH_2	1650 cm ^{1}	mC@O (Amide I)
3300 cm ^{1}	msym NH_2	1595 cm ^{1}	d NH_2 (aminopropyl)
2930 cm ^{1}	masym CH_2	1550 cm ^{1}	dNH/mCAN comb. (Amide II)
2870 cm ^{1}	msym CH_2	1430–1350 cm ^{1}	dCH and dOH

the literature [28,57]. Namely, it is characterized by a broad signal in the high frequency region (top panel), which is characteristic of hydrogen bonding interactions among surface SiAOH groups (silanols) and between these and the grafted aminopropyl functionalities. The presence of the aminopropyl groups is testif ed by the bands (superimposed to the broad band described above) at 3370 and 3300 cm ^{1} (antisymmetric and symmetric NH_2 stretching modes, mNH_2, respectively) and at 2930/2870 cm ^{1} (antisymmetric and symmetric mCH_2). The very weak peak at 3734 cm ^{1} is related to hydrogen bonding acceptors and/or geminal ASi(OH)$_2$ silanols, which were not consumed by the grafting reaction [57]. The corresponding f ngerprints of aminopropyl functional groups in the low frequency region (bottom panel of Fig. 3) are the band at 1595 cm ^{1} due to the NH_2 bending mode (dNH_2) and the weak dCH_2 features between 1500 and 1320 cm ^{1}.

The spectra of MSN/HA samples show interesting differences with respect to parent materials. Namely, in the high frequency region an increase in the intensity and spectral breadth of the absorption between 3700 and 2200 cm ^{1} is observed, in the order HA200A <HA200B ffi HA6.4B. This can be clearly related to the presence of an extended hydrogen bonding network, both among HA residues and between them and the silica surface. Indeed, the weak band at 3734 cm ^{1} related to SiAOH groups is consumed, conf rming the involvement of surface silanols in hydrogen bonding interactions with HA.

Moreover, weak bands can be also observed between 3200 and 3000 cm ^{1}, recalling the typical spectral shape of hydrogen-bonding carboxylic acids. This indicates that not all the D-glucuronic acid residues were involved in the formation of an amidic bond with the amino groups present on silica. In agreement with the structural, textural and quantitative data discussed above, the two samples prepared by method B are very similar and more affected by conjugation, at variance with sample HA200A, showing an intermediate behavior.

The same trend is observed in the low frequency range (Fig. 3, bottom panel). More in detail, broad absorptions develop in the 1700–1500 cm ^{1} and 1450–1350 cm ^{1} ranges, with the same order of intensity described above, i.e. HA200A <HA200B ffi HA6.4B. The dNH_2 signal at 1595 cm ^{1} is clearly evident on sample HA200A, while it is only a shoulder in the other samples. This indicates that not all aminoproyl functionalities reacted with HA, as expected for functional groups lining the inner surface of the pores. Interestingly, the intensity of this band is higher on sample HA200A, where a lower diffusion of HA residues inside the pores was inferred from textural and structural analysis (see above).

Concerning the new features developing in this spectral region after HA conjugation, they can be safely ascribed to the formation of an amidic bond between the NH_2-MSN amino groups and the carboxylic acid functionalities of HA. Namely, the amide I band (mC@O) is observed at 1650 cm ^{1}, the amide II (dNH and mCN combination mode) at 1550 cm ^{1}, while the absorption between 1430 and 1350 cm ^{1} is related to the numerous dCH and dOH vibrations of HA.

Table 4
Langmuir parameters for water vapour sorption process.

Samples	1st cycle			2nd cycle		
	q_m (wt%)	K	R^2	q_m (wt%)	K	R^2
NH_2-MSN[a]	6.83	8.47	0.9267	9.23	8.47	0.9267
HA200A	1.37	17.10	0.9932	1.47	18.29	0.9940
HA200B	1.28	20.14	0.9964	1.43	19.47	0.9964
HA6.4B	1.56	20.87	0.9950	1.66	22.82	0.9968

[a] Parameters calculated from data measured at 25 °C (from Ref. [28]).

3.4. Interaction with water molecules

HA is a hydrophilic macromolecule, with interesting applications as wetting agent [59–61] or as polymer for surfaces modif cation. Indeed, recent studies reported about the use of HA to improve hydrophilicity and biocompatibility of chitosan f lms or scaffolds [62,63]. Moreover, HA has been used to increase surfaces hydrophilicity to provide antifouling properties, as a result of reduced nonspecif c protein adsorption [64–68]. In this work, the effect of HA conjugation on the hydrophilic character of MSN has been studied by carrying out water vapour sorption microgravimetric experiments. This technique has been recently employed by some of us to investigate the effect of different functional groups on the hydrophilic character of MSN [28].

Water adsorption/desorption isotherms at 28 °C were measured on the three MSN/HA, by gradually increasing the equilibrium vapour pressure in the 0–20 mbar range (p/p^0 from 0 to ca 0.55).

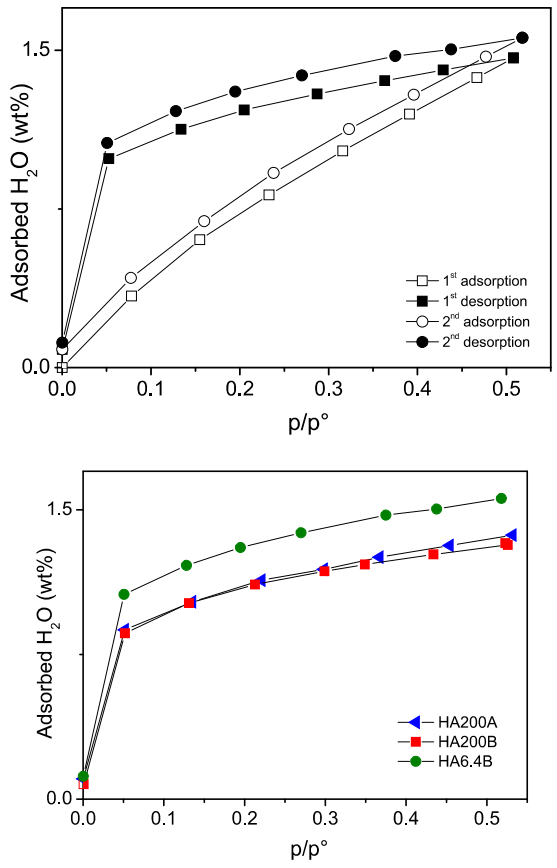

Fig. 4. Water microgravimetric isotherms measured at 28 °C on MSN/HA samples. Top: primary and secondary adsorption/desorption measurements on sample HA6.4B; bottom: comparison of secondary desorption measurements on HA200A (◄), HA200B (j) and HA6.4B (d).

The results obtained on sample HA6.4B are reported in Fig. 4 (top panel). Similar trends were observed on samples HA200A and HA200B (see Fig. S6) and can be summarized as follows. Both primary and secondary adsorption/desorption cycles are characterized by a hysteresis loop, with higher water uptake measured during the desorption step, for each p/p^0 value. This can be explained by the slow diffusion of water interacting with the external HA layer surrounding the MSN. This implies that the equilibrium is probably not reached in the adsorption step within the time frame of the experiment (timeout of 60 min for each p/p^0 dosage). A small water amount is not desorbed after the f rst desorption step, and in all samples the second cycle results in a slightly higher water uptake. When comparing the secondary desorption curves on the three MSN/HA samples, the following order of water uptake is observed: HA6.4B >HA200A ffiHA200B (Fig. 4, bottom panel).

The obtained results are at f rst sight surprising, when compared to what measured on the parent NH_2-MSN material, where a maximum uptake of 6.7 wt% (3.7 mmol/g) was measured at p/p^0 ffi0.3 and 25 °C [28]. This is sensibly higher with respect to what obtained on the MSN/HA samples (1.3–1.7 wt%, see Table 4), indicating a decrease in the water uptake of MSN after HA conjugation, in contrast to what expected for the high hydrophilicity of the polysaccharide. However, the explanation of this apparently puzzling results can be found through a more detailed analysis of the measured isotherms. To this aim, the primary and secondary desorption curves of the samples have been f tted with a Langmuir model, assuming that they are closer to the thermodynamic equilibrium with respect to adsorption ones. The results from this analysis are summarized in Table 4, together with the results for NH_2-MSN parent sample (data from Ref. [28]). First, we acknowledge the fact that for all HA conjugated samples the agreement with the Langmuir model is satisfactory (R^2 >0.99), which is not the case for NH_2-MSN (R^2 =0.9267 for both cycles). Secondly, the set of calculated K values (corresponding to the equilibrium constant of the adsorption process) are consistent for the set of samples, ranging from 17 to ca 23, while for NH_2-MSN a value around 8.5 was found for both sorption cycles. These data clearly indicates that on the conjugated samples water is mainly interacting with the external HA layer, where it is strongly adsorbed and cannot freely diffuse inside the MSN pores, at least in the time frame and experimental conditions of the experiment. This picture f ts well with the higher K values and smaller uptake with respect to parent NH_2-MSN.

Coming back to the comparison among the three samples (Fig. 4, bottom panel) the calculated K values are in the order HA200A <HA200B <HA6.4B. The last sample being the one with the highest uptake, we can infer that the polysaccharide molecular weight inf uences its hydrophilicity. On the contrary, water uptake on HA200A is almost identical to HA200B, irrespective of the different loading. This supports the idea that, when dosed from vapour phase, water is strongly adsorbed on the external HA layer with limited diffusion within the pores. This effect could limit the diffusion of drugs to and from the material pores, as indicated by preliminary studies on drug loading carried out in our group

(not reported). Noticeably, samples HA200B and HA6.4B show a similar water/HA weight ratio (ranging from 0.07 to 0.09) with respect to the sample prepared by method A (0.21–0.22). These data further support the picture obtained by characterization techniques, indicating that sample HA200A is characterized by a different distribution of HA at the pores entrance, with a consistent amount of unreacted amino groups. This could indicate an easier diffusion of adsorbates (such as water molecules) and host drug molecules within the sample.

3.5. Effect of HA on surface charge, aggregation and dispersity

The electrophoretic mobility of the materials was measured to evaluate the effect of conjugation on the particles f potential, which gives an indirect information about the surface charge in the Stern layer. This parameter is affected by both the hydrodynamic diameter and the electric double layer thickness, the latter being strongly inf uenced by the f uid ionic strength and pH. An estimation of the double layer thickness as a function of the ionic strength can be used in the Henry equation, to convert electrophoretic mobility into f potential values [69]. However, in this work f potential values (summarized in Table 2) were calculated with the Smoluchowski equation (representing an approximation valid for thick double layers), for direct comparison with the literature works in the f eld [28,70–73].

In aqueous solution, the amine group is positively charged while the carboxylic ones of HA show a negative charge in relation to their pKa. Assessing the pKa of both covalently linked HA external layer and aminopropyl groups is not straightforward, since both systems are intrinsically complex. Indeed the pKa of amino-functionalized hybrid materials has been the subject of extensive research work, since the covalent bond and interactions with the inorganic surface can affect the amino basicity [28,57,74–78]. In our work, f potential values in water change depending on the amount and on the molecular weight of the conjugated HA. At equal HA molecular weight (compare HA200A and HA200B, 2nd and 3rd lines in Table 2), the f potential decreases as the amount of HA increases. Namely, HA200A (HA loading 6.6 wt%) shows a small but positive value (+14.3 ±1.3 mV), while HA200B, with a HA loading almost triple is characterized by a negative f potential (19.8 ±1.9 mV). Samples obtained by method B showed a more negative surface charge; in fact, according to TGA and carbazole test, this method allows a more eff cient conjugation.

Considering the different HA molecular weights of samples obtained by the same conjugation method, HA200B showed a more negative surface charge with respect to HA6.4B, without clear correlation with the HA loading. Measurements were also carried out on sample HA6.4A, which was discarded for a more detailed characterization because of low HA loading (3.1 wt%as measured by carbazole test, see Table 2) and scarce dispersity (see below). Indeed, this sample shows a f potential value in water almost identical to NH_2-MSN, in agreement with the low derivatization yield.

When the same measurements are carried out in PBS, a different trend is observed, in that almost all samples show more negative f potential values. As recently reported, buffer ions can strongly affect adsorption phenomena at the solid-liquid interphase of charged nanoparticles [73,79,80]. Marucco et al. pointed out how adsorption of phosphate ions from the buffer solution can inf uence the particles surface properties and charge [79]. On the other hand, we cannot exclude the competition of chloride (and Na^+ and K^+ cations, although at a lesser extent) in modifying the effective surface charge of MSNs, in agreement with the work by Cugia et al. [73]. Indeed, in our work all the three considered HA conjugated samples show a similar negative f potential value (around 16 mV), irrespective of the values measured in water. On the contrary, parent NH_2-MSN still shows a positive (though

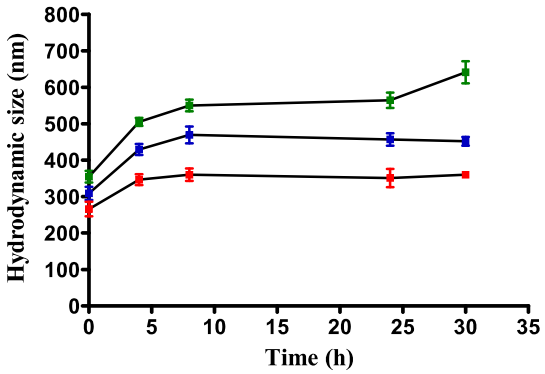

Fig. 5. Dynamic light scattering data of HA200A (blue); HA200B (red) and HA6.4B (green) in PBS measured at 0, 4, 8, 24 and 30 h. The error bars represent the standard deviation of three measurements. (For interpretation of the references to colour in this f gure legend, the reader is referred to the web version of this article.)

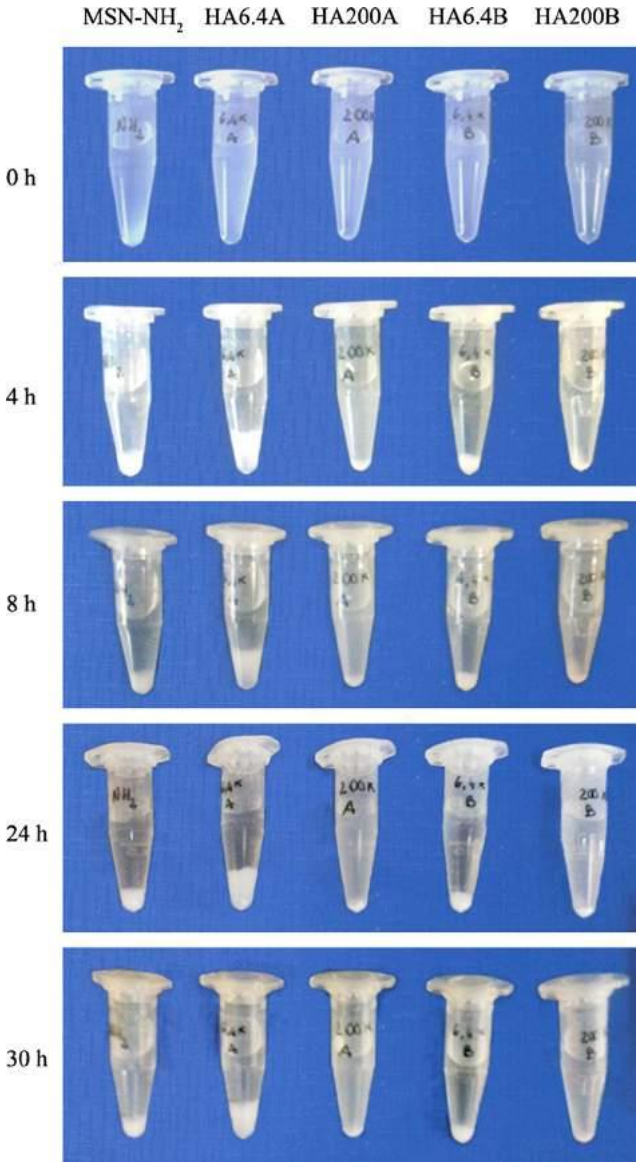

Fig. 6. Images of NH_2-MSN, HA6.4A, HA200A, HA6.4B and HA200B dispersed in PBS with a concentration of 2 mg/ml measured at 0, 4, 8, 24 and 30 h.

minor) charge and sample HA6.4A is almost neutral (1.3 ±0.5 mV). These results cannot easily be rationalized due to the complex interactions of buffer ions with nanoparticles [73].

DLS measurements were carried out to estimate the hydrodynamic sizes of all samples in both water and PBS (Table 2). The average values are always higher than the size of the single particles measured by TEM, indicating agglomeration. A slight decrease in the size is observed after HA conjugation, particularly for high molecular weight and loading, indicating a positive effect of the polymer against the MSNs tendency to agglomeration. Since our attention is focused on the possibility to use these systems for pharmaceutical application, we have followed the evolution of the hydrodynamic size with time. Fig. 5 shows the results obtained on the more stable samples in PBS, i.e. HA6.4B, HA200A and HA200B. The samples show a slight increase of dimensions in the first hours, and then reach a stable value, apart from sample HA6.4B which is characterized by larger size and lower stability. These observations are reflected in the dispersity tests described below.

The pictures acquired during dispersity tests in PBS are shown in Fig. 6. In this case a higher concentration was used (2 mg/ml vs 0.08 mg/ml used for both f potential and DLS measurements), for easier visual observation. The samples with HA of higher molecular weight were better dispersed with respect to parent NH_2-MSN and HA6.4B, which started to precipitate after 4 h. On the contrary, dispersity was dramatically improved after conjugation with high molecular weight HA: HA200A and HA200B formed a stable suspension in PBS for more than 24 h. The enhanced stability of these samples can be explained on the basis of their steric hindrance and of the electrostatic repulsion among the stretched hydrophilic HA chains, reducing the possibility of agglomeration and precipitation. Finally, as concern sample HA6.4A, its precipitation is already complete after 4 h, in agreement with a f potential value close to zero. The dispersity tests carried out in DMEM +10% FBS showed a similar trend (data not reported).

These data confirm the working hypothesis that HA conjugation is a simple and effective method for improving the dispersity and stability of the nanoparticles, which is in turn beneficial for blood

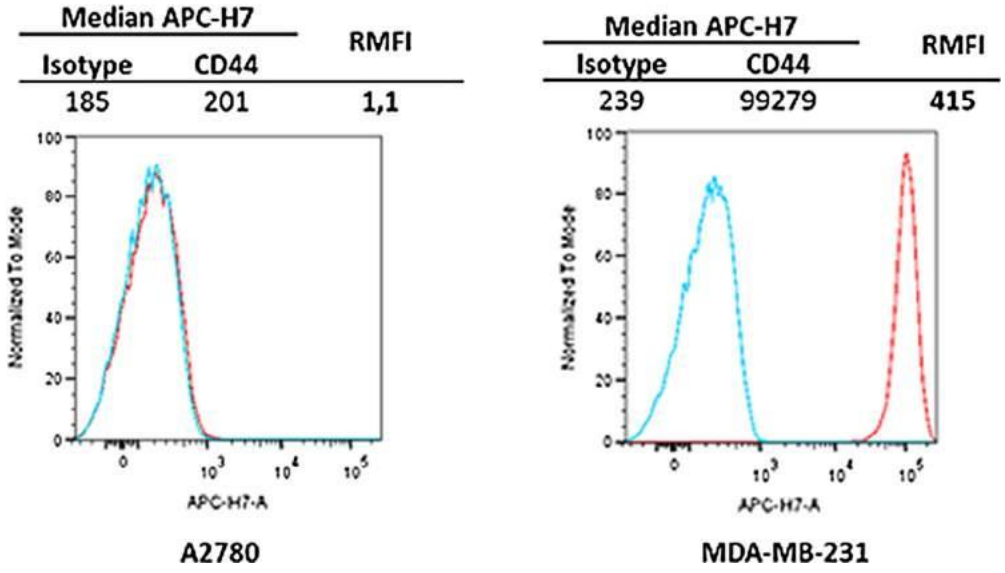

Fig. 7. Flow cytometric histograms of CD44 expression in A2780 cells and MDA-MB-231 cells. Red lines: anti-CD44 antibody; blue lines: isotype control. (For interpretation of the references to colour in this figure legend, the reader is referred to the web version of this article.)

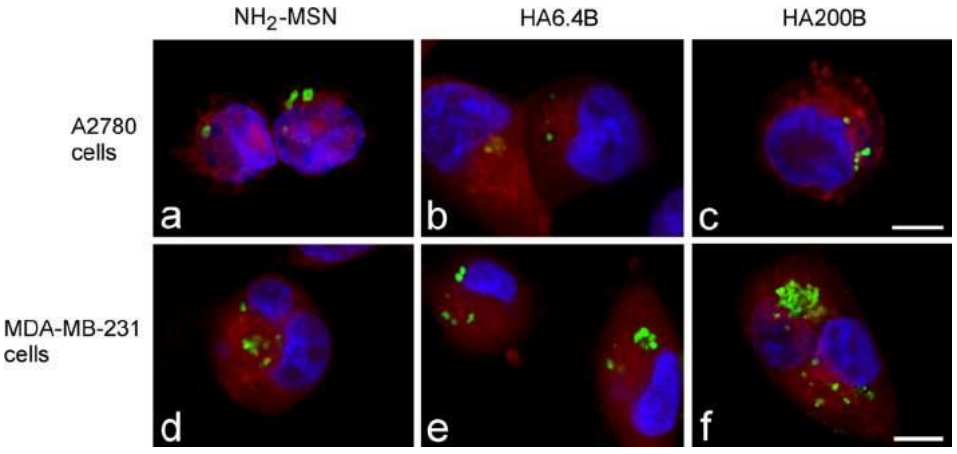

Fig. 8. Confocal micrographs of A2780 cells (a–c) and MDA-MB-231 cells (d–f) after 24 h incubation with different MSN (green fluorescence): NH_2-MSN (a and d), HA6.4B (b and e) and HA200B (c and f). All MSN are distributed in the cytoplasm but are absent from the nucleus (blue fluorescence). The cytoplasm is counterstained with trypan blue (red fluorescence). Note the higher amount of MSN in e and f. Bars: 10 mm. (For interpretation of the references to colour in this figure legend, the reader is referred to the web version of this article.)

circulation making intravenous injection possible. Moreover, our study points out how, irrespective of the similar measured f potential, which is inf uenced by the chemical nature of the buffer medium, the molecular weight of the conjugating macromolecule has a strong inf uence on dispersity.

3.6. Biological characterization

3.6.1. Analysis of cell surface CD44 expression

The HA receptor CD44, an ubiquitous transmembrane molecule, is expressed at low levels on the surface of several normal cells and

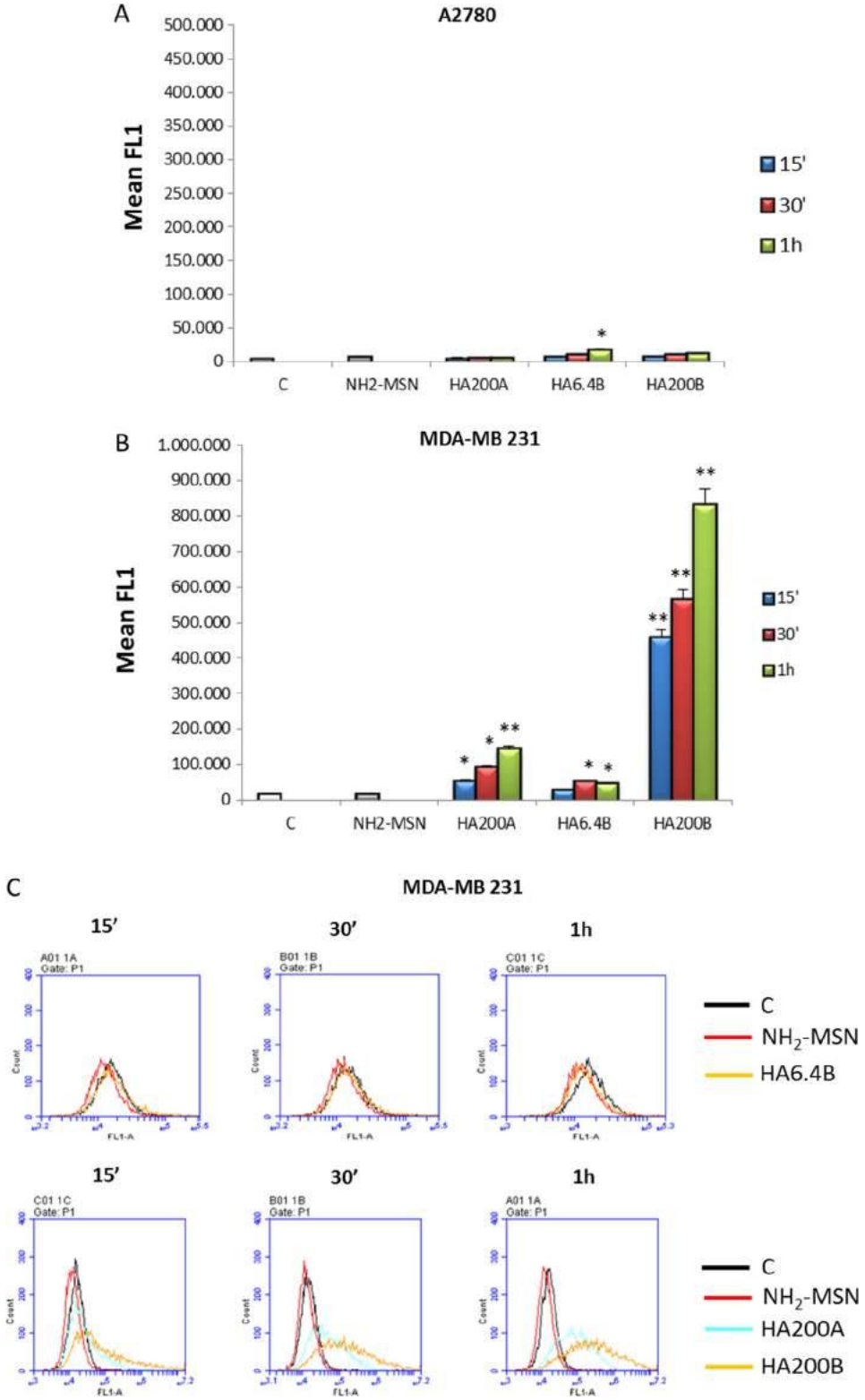

Fig. 9. Cellular uptake of FITC labelled NH_2-MSN with or without HA modif cation in A2780 and MDA-MB-321 cell lines. Analysis of internalization of NH2-MSN, HA6.4B, HA200A and HA200B in A2780 (A) and MDA-MB-231 (B,C) cells by f ow cytometry for the indicated time. Data in graphs are expressed as means ±SEM (*p <.05 and **p <.01 vs FITC-NH_2-MSN) of three independent experiments.

overexpressed in many cancer cells [81]. The levels of receptor cell surface expression were preliminary evaluated on a panel of cancer cell lines (MDA-MB-231, JR8, A459, MCF7 and A2780) using anti-CD44 antibody and flow cytometry, with the aim to identify the cell models to be used for further in vitro studies. The results show that A2780 cells did not express detectable amount of CD44 whereas MDA-MB-231 cells display a very high expression (Fig. 7). Thus, to evaluate the cytotoxic activity and the cellular uptake of the nanoparticles, MDA-MB-231 and A2780 cells were chosen as $CD44^+$ and CD44 cancer cells, respectively.

3.6.2. In vitro cytotoxicity

The in vitro cytotoxicity of NH_2-MSN and MSN/HA was evaluated after treatment of 24, 48 and 72 h in the concentration range of 1.5–25 mg/ml. The results showed that the nanoparticles were non-toxic for both cell lines demonstrating the good safety and biocompatibility of the carriers (data not shown). These data are in agreement with the results obtained with other HA decorated MSN [24,36,37,40].

3.6.3. In vitro targeting analysis

Efficient cellular uptake is a major requirement for the therapeutic efficacy of nanoparticles targeting. To test the targeting ability of our MSN we evaluated the cellular uptake of both FITC-labelled NH_2-MSN and MSN/HA on MDA-MB-231 ($CD44^+$) and A2780 (CD44) cell lines by both CLSM and FACS.

CLSM allowed us to visualize the cellular uptake and biodistribution of the nanoparticles in these two cell lines. As shown in Fig. 8, in both cell lines MSN occurred in the cytoplasm as clusters of different size; accordingly, previous TEM studies demonstrated that these nanoparticles are internalized by the cell via both endocytosis and phagocytosis, and then accumulate into cytoplasmic vacuoles [82]. Moreover, MSNs were never found inside the nucleus of MDA-MB-231 and A2780 cells, consistently with previous observations [23,24,40,82–85]. Although CLSM does not allow precise quantitation of cellular uptake, the amount of internalized NH_2-MSN was apparently similar in the two cell lines, whereas HA6.4B and HA200B were more abundant in MDA-MB-231 than in A2780 cells. This suggests that MSN/HA possess significant selectivity for cells overexpressing CD44 receptors, in agreement with our results obtained with flow cytometry (see below).

In addition, microscopic observation of the samples revealed the absence of evident morphological alterations in both cytoplasm (e.g. vacuolization) and nucleus (e.g. pyknosis, apoptosis), thus confirming the high biocompatibility of NH_2-MSN and MSN/HA at the concentrations tested in this study.

The morphological images obtained by CLSM are consistent with the flow cytometry analysis performed in order to obtain a quantitative comparison between FITC labelled NH_2-MSN and MSN/HA (Fig. 9). After treating A2780 and MDA-MB-231 cells with the different MSN/HA, their uptake in A2780 cells is moderately increased in a time dependent manner, but almost irrelevant in comparison with MDA-MB-231 (Fig. 9A). In particular, the FITC mean intensity of MSN/HA200 (both A and B) was dramatically increased in MDA-MB-231 in comparison to A2780 (Fig. 9A, B). Concerning MDA-MB-231, we observed that the cellular uptake efficiency is increased over incubation time (up to 1 h, when the uptake is near plateau, approximately 80%, Fig. 9C). Moreover, the cellular uptake efficiency is also dependent on the amount of HA on nanoparticles surface and on its molecular weight. In particular, we obtained a higher uptake of HA200B versus HA200A, demonstrating that method B in which the activation of HA was carried out directly in the presence of the nanoparticles improves cells uptake (Fig. 9B). In contrast, the mean intensity of FITC from the cells incubated with FITC labelled NH_2-MSNs without HA modification is lower and similar for both cell lines. These in vitro experiments confirm that MSN/HA can target CD44 overexpressing MDA-MB-231 cancer cells via the HA receptor-mediated endocytosis [84,86] and phagocytosis [87] pathways, strongly highlighting the potential use of MSN/HA as an efficient approach for tumor-targeting treatments.

4. Conclusions

MSN/HA samples were prepared following two different conjugation procedures previously reported [36,37] and using HA of two different molecular weight (6.4 and 200 kDa). The size of HA strongly affects its biological functions and its physico-chemical characteristics [35]. However, to our knowledge this is the first time that such a comparative study is reported, helping the scientific community working in the field to select the best strategy to obtain hybrid nanomaterials with good biological response and potential pharmaceutical applicability. More in detail, our systematic physico-chemical analysis points to the concerted effect of both HA molecular weight and loading in improving dispersity of MSN. With this respect, we have demonstrated that the 'one pot' method - in which HA is directly activated in the presence of the nanoparticles – is the most efficient, also in terms of possible scale-up.

Our results are also in agreement with recent reports about the importance of considering the interaction of buffer ions with nanoparticles when assessing surface charge and related interphase phenomena, which are of fundamental importance to rationalize results in physiological media [73].

Finally, in vitro tests on cancer cell lines demonstrated that MSN/HA are biocompatible and preferentially target cells overexpressing the HA receptor CD44. Also in this context, the best performances are obtained with the 'one pot' sample prepared using HA with high molecular weight (HA200B). All these data suggest the potential use of MSN/HA as efficient approach for tumor-targeting treatments.

Acknowledgements

Funding from Italian Ministry for University and Research (MIUR)—University of Turin, "Fondi Ricerca Locale (ex-60%)" are kindly acknowledged. We thank Maria Carmen Valsania (Mayita) from Department of Chemistry and NIS Centre, University of Torino, for TEM measurements.

Appendix A. Supplementary material

Supplementary data associated with this article can be found, in the online version, at https://doi.org/10.1016/j.jcis.2018.01.072.

References

[1] D.J. Irvine, Drug delivery. One nanoparticle, one kill, Nat. Mater. 10 (5) (2011) 342–343.
[2] D. Yohan, B.D. Chithrani, Applications of nanoparticles in nanomedicine, J. Biomed. Nanotechnol. 10 (9) (2014) 2371–2392.
[3] M. Estanqueiro, M.H. Amaral, J. Conceicao, J.M.S. Lobo, Nanotechnological carriers for cancer chemotherapy: the state of the art, Colloid Surf. B-Biointerfaces 126 (2015) 631–648.
[4] T.M. Sun, Y.S. Zhang, B. Pang, D.C. Hyun, M.X. Yang, Y.N. Xia, Engineered nanoparticles for drug delivery in cancer therapy, Angew. Chem. Int. Edit. 53 (46) (2014) 12320–12364.
[5] A. Wicki, D. Witzigmann, V. Balasubramanian, J. Huwyler, Nanomedicine in cancer therapy: challenges, opportunities, and clinical applications, J. Control. Release 200 (2015) 138–157.
[6] R.R. Castillo, M. Colilla, M. Vallet-Regi, Advances in mesoporous silica-based nanocarriers for co-delivery and combination therapy against cancer, Expert Opin. Drug Deliv. 14 (2) (2017) 229–243.
[7] X. Sun, Y.P. Luo, L.W. Huang, B.Y. Yu, J.W. Tian, A peptide-decorated and curcumin-loaded mesoporous silica nanomedicine for effectively overcoming multidrug resistance in cancer cells, RSC Adv. 7 (27) (2017) 16401–16409.

[8] S. Arpicco, C. Lerda, E.D. Pozza, C. Costanzo, N. Tsapis, B. Stella, M. Donadelli, I. Dando, E. Fattal, L. Cattel, M. Palmieri, Hyaluronic acid-coated liposomes for active targeting of gemcitabine, Eur. J. Pharm. Biopharm. 85 (3) (2013) 373–380.
[9] I. Pedrini, E. Gazzano, K. Chegaev, B. Rolando, A. Marengo, J. Kopecka, R. Fruttero, D. Ghigo, S. Arpicco, C. Riganti, Liposomal nitrooxy-doxorubicin: one step over caelyx in drug-resistant human cancer cells, Mol. Pharm. 11 (9) (2014) 3068–3079.
[10] B.S. Pattni, V.V. Chupin, V.P. Torchilin, New developments in liposomal drug delivery, Chem. Rev. 115 (19) (2015) 10938–10966.
[11] B. Stella, S. Arpicco, M.T. Peracchia, D. Desmaele, J. Hoebeke, M. Renoir, J. D'Angelo, L. Cattel, P. Couvreur, Design of folic acid-conjugated nanoparticles for drug targeting, J. Pharm. Sci. 89 (11) (2000) 1452–1464.
[12] B. Stella, S. Arpicco, F. Rocco, V. Marsaud, J.M. Renoir, L. Cattel, P. Couvreur, Encapsulation of gemcitabine lipophilic derivatives into polycyanoacrylate nanospheres and nanocapsules, Int. J. Pharm. 344 (1–2) (2007) 71–77.
[13] B.E. Grottkau, X.X. Cai, J. Wang, X.M. Yang, Y.F. Lin, Polymeric nanoparticles for a drug delivery system, Curr. Drug Metab. 14 (8) (2013) 840–846.
[14] I.I. Slowing, J.L. Vivero-Escoto, C.-W. Wu, V.S.Y. Lin, Mesoporous silica nanoparticles as controlled release drug delivery and gene transfection carriers, Adv. Drug Deliv. Rev. 60 (11) (2008) 1278–1288.
[15] J. Vivero-Escoto, I. Slowing, B. Trewyn, V. Lin, Mesoporous silica nanoparticles for intracellular controlled drug delivery, Small 18 (2010) 1952–1967.
[16] Y. Chen, H.R. Chen, J.L. Shi, Drug delivery/imaging multifunctionality of mesoporous silica-based composite nanostructures, Expert Opin. Drug Deliv. 11 (6) (2014) 917–930.
[17] V. Mamaeva, C. Sahlgren, M. Linden, Mesoporous silica nanoparticles in medicine-Recent advances, Adv. Drug Deliv. Rev. 65 (5) (2013) 689–702.
[18] J.M. Rosenholm, V. Mamaeva, C. Sahlgren, M. Linden, Nanoparticles in targeted cancer therapy: mesoporous silica nanoparticles entering preclinical development stage, Nanomedicine 7 (1) (2012) 111–120.
[19] H. Meng, M. Xue, J.I. Zink, A.E. Nel, Development of pharmaceutically adapted mesoporous silica nanoparticles platform, J. Phys. Chem. Lett. 3 (3) (2012) 358–359.
[20] S.M. Zhu, Z.Y. Zhou, D. Zhang, Control of drug release through the in situ assembly of stimuli-responsive ordered mesoporous silica with magnetic particles, ChemPhysChem 8 (17) (2007) 2478–2483.
[21] S.H. Wu, Y.S. Lin, Y. Hung, Y.H. Chou, Y.H. Hsu, C. Chang, C.Y. Mou, Multifunctional mesoporous silica nanoparticles for intracellular labeling and animal magnetic resonance imaging studies, ChemBioChem 9 (1) (2008) 53–57.
[22] K.K. Coti, M.E. Belowich, M. Liong, M.W. Ambrogio, Y.A. Lau, H.A. Khatib, J.I. Zink, N.M. Khashab, J.F. Stoddart, Mechanised nanoparticles for drug delivery, Nanoscale 1 (1) (2009) 16–39.
[23] Q.F. Zhao, H.J. Geng, Y. Wang, Y.K. Gao, J.H. Huang, Y. Wang, J.H. Zhang, S.L. Wang, Hyaluronic acid oligosaccharide modified redox-responsive mesoporous silica nanoparticles for targeted drug delivery, ACS Appl. Mater. Interfaces 6 (22) (2014) 20290–20299.
[24] Q.F. Zhao, J. Liu, W.Q. Zhu, C.S. Sun, D.H. Di, Y. Zhang, P. Wang, Z.Y. Wang, S.L. Wang, Dual-stimuli responsive hyaluronic acid-conjugated mesoporous silica for targeted delivery to CD44-overexpressing cancer cells, Acta Biomater. 23 (2015) 147–156.
[25] C. Gimenez, C. de la Torre, M. Gorbe, E. Aznar, F. Sancenon, J.R. Murguia, R. Martinez-Manez, M.D. Marcos, P. Amoros, Gated mesoporous silica nanoparticles for the controlled delivery of drugs in cancer cells, Langmuir 31 (12) (2015) 3753–3762.
[26] J.H. Zhu, Y.M. Niu, Y. Li, Y.X. Gong, H.H. Shi, Q. Huo, Y. Liu, Q.W. Xu, Stimuli-responsive delivery vehicles based on mesoporous silica nanoparticles: recent advances and challenges, J. Mat. Chem. B 5 (7) (2017) 1339–1352.
[27] M. Vallet-Regí, F. Balas, D. Arcos, Mesoporous materials for drug delivery, Angew. Chem. Int. Edit. 46 (2007) 7548–7558.
[28] G.E. Musso, E. Bottinelli, L. Celi, G. Magnacca, G. Berlier, Influence of surface functionalization on the hydrophilic character of mesoporous silica nanoparticles, Phys. Chem. Chem. Phys. 17 (21) (2015) 13882–13894.
[29] S.T. Kim, K. Saha, C. Kim, V.M. Rotello, The role of surface functionality in determining nanoparticle cytotoxicity, Acc. Chem. Res. 46 (3) (2013) 681–691.
[30] M. Zhu, G. Nie, H. Meng, T. Xia, A. Nel, Y. Zhao, Physicochemical properties determine nanomaterial cellular uptake, transport, and fate, Acc. Chem. Res. 46 (3) (2013) 622–631.
[31] J.L. Townson, Y.-S. Lin, J.O. Agola, E.C. Carnes, H.S. Leong, J.D. Lewis, C.L. Haynes, C.J. Brinker, Re-examining the size/charge paradigm: differing in vivo characteristics of size- and charge-matched mesoporous silica nanoparticles, J. Am. Chem. Soc. 135 (43) (2013) 16030–16033.
[32] H. Maeda, Macromolecular therapeutics in cancer treatment: The EPR effect and beyond, J. Control. Release 164 (2) (2012) 138–144.
[33] P. Caliceti, S. Salmaso, S. Bersani, Polysaccharide-based anticancer prodrugs, 2010.
[34] S. Arpicco, P. Milla, B. Stella, F. Dosio, Hyaluronic Acid Conjugates as Vectors for the Active Targeting of Drugs, Genes and Nanocomposites in Cancer Treatment, Molecules 19 (3) (2014) 3193–3230.
[35] F. Dosio, S. Arpicco, B. Stella, E. Fattal, Hyaluronic acid for anticancer drug and nucleic acid delivery, Adv. Drug Deliv. Rev. 97 (2016) 204–236.
[36] M. Ma, H.R. Chen, Y. Chen, K. Zhang, X. Wang, X.Z. Cui, J.L. Shi, Hyaluronic acid-conjugated mesoporous silica nanoparticles: excellent colloidal dispersity in physiological fluids and targeting efficacy, J. Mater. Chem. 22 (12) (2012) 5615–5621.
[37] M.H. Yu, S. Jambhrunkar, P. Thorn, J.Z. Chen, W.Y. Gu, C.Z. Yu, Hyaluronic acid modified mesoporous silica nanoparticles for targeted drug delivery to CD44-overexpressing cancer cells, Nanoscale 5 (1) (2013) 178–183.
[38] A. Salis, M. Fanti, L. Medda, V. Nairi, F. Cugia, M. Piludu, V. Sogos, M. Monduzzi, Mesoporous silica nanoparticles functionalized with hyaluronic acid and chitosan biopolymers. Effect of functionalization on cell internalization, ACS Biomater. Sci. Eng. 2 (5) (2016) 741–751.
[39] M.Z. Zhang, C.L. Xu, L.Q. Wen, M.K. Han, B. Xiao, J. Zhou, Y.C. Zhang, Z. Zhang, E. Viennois, D. Merlin, A hyaluronidase-responsive nanoparticle-based drug delivery system for targeting colon cancer cells, Cancer Res. 76 (24) (2016) 7208–7218.
[40] Z.W. Chen, Z.H. Li, Y.H. Lin, M.L. Yin, J.S. Ren, X.G. Qu, Bioresponsive hyaluronic acid-capped mesoporous silica nanoparticles for targeted drug delivery, Chem. Euro J. 19 (5) (2013) 1778–1783.
[41] L. Chen, X.J. Zhou, W. Nie, Q.Q. Zhang, W.Z. Wang, Y.Z. Zhang, C.L. He, Multifunctional redox-responsive mesoporous silica nanoparticles for efficient targeting drug delivery and magnetic resonance imaging, ACS Appl. Mater. Interfaces 8 (49) (2016) 33829–33841.
[42] D. Tarn, M. Xue, J.I. Zink, pH-responsive dual cargo delivery from mesoporous silica nanoparticles with a metal-latched nanogate, Inorg. Chem. 52 (4) (2013) 2044–2049.
[43] D.R. Radu, C.Y. Lai, K. Jeftinija, E.W. Rowe, S. Jeftinija, V.S.Y. Lin, A polyamidoamine dendrimer-capped mesoporous silica nanosphere-based gene transfection reagent, J. Am. Chem. Soc. 126 (2004) 13216–13217.
[44] K.M. Parida, D. Rath, Amine functionalized MCM-41: an active and reusable catalyst for Knoevenagel condensation reaction, J. Mol. Catal. A -Chem. 310 (1–2) (2009) 93–100.
[45] P. Iliade, I. Miletto, S. Coluccia, G. Berlier, Functionalization of mesoporous MCM-41 with aminopropyl groups by co-condensation and grafting: a physico-chemical characterization, Res. Chem. Intermed. 38 (2012) 785–794.
[46] K.C. Vrancken, K. Possemiers, P. Vandervoort, E.F. Vansant, Surface modification of silica-gels with aminoorganosilanes, Colloid Surf. A 98 (3) (1995) 235–241.
[47] T. Bitter, H.M. Muir, A modified uronic acid carbazole reaction, Anal. Biochem. 4 (4) (1962) 330–334.
[48] F. Rouquerol, J. Rouquerol, K. Sing, Adsorption by Powders & Porous Solids, Academic press, 1999.
[49] V. Vichai, K. Kirtikara, Sulforhodamine B colorimetric assay for cytotoxicity screening, Nat. Protoc. 1 (2006) 1112–1116.
[50] S. Sapino, E. Ugazio, L. Gastaldi, I. Miletto, G. Berlier, D. Zonari, S. Oliaro-Bosso, Mesoporous silica as topical nanocarriers for quercetin: characterization and in vitro studies, Eur. J. Pharm. Biopharm. 89 (2015) 116–125.
[51] A. Malfanti, I. Miletto, E. Bottinelli, D. Zonari, G. Blandino, G. Berlier, S. Arpicco, Delivery of gemcitabine prodrugs employing mesoporous silica nanoparticles, Molecules 21 (4) (2016).
[52] R. Mellaerts, M.B.J. Roeffaers, K. Houthoofd, M. Van Speybroeck, G. De Cremer, J.A.G. Jammaer, G. Van den Mooter, P. Augustijns, J. Hofkens, J.A. Martens, Molecular organization of hydrophobic molecules and co-adsorbed water in SBA-15 ordered mesoporous silica material, Phys. Chem. Chem. Phys. 13 (7) (2011) 2706–2713.
[53] R. Mellaerts, E.J. Fayad, G. Van den Mooter, P. Augustijns, M. Rivallan, F. Thibault-Starzyk, J.A. Martens, In situ FT-IR investigation of etravirine speciation in pores of SBA-15 ordered mesoporous silica material upon contact with water, Mol. Pharm. 10 (2) (2013) 567–573.
[54] L. Medda, M.F. Casula, M. Monduzzi, A. Salis, Adsorption of lysozyme on hyaluronic acid functionalized SBA-15 mesoporous silica: a possible bioadhesive depot system, Langmuir 30 (43) (2014) 12996–13004.
[55] M. Halo, A.M. Ferrari, G. Berlier, I. Miletto, S. Casassa, Experimental and first-principles IR characterization of quercetin adsorbed on a silica surface, Theor. Chem. Acc. 135 (5) (2016).
[56] R. Onnainty, B. Onida, P. Paez, M. Longhi, A. Barresi, G. Granero, Targeted chitosan-based bionanocomposites for controlled oral mucosal delivery of chlorhexidine, Int. J. Pharm. 509 (1–2) (2016) 408–418.
[57] G. Paul, G.E. Musso, E. Bottinelli, M. Cossi, L. Marchese, G. Berlier, Investigating the interaction of water vapour with aminopropyl groups on the surface of mesoporous silica nanoparticles, ChemPhysChem 18 (2017) 839–849.
[58] V. Nairi, L. Medda, M. Monduzzi, A. Salis, Adsorption and release of ampicillin antibiotic from ordered mesoporous silica, J. Colloid Interface Sci. 497 (2017) 217–225.
[59] A. Weeks, D. Luensmann, A. Boone, L. Jones, H. Sheardown, Hyaluronic acid as an internal wetting agent in model DMAA/TRIS contact lenses, J. Biomater. Appl. 27 (4) (2012) 423–432.
[60] A. Weeks, D. Morrison, J.G. Alauzun, M.A. Brook, L. Jones, H. Sheardown, Photocrosslinkable hyaluronic acid as an internal wetting agent in model conventional and silicone hydrogel contact lenses, J. Biomed. Mater. Res. Part A 100A (8) (2012) 1972–1982.
[61] A. Weeks, L.N. Subbaraman, L. Jones, H. Sheardown, The competing effects of hyaluronic and methacrylic acid in model contact lenses, J. Biomater. Sci.-Polym. Ed. 23 (8) (2012) 1021–1038.
[62] Y.J. Wang, L. Guo, L. Ren, S.H. Yin, J. Ge, Q.Y. Gao, T. Luxbacher, S.J. Luo, A study on the performance of hyaluronic acid immobilized chitosan film, Biomed. Mater. 4 (3) (2009).
[63] C.A. Acevedo, E. Sanchez, P. Diaz-Calderon, J.J. Blaker, J. Enrione, F. Quero, Synergistic effects of crosslinking and chitosan molecular weight on the microstructure, molecular mobility, thermal and sorption properties of porous chitosan/gelatin/hyaluronic acid scaffolds, J. Appl. Polym. Sci. 134 (18) (2017).

[64] R.L. Huang, X. Liu, H.J. Ye, R.X. Su, W. Qi, L.B. Wang, Z.M. He, Conjugation of hyaluronic acid onto surfaces via the interfacial polymerization of dopamine to prevent protein adsorption, Langmuir 31 (44) (2015) 12061–12070.
[65] X. Liu, R.L. Huang, R.X. Su, W. Qi, L.B. Wang, Z.M. He, Grafting hyaluronic acid onto gold surface to achieve low protein fouling in surface plasmon resonance biosensors, ACS Appl. Mater. Interfaces 6 (15) (2014) 13034–13042.
[66] M.A.J. Mazumder, Polydimethylsiloxane substrates with surfaces decorated by immobilized hyaluronic acids of different molecular weight for biomedical applications, Arab. J. Sci. Eng. 42 (1) (2017) 271–280.
[67] M.H. Ramadan, J.E. Prata, O. Karacsony, G. Duner, N.R. Washburn, Reducing protein adsorption with polymer-grafted hyaluronic acid coatings, Langmuir 30 (25) (2014) 7485–7495.
[68] M. Van Beek, A. Weeks, L. Jones, H. Sheardown, Immobilized hyaluronic acid containing model silicone hydrogels reduce protein adsorption, J. Biomater. Sci.-Polym. Ed. 19 (11) (2008) 1425–1436.
[69] M. Morga, Z. Adamczyk, D. Kosior, Silica nanoparticle monolayers on a macroion modified surface: formation mechanism and stability, Phys. Chem. Chem. Phys. 19 (34) (2017) 22721–22732.
[70] M. Colilla, I. Izquierdo-Barba, S. Sanchez-Salcedo, J.L.G. Fierro, J.L. Hueso, M. Vallet-Regí, Synthesis and characterization of zwitterionic SBA-15 nanostructured materials, Chem. Mater. 22 (23) (2010) 6459–6466.
[71] J.M. Rosenholm, M. Linden, Towards establishing structure-activity relationships for mesoporous silica in drug delivery applications, J. Control. Release 128 (2) (2008) 157–164.
[72] C. Giaveno, L. Celi, R.M. Aveiro Cessa, M. Prati, E. Bonifacio, E. Barberis, Interaction of organic phosphorus with clays extracted from Oxisols, Soil Sci. 173 (2008) 694–706.
[73] F. Cugia, S. Sedda, F. Pitzalis, D.F. Parsons, M. Monduzzi, A. Salis, Are specific buffer effects the new frontier of Hofmeister phenomena? Insights from lysozyme adsorption on ordered mesoporous silica, RSC Adv. 6 (97) (2016) 94617–94621.
[74] M. Etienne, S. Goubert-Renaudin, Y. Rousselin, C. Marichal, F. Denat, B. Lebeau, A. Walcarius, Multiarm cyclam-grafted mesoporous silica: a strategy to improve the chemical stability of silica materials functionalized with amine ligands, Langmuir 25 (5) (2009) 3137–3145.
[75] M. Etienne, A. Walcarius, Analytical investigation of the chemical reactivity and stability of aminopropyl-grafted silica in aqueous medium, Talanta 59 (6) (2003) 1173–1188.
[76] A. Walcarius, M. Etienne, B. Lebeau, Rate of access to the binding sites in organically modified silicates. 2. Ordered mesoporous silicas grafted with amine or thiol groups, Chem. Mater. 15 (11) (2003) 2161–2173.
[77] M. Morga, Z. Adamczyk, Monolayers of cationic polyelectrolytes on mica – Electrokinetic studies, J. Colloid Interface Sci. 407 (2013) 196–204.
[78] Y. Tataurova, M.J. Sealy, R.G. Larsen, S.C. Larsen, Surface-selective solution NMR studies of functionalized zeolite nanoparticles, J. Phys. Chem. Lett. 3 (3) (2012) 425–429.
[79] A. Marucco, F. Catalano, I. Fenoglio, F. Turci, G. Martra, B. Fubini, Possible chemical source of discrepancy between in vitro and in vivo tests in nanotoxicology caused by strong adsorption of buffer components, Chem. Res. Toxicol. 28 (1) (2015) 87–91.
[80] M. Morga, A. Michna, Z. Adamczyk, Formation and stability of polyelectrolyte/polypeptide monolayers determined by electrokinetic measurements, Colloid Surf. A 529 (2017) 302–310.
[81] R.J.S. Sneath, D.C. Mangham, The normal structure and function of CD44 and its role in neoplasia, J. Clin. Pathol.-Mol. Pathol. 51 (1998) 191–200.
[82] M. Costanzo, F. Carton, A. Marengo, G. Berlier, B. Stella, S. Arpicco, M. Malatesta, Fluorescence and electron microscopy to visualize the intracellular fate of nanoparticles for drug delivery, Eur. J. Histochem. 60 (2) (2016) 107–115.
[83] Z.W. Chen, Z.H. Li, Y.H. Lin, M.L. Yin, J.S. Ren, X.G. Qu, Biomineralization inspired surface engineering of nanocarriers for pH-responsive, targeted drug delivery, Biomaterials 34 (4) (2013) 1364–1371.
[84] M. El-Dakdouki, E. Puré, X. Huang, Development of drug loaded nanoparticles for tumor targeting. Part 1: synthesis, characterization, and biological evaluation in 2D cell cultures, Nanoscale (5) (2013) 3895–3903.
[85] S. Poussard, M. Decossas, O. Le Bihan, S. Mornet, G. Naudin, O. Lambert, Internalization and fate of silica nanoparticles in C2C12 skeletal muscle cells: evidence of a beneficial effect on myoblast fusion, Int. J. Nanomed. 10 (2015) 1479–1492.
[86] R. Racine, M.E. Mummert, Hyaluronan endocytosis: mechanisms of uptake and biological functions, Mol. Regul. Endocytosis (2012) 377–390.
[87] P.P. Ostrowski, S. Grinstein, S.A. Freeman, Diffusion barriers, mechanical forces, and the biophysics of phagocytosis, Dev. Cell 38 (2) (2016) 135–146.

M. Costanzo, F. Boschi, F. Carton, G. Conti, V. Covi, G. Tabaracci, A. Sbarbati, M. Malatesta (2018): Low ozone concentrations promote adipogenesis in human adipose-derived adult stem cells. Eur J Histochem. 62(3), DOI: 10.4081/ejh.2018.2969

Low ozone concentrations promote adipogenesis in human adipose-derived adult stem cells

Manuela Costanzo,[1] Federico Boschi,[2] Flavia Carton,[1] Giamaica Conti,[1] Viviana Covi,[3] Gabriele Tabaracci,[3] Andrea Sbarbati,[1] Manuela Malatesta[1]

[1]Department of Neurosciences, Biomedicine and Movement Sciences, University of Verona
[2]Department of Computer Science, University of Verona
[3]San Rocco Clinic, Montichiari (BS), Italy

Abstract

Ozone is a strong oxidant, highly unstable atmospheric gas. Its medical use at low concentrations has been progressively increasing as an alternative/adjuvant treatment for several diseases. In this study, we investigated the effects of mild ozonisation on human adipose-derived adult stem (hADAS) cells *i.e.*, mesenchymal stem cells occurring in the stromal-vascular fraction of the fat tissue and involved in the tissue regeneration processes. hADAS cells were induced to differentiate into the adipoblastic lineage, and the effect of low ozone concentrations on the adipogenic process was studied by combining histochemical, morphometric and ultrastructural analyses. Our results demonstrate that ozone treatment promotes lipid accumulation in hADAS cells without inducing deleterious effects, thus paving the way to future studies aimed at elucidating the effect of mild ozonisation on adipose tissue for tissue regeneration and engineering.

Introduction

Ozone (O_3) is a naturally occurring atmospheric gas composed of three oxygen atoms; it is highly unstable (rapidly decomposing to normal oxygen, O_2) and is a strong oxidant.

The therapeutic potential of O_3 is known since the end of the 18th century but its medical application has been limited for a long time due to the doubts about its possible toxicity. However, in the last two decades the medical use of O_3 has been progressively increasing all over the world as an alternative/adjuvant treatment for several diseases.[1-3] Some mechanistic evidence has recently been provided for the dose-dependent effects of O_3 treatment.[4-6] In particular, it has been demonstrated that low O_3 concentrations, by inducing the so-called eustress,[7] do activate cell anti-oxidative response pathways[8] which are likely responsible for the therapeutic effects observed in the clinical practice.

However, the potential of mild ozonisation in tissue regeneration and differentiation has been scarcely explored so far. In this view, we investigated the effects of low O_3 concentrations on human adipose-derived adult stem (hADAS) cells *i.e.*, the mesenchymal stem cells which are present in the stromal-vascular fraction of the fat tissue. hADAS cells are able to differentiate *in vitro* into meso-, ecto- and endodermal cell lineages and can also be reprogrammed as pluripotent stem cells more efficiently than other cell types.[9] hADAS cells are therefore considered as a powerful tool in regenerative medicine and tissue engineering.[9-13] In this study, we induced hADAS cells to differentiate into the adipoblastic lineage, and investigated the effect of mild ozonisation on the adipogenic process; histochemical and morphometric analyses at light microscopy were combined with ultrastructural morphology at transmission electron microscopy (TEM).

Materials and Methods

Technical details of cell culture, gas treatment, cell processing for light microscopy and TEM, and morphometric analysis are reported in the Supplementary Material.

Briefly, hADAS cells were isolated from subcutaneous adipose tissue harvested by liposuction and grown in either adipogenic or non adipogenic medium. These cells were exposed to 5, 10 or 20 µg O_3/mL O_2 at early (6 days), intermediate (16 days) and late (20 days) differentiation steps, and the effects were evaluated 2 h and 24 h after gas exposure.

After 6 days in differentiation medium, cell viability was estimated by the Trypan-blue exclusion test 2 h and 24 h after gas treatment. Since 20 µg O_3/mL was found to significantly increase cell death (Figure 1), this concentration was excluded from further analyses.

Oil Red O staining was used to visualize lipid droplets (LDs) at light microscopy. Two h and 24 h after gas treatment, randomly selected cells grown in either adipogenic or non-adipogenic medium were measured to evaluate the percentage of cytoplasmic area covered by LDs, mean LD areas, and LD size distribution. Twenty-four h after treatment, hADAS cells were processed for conventional TEM.

Correspondence: Manuela Malatesta, Department of Neurosciences, Biomedicine and Movement Sciences, University of Verona, Strada Le Grazie 8, 37134 Verona, Italy.
Tel. +39.045.8027569.
E-mail: manuela.malatesta@univr.it

Key words: Ozone; stem cells; adipogenesis; microscopy.

Acknowledgments: This work was supported by the University of Verona (Joint Projects 2017). F.C. is a PhD student in receipt of a fellowship from the Doctoral Program "Nanoscience and Advanced Technologies" of the University of Verona.

Received for publication: 13 July 2018.
Accepted for publication: 20 August 2018.

European Journal of Histochemistry 2018; 62:2969
doi:10.4081/ejh.2018.2969

Results and Discussions

Low O_3 concentrations do not affect hADAS cells viability

Two h after gas exposure, cell death rate significantly raised in samples treated with O_2 or 20 µg O_3/mL in comparison to the untreated control (Figure 1): this suggests that excessive concentrations of O_3 as well as pure O_2 induce the formation of high levels of reactive oxygen species (ROS), which cause cell damage by oxidation and nitration of DNA, RNA, protein and lipids.[14] Conversely, exposure to 5 or 10 µg O_3/mL proved to be safe for hADAS cells at both short and long term post treatment. Regulated ROS levels are known to promote essential signalling pathways involved in cell proliferation, survival and differentiation in mesenchymal stem cells;[14] it is therefore likely that 5 and 10 µg O_3/mL are safe concentrations for hADAS cells, able to activate positive anti-stress cell response involving *e.g.* Nrf2, HSP70, mtHSP70,[15,16] similarly to other cell types submitted to mild ozonisation.[5-8]

Low O_3 concentrations induce adipogenesis in hADAS cells in adipogenic medium

The effects of 5 and 10 µg O_3/mL treatment in hADAS cells grown in adipogenic medium are shown in Figure 2. These results refer to 24 h post treatment, since no change was observed after 2 h (*not shown*).

At early stage of differentiation (6 days), hADAS cells contained few small LDs (Figure 2a-d), although cells exposed to 10 µg O_3/mL showed more numerous LDs than the other samples (Figure 2d). Morphometric evaluation confirmed that 10 µg O_3/mL-treated cells showed both mean LD area and lipid percentage values higher than the controls (Figure 2 f,g), together with numerous large LDs (Figure 2e). At the intermediate stage of differentiation (16 days), hADAS cells contained numerous LDs (Figure 2 a'-d'). Morphometric evaluation demonstrated a decreased mean LD area in cells treated with O_2, 5 µg O_3/mL or 10 µg O_3/mL (Figure 2f'); in addition, cells treated with 5 or 10 µg O_3/mL showed an increase in lipid percentage (Figure 2g'). Accordingly, numerous LDs of small size are present in these samples (Figure 2e'). At late differentiation (20 days) stage, hADAS cells contained a large number of LDs in all samples (Figure 2 a''-d''); however, treatment with 10 µg O_3/mL significantly increased both LD area (Figure 2f'') and lipid percentage (Figure 2g''), consistently with the presence of the highest number of large LDs (Figure 2e'').

LDs are depot of neutral lipids which represent an energy source as well as a substrate for the synthesis of several molecules. Generally, LD formation occurs by steps: first scattered small droplets form in the cytoplasm, then LDs increase in size and finally aggregate into clusters.[17] In white adipocytes, increase in LD size may occur by either addition of neutral lipids to pre-existing droplets[18,19] or LDs fusion.[20,21]

An adipogenic effect of mild ozonisation (especially for 10 µg O_3/mL) on differentiating pre-adipocytes is demonstrated by our data. This effect varies in relation to the differentiation phase: at early and late stages O_3 seems to stimulate lipid addition to LDs and/or LD fusion (as suggested by the increased mean area of LDs) whereas at the intermediate differentiation step O_3 would also stimulate the formation of new LDs (as suggested by the significantly decreased mean area). At this stage, LD size was also affected by O_2; however, the total lipid content did not increase, thus excluding an O_2-induced adipogenic effect. It has been reported that appropriate ROS levels are essential for adipogenic differentiation of mesenchymal stem cells.[14,22] Moreover, Nrf2 has been demonstrated to play a key role in human mesenchymal stem cell differentiation[23,24] together with Heme Oxygenase-1;[25] consistently, mild ozonisation activates an antioxidant cell response through Nrf2 pathway[8] and Heme Oxygenase-1 modulation.[6] It is noteworthy that no LD fission or decrease of the cell lipid content[26,27] was observed even short time post-treatment (*not shown*): since lipolysis may be caused in adipocytes by different stress conditions,[28-30] its absence further supports the safety of the low O_3 concentrations.

This was also confirmed by the ultrastructural analysis. At 6 days (Figure 3 a-c), hADAS cells of all samples were characterized by elongated shapes and one nucleus containing scattered heterochromatin clumps; in the cytoplasm mitochondria were numerous, rough and smooth endoplasmic reticulum and Golgi complex were well developed, while LDs and glycogen were quite scarce. At this differentiation step, in cells treated with 10 µg O_3/mL LDs were frequently found to fuse (Figure 3c), according to the significant increase of the mean LD size. At both 16 and 20 days (Figure 3 d-g), hADAS cells showed roundish shapes and one mostly euchromatic nucleus; in the cytoplasm mitochondria were numerous, rough and smooth endoplasmic reticulum were well developed, Golgi complexes were numerous with many cisternae and vesicles, LDs and glycogen were abundant, especially in cells treated with 10 µg/mL (Figure 3f). Low O_3 concentrations would therefore promote not only lipid but also glycogen accumulation. Taken together, TEM observations revealed that O_3 treatment did not hamper the differentiation process of hADAS cell from elongated,

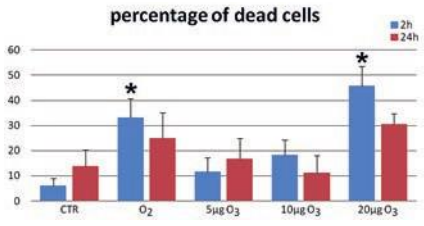

Figure 1. Mean values ± SE of dead cell percentage in the different samples 2 h (blue columns) and 24 h (red columns) after treatment. Asterisks indicate values significantly different from control at the same time point.

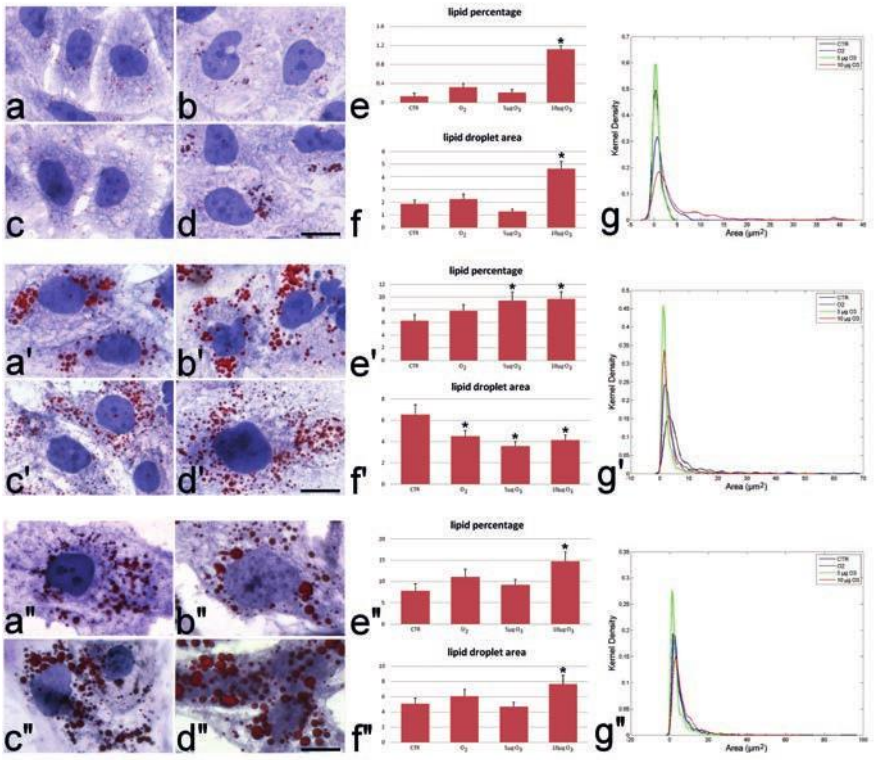

Figure 2. Brightfield micrographs of hADAS cells grown in adipogenic medium. Control (a, a', a"), O_2-treated (b, b', b"), 5 µg O_3-treated (c, c', c") and 10 µg O_3-treated (d, d', d") hADAS cells at day 6 (a-d), 16 (a'-d') and 20 (a"-d"). LDs were stained with Oil Red O and the cell was counterstained with haematoxylin. Note the progressive accumulation of LDs during the differentiation process. Scale bars: 20 µm. Mean values ± SE of percentage of cytoplasmic area covered by LDs (e-e") and of LD area (f-f") at 24 h post-treatment. Asterisks indicate values significantly different from control. Kernel distribution of LD area (g-g").

fibroblast-like cells with heterochromatic nuclei (*i.e.*, containing only partially transcribing DNA), to roundish adipocyte-like cells with euchromatic (i.e., actively transcribing) nuclei and large amounts of lipid and glycogen in the cytoplasm. Moreover, no alteration of the cell organelles occurred in samples treated with low O_3 concentrations at any differentiation step, according to previous ultrastructural observations on other cell types.[5-8]

Notably, cells treated with O_2 showed an evident vacuolization of the cytoplasm and an accumulation of residual bodies at each differentiation step, although no structural damage of cell organelles was observed, suggesting that treatment with pure O_2 induces cell stress, consistently with the observed increase in cell death rate (Figure 1).

Low O_3 concentrations do not affect adipogenesis in the absence of adipogenic factors

When hADAS cells were grown in medium devoid of adipogenic factors, most of the cells maintained fibroblast-like morphology (*not shown*), and only a few clones accumulated LDs. Morphometric evaluation of lipid content was therefore performed exclusively in these cells.

Under this culture condition, no effect was observed for any gas treatment both at short (*not shown*) and long (Figure 4) time. In detail, at 6 days, the cells showed only few small LDs (Figure 4a), with no significant difference in the mean LD area or lipid percentage (Figure 4 b,c), while the Kernel density distribution showed a trend towards larger LD size in O_3 treated cells. At 16 and 20 days, some LDs accumulated in the cytoplasm (Figure 4a'), but no significant difference in LD area, lipid percentage or Kernel density among samples was found (Figure 4 b'-d', b''-d''). Interestingly, the amount of lipid content at 20 days was generally lower than at 16 days, demonstrating a hampered pre-adipocyte differentiation in the absence of adipogenic factors. ROS are known to promote adipogenesis *via* insulin-mediated signal transduction[31] and it is likely that the absence of insulin in the medium may prevent the adipogenic effect of low O_3 concentrations.

In conclusion, our results demonstrate that low O_3 concentrations are able to stimulate lipid accumulation during adipogenic differentiation of hADAS cells without altering cell differentiation process, ultrastructural cytoarchitecture or lipid storage. In particular, lipids play a key role as signaling factors in the regulation of metabolism as well as in cell response (protection and reparation) to damaging stimuli, thus representing a powerful marker of cell func-

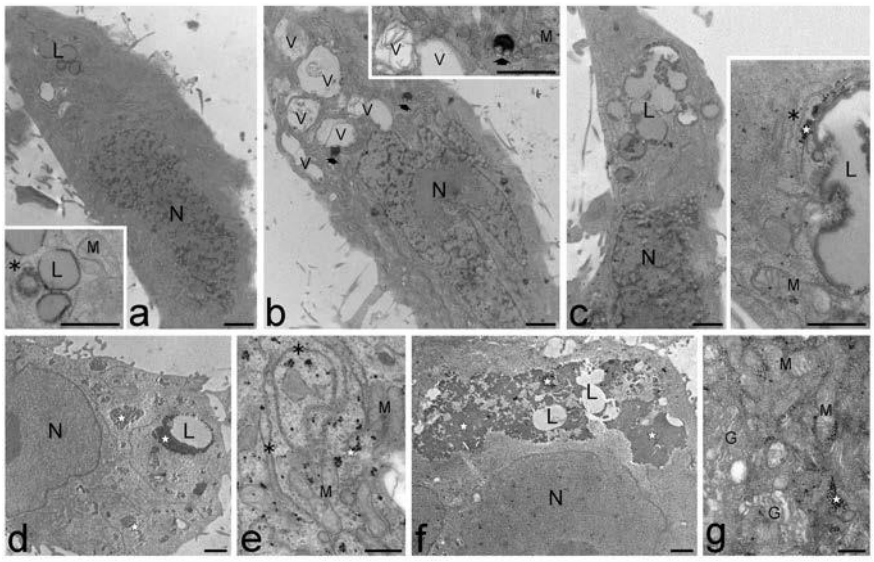

Figure 3. Transmission electron micrographs of hADAS cells. a-c) Control (a), O_2 treated (b) and O_3 10 µg/mL treated (c) cells at early differentiation stage (6 days). The cells are elongated in shape and show nuclei (N) with numerous heterochromatin clumps; in the cytoplasm mitochondria (M) and endoplasmic reticulum (asterisks) are well developed, even after gas exposure while glycogen (star) is scarce. Note the cytoplasmic vacuolization (V) and the residual bodies (arrows) in b, and the merging LDs (L) in c. d-g) Control (d,e), and O_3 10 µg/mL treated (f,g) cells at late differentiation stage (20 days). The roundish cells contain one mostly euchromatic nucleus (N) and numerous mitochondria (M) and Golgi complexes (G); LDs (L) and glycogen (stars) are abundantly distributed in the cytoplasm. Note the large amount of glycogen in f. Scale bars: a-d, f) 2 µm; e,g) 500 nm.

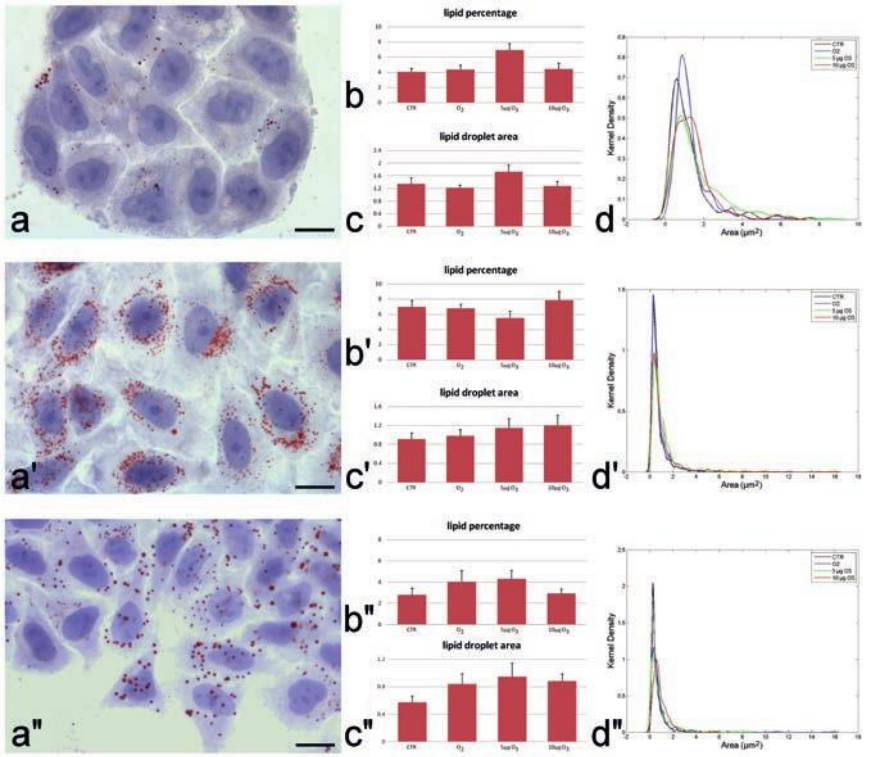

Figure 4. Representative brightfield micrographs of hADAS cells grown in DMEM at day 6 (a), 16 (a') and 20 (a''). LDs were stained with Oil Red O and the cell was counterstained with haematoxylin. Note the increase of LDs at day 16 (a') and the decrease at day 20. Scale bars: 20 µm. Mean values±SE of percentage of cytoplasmic area occupied by LDs (b-b'') and of LD area (c-c'') at 24 h post-treatment. No significant difference was found. Kernel distribution of LD area (d-d'').

tion.[32-34] hADAS cells are a suitable *in vitro* model to explore the effect of mild ozonisation on the regeneration processes since these stem cells are involved in reconstructing the connective matrix and promoting angiogenesis, while supporting epithelial, muscle and even nerve regeneration *in vivo*.[9] Based on the present preliminary findings, future studies *in vitro* and *in vivo* will elucidate the effect of mild ozonisation on human adipose tissue, in the attempt to design targeted protocols of ozone treatment for adipose stem cell-based tissue regeneration and engineering.

References

1. Re L, Mawsouf MN, Menéndez S, León OS, Sánchez GM, Hernández F. Ozone therapy: clinical and basic evidence of its therapeutic potential. Arch Med Res 2008;39:17-26.
2. Elvis AM, Ekta JS. Ozone therapy: A clinical review. J Nat Sc Biol Med 2011;2:66-70.
3. Bocci V. How a calculated oxidative stress can yield multiple therapeutic effects. Free Radic Res 2012;46:1068-75.
4. Sagai M, Bocci V. Mechanisms of action involved in ozone therapy: is healing induced via a mild oxidative stress? Med Gas Res 2011;1:29.
5. Costanzo M, Cisterna B, Vella A, Cestari T, Covi V, Tabaracci G, et al. Low ozone concentrations stimulate cytoskeletal organization, mitochondrial activity and nuclear transcription. Eur J Histochem 2015;59:2515.
6. Scassellati C, Costanzo M, Cisterna B, Nodari A, Galiè M, Cattaneo A, et al. Effects of mild ozonisation on gene expression and nuclear domains organization in vitro. Toxicol in Vitro 2017;44:100-10.
7. Niki E. Oxidative stress and antioxidants: Distress or eustress? Arch Biochem Biophys 2016; 595:19-24.
8. Galiè M, Costanzo M, Nodari A, Boschi F, Calderan L, Mannucci S, et al. Mild ozonisation activates antioxidant cell response by the Keap1/Nrf2 dependent pathway. Free Radic Biol Med 2018; 124:114-21.
9. Ong WK, Sugii S. Adipose-derived stem cells: fatty potentials for therapy. Int J Biochem Cell Biol 2013;45:1083-6.
10. Rigotti G, Marchi A, Galiè M, Baroni G, Benati D, Krampera M, et al. Clinical treatment of radiotherapy tissue damage by lipoaspirate transplant: a healing process mediated by adipose-derived adult stem cells. Plast Reconstr Surg 2007;119:1409-22.
11. Rigotti G, Marchi A, Sbarbati A. Adipose-derived mesenchymal stem cells: past, present, and future. Aesthetic Plast Surg 2009;33:271-3.
12. Salibian AA, Widgerow AD, Abrouk M, Evans GR. Stem cells in plastic surgery: a review of current clinical and translational applications. Arch Plast Surg 2013;40:666-75.
13. Tsuji W, Rubin JP, Marra KG. Adipose-derived stem cells: Implications in tissue regeneration. World J Stem Cells 2014;6:312-21.
14. Atashi F, Modarressi A, Pepper MS. The role of reactive oxygen species in mesenchymal stem cell adipogenic and osteogenic differentiation: a review. Stem Cells Dev 2015;24:1150-63.
15. Wadhwa R, Taira K, Kaul SC. An Hsp70 family chaperone, mortalin/mthsp70/PBP74/Grp75: what, when, and where? Cell Stress Chaperones 2002;7:309-16.
16. Flachbartová Z, Kovacech B. Mortalin - a multipotent chaperone regulating cellular processes ranging from viral infection to neurodegeneration. Acta Virol 2013;57:3-15.
17. Guo Y, Walther TC, Rao M, Stuurman N, Goshima G, Terayama K, et al. Functional genomic screen reveals genes involved in lipid droplet formation and utilization. Nature 2008;453:657-61.
18. Kellner-Weibel G, McHendry-Rinde B, Haynes MP, Adelman S. Evidence that newly synthesized esterified cholesterol is deposited in existing cytoplasmic lipid inclusions. J Lipid Res 2001;42:768-77.
19. Kuerschner L, Moessinger C, Thiele C. Imaging of lipid biosynthesis: how a neutral lipid enters lipid droplets. Traffic 2008;9:338-52.
20. Boström P, Rutberg M, Ericsson J, Holmdahl P, Andersson L, Frohman MA, et al. Cytosolic lipid droplets increase in size by microtubule-dependent complex formation. Arterioscler Thromb Vasc Biol 2005;25:1945-51.
21. Murphy S, Martin S, Parton RG. Lipid droplet-organelle interactions; sharing the fats. Biochim Biophys Acta 2009;1791:441-7.
22. Higuchi M, Dusting GJ, Peshavariya H, Jiang F, Hsiao ST, Chan EC, et al. Differentiation of human adipose-derived stem cells into fat involves reactive oxygen species and Forkhead box O1 mediated upregulation of antioxidant enzymes. Stem Cells Dev 2013;22:878-88.
23. Pi J, Leung L, Xue P, Wang W, Hou Y, Liu D, et al. Deficiency in the nuclear factor E2-related factor-2 transcription factor results in impaired adipogenesis and protects against diet-induced obesity. J Biol Chem 2010;285(12):9292-300.
24. Hou Y, Xue P, Bai Y, Liu D, Woods CG, Yarborough K, et al. Nuclear factor erythroid-derived factor 2-related factor 2 regulates transcription of CCAAT /enhancer-binding protein β during adipogenesis. Free Radic Biol Med 2012;52:462-72.
25. Vanella L, Sanford C Jr, Kim DH, Abraham NG, Ebraheim N. Oxidative stress and heme oxygenase-1 regulated human mesenchymal stem cells differentiation. Int J Hypertens 2012;2012: 890671.
26. Rizzatti V, Boschi F, Pedrotti M, Zoico E, Sbarbati A, Zamboni M. Lipid droplets characterization in adipocyte differentiated 3T3-L1 cells: size and optical density distribution. Eur J Histochem 2013;57:e24.
27. Boschi F, Rizzatti V, Zamboni M, Sbarbati A. Models of lipid droplets growth and fission in adipocyte cells. Exp Cell Res 2015;336:253-62.
28. Deng J, Liu S, Zou L, Xu C, Geng B, Xu G. Lipolysis response to endoplasmic reticulum stress in adipose cells. J Biol Chem 2012;287:6240-9.
29. Conti G, Benati D, Bernardi P, Jurga M, Rigotti G, Sbarbati A. The post-adipocytic phase of the adipose cell cycle. Tissue Cell 2014;46:520-6.
30. Marinozzi MR, Pandolfi L, Malatesta M, Colombo M, Collico V, Lievens PM, et al. Innovative approach to safely induce controlled lipolysis by superparamagnetic iron oxide nanoparticles-mediated hyperthermic treatment. Int J Biochem Cell Biol 2017;93:62-73.
31. Zhang Z, Zhou S, Jiang X, Wang YH, Li F, Wang YG, et al. The role of the Nrf2/Keap1 pathway in obesity and metabolic syndrome. Rev Endocr Metab Disord 2015;16:35-45.
32. Wymann MP, Schneiter R. Lipid signalling in disease. Nat Rev Mol Cell Biol 2008;9:162-76.
33. Carroll B, Donaldson JC, Obeid L. Sphingolipids in the DNA damage response. Adv Biol Regul 2015;58:38-52.
34. Croce AC, Bottiroli G. Lipids: Evergreen autofluorescent biomarkers for the liver functional profiling. Eur J Histochem 2017;61:2808.

.

BIBLIOGRAPHY

Adabi M., Naghibzadeh M., Adabi M., Zarrinfard M.A., Esnaashari S.S., Seifalian A.M., Faridi-Majidi R., Tanimowo Aiyelabegan H., Ghanbari H. "Biocompatibility and nanostructured materials: applications in nanomedicine." Artif Cells Nanomed Biotechnol. (2017), 45(4):833-842.

Afzal E., Zakeri S., Keyhanvar P., Bagheri M., Mahjoubi P., Asadian M., Omoomi N., Dehqanian M., Ghalandarlaki N., Darvishmohammadi T., Farjadian F., Golvajoee M.S., Afzal S., Ghaffari M., Cohan R.A., Gravand A., Ardestani M.S. "Nanolipodendrosome-loaded glatiramer acetate and myogenic differentiation 1 as augmentation therapeutic strategy approaches in muscular dystrophy." Int J Nanomedicine. (2013), 8:2943-2960.

Andersen G., Hedermann G., Witting N., Duno M., Andersen H., Vissing J. "The antimyotonic effect of lamotrigine in non-dystrophic myotonias: a double-blind randomized study." Brain. (2017), 140(9):2295-2305.

Andrew G. Engel. "Myology." McGraw-Hill Medical. (2004), :1-180

Arpicco S., Lerda C., Dalla Pozza E., Costanzo C., Tsapis N., Stella B. "Hyaluronic acid-coated liposomes for active targeting of gemcitabine." Eu. J Pharm Biopharm. (2013), 85(3 Pt A), 373-380.

Auffan M., Achouak W., Rose J., Roncato M.A., Chanéac C., Waite D.T., Masion A., Woicik J.C., Wiesner M.R., Bottero J.Y. "Relation between the redox state of iron-based nanoparticles and their cytotoxicity toward Escherichia coli." Environ Sci Technol (2008), 42(17):6730-6735.

Baeza A., Colilla M., Vallet-Regí M. "Advances in mesoporous silica nanoparticles for targeted stimuli-responsive drug delivery." Expert Opin Drug Deliv. (2015), 12(2):319-337.

Baeza A., Guisasola E., Ruiz-Hernández E., Vallet-Regí M. "Magnetically Triggered Multidrug Release by Hybrid Mesoporous Silica Nanoparticles." Chem. Mater. (2012), 24, 3, 517-524

Baldwin K., Haddad F. “Effects of different activity and inactivity paradigms on myosin heavy chain gene expression in striated muscle.” J Appl Physiol. (2001), 90:345–357.

Bennett C.F., Swayze E.E. “RNA targeting therapeutics: molecular mechanisms of antisense oligonucleotides as a therapeutic platform.” Annu Rev Pharmacol Toxicol. (2010), 50:259-293.

Bibee K.P., Cheng Y.J., Ching J.K., Marsh J.N., Li A.J., Keeling R.M., Connolly A.M., Golumbek P.T., Myerson J.W., Hu G., Chen J., Shannon W.D., Lanza G.M., Weihl C.C., Wickline S.A. “Rapamycin nanoparticles target defective autophagy in muscular dystrophy to enhance both strength and cardiac function.” FASEB J. (2014), 28(5):2047-2061.

Bozzuto G., Molinari A. “Liposomes as nanomedical devices”. Int J Nanomedicine. (2015), 10:975-999.

Briolay A., Jaafar R., Nemoz G., Bessueille L. “Myogenic differentiation and lipid-raft composition of L6 skeletal muscle cells are modulated by PUFAs.” Biochim. Biophys. Acta. (2013), 1828(2): 602-613.

Brook J.D., McCurrach M.E., Harley H.G., Buckler A.J., Church D., Aburatani H., Hunter K., Stanton V.P., Thirion J.P., Hudson T. “Molecular basis of myotonic dystrophy: expansion of a trinucleotide (CTG) repeat at the 3′ end of a transcript encoding a protein kinase family member.” Cell. (1992), 68:799–808.

Büller H.R., Bethune C., Bhanot S., Gailani D., Monia B.P., Raskob G.E., Segers A., Verhamme P., Weitz J.I. “Factor XI antisense oligonucleotide for prevention of venous thrombosis.” N Engl J Med. (2014), 372:232- 240.

Burel S.A., Han S.R., Lee H.S., Norris D.A., Lee B.S., Machemer T, Park S.Y., Zhou T., He G., Kim Y., MacLeod A.R., Monia B.P., Lio S., Kim T.W., Henry S.P. “Preclinical evaluation of the toxicological effects of a novel constrained ethyl modified antisense compound targeting signal transducer and activator of transcription 3 in mice and cynomolgus monkeys.” Nucleic Acid Ther. (2013), 23:213-227.

Cadete A., Alonso M.J. “Targeting cancer with hyaluronic acid-based nanocarriers: recent advances and translational perspectives.” Nanomedicine (Lond). (2016), 11(17):2341-2357.

Cao F., Yan M., Liu Y., Liu L., Ma G. “Photothermally controlled MHC class I restricted CD8+ T-cell responses elicited by hyaluronic acid decorated gold nanoparticles as a vaccine for cancer immunotherapy.” Adv Healthc Mater. (2018), 7(10): e1701439.

Carton F., Calderan L., Malatesta M. “Incubation under fluid dynamic conditions markedly improves the structural preservation in vitro of explanted skeletal muscles.” Eur J Histochem. (2017), 61:2862:1-5.

Cavalli M., Fossati B., Vitale R., Brigonzi E., Ricigliano V.A.G., Saraceno L., Cardani R., Pappone C., Meola G. “Flecainide-Induced Brugada Syndrome in a Patient with Skeletal Muscle Sodium Channelopathy: A Case Report with Critical Therapeutical Implications and Review of the Literature.” Front Neurol. (2018), 9:385.

Chang H.I., Yeh M.K. “Clinical development of liposome-based drugs: formulation, characterization, and therapeutic efficacy.” Int J Nanomedicine. (2012), 7: 49–60.

Chang J.S., Chang K.L., Hwang D.F., Kong Z.L. “In vitro cytotoxicitiy of silica nanoparticles at high concentrations strongly depends on the metabolic activity type of the cell line. Environ Sci Technol.” (2007), 41(6), 2064-2068.

Chen C.A., Wang C.C., Jong Y.J., Wu S.M. “Label-Free Fluorescent Copper Nanoclusters for Genotyping of Deletion and Duplication of Duchenne Muscular Dystrophy.” Anal Chem. (2015), 87(12):6228-6232.

Chen M., Von Mikecz A. “Formation of nucleoplasmic protein aggregates impairs nuclear function in response to SiO2 nanoparticles.” Exp Cell Res. (2005), 305(1):51-62.

Chen Y. “A perfusion system for high productivity of monoclonal antibody by hybridoma cells in a CelliGen bioreactor.” Chin J Biotechnol. (1992), 8(3):179-186.

Childs-Disney J.L., Hoskins J., Rzuczek S.G., Thornton C.A., Disney M.D. “Rationally designed small molecules targeting the RNA that causes myotonic dystrophy type 1 are potently bioactive.” ACS ChemBiol. (2012), 7:856–862.

Coonrod L.A., Nakamori M., Wang W., Carrell S., Hilton C.L., Bodner M.J., Siboni R.B., Docter A.G., Haley M.M., Thornton C.A., Berglund J.A. “Reducing levels of toxic RNA with small molecules.” ACS Chem Biol. (2013), 8:2528–2537.

Costanzo M., Boschi F., Carton F., Conti G., Covi V., Tabaracci G., Sbarbati A., Malatesta M. “Low ozone concentrations promote adipogenesis in human adipose-derived adult stem cells.”Eur J Histochem. (2018), 62(3): 253-256.

Costanzo M., Carton F., Malatesta M. "Microscopy techniques in nanomedical research." Microscopie. (2017a), 27:66-71.

Costanzo M., Carton F., Malatesta M. "Monitoring the uptake and intracellular fate of nanovectors by microscopical technique." In: "Small is beautiful: nanovectors for biomedical research and therapy." Istituto Lombardo - Accademia di Scienze e Lettere. Incontri di studio (2017b), 91:51-70, http://www.ilasl.org/index.php/Incontri/article/view/269.

Costanzo M., Carton F., Marengo A., Berlier G., Stella B., Arpicco S., Malatesta M. "Fluorescence and electron microscopy to visualize the intracellular fate of nanoparticles for drug delivery." Eur J Histochem. (2016), 60:2640:107-115.

Danhier F., Ansorena E., Silva J.M., Coco R., Le Breton A., Préat V. "PLGA-based nanoparticles: an overview of biomedical applications." J Control Release. (2012), 161(2):505-22.

Darvishi B., Manoochehri S., Kamalinia G., Samadi N., Amini M., Mostafavi S.H., Maghazei S., Atyabi F., Dinarvand R. "Preparation and Antibacterial Activity Evaluation of 18-β-glycyrrhetinic Acid Loaded PLGA Nanoparticles." Iran J Pharm ResSpring. (2015), 14(2):373-383.

De Bartolo L., Salerno S., Morelli S., Giorno L., Rende M., Memoli B., Procino A., Andreucci V.E., Bader A., Drioli E. "Long-term maintenance of human hepatocytes in oxygen-permeable membrane bioreactor." Biomaterials. (2006), 27(27):4794-4803.

Dosio F., Arpicco S., Stella B., Fattal E. "Hyaluronic acid for anticancer drug and nucleic acid delivery." Adv Drug Deliv Rev. (2016), 97:204-236.

Ebner D.C., Bialek P., El-Kattan A.F., Ambler C..M, Tu M. "Strategies for skeletal muscle targeting in drug discovery." Curr Pharm Des. (2015), 21(10):1327-1336.

Elsaesser A., Howard C.V. "Toxicology of nanoparticles." Adv Drug Deliv Rev (2012), 64(2):129-137.

El-Say K.M., El-Sawy H.S. "Polymeric nanoparticles: Promising platform for drug delivery." Int J Pharm. (2017), 528(1-2):675-691.

Eroglu M.S., Oner E.T., Mutlu E.C., Bostan M.S. "Sugar Based Biopolymers in Nanomedicine; New Emerging Era for Cancer Imaging and Therapy." Curr Top Med Chem. (2017), 17(13):1507-1520.

Evers-van Gogh I.J., Alex S., Stienstra R., Brenkman A.B., Kersten S., Kalkhoven E. "Electric Pulse Stimulation of Myotubes as an In Vitro Exercise Model: Cell-Mediated and Non-Cell-Mediated Effects." Sci Rep. (2015), 5:10944.

Falzarano M.S., Bassi E., Passarelli C., Braghetta P., Ferlini A. "Biodistribution studies of polymeric nanoparticles for drug delivery in mice." Hum Gene Ther. (2014), 25(11):927-928.

Falzarano M.S., Passarelli C., Bassi E., Fabris M., Perrone D., Sabatelli P., Maraldi N.M., Donà S., Selvatici R., Bonaldo P., Sparnacci K., Laus M., Braghetta P., Rimessi P., Ferlini A."Biodistribution and molecular studies on orally administered nanoparticle-AON complexes encapsulated with alginate aiming at inducing dystrophin rescue in mdx mice." Biomed Res Int. (2013), 527418.

Falzarano M.S., Passarelli C., Ferlini A. "Nanoparticle Delivery of Antisense Oligonucleotides and Their Application in the Exon Skipping Strategy for Duchenne Muscular Dystrophy". Nucleic Acid Ther. (2014), 24(1): 87–100.

Fessi H., Devissaguet J.P., Puisieux F., Thies C. "Nanocapsule formation by interfacial polymer deposition following solvent displacement." Int. J Pharm. (1989), 55: R1-R4.

Foley S., Crowley C., Smaihi M., Bonfils C., Erlanger B.F., Seta P., Larroque C. "Cellular localisation of a water-soluble fullerene derivative." Biochem Biophys Res Commun (2002), 294(1):116-119.

Forterre A., Jalabert A., Berger E., Baudet M., Chikh K., Errazuriz E., De Larichaudy J., Chanon S., Weiss-Gayet M., Hesse A.M., Record M., Geloen A., Lefai E., Vidal H., Couté Y., Rome S. "Proteomic analysis of C2C12 myoblast and myotube exosome-like vesicles: a new paradigm for myoblast-myotube cross talk?" PLoS One. (2014), 9(1): e84153.

Freichels H., Danhier F., Préat V., Lecomte P., Jérôme C. "Fluorescent labeling of degradable poly(lactide-co-glycolide) for cellular nanoparticles tracking in living cells." Int J Artif. Organs (2011), 34(2), 152-160.

Fu Y.H., Pizzuti A., Fenwick R.G. Jr, King J., Rajnarayan S., Dunne P.W., Dubel J., Nasser G.A., Ashizawa T., de Jong P., Wieringa P., Korneluk R., Perryman M.B., Epstein H.F., Thomas Caskey C. "An unstable triplet repeats in a gene related to myotonic muscular dystrophy." Science. (1992), 255:1256-1258.

Gaudet D., Brisson D., Tremblay K., Alexander V.J., Singleton W., Hughes S.G., Geary R.S., Baker B.F., Graham M.J., Crooke R.M., Witztum J.L. "Targeting APOC3 in the familial chylomicronemia syndrome." N Engl J Med. (2014), 371:2200-2206.

Giusti S., Sbrana T., La Marca M., Di Patria V., Martinucci V., Tirella A., Domenici C., Ahluwalia A. "A novel dual-flow bioreactor simulates increased fluorescein permeability in epithelial tissue barriers." Biotechnol J. (2014), 9(9):1175-1184.

Glass Z., Li Y., Xu Q. "Nanoparticles for CRISPR-Cas9 delivery. " Nat Biomed Eng. (2017), 1(11) :854-855.

Goemans N.M., Tulinius M., van den Akker J.T., Burm B.E., Ekhart P.F., Heuvelmans N., Holling T., Janson A.A., Platenburg G.J., Sipkens J.A., Sitsen J.M., Aartsma-Rus A., van Ommen G.J., Buyse G., Darin N., Verschuuren J.J., Campion G.V., de Kimpe S.J., van Deutekom J.C. "Systemic administration of PRO051 in Duchenne's muscular dystrophy." N Engl J Med. (2011), 364:1513-1522.

Gourdon G., Meola G. "Myotonic Dystrophies: State of the Art of New Therapeutic Developments for the CNS." Front Cell Neurosci. (2017), 101:1-14.

Gu W., Wu C., Chen J., Xiao Y. "Nanotechnology in the targeted drug delivery for bone diseases and bone regeneration." Int J Nanomedicine. (2013), 8:2305-2317.

Harper P.S." Myotonic Dystrophy". (2001), London: WB Saunders. Hill CR.

Hauck T.S., Ghazani A.A., Chan W.C. "Assessing the effect of surface chemistry on gold nanorod uptake, toxicity, and gene expression in mammalian cells." Small. (2008), 4(1):153-159.

He W.W., Kuang M.J., Zhao J., Sun L., Lu B., Wang Y., Ma J.X., Ma X.L." Efficacy and safety of intraarticular hyaluronic acid and corticosteroid for knee osteoarthritis: A meta-analysis." Int J Surg. (2017), 39:95-103.

He Z., Wang B., Hu C., Zhao J. "An overview of hydrogel-based intra-articular drug delivery for the treatment of osteoarthritis." Colloids Surf B Biointerfaces (2017), 154:33-39.

Hill C.R., Cole M., Errington J., Malik G., Boddy A.V., Veal G.J. "Characterisation of the clinical pharmacokinetics of actinomycin D and the influence of ABCB1 pharmacogenetic variation on actinomycin D disposition in children with cancer." Clin Pharmacokinet. (2014), 53(8):741-751.

Hudson R., Feng Y., Varmab R., Moores A. "Bare magnetic nanoparticles: sustainable synthesis and applications in catalytic organic transformations". Green Chem. (2014), 16:4493-4505

Hussain S.M., Hess K.L., Gearhart J.M., Geiss K.T., Schlager J.J. "In vitro toxicity of nanoparticles in BRL 3A rat liver cells." Toxicol In Vitro (2005), 19(7):975-983.

Ikoba U., Peng H., Li H., Miller C., Yu C., Wang Q. "Nanocarriers in therapy of infectious and inflammatory diseases." Nanoscale. (2015), 7(10):4291-4305.

Jog S.P., Paul S., Dansithong W., Tring S., Comai L., Reddy S. "RNA splicing is responsive to MBNL1 dose." PLoS One. (2012), 7(11): e48825.

Jonderian A., Maalouf R. "Formulation and In vitro Interaction of Rhodamine-B Loaded PLGA Nanoparticles with Cardiac Myocytes." Front Pharmacol. (2016), 7, 458:1-7.

Kabakov A.E., Kudryavtsev V.A., and Gabai V.L. "Determination of Cell Survival or Death." In: Calderwood S.K. and Prince T.L. (eds.), "Molecular Chaperones: Methods and Protocols." Methods in Molecular Biology (2011), 787: 231-244.

Kamat J.P., Devasagayam T.P., Priyadarsini K.I., Mohan H. "Reactive oxygen species mediated membrane damage induced by fullerene derivatives and its possible biological implication." Toxicology (2000), 155(1-3):55-61.

Kamitori S., Takusagawa F. "Crystal structure of the 2:1 complex between d(GAAGCTTC) and the anticancer drug actinomycin D." J Mol Biol. (1992), 225:445–456.

Kandarian S., Stevenson E. "Molecular events in skeletal muscle during disuse atrophy." Exerc Sport Sci Rev. (2002), 30:111–116.

Kavoosi F., Modaresi F., Sanaei M., Rezaei Z. "Medical and dental applications of nanomedicines." APMIS. (2018), 126(10): 795-803.

Kislinger T., Gramolini A.O., Pan Y., Rahman K., MacLennan D.H., Emili A. "Proteome dynamics during C2C12 myoblast differentiation." Mol Cell Proteomics. (2005), 4(7):887-901.

Koebis M., Kiyatake T., Yamaura H., Nagano K., Higashihara M., Sonoo M., Hayashi Y., Negishi Y., Endo-Takahashi Y., Yanagihara D., Matsuda R., Takahashi M.P., Nishino I., Ishiura S. "Ultrasound-enhanced delivery of morpholino with Bubble liposomes ameliorates the myotonia of myotonic dystrophy model mice." Sci Rep. (2013), 3:2242.

Kumar R., Sahoo G.C., Pandey K., Das V., Das P. "Study the effects of PLGA-PEG encapsulated amphotericin B nanoparticle drug delivery system against Leishmania donovani." Drug Deliv. (2015), 22(3):383-388.

Lalatsa A., Barbu E. "Carbohydrate Nanoparticles for Brain Delivery." Int Rev Neurobiol. (2016), 130:115-153.

Lee H.L., Boccazzi P., Ram R.J., Sinskey A.J. "Microbioreactor arrays with integrated mixers and fluid injectors for high-throughput experimentation with pH and dissolved oxygen control." Lab Chip. (2006), 6(9):1229-1235.

Lee J.E., Bennett C.F., Cooper T.A. "RNase H-mediated degradation of toxic RNA in myotonic dystrophy type 1." Proc Natl Acad Sci USA. (2012), 109:4221–4226.

Lee K., Conboy M., Park H.M., Jiang F., Kim H.J., Dewitt M.A., Mackley V.A., Chang K., Rao A., Skinner C., Shobha T., Mehdipour M., Liu H., Huang W.C., Lan F., Bray N.L., Li S., Corn J.E., Kataoka K., Doudna J.A., Conboy I., Murthy N. "Nanoparticle delivery of Cas9 ribonucleoprotein and donor DNA in vivo induces homology-directed DNA repair. " Nat Biomed Eng. (2017), 1 :889-901.

Lee M.M., Pushechnikov A., Disney M.D. "Rational and modular design of potent ligands targeting the RNA that causes myotonic dystrophy 2." ACS Chem Biol. (2009), 4:345–355.

Lee R.G., Crosby J., Baker B.F., Graham M.J., Crooke R.M. "Antisense technology: an emerging platform for cardiovascular disease therapeutics." J Cardiovasc Transl Res. (2013), 6:969-680.

Leger A.J., Mosquea L.M., Clayton N.P., Wu I.H., Weeden T., Nelson C.A., Phillips L., Roberts E., Piepenhagen P.A., Cheng S.H., Wentworth B.M. "Systemic delivery of a Peptide-linked morpholino oligonucleotide neutralizes mutant RNA toxicityin a mouse model of myotonic dystrophy." Nucleic Acid Ther. (2013), 23(2):109-117.

Li M., Reineke J. “Physiologically based pharmacokinetic modeling for nanoparticle toxicity study.” Methods Mol Biol. (2012), 926:369-382.

Liong M., Lu J., Kovochich M., Xia T., Ruehm S.G., Nel A.E., Tamanoi F., Zink J.I. “Multifunctional inorganic nanoparticles for imaging, targeting, and drug delivery.” ACS Nano. (2008), 2(5):889-896.

Liquori C.L., Ricker K., Moseley M.L., Jacobsen J.F., Kress W., Naylor S.L., Day J.W., Ranum L.P. “Myotonic dystrophy type 2 caused by a CCTG expansion in intron 1 of ZNF9.” Science. (2001), 293:864-867.

Lu J., Liong M., Li Z., Zink J.I., Tamanoi F. “Biocompatibility, biodistribution, and drug-delivery efficiency of mesoporous silica nanoparticles for cancer therapy in animals.” Small. (2010), 6(16):1794-1805.

Mahadevan M., Tsilfidis C., Sabourin L., Shutler G., Amemiya C., Jansen G., Neville C., Narang M., Barceló J., O'Hoy K. “Myotonic dystrophy mutation: an unstable CTG repeat in the 3’ untranslated region of the gene.” Science. (1992), 255:1253-1255.

Mahmoudi K., Bouras A., Bozec D., Ivkov R., Hadjipanayis C. “Magnetic hyperthermia therapy for the treatment of glioblastoma: a review of the therapy's history, efficacy and application in humans.” Int J Hyperthermia. (2018), 34(8):1316-1328.

Manzano M., Colilla M., Vallet-Regí M. “Drug delivery from ordered mesoporous matrices.” Expert Opin Drug Deliv. (2009), 6(12):1383-1400.

Manzano M., Vallet-Regí M. “Mesoporous silica nanoparticles in nanomedicine applications.” J Mater Sci Mater Med. (2018), 8;29(5):65.

Markhorst J.M., Stunnenberg B.C., Ginjaar I.B., Drost G., Erasmus C.E., Sie L.T. “Clinical experience with long-term acetazolamide treatment in children with nondystrophic myotonias: a three-case report.” Pediatr Neurol. (2014), 51(4):537-41.

Mazzei D., Guzzardi M.A., Giusti S., Ahluwalia A. “A low shear stress modular bioreactor for connected cell culture under high flow rates.” Biotechnol Bioeng. (2010), 106(1):127-37.

Meola G., Cardani R. “Myotonic dystrophies: An update on clinical aspects, genetic, pathology, and molecular pathomechanisms.” Biochim Biophys Acta. (2015), 1852:594-606.

Meola G., Cardani R. “RNA binding proteins in myotonic dystrophies.” In: Denman RB, editor. Kerala: Research Signpost. (2009), :153–166.

Meola G., Sansone V., Marinou K., Cotelli M., Moxley R.T., Thornton C.A., De Ambroggi L. “Proximal myotonic myopathy: a syndrome with a favourable prognosis?” J Neurol Sci. (2002), 193:89-96.

Miller J.W., Urbinati C.R., Teng-Umnuay P., Stenberg M.G., Byrne B.J., Thornton C.A., Swanson M.S. “Recruitment of human muscleblind proteins to (CUG)(n) expansions associated with myotonic dystrophy.” EMBO J. (2000), 19:4439-4448.

Mori H., Kawai N., Kinouchi N., Hichijo N., Ishida T., Kawakami E., Noji S., Tanaka E. “Effectiveness of cationic liposome-mediated local delivery of myostatin-targeting small interfering RNA in vivo.” Dev Growth Differ. (2014), 56(3):223-232.

Morra M. “Engineering of biomaterials surfaces by hyaluronan.” Biomacromolecules. (2005), 6:1205-1223.

Nagavarma B.N.V, Hemant K.S.Y, Ayaz A., Vasudha L.S, Shivakumar H.G. “Different techniques for preparation of polymeric nanoparticles- A review.” (2012), Asian Journal of Pharmaceutical and Clinical Research. 5(3):16-23.

Nance M.E., Hakim C.H., Yang N.N., Duan D. “Nanotherapy for Duchenne muscular dystrophy.” Wiley Interdiscip Rev Nanomed Nanobiotechnol. (2018), 10(2): 1-30.

Navarro E., Baun A., Behra R., Hartmann N.B., Filser J., Miao A.J., Quigg A., Santschi P.H., Sigg L. “Environmental behavior and ecotoxicity of engineered nanoparticles to algae, plants, and fungi.” Ecotoxicology (2008), 17(5):372-386.

Negishi Y., Endo-Takahashi Y., Ishiura S. “Exon Skipping by Ultrasound-Enhanced Delivery of Morpholino with Bubble Liposomes for Myotonic Dystrophy Model Mice.” Methods Mol Biol. (2018), 1828:481-487.

Negishi Y., Ishii Y., Shiono H., Akiyama S., Sekine S., Kojima T., Mayama S., Kikuchi T., Hamano N., Endo-Takahashi Y., Suzuki R., Maruyama K., Aramaki Y. “Bubble liposomes and ultrasound exposure improve localized morpholino oligomer delivery into the skeletal muscles of dystrophic mdx mice.” Mol Pharm. (2014), 11(3):1053-1061.

Nel A.E., Mädler L., Velegol D., Xia T., Hoek E.M., Somasundaran P., Klaessig F., Castranova V., Thompson M. "Understanding biophysicochemical interactions at the nano-bio interfac." Nat Mater. (2009), 8(7):543-557.

Nguyen L., Lee J.Y., Wong C.H., Zimmerman S.C. "Small Molecules that Target the Toxic RNA in Myotonic Dystrophy Type 2." Chem Med Chem. (2014), 9: 2455-2462.

Nguyen L., Luu L.M., Peng S., Serrano J.F., Edwin Chan H.Y., Zimmerman S.C. "Rationally designed small molecules that target both the DNA and RNA causing Myotonic Dystrophy Type 1." J Am Chem Soc. (2015), 137:14180–14189.

Nie Y., Zhang Z.R., He B., Gu Z. "Investigation of PEG-PLGA-PEG nanoparticles-based multipolyplexes for IL-18 gene delivery." J Biomater Appl. (2012), 26(8): 893-916.

Niles A.L., Moravec R.A., Riss T.L. "Update on in vitro cytotoxicity assays for drug development." Expert Opin Drug Discov. (2008), 3(6):655-669.

Osborne R.J., Filiaci V., Schink J., Mannel R.S., Alvarez Secord A., Kelley J.L., Provencher D., Scott Miller D., Covens A.L., Lage J.M. "Phase III trial of weekly methotrexate or pulsed actinomycin for low risk gestational trophoblastic neoplasia: a gynecologic oncology group study." J Clin Oncol. (2011), 29:825–831.

Øvrevik J., Låg M., Schwarze P., Refsnes M. "p38 and Src-ERK1/2 pathways regulate crystalline silica-induced chemokine release in pulmonary epithelial cells." Toxicol Sci (2004), 81(2):480-490.

Pan Y.J., Chen Y.Y., Wang D.R., Wei C., Guo J., Lu D.R. Chu C.C., Wang C.C. "Redox/pH dual stimuli-responsive biodegradable nanohydrogels with varying responses to dithiothreitol and glutathione for controlled drug release." Biomaterials. (2012), 33(27), 6570-6579.

Pandey S.K., Wheeler T.M., Justice S.L., Kim A., Younis H.S., Gattis D., Jauvin D., Puymirat J., Swayze E.E., Freier S.M., Bennett C.F., Thornton C.A., MacLeod A.R. "Identification and characterization of modified antisense oligonucleotides targeting DMPK in mice and nonhuman primates for the treatment of myotonic dystrophy type 1." J Pharmacol Exp Ther. (2015), 355:329-340.

Park M.V., Annema W., Salvati A., Lesniak A., Elsaesser A., Barnes C., McKerr G., Howard C.V., Lynch I., Dawson K.A., Piersma AH, de Jong WH. "In vitro

developmental toxicity test detects inhibition of stem cell differentiation by silica nanoparticles." Toxicol Appl Pharmacol. (2009), 240(1):108-116.

Parkesh R., Childs-Disney J.L., Nakamori M., Kumar A., Wang E., Wang T., Hoskins J., Tran T., Housman D., Thornton C.A., Disney M.D. "Design of a bioactive small molecule that targets the myotonic dystrophy type 1 RNA via an RNA motif-ligand database and chemical similarity searching." J Am Chem Soc. (2012), 134:4731–4742.

Pascual-Gil S., Simón-Yarza T., Garbayo E., Prósper F., Blanco-Prieto M.J. "Cytokine-loaded PLGA and PEG-PLGA microparticles showed similar heart regeneration in a rat myocardial infarction model." Int J Pharm. (2017), 523(2):531-533.

Patra J.K., Das G., Fraceto L.F., Campos E.V.R., Rodriguez-Torres M.D.P., Acosta-Torres L.S, Diaz-Torres L.A., Grillo R., Swamy M.K., Sharma S., Habtemariam S., Shin H.S. "Nano based drug delivery systems: recent developments and future prospects." J Nanobiotechnology. (2018), 19:16-71.

Perdoni F., Malatesta M., Cardani R., Giagnacovo M., Mancinelli E., Meola G., Pellicciari C. "RNA/MBNL1-containing foci in myoblast nuclei from patients affected by myotonic dystrophy type 2: an immunocytochemical study." Eur J Histochem. (2009), 53:151-158.

Peretti E., Miletto I., Stella B., Rocco F., Berlier G., Arpicco S. "Strategies to Obtain Encapsulation and Controlled Release of Pentamidine in Mesoporous Silica Nanoparticles." Pharmaceutics. " (2018), 19;10(4): 1-15.

Poussard S., Decossas M., Le Bihan O., Mornet S., Naudin G., Lambert O. "Internalization and fate of silica nanoparticles in C2C12 skeletal muscle cells: evidence of a beneficial effect on myoblast fusion." Int J Nanomedicine. (2015), 10:1479-92.

Powers M.J., Janigian D.M., Wack K.E., Baker C.S., Beer Stolz D., Griffith L.G. "Functional behaviour of primary rat liver cells in a three-dimensional perfused microarray bioreactor." Tissue Eng. (2002), 8(3):499-513.

Pradhan R., Ramasamy T., Choi J.Y., Kim J.H., Poudel B.K. Tak J.W., Nukolova N., Choi H.G., Yong C.S., Kim J.O. "Hyaluronic acid-decorated poly (lactic-co-glycolic acid) nanoparticles for combined delivery of docetaxel and tanespimycin." Carbohydr Polym. (2015), 123:313-23.

Qin W.J., Yim O.S., Lai P.S., Yung L.Y. "Dimeric gold nanoparticle assembly for detection and discrimination of single nucleotide mutation in Duchenne muscular dystrophy." Biosens Bioelectron. (2010), 25(9):2021-2025.

Quagliariello V., Iaffaioli R.V., Armenia E., Clemente O., Barbarisi M., Nasti G. "Hyaluronic Acid Nanohydrogel Loaded with Quercetin Alone or in Combination to a Macrolide Derivative of Rapamycin RAD001 (Everolimus) as a New Treatment for Hormone-Responsive Human Breast Cancer." J. Cell Physiol. (2017), 232(8), 2063-2074.

Raal F.J., Santos R.D., Blom D.J., Marais A.D., Charng M.J., Cromwell W.C., Lachmann R.H., Gaudet D., Tan J.L., Chasan-Taber S., Tribble D.L., Flaim J.D., and Crooke S.T. "Mipomersen, an apolipoprotein B synthesisinhibitor, for lowering of LDL cholesterol concentrations." Science. (2010), 293:864-867.

Reuss M. "Stirred tank bioreactors." Bioprocess Technol. (1995), 21:207-255.

Ricci V., Zonari D., Cannito S., Marengo A., Scupoli M.T., Malatesta M., Carton F., Boschi F., Berlier G., Arpicco S. "Hyaluronated mesoporous silica nanoparticles for active targeting: influence of conjugation method and hyaluronic acid molecular weight on the nanovector properties." J Colloid Interface Sci. (2018), 516:484-497.

Rimessi P., Sabatelli P., Fabris M., Braghetta P., Bassi E., Spitali P., Vattemi G., Tomelleri G., Mari L., Perrone D., Medici A., Neri M., Bovolenta M., Martoni E., Maraldi N.M., Gualandi F., Merlini L., Ballestri M., Tondelli L., Sparnacci K., Bonaldo P., Caputo A., Laus M., Ferlini A. "Cationic PMMA nanoparticles bind and deliver antisense oligoribonucleotides allowing restoration of dystrophin expression in the mdx mouse." Mol Ther. (2009), 17(5):820-827.

Riss T.L., Moravec R.A., Niles A.L., Duellman S., Benink H.A., Worzella T.J., Minor L. "Cell Viability Assays." In: Sittampalam GS et al. (Eds): "Assay Guidance Manual Eli Lilly & Company and the National Center for Advancing Translational Sciences." Bethesda (MD) (2016).

Russell W.M.S., Burch R.L. The principles of humane experimental technique. London: Methuen; (1959).

Saad F., Hotte S., North S., Eigl B., Chi K., Czaykowski P., Wood L., Pollak M., Berry S., Lattouf J.B., Mukherjee S.D., Gleave M., Winquist E. "Randomized phase II trial of Custirsen (OGX-011) in combination with docetaxel or mitoxantrone as second-line

therapy in patients with metastatic castrate-resistant prostate cancer progressing after first-line docetaxel: CUOG trial P-06c." Clin Cancer Res. (2011), 17:5765-5773.

Sahay G., Alakhova D.Y., Kabanov A.V. "Endocytosis of nanomedicines." J Control Release (2010), 145(3):182-95.

Salova A.V., Leontieva E.A., Mozhenok T.P., Kornilova E.S., Krolenko S.A., Belyaeva T.N. "Change in localization of cellular vesicular apparatus during differentiation of myoblasts into myotubules in cell culture." Cell Tissue Biol. (2011), 5(3), 255-263.

Sang M., Zhang Z., Liu F., Hu L., Li L., Chen L., Feng F., Liu W., Qu W. "Multifunctional hyaluronic acid-decorated redox-responsive magnetic complex micelle for targeted drug delivery with enhanced antitumor efficiency and anti-cell-migration activity." J Biomed Nanotechnol. (2018), 14(3):477-495

Saxena R., Pan G., McDonald J.M. Km. "Osteoblast and osteoclast differentiation in modeled microgravity." Ann N Y Acad Sci. (2007), 1116:494-498.

Sbrana T., Ahluwalia A. "Engineering Quasi-Vivo in vitro organ models." Adv Exp Med Biol. (2012), 745:138-153.

Schwartlander R., Schmid J., Brandenburg B., Katenz E., Vondran F.W., Pless G., Cheng X., Pascher A., Neuhaus P., Sauer IM. "Continuously microscopically observed and process-controlled cell culture within the SlideReactor: proof of a new concept for cell characterization." Tissue Eng. (2007), 13(1):187-196.

Seth P.P., Siwkowski A., Allerson C.R., Vasquez G., Lee S., Prakash T.P., Wancewicz E.V., Witchell D., Swayze E.E. "Short antisense oligonucleotides with novel 2'-4' conformationaly restricted nucleoside analogues show improved potency without increased toxicity in animals." J Med Chem. (2009), 52:10-13.

Shen J., Kim H.C., Su H., Wang F., Wolfram J., Kirui D., Mai J., Mu C., Ji L.N., Mao Z.W., Shen H. "Cyclodextrin and polyethylenimine functionalized mesoporous silica nanoparticles for delivery of siRNA cancer therapeutics." Theranostics. (2014), 4(5):487-497.

Si X.Y., Merlin D., Xiao B. "Recent advances in orally administered cell-specific nanotherapeutics for inflammatory bowel disease." World J Gastroenterol. (2016), 22(34):7718-7726.

Siboni R.B., Nakamori M., Wagner S.D., Daniel M.C., Matthew K.T., Berglund J.A. "Actinomycin D specifically reduces expanded CUG repeat RNA in myotonic dystrophy models." Cell Rep. (2015), 13:2386–2394.

Sicot G., Gourdon G., Gomes-Pereira M. "Myotonic dystrophy, when simple repeats reveal complex pathogenic entities: new findings and future challenges." Hum Mol Genet. (2011), 20: 116-123.

Sirsi S.R., Schray R.C., Wheatley M.A., Lutz G.J. "Formulation of polylactide-co-glycolic acid nanospheres for encapsulation and sustained release of poly (ethylene imine)-poly(ethylene glycol) copolymers complexed to oligonucleotides." J Nanobiotechnology. (2009), 7(1): 1-12.

Sithole M.N., Choonara Y.E., du Toit L.C., Kumar P., Pillay V. "A review of semi-synthetic biopolymer complexes: modified polysaccharide nano-carriers for enhancement of oral drug bioavailability." Pharm Dev Technol. (2017), 22(2):283-295.

Slowing I., Trewyn B.G., Lin V.S. "Effect of surface functionalization of MCM-41-type mesoporous silica nanoparticles on the endocytosis by human cancer cells." J Am Chem. Soc. (2006), 128(46), 14792-14793.

Slowing I.I., Vivero-Escoto J.L., Wu C.W., Lin V.S. "Mesoporous silica nanoparticles as controlled release drug delivery and gene transfection carriers." Adv Drug Deliv Rev. (2008), 60(11):1278-88.

Soares S., Sousa J., Pais A., Vitorino C. "Nanomedicine: Principles, Properties, and Regulatory Issues." Front Chem. (2018), 20;360: 1-15.

Sosa-Hernández J.E., Villalba-Rodríguez A.M., Romero-Castillo K.D., Aguilar-Aguila-Isaías M.A., García-Reyes I.E., Hernández-Antonio A., Ahmed I., Sharma A., Parra-Saldívar R., Iqbal HMN. "Organs-on-a-Chip module: A review from the development and applications perspective." Micromachines (Basel). (2018), 9(10): E536.

Su C., Liu Y., He Y., Gu J. "Analytical methods for investigating in vivo fate of nanoliposomes: A review." J Pharm Anal. (2018), 8(4):219-225.

Sun X., Xu C., Wu G.,Ye Q., Wang C. "Poly (lactic-co-glycolic acid): Applications and future prospects for periodontal tissue regeneration." Polymers. (2017), 9:189:1-19.

Sung J.H., Shuler M.L. “A micro cell culture analog (microCCA) with 3-D hydrogel culture of multiple cell lines to assess metabolism-dependent cytotoxicity of anti-cancer drugs.” Lab Chip. (2009), 9(10):1385-1394.

Swierczewska M., Han H.S., Kim K., Park J.H., Lee S. “Polysaccharide-based nanoparticles for theranostic nanomedicine.” Adv Drug Deliv Rev. (2016), 99(Pt A):70-84.

Trewyn B.G., Slowing I.I., Giri S., Chen H.T., Lin V.S. “Synthesis and functionalization of a mesoporous silica nanoparticle based on the sol-gel process and applications in controlled release.” Acc Chem Res. (2007), 40(9):846-53.

Van Deutekom J.C., Janson A.A., Ginjaar I.B., Frankhuizen W.S., Aartsma-Rus A., Bremmer-Bout M., den Dunnen J.T., Koop K., van der Kooi A.J., Goemans N.M., de Kimpe S.J., Ekhart P.F., Venneker E.H., Platenburg G.J., Verschuuren J.J, van Ommen G.J. “Local dystrophin restoration with antisense oligonucleotide PRO051.” N Engl J Med. (2007), 357:2677-2686.

Vivero-Escoto J.L., Slowing I.I., Trewyn B.G., Lin V.S. “Mesoporous silica nanoparticles for intracellular controlled drug delivery.” Small. (2010), 6(18):1952-1967.

Vozzi F., Heinrich J.M., Bader A., Ahluwalia A.D. “Connected culture of murine hepatocytes and HUVEC in a multicompartmental bioreactor.” Tissue Eng Part A. (2009), 15(6):1291-1299.

Vozzi F., Mazzei D, Vinci B, Vozzi G, Sbrana T, Ricotti L, Forgione N, Ahluwalia A. “A flexible bioreactor system for constructing in vitro tissue and organ models”. Biotechnol Bioeng. (2011), 108(9):2129-2140.

Wang H., Agarwal P., Zhao S., Xu R.X., Yu J., Lu X., He X. “Hyaluronic acid-decorated dual responsive nanoparticles of Pluronic F127, PLGA, and chitosan for targeted co-delivery of doxorubicin and irinotecan to eliminate cancer stem-like cells.” Biomaterials. (2015), 72:74-89.

Wang M., Wu B., Lu P., Tucker J.D., Milazi S., Shah S.N., Lu Q.L. “Pluronic-PEI copolymers enhance exon-skipping of 2'-O-methyl phosphorothioate oligonucleotide in cell culture and dystrophic mdx mice.” Gene Ther. (2014), 21(1):52-59.

Warf M.B., Nakamori M., Matthys C.M., Thornton C.A., Berglund J.A. “Pentamidine reverses the splicing defects associated with myotonic dystrophy.” Proc Natl Acad Sci USA. (2009), 106:18551–18556.

Wei C.W., Cheng J.Y., Young T.H. “Elucidating in vitro cell-cell interaction using a microfluidic coculture system.” Biomed Microdevices. (2006), 8(1):65-71.

Weinhart M., Hocke A., Hippenstiel S., Kurreck J., Hedtrich S. “3D Organ Models - Rrvolution in pharmacological research?” Pharmacol Res. (2018), accepted manuscript.

Wheeler T.M., Leger A.J., Pandey S.K., MacLeod A.R., Nakamori M., Cheng S.H., Wentworth B.M., Bennett C.F., Thornton C.A. “Targeting nuclear RNA for in vivo correction of myotonic dystrophy.” Nature. (2012), 488:111- 115.

Williams D.F. “Definitions in biomaterials.” Amsterdam: Elsevier; (1987): 72.

Wong C.H., Fu Y., Ramisetty S.R., Baranger A.M., Zimmerman S.C. “Selective inhibition of MBNL1- CCUG interaction by small molecules toward potential therapeutic agents for myotonic dystrophy type 2 (DM2).” Nucleic Acids Res. (2011), 39:8881–8890.

Xia T., Kovochich M., Liong M., Mädler L., Gilbert B., Shi H., Yeh J.I., Zink J.I., Nel A.E. “Comparison of the mechanism of toxicity of zinc oxide and cerium oxide nanoparticles based on dissolution and oxidative stress properties.” ACS Nano (2008), 2(10):2121-2134.

Ye H., Xia Z., Ferguson D.J., Triffitt J.T., Cui Z. “Studies on the use of hollow fibre membrane bioreactors for tissue generation by using rat bone marrow fibroblastic cells and a composite scaffold.” J Mater Sci Mater Med. (2007), 18(4):641-648.

Yin H., Price F., Rudnicki M.A. “Satellite cells and the muscle stem cell niche.” Physiol Rev. (2013), 93(1):23-67.

Yukihara M., Ito K., Tanoue O., Goto K., Matsushita T., Matsumoto Y., Masuda M., Kimura S., Ueoka R. “Effective drug delivery system for duchenne muscular dystrophy using hybrid liposomes including gentamicin along with reduced toxicity.” Biol Pharm Bull. (2011), 34(5):712-716.

Zylberberg C., Matosevic S. “Pharmaceutical liposomal drug delivery: a review of new delivery systems and a look at the regulatory landscape.” Drug Deliv. (2016), 23(9):3319-3329.